BIOMECHANICAL PROPERTIES OF PARASPINAL MUSCLES AND THEIR INFLUENCE ON SPINAL LOADING

AN EXPERIMENTAL AND COMPUTATIONAL INVESTIGATION

by

Masoud Malakoutian

B.A.Sc., The University of Tehran, 2011

M.A.Sc., The University of British Columbia, 2014

A THESIS SUBMITTED IN PARTIAL FULFILLMENT OF

THE REQUIREMENTS FOR THE DEGREE OF

DOCTOR OF PHILOSOPHY

in

The Faculty of Graduate and Postdoctoral Studies

(Mechanical Engineering)

THE UNIVERSITY OF BRITISH COLUMBIA

(Vancouver)

May 2021

The following individuals certify that they have read, and recommend to the Faculty of Graduate and Postdoctoral Studies for acceptance, the dissertation entitled:

Biomechanical Properties of Paraspinal Muscles and Their Influence on Spinal Loading: An Experimental and Computational Investigation

submitted by Masoud Malakoutian in partial fulfillment of the requirements for

the degree of Doctor of Philosophy

in Mechanical Engineering

Examining Committee:

Dr. Thomas R. Oxland, Professor, Departments of Orthopaedics and Mechanical Engineering, UBC
Supervisor

Dr. Sidney Fels, Professor, Department of Electrical and Computer Engineering , UBC
Supervisory Committee Member

Dr. Stephen H. M. Brown, Associate Professor, Department of Human Health and Nutritional Sciences, University of Guelph
Supervisory Committee Member

Anasavarapu Srikantha Phani, Associate Professor, Department of Mechanical Engineering, UBC
University Examiner

Jean-Sébastien Blouin, Professor, School of Kinesiology, UBC
University Examiner

Additional Supervisory Committee Members:

Dr. David Wilson, Professor, Departments of Orthopaedics and Mechanical Engineering, UBC
Supervisory Committee Member

Abstract

Adult spinal deformity (ASD) is prevalent among ~30% of the population above 65 years old. While decreased back extensor strength in the form of muscle weakness/dysfunction is well-documented for these patients, it is unclear what muscle properties lead to such decreased strength. The overall goal of this research project was to investigate if biomechanical properties of the paraspinal muscles are different in ASD patients; and whether those differences could influence spinal loading and be associated with the initiation/progression of ASD. To achieve this goal, four studies were conducted. The first study examined the effect of spinal level on elastic modulus, slack sarcomere length, and collagen deposition in paraspinal muscles of 13 rats revealing independence of those properties on the spinal level. In the second study, the influence of the size of single muscle fibers and fiber bundles on elastic modulus was investigated for both rodents and humans. Smaller fibers and fiber bundles manifested larger elastic moduli, highlighting the necessity of aiming for consistent bundle sizes for passive property measurement. For the third study, ethical and technical requirements for intraoperative human muscle biopsy acquisition were addressed and paraspinal muscle biopsies were collected from nine ASD patients. Although patient-recruitment halted because of COVID-19 and thus the small number of patients did not allow performing a statistical comparison between the patients, thought-provoking observations were made. In situ- and slack sarcomere lengths had large variations; several fiber bundles exhibited substantially high stiffnesses, and histopathological analysis unveiled a variety of extracellular and intracellular case-specific abnormalities. The variations observed for the biomechanical properties were input to an enhanced musculoskeletal model of the thoracolumbar spine, which predicted increases in the intradiscal pressures by several orders of magnitudes in some cases. This fourth study highlighted the importance of

biomechanical properties along with the muscle force-length curve to the spinal forces. The entire thesis demonstrated that biomechanical properties of paraspinal muscles do vary among ASD patients and this can dramatically influence the spinal loads. Therefore, future experimental and computational studies should be conducted to provide further insight on the potential role of these properties in the initiation/progression of ASD.

Lay Summary

About 30% of the people above 65 years old acquire spinal deformity including hunchback. Back muscle weakness is considered a primary factor in causing spinal deformity. This thesis mainly aimed to investigate what muscle properties in these patients are different that result in their back muscles being weak, leading to spinal deformity.

After addressing two fundamental questions on muscle-mechanics using rat models, intraoperative muscle biopsies were collected from adult spinal deformity patients to study their passive properties and biological structures. Large variability for muscle passive properties and various abnormalities including muscle fiber degeneration and increased connective-tissue were present. The effect of the observed variations in muscle passive properties was examined in a computational model, which suggested substantial increases in spinal loading. Further studies should be conducted to better understand the role of muscle properties in causing age-related spinal deformities. That knowledge can help in the development of better treatments/preventative strategies.

Preface

This thesis was written in its entirety by Masoud Malakoutian. The supervisory committee including Dr. Thomas Oxland, Dr. Stephen Brown, Dr. Sidney Fels, and Dr. David Wilson provided invaluable insight and feedback throughout the project and in editing of the thesis. Dr. Thomas Oxland supervised the entire project, guided its direction, provided the required facilities and collaborations for conducting the studies, and took leadership on writing the grant to fund this project. Dr. Stephen Brown provided priceless insight on muscle mechanics and its physiology, trained the author and transferred knowledge for testing muscle mechanical properties, and provided further insight in musculoskeletal modeling of the lumbar spine. Drs. Sidney Fels and John Lloyd provided guidance and facilitated using of ArtiSynth software package for development of the musculoskeletal model and enhancing its performance. Dr. John Street and his amazing research team provided the clinical perspective and assisted in obtaining ethics approval, patient recruitment, muscle biopsy acquisition, and coordination with various departments in Vancouver General Hospital. Dr. David Wilson provided imaging and biomechanical insight. Drs. Fabio Rossi and Marine Theret provided insight and training for tissue processing, immunostaining, and histology. Dr. Peter Schutz made histological assessment of muscle biopsies and provided myopathological insight.

A version of Chapter 2 has been accepted for publication in the Journal of the Mechanical Behavior of Biomedical Materials:

- **M. Malakoutian**, S. Yamamoto, S. Sadaram, J. Speidel, J. Liu, J. Street, S. H.M. Brown, and T. R. Oxland. *The Effect of Vertebral Level on Biomechanical Properties of the Lumbar Paraspinal Muscles in a Rat Model.*

The study was designed by MM, SHMB, and TRO. MM and SS designed, developed, and verified an apparatus for testing muscle mechanical properties. MM conducted all mechanical testing. MM and JS wrote the protocol for animal care and ethics approval. JL performed surgery on rats. MM, SY, and JS obtained biopsies and performed animal care. JS (the surgeon) provided clinical insight for surgery simulation. MM drafted the manuscript. TRO and SHMB provided insight, supervised the entire study, and edited the manuscript. All coauthors read and approved the final manuscript. The UBC ethics number for the animal study was A18-0261.

A version of Chapter 3 is submitted for publication in a scientific journal:

- **M. Malakoutian,** M. Theret, S. Yamamoto, I. Dehghan-Hamani, M. Lee, J. Street, F. Rossi, S.H.M. Brown, and T. R. Oxland. *Larger Muscle Fibers and Fiber Bundles Manifest Smaller Elastic Modulus in Paraspinal Muscles of Rats and Humans.*

The study was designed by MM, SHMB, and TRO. MM, SY, and IDH conducted mechanical testing of specimens belonging to study groups 1,2,3, respectively. ML and SY sectioned and stained the specimens; MT and FR provided insight and training in immunostaining and image analysis; JS provided clinical insight and collected human specimens; MM and SY performed data analysis; MM drafted the manuscript; TRO and SHMB provided insight, supervised the entire study and edited the manuscript. All coauthors read and approved the final manuscript. The UBC ethics numbers were A18-0261 and H18-01072 for the animal and human studies, respectively. The VCH number for the human study was V18-01072.

A version of Chapter 4 is being prepared to be submitted for publication in a scientific journal:

- **Malakoutian M**, I. Dehghan Hamani, S.H.M. Brown, M. Doroudi, P. Schutz, T. Ailon, J. Street, and T. R. Oxland, *Biomechanical Properties of Paraspinal Muscles in Adult Spinal Deformity Patients – A Preliminary Analysis.*

The study was designed by MM, SHMB, JS and TRO. MM designed tools and developed procedures for obtaining biopsies. MD provided anatomical insight for muscle biopsy acquisition. TA and JS identified patient groups, performed the surgeries, and collected muscle biopsies. MM and IDH received biopsies, processed them, and conducted the mechanical testing. PS made histopathological assessment of the biopsies. TRO supervised the entire study. TRO and SHMB provided biomechanical insight and edited the manuscript. The UBC ethics and VCH numbers for this study were H18-01072 and V18-01072, respectively.

A version of Chapter 5 is submitted for publication in a scientific journal:

- **Malakoutian M**, C. A. Sanchez, S.H.M. Brown, J. Street, Sidney Fels, and T. R. Oxland, *Biomechanical Properties of Paraspinal Muscles Influence Spinal Loading - A Musculoskeletal Simulation Study*.

The study was designed by MM. MM developed the musculoskeletal model, improved its solution methods, and enhanced its validation. CAS and SF provided insight and assisted MM in using ArtiSynth software package for development of the model. JS provided clinical perspective. TRO supervised the entire study. TRO and SHMB provided biomechanical and musculoskeletal modeling insight and edited the manuscript.

Table of Contents

List of Tables

List of Figures

List of Abbreviations

ACSA – Anatomical Cross-Sectional Area

ASD – Adult Spinal Deformity

CM – Compensatory Mechanisms

COVID-19 – Coronavirus Disease 2019

CSA – Cross-Sectional Area

DEG – Degenerative Spine

DEG+ COMP – Degenerative Spine with Compensatory Mechanisms

DEG+COMP+UNBAL – Degenerative spine with Compensatory Mechanisms but Unbalanced

ECM – Extracellular Matrix

EXT – Extensor Muscles

EXT+PS – Extensor Muscles and Psoas Major

FAP – Fibro Adipogenic Progenitor

IDP – Intradiscal Pressure

IQR – Inter Quartile Range

MDRD – Medical Device Reprocessing Department

MUL – Multifidus

O.C.T. – Optimal Cutting Temperature

PCSA – Physiological Cross-Sectional Area

SI – Sagittal Imbalance

SpT – Scaling factor for Specific Tension

SSL – Slack Sarcomere Length

UBC CREB – University of British Columbia Clinical Research Ethics Board

VCHRI – Vancouver Coastal Health Research Institute

Acknowledgments

First, I would like to acknowledge the support of my research supervisor, Dr. Thomas R. Oxland. I wish to thank you for your continuous support, encouragement, optimism, openness, trust, and for embodying any characteristics I can imagine an academic role model would have. Thanks for caring about your students and helping them maintain their balance of life. I would like to thank you the most for your honesty and sticking to the ethical and moral values in every single step of the research. I learned a lot from you and that will continue.

I also wish to acknowledge the support of my supervisory committee: Drs. Sidney Fels, Stephen Brown, and David Wilson. Thank you for sharing your insights and providing me with your invaluable comments and feedback throughout my project. Special thanks to you Dr. Stephen Brown for your never-ending support and always accommodating my requests/questions in your busy schedule. Without your help, I could not have ever established our muscle testing lab at the ICORD.

I would like to acknowledge the support and funding received from Medtronic Canada and Natural Sciences and Engineering Research Council of Canada (NSERC) as well as the four-year fellowship (4YF) form the department of Mechanical Engineering at UBC.

I wish to acknowledge the tremendous support from Dr. John Street and his research team, particularly Leilani Reichl and Allan Aludino. Without your help at the clinical front I cannot imagine how conduction of the human study would have been possible. Many thanks to Dr. John Lloyd for his technical support for using ArtiSynth. I wish to express my sincere gratitude to Drs.

Peter Schutz, Fabio Rossi, Marine Theret, Aziz Ghahary, and Reza Jalili, for their help on the histology aspect of my project.

Special thanks to the muscle project team in our lab including Iraj Dehghan-Hamani, Dr. Shun Yamamoto, Dr. Jie Liu, Sandeep Sadaram, Jason Speidel, Sophie Ramsden, Rafael Lustosa de Lima, and Alex Burden, who helped in various aspects of my studies including tool design, manufacturing, testing, and animal care. Also, many thanks to the rest of OIBG labmates who were always there for help and support including Kurt McInnes, Dr. Stephen Mattucci, Loay Al-Salehi, Luis Dias, Angela Melnyk, and so many others.

I would like to express my greatest gratitude to my family, especially my kind parents and brother, Taha. Your unconditional love and prayers for me were invaluable assets I had for accomplishing my goals. I do not know how to thank you more for everything you gave me to be who I am today. I also wish to thank my parents, sisters, and brother in-law for their warm hospitality, support and help particularly during the phase of my thesis writing.

My deepest heart-felt thanks goes to my dear, lovely wife, Zahra. Thanks for your continuous encouragement, positive energy, and endless love. Thanks a ton for making the taste of my PhD studies so sweet with your patience and presence by my side.

Dedication

To whom I have dedicated my entire life to

Chapter 1 Introduction

1.1 Overview

By 2050, more than 1.5 billion (16%) people in the world will be above 65 years old [1]. Associated with that rise in elderly population, the number of patients with adult spinal deformity (ASD), which is prevalent among ~30% of adult population [2][3][4], will increase causing significant effects on quality of life and social costs [5]. While various risk factors such as vertebral fractures, postural changes, degenerative disc disease, and genetic predisposition are identified for adult spinal deformity [2][6], many original and recent review studies believe the main causative role is played by muscular dysfunction [7][8][9][10][11][12] and decreased back extensor strength.

A decrease in back extensor strength may arise from changes in different muscle parameters including smaller anatomical cross-sectional area, lower level of activation, or muscle moment arm, all of which have been observed to some extent in patients with adult spinal deformity [13][14][15]. While each of these parameters can have an effect on muscle strength, they are not sufficient for assessment of the torque generation capacity (strength) of a muscle across a joint. Information about other muscle parameters such as fascicle length, pennation angle, sarcomere number, specific tension and passive stiffness, which can each play significant roles on muscle force generation capacity, is also necessary.

The overall goal of this thesis is to investigate which biomechanical properties of the paraspinal muscles are different in adult spinal deformity patients; and whether those differences could influence spinal loading and be associated with initiation/progression of adult spinal deformity.

Understanding the effect of each of the muscle biomechanical properties on muscle function requires a deeper look into its structure and mechanism of force production which is provided in the following sections. Furthermore, musculoskeletal modeling is required to provide insight into the influence of these parameters on spinal forces.

In this chapter, a brief anatomy of the spine and paraspinal muscles is presented followed by a review of recent findings on the etiology of adult spinal deformity. A background on muscle mechanics, its structure, and its adaptation in different environments is provided. Hill-type musculotendon actuator model and recent advances in musculoskeletal modeling of the thoracolumbar spine are reviewed and discussed. Finally, the conclusions from these sections lead to my research questions and the objectives of this thesis.

1.2 Spine Anatomy

The spine is a pivotal structure in the body that connects the head to the pelvis. The main functions of the spine include transferring loads of the upper body to the pelvis, providing physiological mobility to the trunk, and most importantly protecting the spinal cord and nerve roots [16]. Twenty-four articulated vertebrae along with the sacrum and coccyx comprise the spine. The spine has several regions including cervical spine with seven vertebrae, thoracic spine with twelve vertebrae, lumbar spine with five vertebrae, the sacrum with four to five fused vertebrae, and the coccyx with four to five fused vertebrae (Figure 1-1).

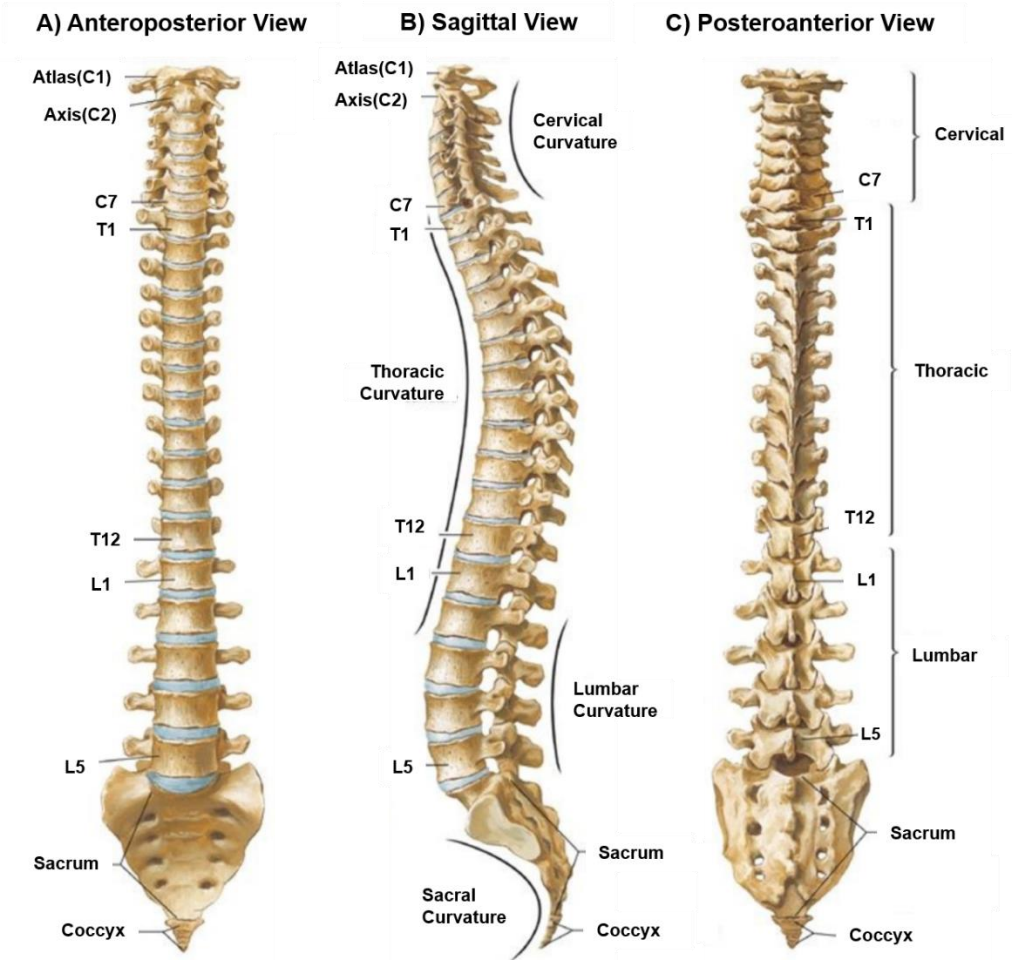

Figure 1-1. Spine from three different views. Adapted from [17] **with permission from Elsevier Health Sciences.**

A vertebra is a bony element with two main regions: the anterior region known as the vertebral body and the posterior region called the neural arch. A triangular opening is formed between the two regions, known as the vertebral foramen, through which the spinal cord and cauda equina pass and are protected along the spinal column (Figure 1-2).

The neural arch of the vertebra has a particular shape with various protrusions, known as processes. The spinous process is directed posteriorly, whereas transverse processes are directed laterally. Two superior and two inferior articular processes of each vertebra articulate with inferior and superior processes of the adjacent vertebrae, respectively, forming the facet joints. There are also some minor processes which are helpful landmarks for describing muscle attachment sites. These processes include mammillary processes and accessory processes (Figure 1-2). The pedicle is a thick bridging protrusion between the vertebral body and posterior elements; and lamina is a wide bony plate connecting the pedicle to the spinous process.

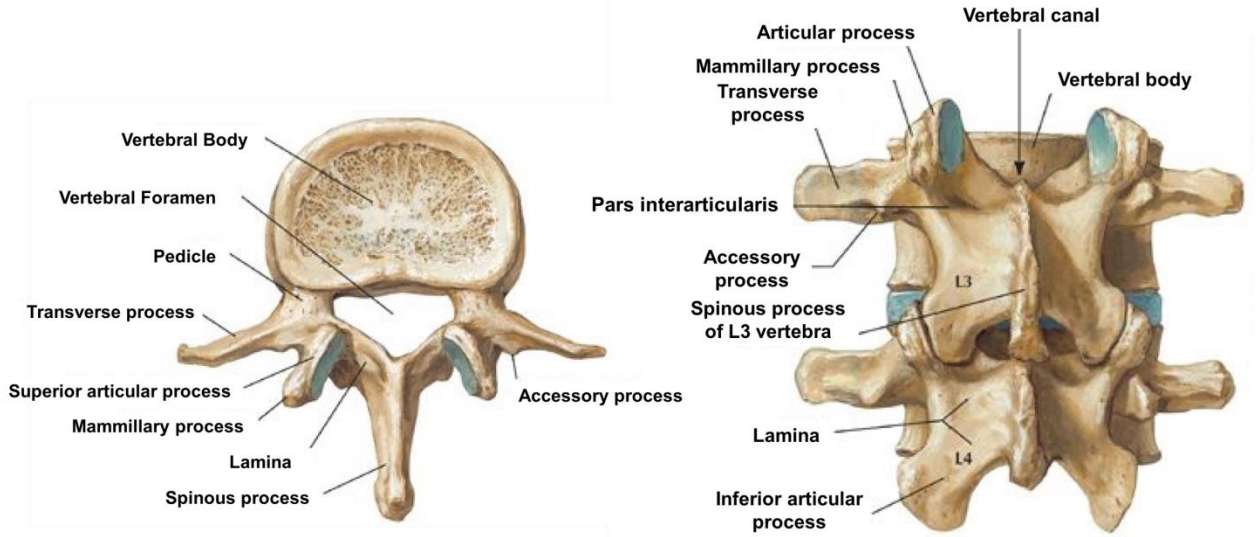

Figure 1-2. Landmarks of a lumbar vertebra. Adapted from [17] **with permission from Elsevier Health Sciences.**

While facet joints articulate the posterior elements of the adjacent vertebrae, intervertebral discs connect their vertebral bodies. Intervertebral discs are comprised of a nucleus pulposus, annulus fibrosus, and cartilaginous endplates (Figure 1-3A&B). The major volume of the intervertebral disc is filled by the nucleus pulposus, which is a fluid like substance in the middle of the intervertebral disc, surrounded by the annulus fibrosus circumferentially and by cartilaginous endplates on the top and bottom. The annulus fibrosis consists of several concentric layers of fibrocartilaginous bands whose fibers have a small angle of ~30° with the transverse plane but are in opposite direction to their adjacent layers (Figure 1-3C) [16].

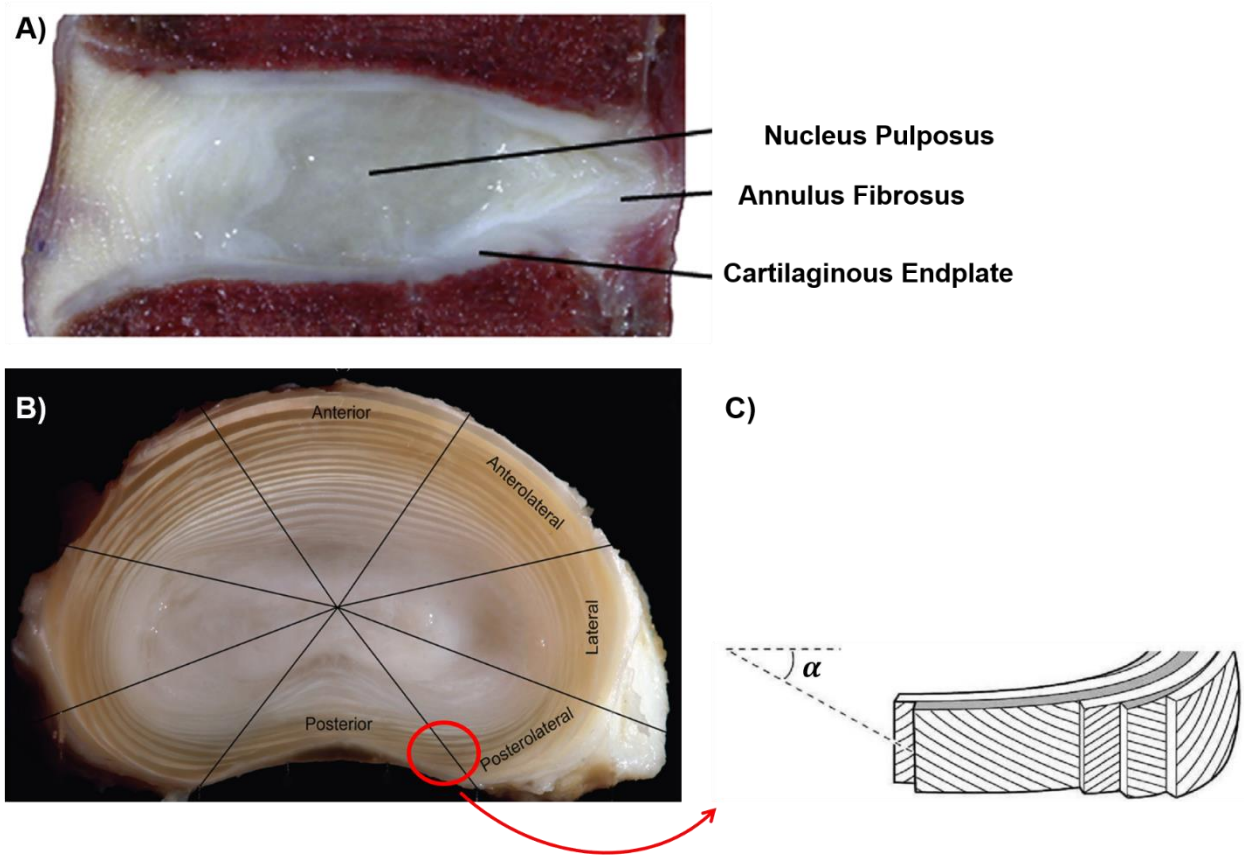

Figure 1-3. Intervertebral disc structure. (A) sagittal plane view of the disc, (B) superior view of the disc, (C) and crisscross pattern of the lamellae fibers at about $\alpha = \pm 30°$ from the vertebral end plates. Adapted from [18]**,** [19]**, and** [20] **with permission from Schmidt, Cambridge university press, and Wolters Kluwer HealthInc.**

The vertebrae of the spine are connected through several ligaments. Anterior longitudinal and posterior longitudinal ligaments cover the anterior and posterior of the vertebral bodies, respectively, along the entire spine. The outer layer of annulus fibrosus is also a vertebral body ligament as it connects two bones, i.e. the adjacent vertebrae. The ligamentum flavum with its short thick bands lies posterior to the spinal canal and spans between the laminae of the adjacent vertebrae. The bottom and top edges of spinous processes of adjacent vertebrae are connected via interspinous ligaments, while their posterior edges are connected and shielded by supraspinous ligament. Several iliolumbar ligaments attach transverse processes of L5 to multiple sites on the ilium. In general, the main role of the spinal ligaments is to assist in stabilizing and supporting the spine in various postures especially under distraction, bending, and twisting (Figure 1-4)[21].

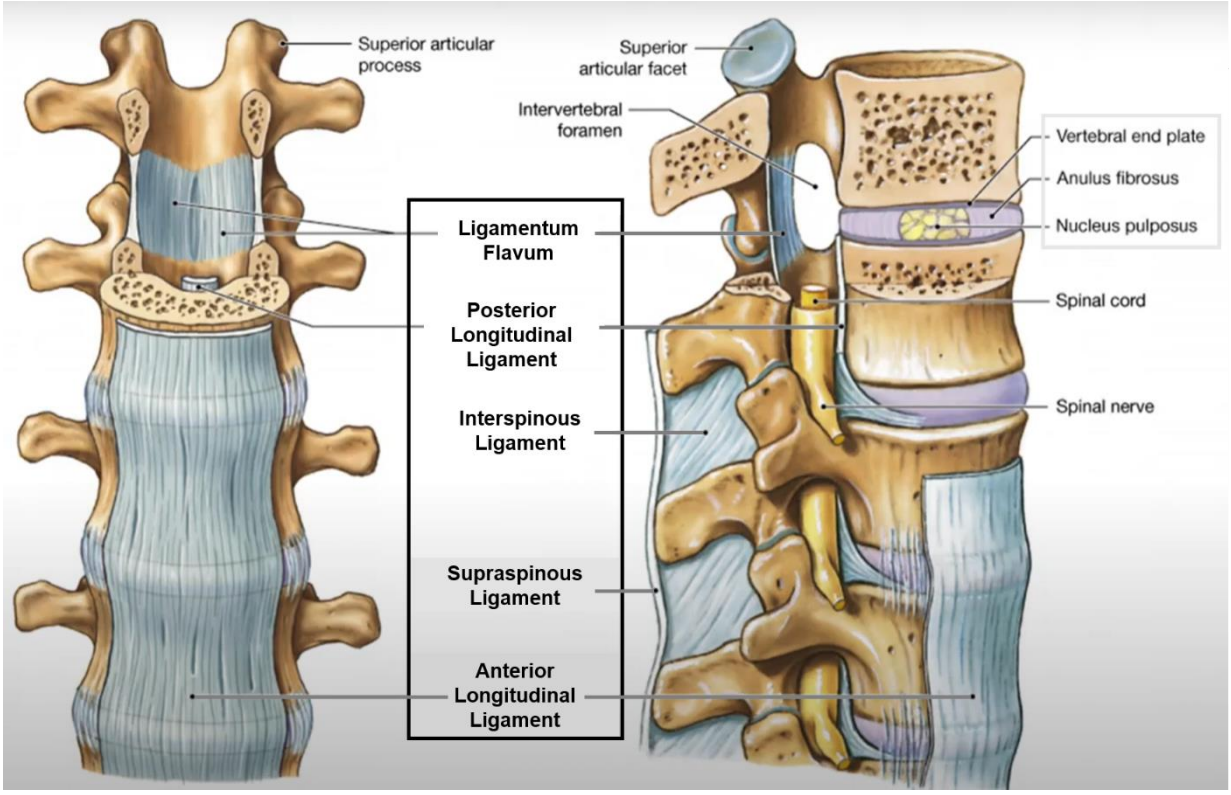

Figure 1-4. Major ligaments of the spine. Adapted from [22] **with permission from Kevin Tokoph.**

1.3 Paraspinal Muscle Anatomy

Functionally and anatomically, back muscles can be divided into extrinsic and intrinsic groups. Intrinsic muscles contribute to spinal movement, maintaining its balance, and controlling its posture, whereas extrinsic muscles are more involved in limb movements and respiration [23][24] (Figure 1-5). Extrinsic muscles are mostly present at the superficial layer and include trapezius, latissimus dorsi, levator scapulae, rhomboids, and serratus posterior (Figure 1-6).

Intrinsic muscles exist mostly at the intermediate and deep layers (Figure 1-7). The only intrinsic muscle at the superficial layer is the splenius, which belongs to the cervical spine as the extensor of the head and neck (Figure 1-7A). At the intermediate layer, erector spinae muscle is present and consists of spinalis, longissimus, and iliocostalis, respectively from most medial to most lateral (Figure 1-7B). These muscles are further classified based on the region into which they are inserted. For example, superior insertion points of iliocostalis lumborum are in the lumbar region, whereas those for iliocostalis cervicis lie in the cervical region. A further classification can be made based on the origin points of these muscles.

At the deep layer of intrinsic muscles, transversospinalis muscle group consists of multifidus, semispinalis, and rotatores. Multifidus is present along the entire spine but is the only transversopinalis muscle that exists in the lumbar region (Figure 1-7C). Multifidus is well-known for its stabilizing role at the lumbar spine region [25]. Interspinalis, intertransversarii, and levatores costarum are named minor deep muscles, as with their small sizes they are not expected to assist in taking substantial spinal loads; rather, they are postulated to have a proprioceptive function [26][23] (Figure 1-7D).

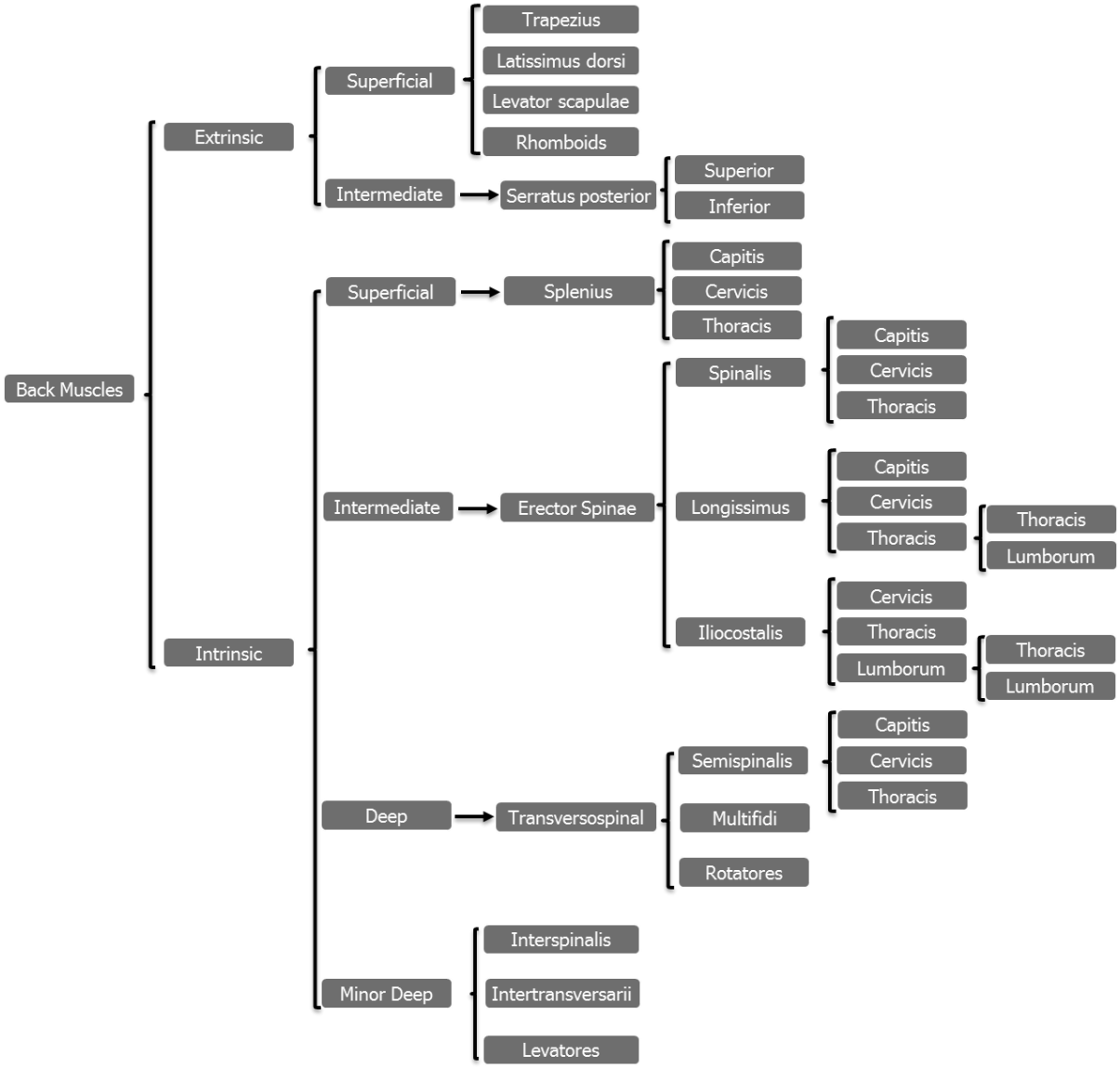

Figure 1-5. A summary of spinal muscles according to the classifications presented in Gray's anatomy [24] **and Clinically Oriented Anatomy** [23]**. Adapted from** [27] **with permission from the University of British Columbia.**

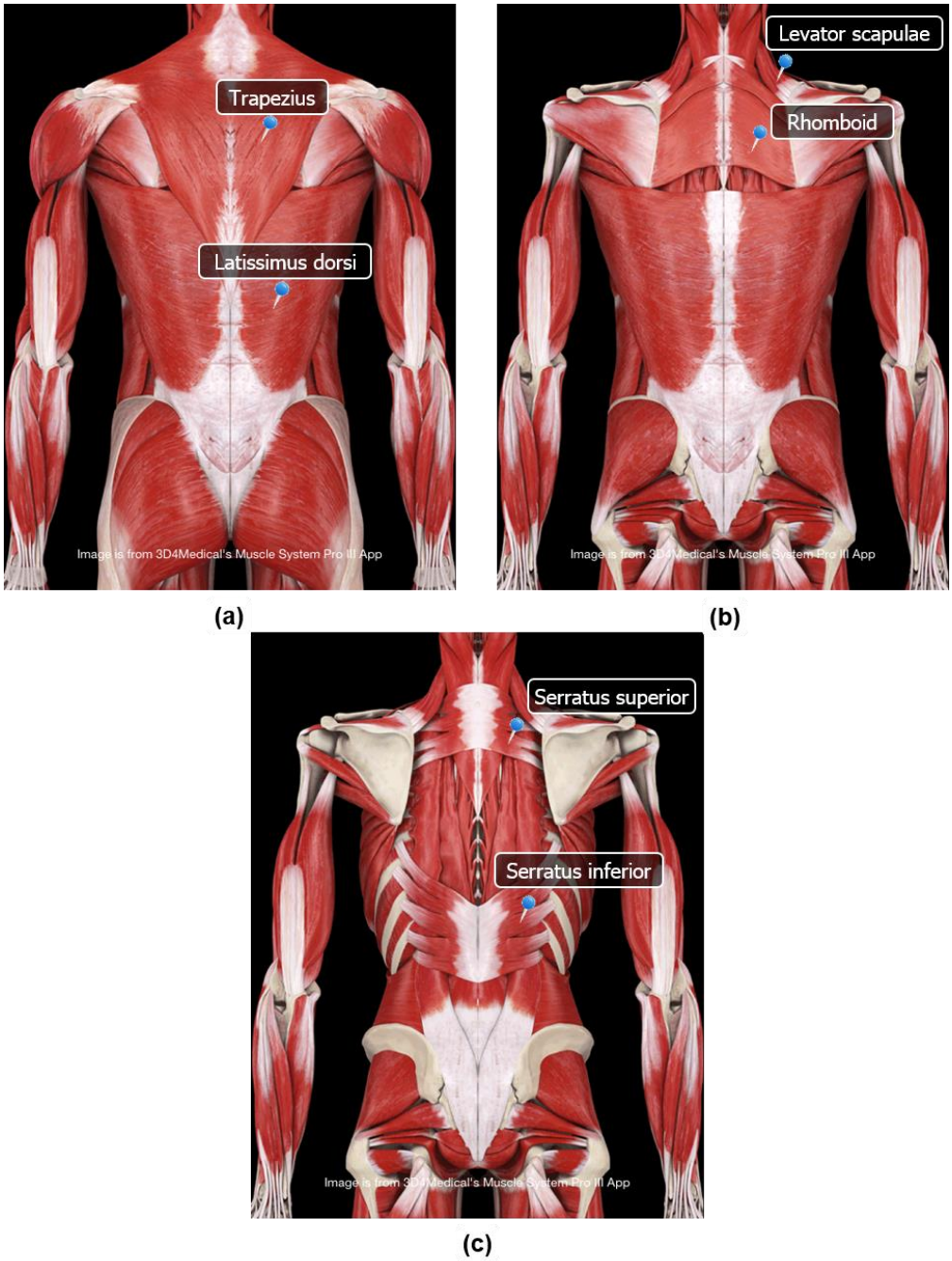

Figure 1-6. The extrinsic back muscles. (a) trapezius and latissimus dorsi; (b) levator scapulae and rhomboids; and (c) serratus inferior and posterior. Adapted from Muscle System Pro III app with permission from 3D4Medical company.

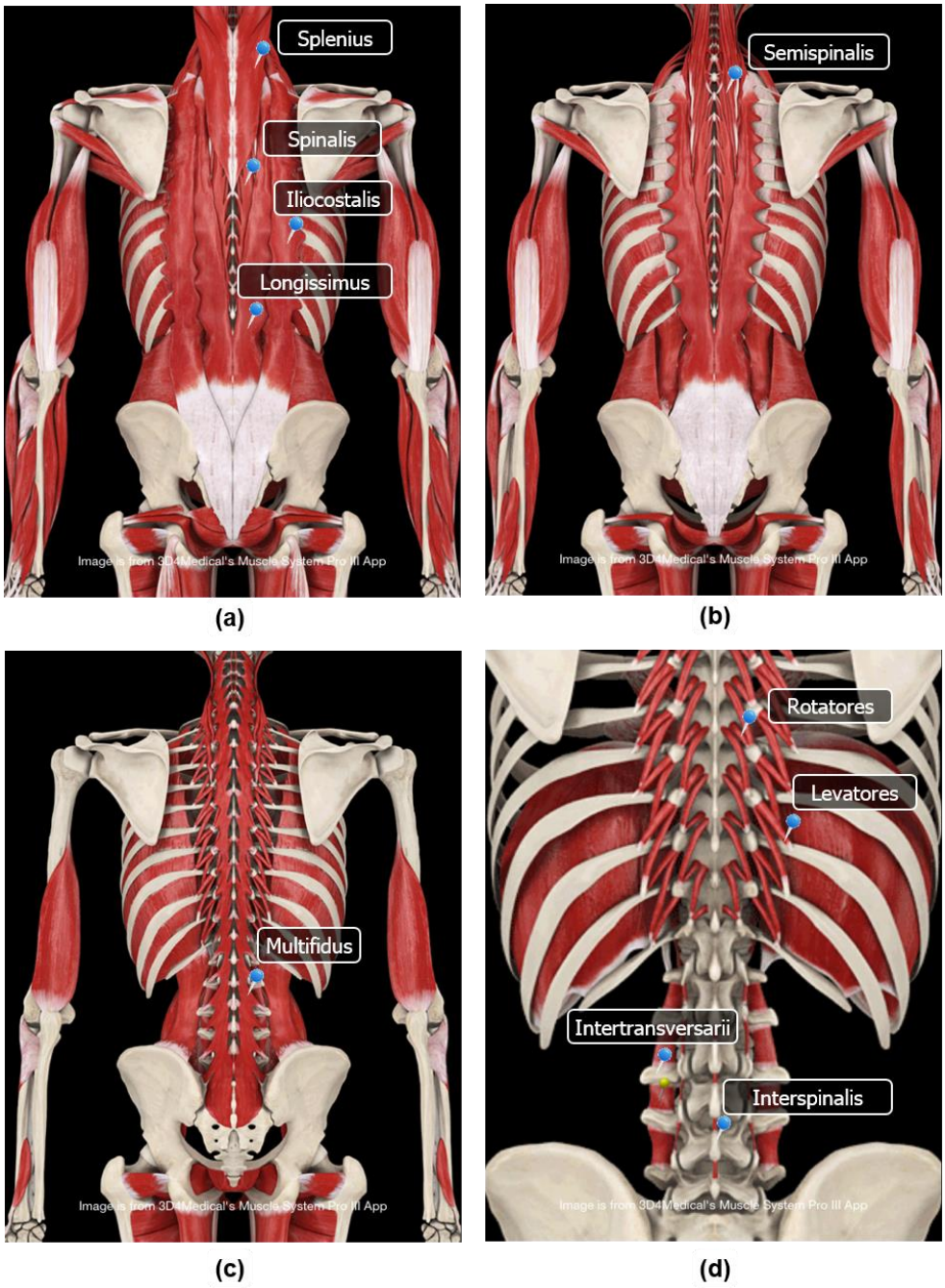

Figure 1-7. The intrinsic back muscles. (a) splenius, spinalis, longissimus, and iliocostalis; (b) semispinalis; (c) multifidus; and (d) rotatores, interspinalis, intertransversarii, and levatores. Adapted from Muscle System Pro III app with permission from 3D4Medical company.

While quadratus lumborum and psoas major may not be included in anatomy books under spinal muscles [24][23], they do have attachment sites on lumbar spine vertebrae and contribute to its loading (Figure 1-8). Quadratus lumborum originates from the iliac crest and is attached to the twelfth rib, sometimes after passing through transverse processes of the lumbar vertebrae [23]. Psoas major is known primarily as a hip flexor but it can also flex the spine when the lower limb is fixed [28].

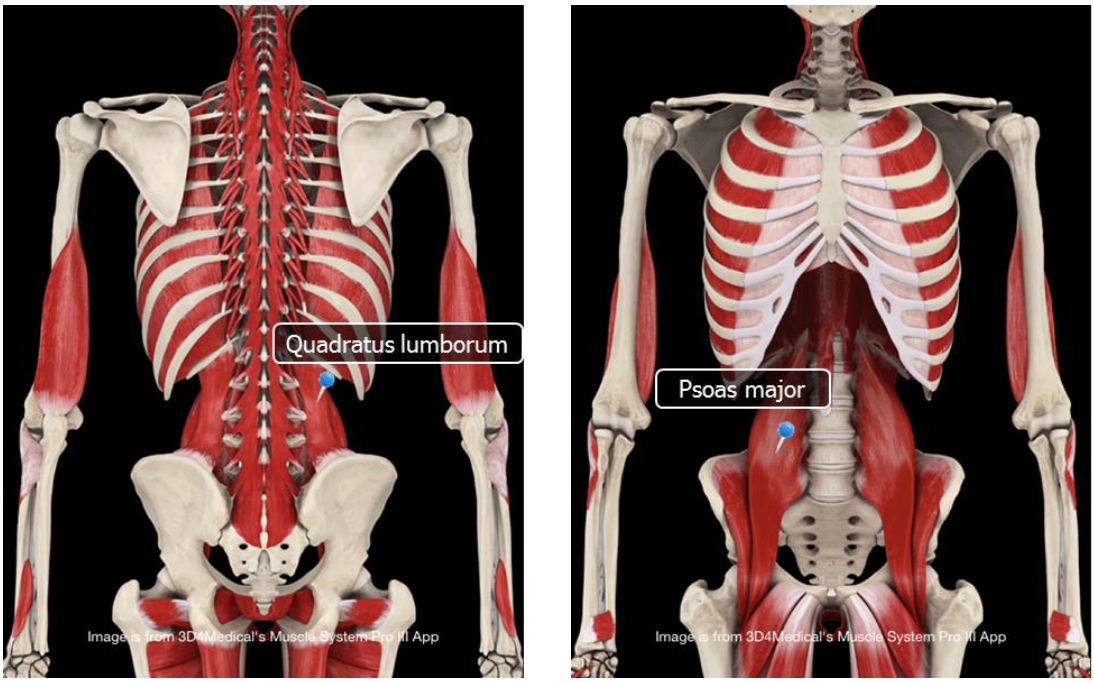

Figure 1-8. Quadratus lumborum and psoas major. Adapted from Muscle System Pro III app with permission from 3D4Medical company.

1.4 Adult Spinal Deformity

Globally, the number of people above 65 years old is expected to almost double from 2020 to 2050, increasing from 727 million (9% of the population) to above 1.5 billion (16% of the population) [1]. With this growing aged population, the prevalence of degenerative spinal disorders including adult spinal deformity will increase, causing significant effect on quality of life and social costs [5][29]. The prevalence of adult spinal deformity has been reported to be up to ~30% [2][3][4] and in some cases as high as 68% [30] for people above 65 years old. Therefore, a better understanding of this condition and its etiology is crucial for development of preventative strategies or improved treatments.

1.4.1 Definition

Adult spinal deformity can occur within the sagittal, coronal, or axial planes. Such deformity can be in the form of a malalignment between two adjacent vertebrae (segmental deformity), within any of the lumbar, thoracic, or cervical regions of the spine (regional deformity), or between the upper spine and sacrum (global deformity) [31]. To quantify these deformities, several measurements are made on posteroanterior (coronal plane) and lateral (sagittal plane) full-length (36-in) standing radiographs (Figure 1-9 & Figure 1-10).

Global spinal alignment in the sagittal plane is defined by a plumb line dropped from the C7 centroid [32][33](Figure 1-9a). If the C7 plumb line, also known as the sagittal vertical axis (SVA), falls further than 5 cm anterior to the posterior corner of the S1 endplate, the patient has global sagittal deformity [34]. Such deformity could arise from regional deformities including a thoracic hyperkyphosis and/or lumbar hypolordosis. The normal kyphosis of the thoracic spine is

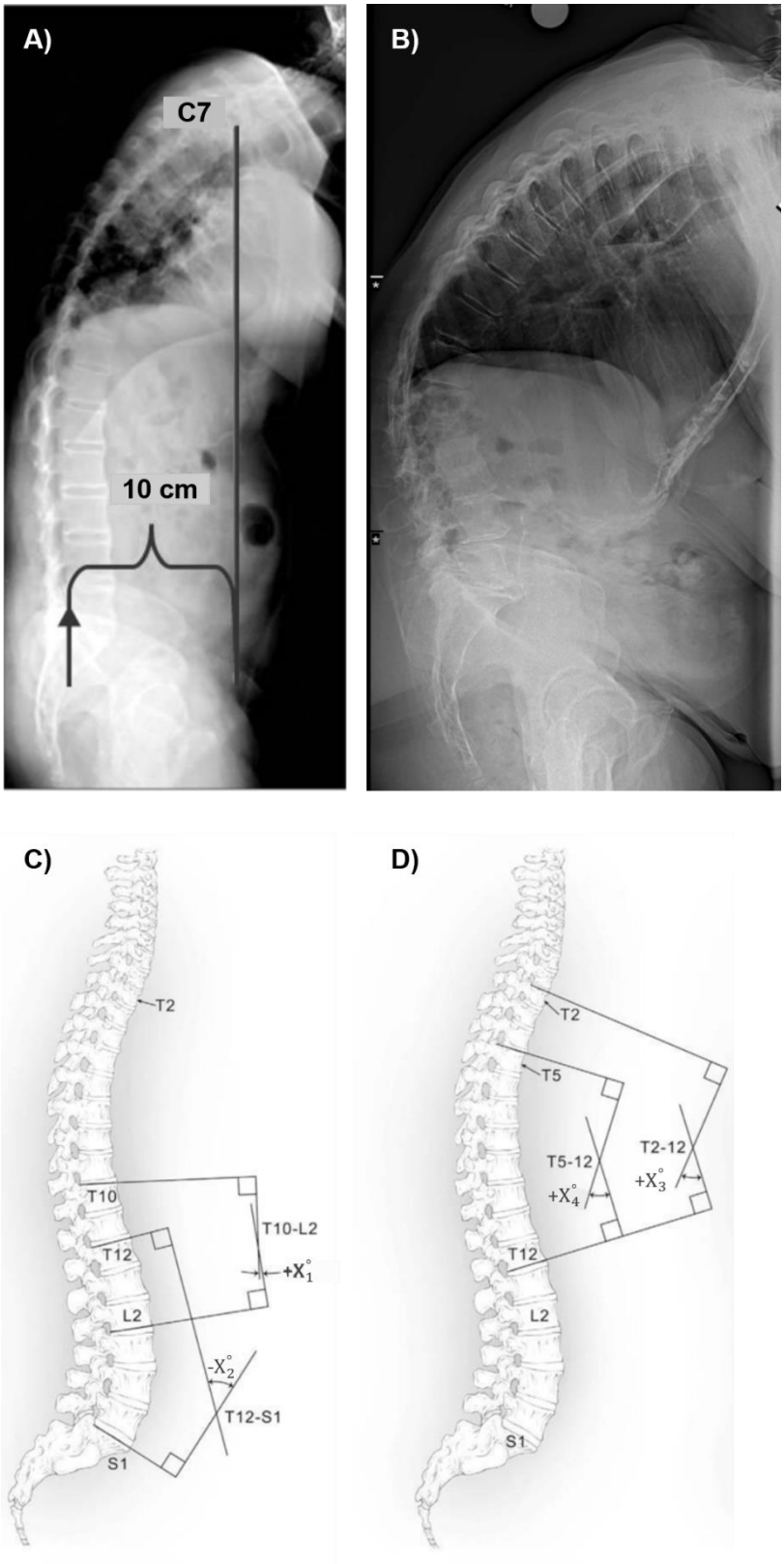

Figure 1-9. Sagittal spinal deformity as a result of A) hypolordosis or B) hyperkyphosis. Regional deformities are typically reported in terms of C) lordosis angle in the lumbar (X_2°) and lumbosacral regions or kyphosis angles in the thoracolumbar region (X_1°) or D) the thoracic region (either X_3° or X_4°) . Adapted from [35]**,** [36]**, and** [34] **with permission from the Korean Orthopaedic Association, Congress of Neurological Surgeons, Radiological Society of North America (RSNA), and Oxford university press.**

considered between 20 to 60 degrees [36] (Figure 1-9D). Therefore, a kypohosis greater than 60 degrees is referred to as hyperkyphosis [31]. On the other hand, the lumbar lordosis ranges between 30-80 degrees [31] (Figure 1-9C). Therefore, a smaller lordosis is deemed insufficient and is referred to as a hypolordotic or flatback deformity [37].

Global spinal alignment in the coronal plane is also defined by the C7 plumb line [38] (Figure 1-10A). If this line falls 5 cm or more lateral to the mid sacral line the patient has global coronal deformity [31]. This deformity may arise from a variety of regional deformities including thoracic, thoracolumbar, or lumbar coronal curvature (scoliosis). The location of the curvature is determined by locating its apex [34] (Figure 1-10B). The apex of the curve is identified by the disc or vertebra that is maximally displaced from the midline and minimally angulated [34]. Regional scoliosis is quantified by the Cobb angle, which is the angle between maximally angulated (end) vertebrae above and below the apex [38] (Figure 1-10B).

Typically, adjacent to the major curve which has the largest Cobb angle, there are minor curves present in the coronal plane that are further categorized as compensatory or structural [39] (Figure 1-11A). Surgical correction of the major curve usually leads to spontaneous correction of the compensatory minor curve, while it does not correct the structural curve. Therefore, supine side-bending radiographs are required to distinguish between these two curves - compensatory curves are less than 25 degrees, while structural curves are above 25 degrees [34] (Figure 1-11B&C).

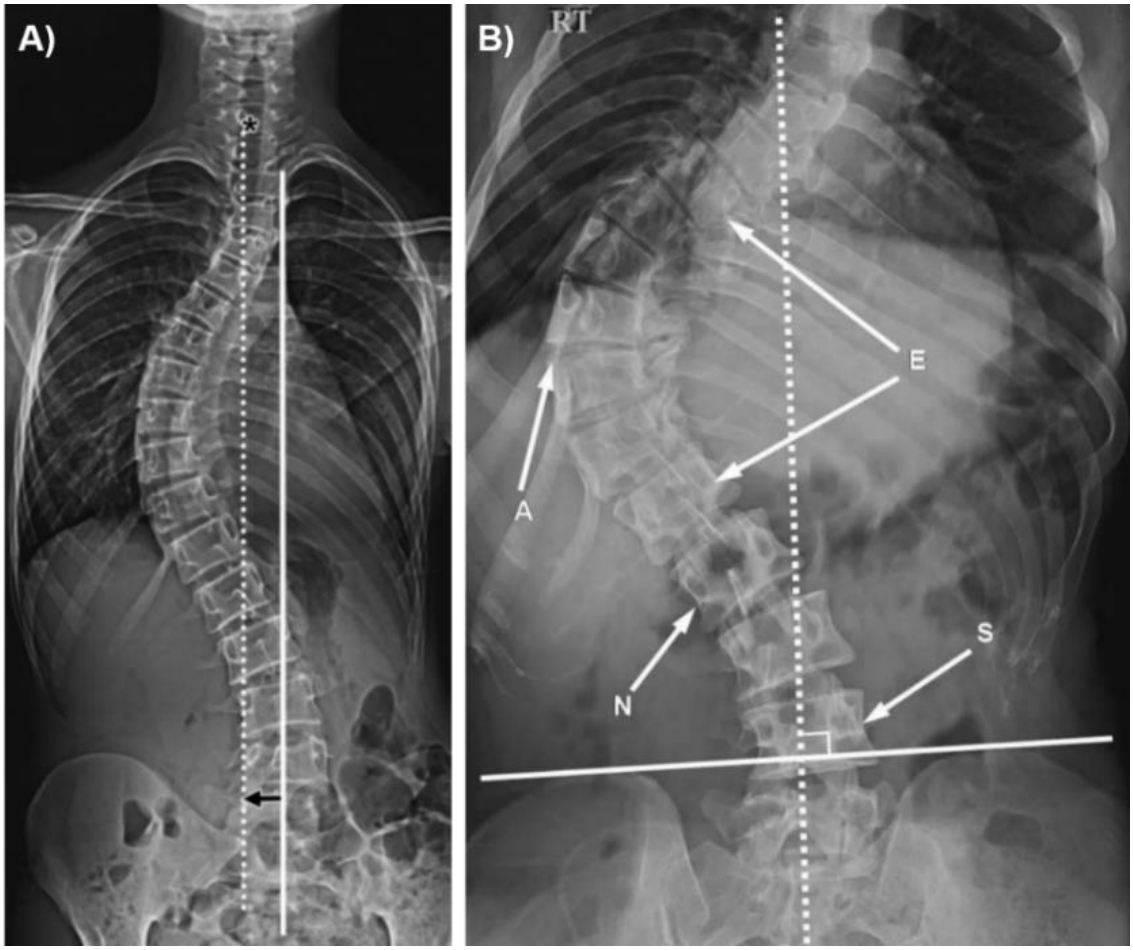

Figure 1-10. Characteristics of coronal-plane deformity. Global coronal-plane deformity is determined by the deviation of the C7 plumb line from the central sacral vertical line (A). A scoliotic curve is characterized by its apex, A, and its end vertebrae, E, which are the most angulated vertebrae above and below the apex, and are used for Cobb angle measurement (B). A neutral vertebra, N, is the one that is not tilted with respect to its adjacent vertebrae, and a stable vertebra, S, is the most distant above the sacrum that is still (nearly) bisected by the central sacral vertical line. Adapted from [38] **with permission from Radiological Society of North America.**

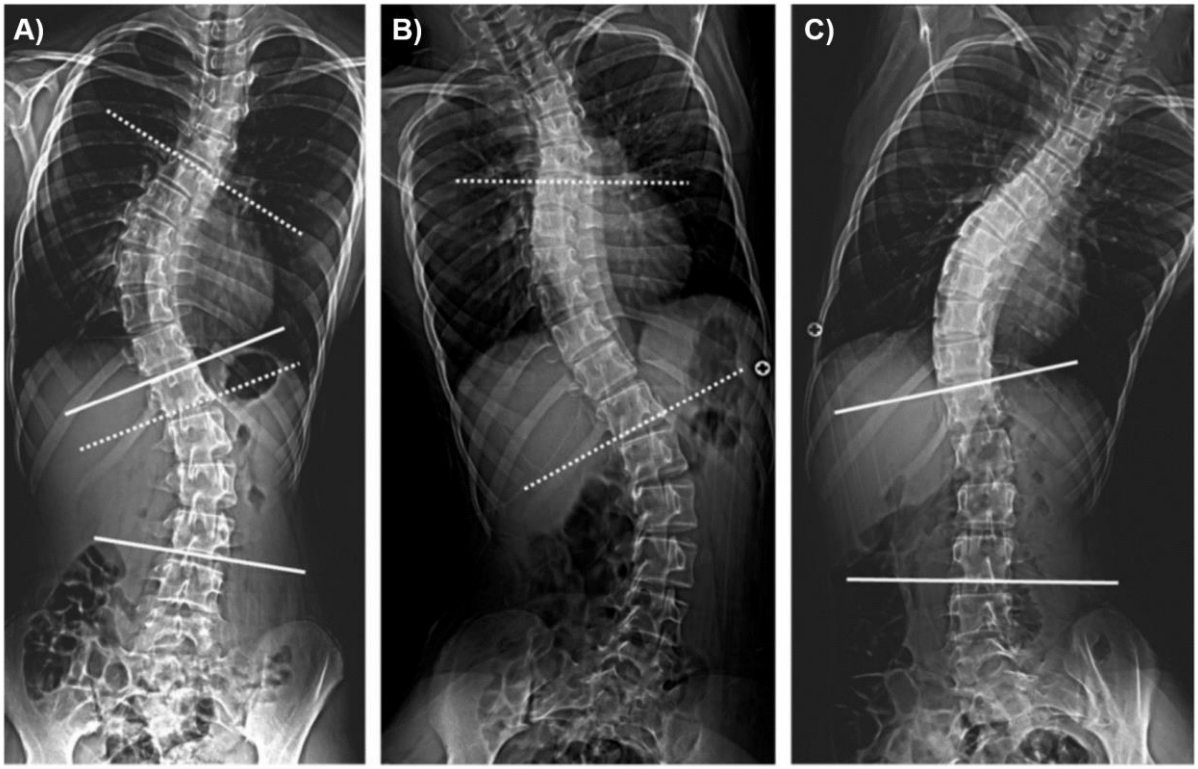

Figure 1-11. Structural versus compensatory curves in coronal plane deformity. In the neutral standing image (A), the curve between the solid lines and the curve between the dotted line are both greater than 25°. However, by bending to the right (B), the curve between the dotted lines remains greater than 25°, while when bending to the left (C), the curve between the solid lines decreases to less than 25°. Therefore, the curve between the dotted lines is the structural and the one between the solid lines is the compensatory curve. Adapted from [38] **with permission from Radiological Society of North America (RSNA).**

This thesis primarily focuses on global sagittal plane deformity (Figure 1-9), especially given that its occurrence is more common [40]. In fact, such deformity is estimated to be prevalent among 20-40% of older adults [2]. Yet, the exact etiology of sagittal plane deformity remains unknown.

1.4.2 Etiology

While various risk factors such as vertebral fractures [41][42], disc degeneration [2][43][6], ligamentous degeneration [44], proprioceptive deficits [11] and genetic predisposition [42] are identified for adult spinal deformity, many original and recent review studies believe a primary

causative role is played by muscle weakness/dysfunction [45][11][46][7][8][9][12][47][48][49][50].

Paraspinal muscle is pivotal to maintaining the upright posture [50][51]. The weight of the upper body generates a flexion moment on the spine which needs to be counterbalanced by extensor muscles. In addition to preserving the equilibrium, extensor muscles contribute to guaranteeing the mechanical stability of the spine [51]. Therefore, it is reasonable that muscle dysfunction may be involved in the development of the spine deformity. In fact, multiple studies have observed lower muscle strength in adult deformity patients [46][7][8][9].

A decrease in back extensor strength may arise from changes in different muscle properties including smaller anatomical cross-sectional area, lower level of activation, or shorter muscle moment arm, all of which have been observed to some extent in spinal deformity patients compared to the normal population [13][14][15]. However, there are other muscle biomechanical properties that could contribute to force production capacity of a muscle, but no study to date has measured them in adult deformity patients in contrast to the normal population. Those muscle properties include passive elastic modulus, slack sarcomere length (beyond which passive force starts to develop), in situ sarcomere length (measured inside the body for a certain posture), specific tension, fascicle length, and pennation angle. These properties relate to multi-scale muscle structure and its function, therefore a review of them is provided in the next section.

1.5 Muscles

1.5.1 Structure

Muscle is an organized material with several structural levels (Figure 1-12). The functional building blocks of muscles are sarcomeres, which consist of interdigitated thin and thick

myofilaments mainly comprised of actin and myosin contractile proteins, respectively [52]. Actin myofilaments are coupled to one another at the two ends of each sarcomere, forming the so-called Z discs, whereas the myosin myofilaments are first linked to titin filaments and then connected to the Z discs. A large number of sarcomeres in series form a myofibril. Parallel alignment of myofibrils forms a muscle fiber (muscle cell) which contains sarcolemma immediately surrounding those myofibrils in addition to a membrane over that known as basal lamina. Muscle fibers lie in parallel within an extracellular matrix known as endomysium which bonds them together and form muscle fascicles. Muscle fascicles are individually covered by perimysium but altogether are wrapped by epimysium forming a muscle [53][54] (Figure 1-12).

While not considered in classic studies as an independent part of muscle structural hierarchy, “muscle fiber bundle” is defined and extensively used in studying muscle biomechanical (passive) properties. Fiber bundle is defined as a small number of (~10 - 20) fibers surrounded by their connective tissue [52]. In contrast to a fascicle or the whole muscle, which are wrapped by perimysium and epimysium, respectively, no biological tissue is identified as the boundary for a fiber bundle. In terms of order of magnitudes, a typical bundle has ~20 fibers, while a fascicle may contain ~300 fibers [55]. Depending on the number of fascicles, at the whole muscle one may expect ~1000 fibers or more in parallel.

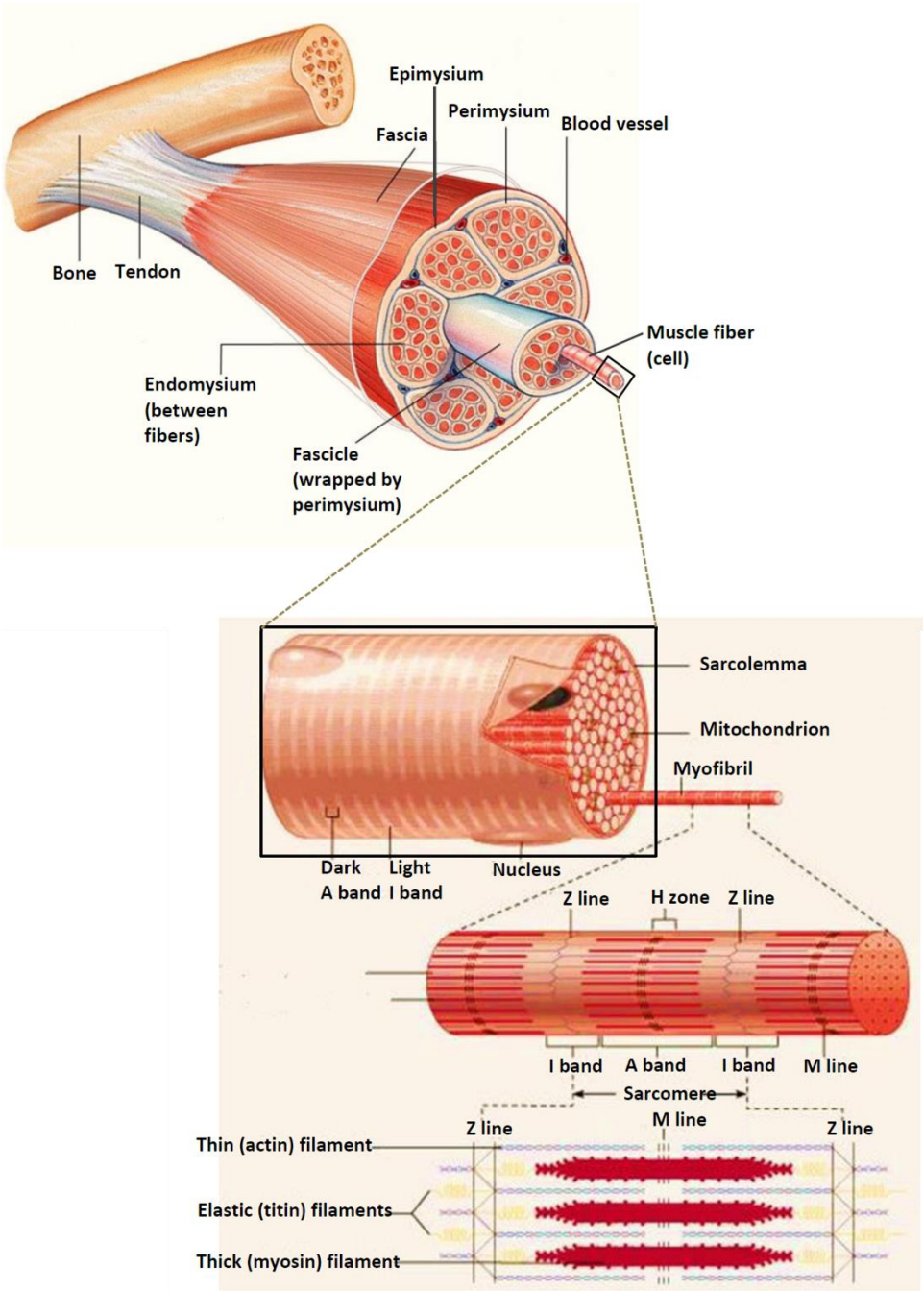

Figure 1-12. Muscle hierarchical structure. Adapted from Fig. 6.1 and 6.3 of [56] **with permission from Pearson Education, Inc.**

1.5.2 Force Production Mechanism

For a muscle fiber to contract (twitch), the central nervous system sends a neural signal in form of an action potential to the neuromuscular junction of that muscle fiber. The action potential is transmitted to the fiber through depolarization of the sarcolemma and is propagated deep into the fiber by the transverse tubular system (Figure 1-13). The transverse tubular system signals the sarcoplasmic reticulum (a sac-like reservoir for calcium ions surrounding the myofibrils) to release calcium ions into the myofilaments region. The calcium ions then initiate a series of chemical reactions that lead to formation of cross-bridges between the myosin and actin myofilaments. Through myosin-actin interaction (the cross-bridge cycle), the myosin grabs the actin filament and slides it toward the center of the sarcomere creating muscle contraction. This force generation process continues until the neural signal stops, which results in uptake of calcium ions into the sarcoplasmic reticulum and therefore, muscle relaxation [57][52].

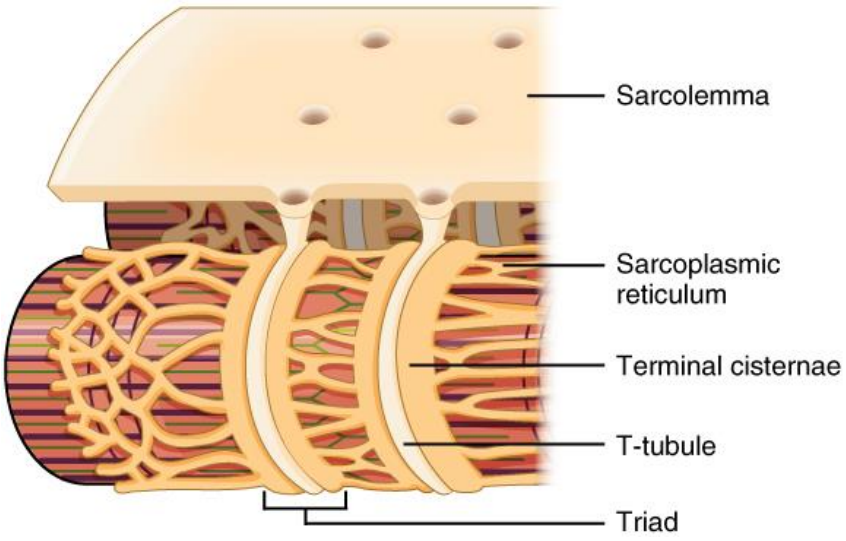

Figure 1-13. Transverse tubular system as the interface between sarcolemma and sarcoplasmic reticulum for propagating action potential deep into the myofilament regions. Adapted from [58] **with permission under the Creative Commons Attribution 4.0 International license.**

The amount of force a muscle generates depends on the position of its myofilaments. The more overlap between actin and myosin myofilaments, the higher the number of cross bridges forming between them and the larger the amount of active force generated by the sarcomere. On the other hand, when the sarcomere is stretched beyond its resting length, titin filaments and other molecules act as springs and demonstrate passive resistance to stretch. Such active and passive behavior of muscle leads to a force-length relationship as the one shown in Figure 1-14. Therefore, the status of sarcomere length, the form of the passive tension curve, and the slack sarcomere length (where the passive curve starts to develop) are all factors involved in the amount of force a muscle can produce [52].

The force production of the muscle is also dependent on the type of myosin heavy chain (MHC) isoforms [59]. The main MHC isoforms in muscles are slow-twitch Type I, and fast-twitch type IIa and type IIb. As for a certain amount of force, the corresponding shortening velocities vary between these fibers, they are classified as slow and fast fibers. The effect of these fibers on muscle force-velocity curve can be seen in Figure 1-14. Although their effect is significant at high shortening speed, they do not differ much in isometric forces or forces at small velocities. The ratios between these fiber types however vary between muscles and are dependent on the type of activity and conditions [52].

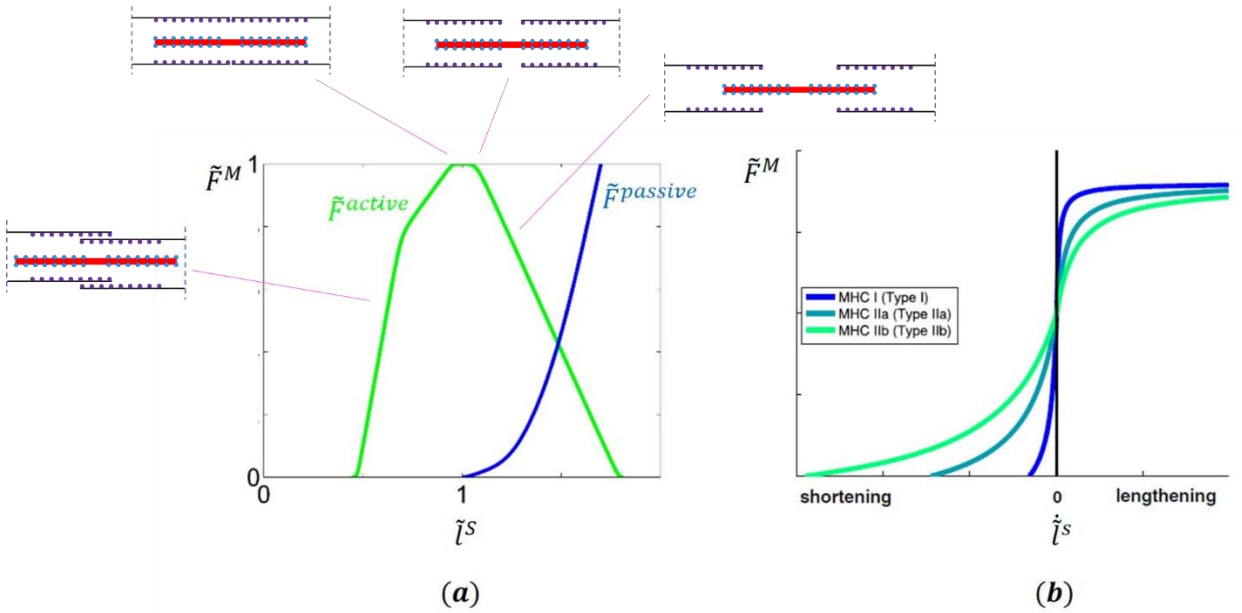

Figure 1-14. Muscle force-length relationship (a), and force-velocity curves for three different fiber types (b). $\tilde{l}^S$ is the sarcomere length normalized by the optimum sarcomere length, which is assumed to be 2.8 μm in human. Depending on the sarcomere length of a muscle, the amount of overlap between the myosin and active myofilaments, and therefore the number of cross-bridges between them varies. This affects the amount of force ($\tilde{F}^{active}$) a muscle can produce when fully activated (green curve), such that in the vicinity of the optimum sarcomere length, maximum isometric force is produced, while on the ascending and descending limb a smaller force is generated in full activation. When a muscle is stretched beyond its resting length, passive force develops ($\tilde{f}^{passive}$). Total muscle force $\tilde{F}^M$ is a summation of active and passive forces. Adapted from [295] with permission from Springer Nature.

1.5.3 Adaptation

As one of the most adaptive tissues of the body, muscles can change due to various stimuli, including neural activation, denervation, exercise, stretch, and overload [54]. Changes can occur at all different scales and affect the muscle force generation capability. For example, at the molecular scale, the fiber type and the speed of force generation in animals have been shown to be changed to slower types in response to overstretch or overload [60][61], though such transformation has not been as evident in humans [62][63][64][65].

At the subcellular level, the number of sarcomeres in series and parallel can change, leading to differences in fiber length and cross-sectional area, respectively. In general, the number of sarcomeres in series increases in a muscle when chronically stretched [66][67][68][69][70] and decreases when chronically understretched [71][72][73][74][75]. When supplemented with overload, protein synthesis accelerates and passive stretch of a muscle leads to even greater extent of sarcomere addition[76]. Sarcomeres are therefore thought to adjust their numbers when subjected to a change so as to restore their original or optimal length, where maximum force production occurs [77]. However, that is not necessarily true. A few studies found an increase in sarcomere lengths when subjected to overstretch rather than an increase in sarcomere numbers [67][66][78]. Nonetheless, it is well accepted that an increase/decrease in cross-sectional area is due to addition/subtraction of sarcomeres in parallel[79]; and that overload increases [65][80], while disuse decreases the number of parallel sarcomeres [79].

At the cellular level, the peak isometric fiber stress has been shown to increase when overloaded [64], and decrease in disuse[81][82]; while at the tissue level, the passive stiffness of the muscle has demonstrated adaptation through changes in the composition and volume of the extracellular matrix [71][83].

Finally, at the organ level, the muscle architecture may change in contribution to muscle adaptation. It is well documented that overload, especially in form of eccentric exercise, increases the cross-sectional area and volume of the muscle [80][65][76], and in contrast underload leads to decrease in both [75]. Also, hypertrophy, which can be the result of overload, leads to an increase in pennation angle, probably for the muscle to keep its size as small and compact as possible, while atrophy or underload, has an opposite effect.

1.5.4 Biomechanical Properties

A change in the parameters discussed in the previous section including muscle cross-sectional area, pennation angle, maximum isometric force, sarcomere length, and passive properties can have an influence on muscle force production. It is tempting to explore the extent of influence that a change in any of these parameters imposes on paraspinal muscles and consequently the spinal forces. However, for the scope of this thesis we only focus on three fundamental biomechanical properties given the preponderance of the muscle adaptation literature on them. These properties include the sarcomere length of the muscle at a certain joint/limb/body position, passive elastic modulus, and the slack sarcomere length, beyond which muscle passive forces start to develop.

1.5.4.1 Sarcomere Length

For a certain body posture, sarcomere length of human paraspinal muscles varies between different muscle groups. For example, in a prone posture multifidus typically manifests an average in situ sarcomere length of ~2.3 µm [20][21] while psoas typically has an average in situ sarcomere length of ~3.3 µm [21][23]. When the spine moves from prone to a flexed posture, multifidus fascicles elongate and accordingly their sarcomere length increases, while psoas fascicles shorten and so do their sarcomeres.

As stated in the previous section, when a muscle is put in a new mechanical condition for a long time it seems to remodel to restore its original sarcomere length, but such a phenomenon may not necessarily occur in some cases. Elsalanty *et al.* [67] analyzed 9 adult goats that had underwent 20% tibial lengthening in one of their hind limbs. They observed after 60 days the fiber length of tibialis caudalis muscle had increased 36.7% and that the pennation angle had decreased 37.2%.

Interestingly, the increase in fiber length was due to the increase in sarcomere length from 2.18 µm to 2.97 µm, while muscle mass and PCSA remained constant.

Makarov *et al.* [66] studied all 13 different muscles of goat's tibia in 9 animals after 20% tibia lengthening. After distraction, posterior compartments of muscles had 42% increase in fiber length and 38% increase in sarcomere length, whereas the muscles at the anterior compartments showed a 10% increase in fiber length but 12% decrease in sarcomere length. This study demonstrated surprising differences between individual muscles in response to overstretch (limb lengthening) and indicated that poor mechanism of sarcomere addition of posterior muscles resulted in sarcomere elongation and contracture of the joint.

In a more recent study [78], it was shown in human soleus muscle, that although fascicle length was similar in both cerebral palsy patients and typically developing children, the sarcomere length was dramatically different (4.07±0.45 µm vs. 2.17±0.24 µm). While that parameter has been measured for various spinal muscles, including psoas, multifidus, iliocostalis and longissimus, they have been all measured in normal cadavers or in a mixed heterogeneous group of patients undergoing spine surgery [25][84]. No studies to the best of author's knowledge has measured such a difference in patients with a specific spinal disorder including those with adult spinal deformity.

1.5.4.2 Passive Elastic Modulus

While at the molecular level, actin and myosin, the cross bridge between them, and desmin (protein filament that interconnects myofibrils to one another) may contribute to the passive properties of a fiber, titin is assumed to be the main element corresponding to passive forces within a stretched fiber [85][86][87]. Titin is a giant protein in sarcomeres spanning almost half

of the size of a sarcomere and has been shown to have a negative correlation between its size and fiber stiffness (i.e. smaller (or shorter) titin leads to higher fiber stiffness and vice versa) [86][88][89]. Nonetheless, some studies have cast doubt about this as they did not find any correlation between them [25][90][91]. Therefore, further studies remain to be conducted to indicate the main mechanism behind the passive behavior of a fiber.

While the elastic modulus of an animal single muscle fiber can take values as small as ~6 kPa (in mice [92]) to values more than 150 kPa (in rabbits [86]), the average elastic modulus of a human muscle fiber lies between 20 and 40 kPa [25][93][94]. However, this is only true for healthy individuals. It has been shown that in patients with cerebral palsy the spastic muscle fibers had an average elastic modulus of up to 55 kPa [25]. Interestingly, fiber elastic modulus of spastic muscles is not equal for all muscles and depends on the location of the studied muscle. Friden and Lieber [93] studied the muscles of upper extremities, including biceps brachialis, extensor carpi radialis, flexor carpi ulnaris, pronator teres, and subcapularis and found on average about two times stiffer fibers in cerebral palsy patients. Mathewson *et al.* [95] also found gastrocnemius and soleus in cerebral palsy patients to be stiffer than normal individuals. However, Smith *et al.* [94] did not observe any difference between cerebral palsy patients and the control group in terms of the fiber stiffness of gracilis and semitendinosus. This implies different remodeling mechanisms of the muscles at different locations in the body.

The elastic modulus of a bundle of fibers (~3 to ~30 fibers ensheathed in their connective tissue matrix) is not the same as the elastic modulus of single fibers. This is due to the extracellular matrix, despite its low percentage (~10% of the muscle volume), playing a significant role in stiffening the muscle fiber bundles. In contrast to single fiber elastic modulus, muscle fiber bundles demonstrate a wide range of elastic moduli **(**Table 1-1**).** Values as low as 25 kPa, as was

measured for semitendinosus in [94], up to 463 kPa (16 times stiffer than its single fiber), as was in upper extremities [96]) have been measured for elastic modulus of human muscle fiber bundles. Lieber *et al.* [96] showed that in subjects of their study, while spastic muscles had higher fiber elastic modulus compared to the control group, the bundle elastic modulus was much lower due to lower quality of ECM in the muscles of cerebral palsy patients. The influence of ECM on stiffness of muscle bundles is also muscle specific. The cerebral palsy patients in the study by Mathewson *et al.* [95] had stiffer single fibers compared to the control group, but not different fiber bundle stiffnesses in their gastrocnemius and soleus, whereas an opposite observation was reported by Smith *et al.* [94] for gracilis and semitendinosus: stiffer bundles with no difference in fiber stiffness.

The elastic modulus of single fiber and fiber bundles has been measured for human spinal muscles but has not been contrasted against different groups of patients. Ward *et al.* [25] collected muscle biopsies from three sub groups of erector spinae: multifidus, iliocostalis lumborum, and longissimus thoracis. They found similar single fiber elastic modulus for the three subgroups (~30kPa), but larger elastic modulus for fiber bundles of multifidus (~90kPa) compared to iliocostalis and longissimus (~60 kPa). Whether elastic modulus of these muscles in patients with spinal conditions, particularly those with adult spinal deformity, is any different than others is unknown.

Table 1-1. Summary of passive elastic modulus of muscle fiber and muscle fiber bundle in various human and animal studies.

Study	Subject	Muscle	Fiber Elastic Modulus (kPa)	Fiber Bundle Elastic Modulus (kPa)
Ward 2009 [25]	Human	Multifidus	33.7 ± 1.9	91.3 ± 6.9
		Iliocostalis Lumborum	37.1 ± 3.7	58.8 ± 7.7
		Longissimus Thoracis	32.8 ± 3.2	62.9 ± 14.7
Friden 2003 [93]	Human	Upper extremity (Spastic)	55.0 ± 6.6	Not Measured
		Upper extremity (Normal)	28.2 ± 3.3	Not Measured
Lieber 2003 [96]	Human	Biceps brachialis, extensor carpi radialis, flexor carpi ulnaris, pronator teres, and subcapularis (Spastic)	55.0 ± 6.6	111.2 ± 35.5
		Adductor pollicis longus, brachioradialis, extensor carpi radialis longus, flexor digitorum superficialis, flexor digitorum superficialis (Normal)	28.2 ± 3.3	462.5 ± 99.6
Smith 2011a[94]	Human	Gracilis (cerebral palsy)	21.5 ± 2.4	60.4 ± 11.8
		Gracilis (Normal)	21.5 ± 1.8	36.1 ± 3.9
		Semitendinosus (cerebral palsy)	23.6 ± 1.7	40.7 ± 4.9
		Semitendinosus (Normal)	22.47 ± 1.8	25.2 ± 2.9
Mathewson 2014 [95]	Human	Gastrocnemius (cerebral palsy vs. Normal)	Stiffer	No Difference
		Soleus (cerebral palsy vs. Normal)	Stiffer	No Difference
Brown 2011 [90]	Rabbit	Multifidus (Injured) L3	~95	~115
		Multifidus (Normal) L3	~70	~50
		Multifidus (Injured) L7	~70	~105
		Multifidus (Normal) L7	~55	~55
Brown 2012 [91]	Rat	Rectus Abdominis External Oblique Internal Oblique Transverse Abdominis	~50	~55
Meyer 2011 [92]	Mouse	Extensor Digital Longus	6.3	40.5
Prado 2005 [86]	Rabbit	Extensor Digital Longus	70.9	158.5
		Gastrocnemius	53.5	106.5
		Psoas	157.1	91.6

Elastic modulus of muscle fibers and fiber bundles are determined typically through a uniaxial stretch test. Single fibers and fiber bundles of different sizes are tested and normalized for cross-sectional area under the assumption that this eliminates the effect of size (i.e. cross-sectional area). The size of muscle fiber bundles tested for their elastic modulus varies from 3 to 30 fibers in the literature [96][90][97][98][55][99]. Whether the effect of size on elastic modulus disappears after normalizing for cross-sectional area is unclear. Noonan et al. [100] recently demonstrated that elastic modulus does depend on the size of the muscle fiber. This question, however, has not been solved for bundles of muscle fibers.

Another consideration in measurement of elastic modulus is that most studies of single muscle fibers or bundles of muscle fibers assumed a cylindrical shape and only measured diameter of those specimens in one plane [98][55][101][86][91][102]. Other researchers believe measurement of diameters in two different planes (i.e. both top and side views) is required [103][99]. Blinks [104] investigated 16 frog fibers and observed ~20% difference in the calculated cross-sectional area when measuring only one diameter versus two. For humans or rodents, whether the assumption of a cylindrical shape is trustworthy and to what extent it impacts the measured cross-sectional area of a muscle fiber or a bundle of muscle fibers remains unclear.

It should be noted that as shown in Figure 1-14, the passive behavior of a muscle fiber/fiber bundle demonstrates a nonlinear curve, in most cases an exponential curve with a toe region at its beginning. Hence, depending on where the slope is tangent to the curve the reported stiffness may vary. However, for the sake of comparison, in order to represent the curve by one single value, some studies have neglected the toe region and approximated the second part of the curve

by a line and reported its slope [93][96][90], while some have selected an arbitrary point (e.g. 4 microns) and reported the tangent at that point as the stiffness [91][94].

1.5.4.3 Slack Sarcomere Length

Slack sarcomere length, the point where the passive force starts to develop, is another characteristic of the passive curve that should be considered when studying the muscle passive behavior. This parameter has been shown to vary between different muscles as well as for different patient groups. For instance, the spastic patients of the study by Friden and Lieber [93] had smaller slack sarcomere length compared to the control group (1.84±0.05 μm vs. 2.20±0.04 μm). This obviously has influence on muscle force calculations and thus, should be considered.

1.5.5 Extracellular Matrix

Extracellular matrix plays an important role in modulating the passive properties of the muscle at the tissue level. The larger stiffness of fiber bundles than single fibers arises from the extracellular matrix and properties of its constituents [105]. The largest constituents of muscle extracellular matrix are collagen isoforms [106][105], among which fibrillar collagens, specifically type I (~70% of total collagen) and type III, are the most prevalent [107][105][108]. Collagen I is associated with increasing tensile stiffness of the tissue [107][109] while collagen III is deemed to act in opposite and make the tissue more compliant [109][110].

Smith et al. [108] studied the contribution of extracellular components to the stiffness of semitendinosus muscle in typically developing children in contrast to those with contractures due to cerebral palsy. In total, collagen I and total proteoglycan acted as positive and collagen III and

biglycan as negative predictors of muscle stiffness. When analyzing the groups separately, however, the determining collagenous factors for typically developing children were collagen I and collagen IV, while for cerebral palsy patients it was the ratio of collagen I to collagen III.

In a recent study by Ward et al. [55] collagen content and passive stiffness of several lower extremity muscles were measured in six rabbits. The measurements were made at multiple scales including fiber bundle (~20 fibers), fascicle (~300 fibers), and whole muscle. The results revealed a nonlinear increase in both stiffness and collagen content from smaller to larger scales. At the whole muscle level, collagen was the strongest predictor of muscle passive function. However, not just the content but the organization and quality of collagen also seem to influence the muscle stiffness [111].

1.6 Musculoskeletal Modeling

Knowledge of the muscle forces and human body joint loads is important to a variety of applications including implant design, surgical planning, rehabilitation and ergonomics. Currently, non-invasive direct measurement of muscle forces and joint loads is not feasible. Calculation of muscle forces is not trivial and depends on several muscle parameters. Furthermore, the intricate anatomy and architecture of the musculoskeletal system, particularly in the spine region, adds to its complexity. Therefore, musculoskeletal models are developed to offer a unique opportunity in providing estimations of the muscle forces and joint loads of the human body for a variety of activities and scenarios. Obviously, the predictive accuracy of these models depends on their input material properties and the solution method they adopt, which is discussed in this section.

1.6.1 Hill Type Muscle-Tendon Actuator

Given the special force production mechanism of muscles and their force-length and force-velocity relationships, a muscle can be represented by a combination of a contractile element in parallel with a passive spring (Figure 1-15). The tendon attaching the muscle to its anchor sites on bones can also be represented by a passive spring in series with that muscle. This entire unit is defined as a Hill-type muscle-tendon actuator, per the classical description by Hill [112] and is adopted by most musculoskeletal models throughout the literature for modeling an entire muscle-tendon [113].

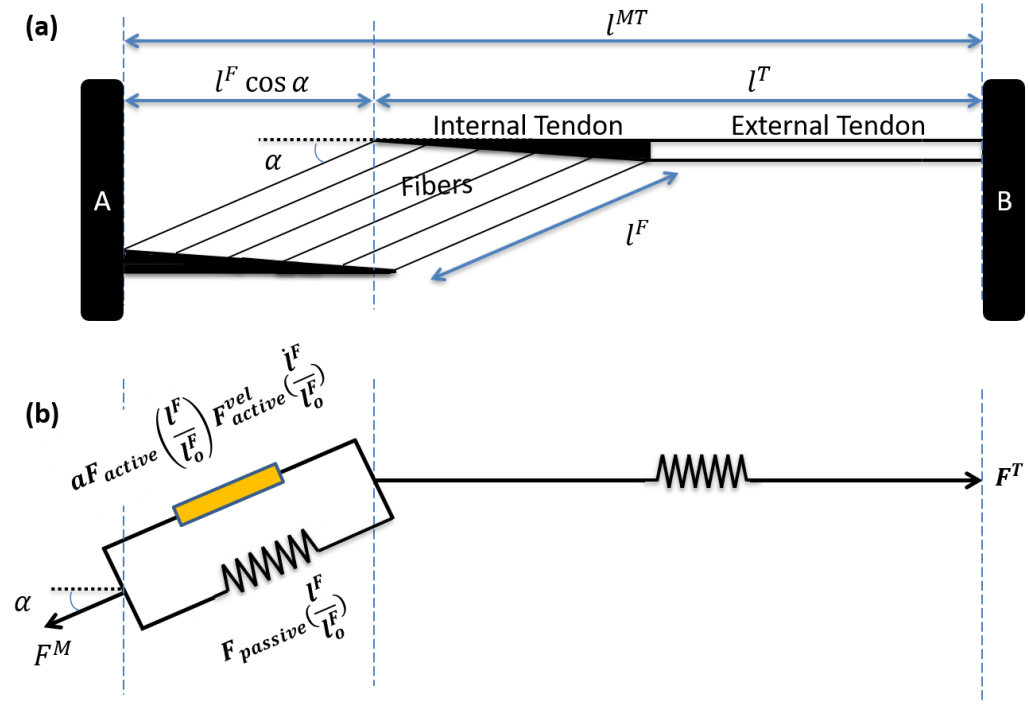

Figure 1-15. Illustration of a muscle-tendon unit and its equivalent model as Hill-type musculotendon actuator.

The force of the muscle component in Hill-type muscle-tendon model is computed in form of:

$$
\begin{aligned}
F^T = F^M\left(a, l^F, \dot{l}^F\right) \times \cos\alpha \\
&= PCSA \\
&\times \left(a \times ST \times \tilde{F}_{active}\left(\frac{l^F}{l_o^F}\right) \times \tilde{F}_{active}^{vel}\left(\frac{\dot{l}^F}{l_o^F}\right) + K \times \tilde{F}_{passive}\left(\frac{l^F}{l_o^F}\right)\right) \qquad (1\text{-}1) \\
&\times \cos\alpha
\end{aligned}
$$

where on the left hand side, F^M is the muscle force as a function of three state variables of the muscle, namely the activation level of the muscle (a), muscle fiber length (l^F), and muscle fiber

contraction velocity ($\dot{l}^F$). In the right-hand side, however, in addition to the three state variables, several biomechanical and anatomical properties of the muscle are required to compute the muscle force. These parameters include physiological cross-sectional area ($PCSA$), specific tension (ST), passive curve scaling factor (K), pennation angle (α), and optimum fiber length (l_o^F). In the above equation, $\tilde{F}_{passive}$, $\tilde{F}_{active}$, and $\tilde{F}_{active}^{vel}$ are the force multipliers obtained from the muscle force-length and force-velocity curves as functions of normalized fiber length and normalized fiber velocity. A description of these anatomical and biomechanical properties follows.

1.6.1.1 Optimal Fiber Length

Optimum fiber length is the muscle fiber length at which the maximum isometric force is produced. Based on cross-bridge theory on muscle force production mechanism, this happens when the sarcomere length is at its optimum point, which is considered to be the middle point of the plateau in the active force-length curve (Figure 1-14a). For humans, the optimum sarcomere length is assumed to be between 2.7 μm [114] to 2.8 μm [115]; we used 2.8 μm throughout this manuscript.

Currently, most anatomical muscle parameters of the human body, particularly those used in musculoskeletal models, are measured in cadavers. Therefore, optimum fiber length is not measured experimentally, but calculated based on muscle current fiber length and its corresponding sarcomere length. With the optimum sarcomere length equal to 2.8 μm, the optimum fiber length is computed as:

$$l_o^F = l^F \times \frac{l_o^S}{l^S} = l^F \times \frac{2.8\,\mu m}{l^S} \tag{1-2}$$

Therefore, note that for using the force-length and force-velocity curves appropriately, one needs to know the sarcomere length corresponding to the fiber length measured for a muscle [116]. Otherwise, optimum fiber length cannot be calculated, and consequently the force-length and force-velocity curves cannot be used for calculation of Hill-type muscle forces.

Experimentally, the length of a muscle fiber can be measured using a caliper (or ruler). Measurement of its corresponding sarcomere length, however, requires special tools or techniques. Sarcomere length manifests a range between ~1.5 μm to ~5μm for human muscles. For measurement in such scale, either a microscope should be used or more commonly the laser diffraction technique is employed [115][117][118].

In this method, a laser beam is used to transilluminate a fixated muscle sample. Light interference occurs when the beam passes through the striated pattern of the muscle and results in a diffraction pattern consisting of light and dark points on the projected plane (Figure 1-16). Knowing the wavelength of the laser beam (e.g. $\lambda = 660\,nm$), in addition to the distance between the center light dot and the first light dot next to it (Y), and the distance from the muscle sample to the plane (L), the length of the sarcomere (d) can be obtained as:

$$d = \frac{\lambda\sqrt{Y^2 + L^2}}{Y} \tag{1-3}$$

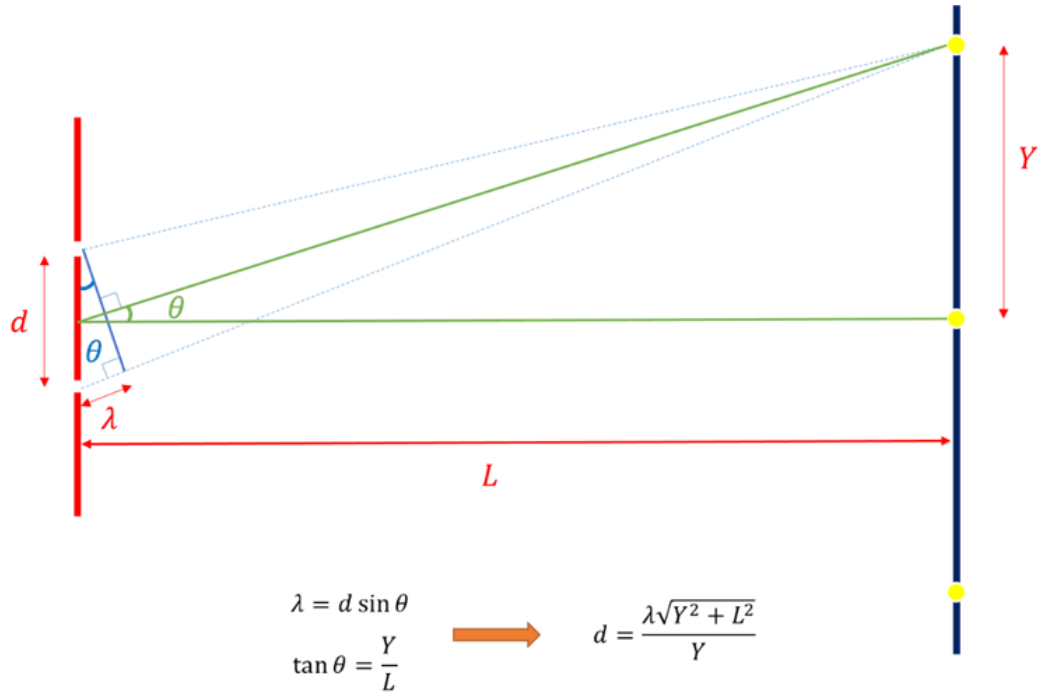

Figure 1-16. Measurement of sarcomere length using laser diffraction technique. When a coherent beam hits a myofibril, consisting of in-series sarcomeres (denoted here by vertical red line segments), the beam passes through the slits/gaps between the sarcomeres and thus, light interference (dotted blue lines) occurs which results in a diffraction pattern consisting of light (yellow dots) and dark points on the projected plane. By knowing the laser wavelength, λ, and measuring the dimensions indicated here, one can measure the sarcomere length, d, using the formula above.

1.6.1.2 Specific Tension

The maximum isometric force per unit area a muscle can generate actively is defined as its specific tension. Based on cross-bridge theory for muscle force production mechanism, this force takes place when its sarcomere is at its optimum length, which is within the plateau of the force-length curve.

Experimentally, this parameter is measured using fresh muscle samples. A single muscle fiber can be extracted from a fresh biopsy and placed in a physiological solution bath, where it is mounted on two fixed colinear pins and secured to them by suture loops. A microscope or laser diffraction technique can be used to ensure the sarcomeres of the fiber are at their optimum

length by adjusting the position of one of the pins. By saturating the concentration of calcium ions in the bath and having a uniaxial force transducer attached to one of the pins, the maximum isometric force of the fiber can be measured. Dividing that force by the cross-sectional area of the fiber gives us the specific tension. The same concept can be applied at the bundle, fascicle, or whole muscle levels to obtain the specific tension. Theoretically, those measurements should all result in similar values. The average specific tensions measured experimentally through this manner ranges between ~10 to ~40 N/cm^2 for human muscles [119][120]. This parameter, however, has never been measured for human paraspinal muscles to date.

1.6.1.3 Pennation Angle

The fibers in a muscle-tendon unit are not necessarily all along its line of action, rather in some muscles they insert onto the tendon at a certain angle (Figure 1-15). The angle between muscle fibers and the line of action of the muscle-tendon unit is called the pennation angle (α). This angle decomposes the force a muscle produces into two components, one component along the line of action, and the other component perpendicular to that. Equation (1-1) provides the effective component along the line of action, while the other component in Hill-type muscle-tendon model is deemed to compress the tendon against the muscle belly and cancels out by muscle incompressibility. In the Hill-type model, the assumption of muscle incompressibility dictates that the muscle fiber length times the sine of the pennation angle at any state remains constant (Figure 1-15).

1.6.1.4 Physiological Cross-Sectional Area (PCSA)

Physiological cross-sectional area (PCSA) of a muscle is an important anatomical property for calculation of muscle force. This property is defined to reflect the sum of cross-sectional areas of

all fibers in a muscle when they are at their optimum lengths. This definition allows calculation of the maximum active force of a muscle simply by multiplying its PCSA by the specific tension. If the muscle is pennated, the muscle maximum active force along its line of action would be a product of PCSA, specific tension, and the cosine of the pennation angle (equation (1-1)).

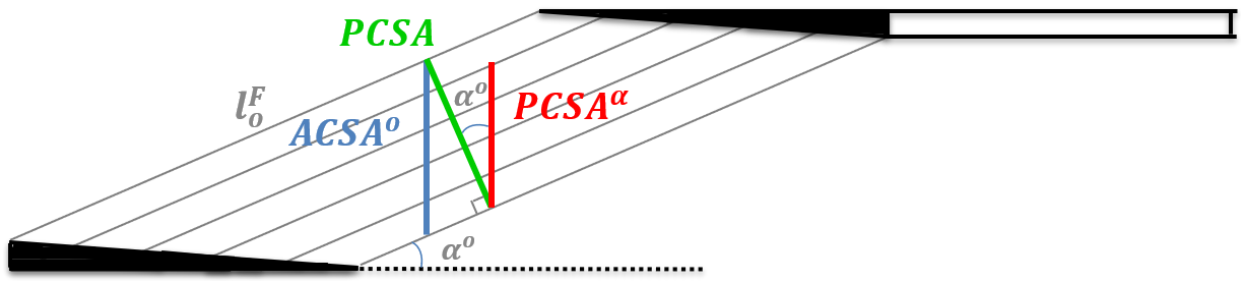

Figure 1-17. Illustration of $PCSA$, $PCSA^\alpha$, and $ACSA^o$ on a muscle-tendon unit.

To calculate PCSA, the volume of a muscle can be measured by immersing it into a volumetric cylinder [28] or by dividing its mass by the density of muscle, known to be 1.056 kg/m^3, through the following formula:

$$PCSA = \frac{M}{\rho \times l_o^F} \tag{1-4}$$

where M is the muscle mass, ρ is its density, and l_o^F is the fiber optimum length. Note that all parameters on the right-hand side of equation (1-4) are constant for any individual muscle. Therefore, PCSA is a constant for any muscle, independent of its position.

While some studies used the PCSA definition presented above [115][28][121], some other studies [122][116][52] adopted an alternative definition as:

$$PCSA^{\alpha} = \frac{M \times \cos \alpha^{o}}{\rho \times l_{o}^{F}} \tag{1-5}$$

where $\alpha^{o}$is the pennation angle of the muscle when its fibers are at their optimum lengths. The superscript α in $PCSA^{\alpha}$ is used to differentiate between the two definitions by referring to the usage of pennation angle in the formula of the latter (Figure 1-1). In this manuscript, the first definition of $PCSA$ is preferred. The reason is that for calculation of muscle force in equation (1-1), $\cos \alpha$ changes with the muscle fiber length. It is noteworthy that $PCSA^{\alpha}$ is equal to $PCSA$ times $\cos \alpha^{o}$; thus $PCSA^{\alpha}$ is also a constant.

The optimum pennation angle terminology is not commonly used, but in the author's opinion is necessary to avoid confusion. In fact, many studies have measured the surface pennation angle of a muscle which was not necessarily at its optimum fiber length and used that value for calculation of $PCSA^{\alpha}$ in equation (1-5) [115][28]. This can result in incorrect values as when the fiber length changes, its pennation angle also changes [123]. Therefore, depending on at what fiber length a muscle is fixed in a cadaver, its pennation angle may vary and be different than the optimum pennation angle.

Advances in medical imaging have provided a great opportunity for measurement of muscle cross-sectional areas in a live human body. Care should be taken, however, when transforming those measurements into PCSA. Some studies have measured the cross-sectional area perpendicular to the line of action of the muscle, which can be named anatomical cross-sectional area (ACSA). One cannot simultaneously measure the pennation angle and calculate PCSA by multiplying the ACSA by the sine of that pennation angle. Note that ACSA changes with changes in muscle fiber length. Therefore, only $ACSA°$, which is the ACSA measured when the

muscle is at its optimum fiber length, can be converted to PCSA through multiplication by $\cos \alpha^o$ (Figure 1-17). Calculation of the optimum fiber length requires knowledge of the muscle fiber length and its corresponding sarcomere length. Therefore, only imaging studies that have measured those two lengths in the same muscle position as its ACSA was measured can provide a valid estimation of PCSA.

1.6.1.5 Passive Curve Scaling Factor

In equation (1-1), K is a scaling factor for the normalized passive force-length curve. It has the same unit and functionality as the specific tension has for scaling the normalized active force-length curve. In Figure 1-14, active forces measured experimentally for different lengths are normalized by the maximum isometric force. To present both active and passive curves in one plot, one may choose to normalize the passive forces measured experimentally for different lengths by the maximum isometric force. In that case the value of K value is equal to ST.

Experimentally, passive behaviour of a muscle is tested using fresh muscle samples. Similar to the method described for active testing, a single muscle fiber can be extracted and mounted on two collinear pins in a physiological relaxing solution bath. One of the pins is connected to a uniaxial force transducer, while the other pin is attached to a length controller. Starting from a slack length, one can stretch the muscle fiber by certain increments and read the force data at the end of each increment after ~2 to ~4 minutes of relaxation time. Using a microscope or laser diffraction technique the sarcomere lengths can be measured at the end of each increment. By dividing the measured forces by the cross-sectional area of the muscle fiber, passive stresses at different sarcomere lengths are obtained. One can normalize the stresses by dividing them by an arbitrary K values; or by $K = ST$ to present it side-by-side the normalized active force-length

curve. Following the same concept, the passive behaviour of a fiber bundle, a fascicle, or whole muscle can be tested.

As discussed in section 1.5.5, in contrast to specific tension, the passive elastic modulus of a muscle increases nonlinearly from smaller to larger ones. Therefore, for passive muscle behaviour, testing at the whole muscle level is ideal. Nonetheless, such measurement is technically challenging for paraspinal muscles and has never been conducted in any species to date. In that case, one may measure muscle constituents at the whole muscle level and indirectly estimate the stiffness using the existing correlations in the literature [55][108].

1.6.2 Approaches for Determining Muscle Forces

1.6.2.1 Forward-Dynamics versus Inverse-Dynamics

With the Hill-type muscle-tendon model, a musculoskeletal model turns into a typical mechanical system comprised of several masses connected through various joints, springs, dampers, and actuators. The equilibrium equations for such a system can be formed as functions of muscle activations and two other state variables including position and velocity of the generalized coordinates corresponding to the degrees of freedom of the system [27]. With known boundary conditions and external forces including the gravity force, the equilibrium equations of the system are complete and ready to be solved.

To solve the equilibrium equations of the system, two approaches could be adopted. When muscle activations are treated as known inputs into the equilibrium equations to solve for the generalized coordinates of the system, the approach is called forward-dynamics. The alternative is to have generalized coordinates as known inputs to the system of equations to solve for muscle

forces and consequently muscle activations. This method is known as inverse-dynamics approach.

To simulate a certain activity using a forward-dynamics approach, muscles' activation level can be measured for that activity through electromyography (EMG). By feeding the measured activation levels as input to the model, body positions, muscle forces and consequently joint loads can be determined. Alternatively, inverse-dynamics approach may be adopted using experimental kinematics data captured for that activity in a gait lab as input to the model. By two times derivation of input kinematic data with respect to time, accelerations of body segments are obtained and used in equilibrium equations to solve for the joint torques. Joint torques are then distributed among the muscles crossing that joint, through which muscle forces and consequently joint loads can be determined. A limitation of this approach is the sensitivity of the calculated joint torques to the input kinematics, especially since it involves double differentiation of such data. Forward-dynamics approach is also limited when it relies on EMG data, as EMG from all muscles involved in an activity is not always feasible, particularly where compact and dense presence of motoneurons requires multiple needles, leading to crosstalk issues. Either of these two approaches could be utilized depending on the availability of the input data and the type of the problem to be solved [124].

1.6.2.2 Addressing Muscle Redundancy

For most musculoskeletal models, the number of muscles crossing a joint is more than the degrees of freedom of the system. Therefore, the system is indeterminate, meaning that different sets of muscle forces (or equivalently muscle activation levels) can result in the same joint torques and kinematics. Regardless of the utilized approaches, i.e. forward dynamics or inverse

dynamics, optimization is required to find a unique set of muscle forces (or equivalently muscle activation levels) for a simulated activity.

In an optimization problem, a cost function is defined and the unique set of variables that minimize that cost function and meet the optimization constraints is sought. For addressing muscle redundancy in musculoskeletal models, a variety of optimization cost functions have been introduced throughout the literature [124]. These cost functions can be classified into three sub-groups: kinematics-based, neuromuscular performance, and bone/joint loading cost functions [125]. Examples of kinematics-based cost functions include trajectory tracking error [126], jerk [127], negative of maximum height a model can jump [128] or negative of maximum velocity a model can reach [129] (negative is required, as cost functions are defined to be minimized). Sums of different powers of muscle forces, muscle activations, muscle stresses, and muscle energy consumption are examples of neuromuscular performance cost functions [130][131][132][133]. Sum of joint forces [130], negative of maximum joint moments [132], or negative of maximum producible force by a limb along a certain direction have been used as joint/bone loading criteria [134]. Although an optimization problem can only have one cost function, it can be a weighted summation of many sub-cost functions.

Depending on the type of simulation activity and the research question, static or dynamic optimization may be used. In addition to static activities, dynamics activities can also be simulated using static optimization. In this technique, complete optimization problem is solved independently for each instant of time before moving to the next time step in solution. Most musculoskeletal models for gait analysis use static optimization. However, to simulate an activity like the maximum height a model can jump, especially when no gait kinematics is available, a dynamic optimization is adopted. In this technique, the optimization problem is solved once and

that is for the entire cycle of movement. For activities where both static and dynamic optimization could be applied, similar results for muscle and joint forces were achieved [135]. Therefore, wherever possible, static optimization is used due to its much faster solution than dynamic optimization [126].

An exemplar static optimization approach is the forward-dynamics assisted data tracking [124][136]. In this method, the gait kinematics are used but not as input to the equilibrium equations of the system (as is the case for inverse dynamics), rather as reference trajectories in the optimization cost function. For each instant of time, the best set of values for muscle activation levels are sought through optimization, so when fed to the forward dynamics solver, they produce the closest kinematics to the reference trajectories [137]. In contrast to inverse dynamics approach that requires segmental kinematics of all rigid bodies of the system as input, in this approach the reference trajectory of a single target point in the entire model is sufficient although the trajectories of as many target points/bodies as desired could be assigned to the solver. In comparison to inverse dynamics, the predictions of this approach are less sensitive to input kinematics [124].

1.6.3 Musculoskeletal Models of the Lumbar Spine

Since the first application of finite element method (FEM) to the spine by Belytschko et al. [138], more than four decades have passed, through which computational modeling of the lumbar spine has evolved tremendously providing invaluable insight into spine biomechanics [139][140][141]. In 1980s, several musculoskeletal models of the lumbar spine were introduced by Schultz et al. [142], McGill & Norman [143], and Bean et al. [144] highlighting the importance of paraspinal muscles on spinal loading. Since then considerable efforts were

devoted by Macintosh and Bogduk [145][146][147][28][121] amongst others to provide quantitative fascicular anatomy of the paraspinal muscles. More detailed musculoskeletal models [148][149][26] revealed that even a slight change in muscles' line of action (between 5° to 15°) can result in large variations (greater than 100 N) in spinal forces [26]. Therefore, musculoskeletal models of the lumbar spine moved toward incorporation of more anatomical data, thanks to further quantitative anatomical studies [150][115]. Although other forms of muscle models have been used [51], most models of the lumbar spine have used the Hill-type muscle-tendon model. Physiologically detailed models of the lumbar spine require knowledge of sarcomere lengths of all muscles in the model to use force-length curves appropriately. This has become possible recently [151][152][153] with the recent anatomic and experimental studies [154][155][114][156].

An important aspect of musculoskeletal models is their methodology in determining the muscle forces. Based on that methodology, musculoskeletal models of the lumbar spine can be categorized as EMG-driven [143][157][158], optimization-driven [159][160][151], or driven by EMG-assisted optimization (EMGAO) [161][162]. The superiority of EMG-driven models is their ability to include activations of both agonist and antagonist muscles, although they are limited in satisfying moment equilibrium at all vertebral joints [158]. On the other hand, optimization-driven models are typically not able to predict muscle co-activations [163][164]. EMGAO, combines these two methods to benefit from their advantages [161]. When comparing the results of these three techniques for simulation of a flexion/extension task, Cholewicki et al. [158] found significantly different muscle activation pattern predicted by the optimization-driven model as opposed to EMG-driven and EMGAO. The compressive joint loads, however, were only lower by 32% in extension and 43% in flexion in the optimization-driven model. A recent

study compared two optimization-based models to an EMGAO model for simulating the spinal loads during walking with backpack loads. They observed slight differences in maximum joint loads (less than 19%) and joint force profiles (root-mean-square of less than 25%) [165]. Given the complexity of collecting and processing EMG data for EMGAO, most recent models suffice to the optimization technique alone[165].

With the advent of multi-body-dynamics based software packages specialized for musculoskeletal modeling including OpenSim [166], AnyBody [167], and ArtiSynth [168] a variety of models of the spine has evolved. These software packages provide a convenient framework for sharing models between groups all over the world, which has had an enormous contribution to fast improvement of the models being built on top of each other.

Using AnyBody, de Zee et al. [160] pioneered in making a lumbar spine model with 154 muscle fascicles. By enhancing that model through adding non-linear intervertebral joint stiffness, short-segmental muscles, and considering the effect of intra abdominal pressure, Han et al. [169] validated that model by comparing the predicted spinal forces by their model normalized to upright standing against the similar normalized loads measured in vivo by Rohlmann et al. [170] and Wilke et al.'s [171]. Christophy et al. [151] developed the first OpenSim lumbar spine model, similar to the de Zee et al. AnyBody model. The advantage of Christophy et al.'s model was inclusion of muscle force-length and force-velocity curves along with the required biomechanical muscle properties for the Hill-type modeling of all 238 muscle fascicles used in their model.

By combining Christophy et al.'s model with the neck [172] and upper extremity models [173], Bruno et al. [153] built their fully articulated thoracolumbar spine model using OpenSim and

validated the spinal forces predicted by their model for several static activities against the experimental data in the literature [169][142][174]. Similarly, Ignasiak et al. [175] enhanced de Zee et al.'s model and built the first AnyBody articulated thoracolumbar spine model. Various lumbar, thoracolumbar, or even full body models have been introduced since then for studying jogging biomechanics [176], sit-to-stand [177], lifting activities [178], or simulating children's spine [179].

Musculoskeletal models of the spine have been used to address a variety of clinical questions including the dependence of spinal loads on disc degeneration [180], spine posture [181][182], aging and sarcopenia [183], post-surgical muscle damage [184][185], efficacy of braced arm-to-thigh lifting technique [186], asymmetric load handling [187][188], obesity [189], and flexion-relaxion phenomenon [190].

Recently, a few studies have focused on modeling spinal deformity patients [191]. Subject-specific models have been developed from patients' radiographs [192][193] and used for assessment of spinal compressive forces in adolescent scoliosis patients [194][195][196]. The effect of different bony geometries such as spinopelvic parameters have been studied on post-surgical alignment [197] and lumbar spinal loads [198][199], but the influence of muscle biomechanical properties other than PCSA has not yet been investigated.

In fact, only a relatively few optimization-based spine models have included both active and passive force-length curves and the biomechanical parameters associated with them in their solution methods. Currently, spine models developed using OpenSim and ArtiSynth include those parameters and use them appropriately in their solution method. Even in those models, no study to date has explored the effect of muscle properties such as sarcomere length, specific

tension, passive stiffness, or slack sarcomere length on spinal forces; therefore, their significance on spinal loads remains unknown.

1.6.4 UBC Musculoskeletal Model of The Thoracolumbar Spine

In a previous study in our research group at UBC, a musculoskeletal model of the thoracolumbar spine was created using ArtiSynth, an open source biomechanical modeling software toolkit [27]. The main superiority of ArtiSynth over its peers such has OpenSim or AnyBody is its ability in combining FEM and Multibody dynamics in one model and solving them in a convenient fashion. The vertebral and muscular geometries in our model were based on Christophy et al's model and included the entire spine and rib cage, with the lumbar vertebrae being mobile, and 210 muscle fascicles. Muscle properties required for a full Hill-type musculotendon model were incorporated. This included tendon ratios and pennation angles along with muscle force-length and force-velocity curves. The nonlinear stiffness of the functional spinal units was represented by special six-dimensional springs connecting the adjacent vertebrae. These springs generated restoring forces and moments by relative displacements and rotations between two adjacent vertebrae and applied them equally but in opposite directions at the centers of the two vertebrae. The effect of intra-abdominal pressure was simulated as an upward force applied to the thorax. Forward-dynamics-assisted data tracking was adopted for prediction of muscle forces [200][201]. The solution method was validated by contrasting the estimated spinal forces against the results of two in vivo studies in the literature [171][26].

The model predicted the ratios of axial forces at L4-L5 as measured in vivo intradiscal pressures for three activities of standing erect, holding a weight of 190N close, and far from the chest (i.e. 25 and 55 cm anterior to the L5-S1 disc, respectively)[152]. Using that model, we investigated

the effect of iatrogenic muscle damage on spinal loads, which is common in open fusion surgeries, and found that surprisingly, damaging the muscles increased the loads at the levels adjacent to a spinal fusion, more substantially at the rostral level [185].

The solution method for estimation of muscle forces was based on tracking the trajectories of a set of target points. Due to the high axial stiffness of the spine, the solution method was very sensitive to input kinematics, for which submillimeter kinematic accuracy was required. Such accuracy, however, is very challenging to obtain for the lumbar spine and therefore, limited our studies to only a static case of upright standing. This limitation needed to be addressed by modifying the solution method to only track the angular motion of the targets, so as to enhance the validation of the model to postures other than standing and to use the model for investigating the influence of muscle biomechanical properties on spinal loading.

1.7 Objectives

While decreased back extensor strength of adult spinal deformity patients could arise from smaller cross-sectional area of their paraspinal muscles, there are other muscle biomechanical properties that could be also responsible but their role remains unclear. These parameters include in situ sarcomere length at a certain posture, passive elastic modulus, and slack sarcomere length. Musculoskeletal models could provide insight into identifying the significance of these muscle properties and their role in progression of spinal deformity. The results of musculoskeletal models, however, rely on their input material properties, and therefore, it is important to provide correct and physiological input data for them. No study to date has investigated these properties for human paraspinal muscles in adult spinal deformity patients, likely due to the technical and ethical challenges associated with obtaining the muscle biopsies from these patients.

Furthermore, due to the paucity of experimental data in the literature, musculoskeletal models make assumptions that may not be valid. For example, it is assumed that biomechanical properties of paraspinal muscles are similar between different vertebral levels; but this has never been demonstrated experimentally. Additionally, for testing mechanical properties of paraspinal muscles, the size of muscle fiber bundles tested throughout the literature has a wide variation (form ~3 to ~30 fibers). Whether this size variation influences the obtained elastic modulus is unknown. Addressing these foundational questions are necessary for better representation of muscles in musculoskeletal models and using their predictions for understanding etiology of spinal conditions, specifically adult spinal deformity. My PhD project was defined to address these questions through the following chapter-specific objectives:

1- To investigate the effect of vertebral level on the biomechanical properties of paraspinal muscles in a rat model. The primary objective was to explore whether tangent modulus and slack sarcomere length of a fiber or a fiber bundle in multifidus or longissimus depend on the vertebral level. The secondary objective was to examine the collagen content of muscle fascicles at different vertebral levels.

2- To explore whether the size of a single muscle fiber or a bundle of muscle fibers has an influence on its measured elastic modulus and to examine whether the assumption of a circular shape for the cross section of a muscle fiber or a bundle of fibers is valid.

3- To develop protocols to acquire biopsies of human multifidus and longissimus from adult deformity patients, and to evaluate them biomechanically and histopathologically.

4- To explore changes in spinal loading due to variation in the paraspinal muscle parameters, specifically slack sarcomere length, passive stiffness, in situ sarcomere length, specific tension, and pennation angle.

The overall goal of this research project was to investigate if biomechanical properties of the paraspinal muscles are different in adult spinal deformity patients; and whether those differences could influence spinal loading and be associated with initiation/progression of adult spinal deformity.

The results of this line of research in the long term will provide insight into the significance of muscle functional properties in the development of spinal disorders and may suggest shifting the focus of future treatments toward muscle-preserving strategies, pharmaceutical approaches such as botulinum toxin injections, or advent of muscle remodeling techniques to prevent progression of such spinal conditions.

The following sections of the thesis consist of four manuscripts (chapters 2 to 5), which address the specific objectives listed above, followed by an integrated discussion (chapter 6).

Chapter 2 The Effect of Vertebral Level on Biomechanical Properties of the Lumbar Paraspinal Muscles in a Rat Model

Passive mechanical properties of the paraspinal muscles are important to the biomechanical functioning of the spine. In most computational models, the same biomechanical properties (including passive properties) are assumed for each paraspinal muscle group, while cross-sectional area or fatty infiltration in these muscles have been reported to differ between the vertebral levels. The study presented in this chapter explored validity of this assumption and investigated the effect of vertebral level on the biomechanical properties of paraspinal muscles. As direct measurement of paraspinal muscle passive properties was not feasible in healthy humans, this study was conducted in a rat model. The results of this study inform whether measurement of biomechanical properties at one vertebral level suffices or measurements at multiple vertebral levels are necessary for more accurate representation of the paraspinal muscles in a normal musculoskeletal model of the spine.

2.1 Introduction

Paraspinal muscles play a major role in maintaining the health and functionality of the spine [16][51]. Studies on the etiology of a variety of spinal disorders including spinal deformity [7][45], adjacent segment disease [202][185] and low back pain [203][204][205][206] have reported dysfunction of paraspinal muscles as a major risk factor. There are a number of muscle parameters that can be responsible for paraspinal muscle dysfunction as having direct influence on muscle force generation capacity. These parameters include physiological cross-sectional area, muscle fiber length, sarcomere length, specific tension, and passive tangent modulus [52].

Musculoskeletal models incorporate these muscle parameters along with the osteoligamentous structure together in one platform to investigate a variety of clinical problems [207][208][185][183][209]. These muscle parameters have an important effect on the kinematic and kinetic outputs of the musculoskeletal models [210][152][211]. Due to scarcity of data in the literature, almost all models assume similar mechanical properties for a muscle group [159][212][151][153][175].

The assumption of uniform mechanical properties may not be valid for paraspinal muscles due to their complex structure and architecture. Anatomically, in many cases fascicles that belong to the same paraspinal muscle group (e.g. multifidus) have varying insertion (and/or origin) points located on different vertebrae, and therefore have independent functions. For example, one multifidus fascicle only extends between L1-L3 segments while another acts on L3-S1. Even superficial and deep multifidus differ in functionality as suggested by both anatomical and EMG studies such that superficial multifidus is well suited for axial rotation and total lumbar extension while deep multifidus is more involved in controlling intersegmental motion [154][213]. Some studies have reported that muscle parameters such as cross-sectional area (CSA) and fatty infiltration significantly differ between lumbar spinal levels [214][215][216][217]. Those studies, therefore, recommend more than a single-level measurement of muscle properties for more accurate representation of the entire lumbar spine musculature. A recent elastography study explored feasibility of ultrasound shear wave in measurement of human multifidus stiffness and reported larger elasticity at the L4-L5 level than L2-L3 [218]. This body of evidence provokes the question if other mechanical properties of paraspinal muscles differ between the vertebral levels such that to be considered in musculoskeletal modeling.

Passive behavior of muscles, as one of the main contributing factors to muscle force generation and transmission, has been studied extensively throughout the literature, both at cellular (i.e. single fiber) and tissue levels (i.e. bundle of ~10-20 fibers ensheathed in their connective tissue) [93][96][94][86][90][91][92][97]. Tangent modulus of fibers and bundles of fibers in human paraspinal muscles, however, have been only examined in the study by Ward et al. [25] where bundles of fibers showed larger stiffness compared to single fibers and were ~1.5 times stiffer in multifidus than longissimus. However, the biopsies in that study were taken from mixed spinal levels and not contrasted among the studied spinal levels, and they were also from degenerative spine patients undergoing spinal surgery and were not able to be compared to healthy individuals. Studying muscle passive stiffness in healthy individuals presents substantial technical and ethical challenges. Therefore, animal models are required to study tangent modulus of healthy paraspinal muscle.

The tangent modulus of single fibers and fiber bundles of the lumbar paraspinal muscles has been measured in other species including rabbits [219][90], mice [97], and rats [220][102]. To the best of our knowledge no study has explicitly explored the effect of vertebral level on tangent modulus of healthy paraspinal muscles across multiple lumbar spinal levels. Brown et al. [90] measured the stiffness of multifidus at two different spinal levels (L3 and L7), but it was performed only in one muscle group (multifidus) and in a small group of 4 rabbits.

For the purpose of musculoskeletal modeling, knowledge of the tangent modulus at the fascicle level (~300 fibers) or whole muscle is of great interest. However, measurement of those properties, especially for the paraspinal muscles is technically challenging and requires special considerations. In a recent study by Ward et al. [55] collagen content of lower extremity muscles was demonstrated as the strongest predictor of passive function of the whole muscle. Therefore,

to investigate the effect of vertebral level on whole muscle passive properties, one may measure and contrast the collagen content of those muscles between the different vertebral levels.

This study aimed to investigate the effect of vertebral level on the biomechanical properties of paraspinal muscles in a rat model. The primary objective was to explore whether tangent modulus and slack sarcomere length of a fiber or a fiber bundle in multifidus or longissimus depend on the vertebral level. The secondary objective was to examine the collagen content of muscle fascicles at different vertebral levels.

2.2 Materials and Methods

The left paraspinal muscles of 13 male Sprague-Dawley rats (330±14g) were exposed under anesthesia (approved by the University of British Columbia animal care committee, Vancouver, Canada). In total, six muscle biopsies were collected from each rat: three from multifidus (one per each of the L1, L3, and L5 levels) and three from longissimus (one per each of the L1, L3, and L5 levels; Figure 2-1). The biopsies were divided through a transverse cut into two halves: one half was placed in a physiological storage solution for mechanical testing and the other half was immediately frozen for histology analysis.

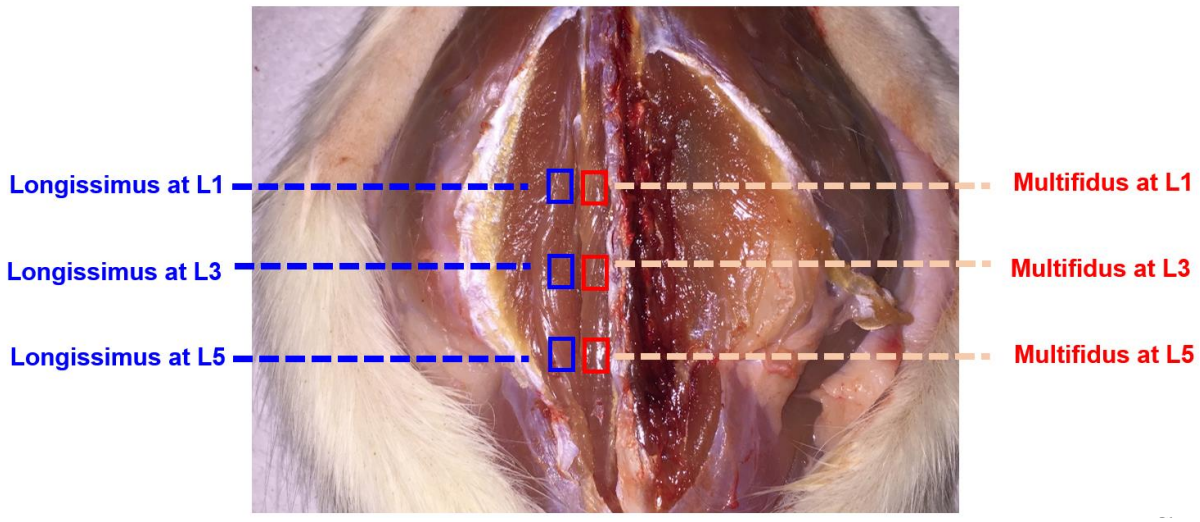

Figure 2-1. Anatomical locations of collected muscle biopsies. From each rat, six muscle biopsies were taken: three multifidus biopsies and three longissimus biopsies at L1, L3, and L5.

2.2.1 Mechanical Testing

The portion of each muscle biopsy for mechanical testing was placed in a physiological storage solution (same as the one used by Zwambag et al. [102]) containing (mmol): KPr (170), Na2ATP (21.2), imidazole (10), MgCl2 (5.3), EGTA (5.0), glutathione (2.5), NaN3 (1), leupeptin (0.05) and 50% (v/v) glycerol. The samples were first incubated at 4 °C for 24 hours and then kept at -20 °C for minimum 24 hours. Samples stored in this way have been reported to remain stable for up to three months [221][222]. All tests in this study were conducted within 21 days. In preparation for testing, samples were transferred to a physiological relaxing solution (same as the one used by Zwambag et al. [102]) containing (mmol): KMSA (86), imidazole (59.4), Mg(MSA)2 (10.8), K3EGTA (5.5), Na2ATP (5.1), KH2PO4 (1.0), and Ca(MSA)2 (0.13) (Shah and Lieber 2003) and were dissected under a stereomicroscope (SteREO Discovery.V8, Zeiss, Plan-Apochromat 0.63x) to extract single fibers and fiber bundles. Extreme care was taken to

preserve the integrity of the extracellular connective tissue matrix during separation of bundles. Therefore, when necessary separating extra fibers from a bundle that could result in loss of bundle integrity was avoided resulting in bundles without a perfect cylindrical shape or certain number of fibers aimed for.

From each biopsy two to three fibers and two to six fiber bundles were extracted. The extracted fiber or fiber bundle was transferred to a solution bath of physiological relaxing solution and mounted on two collinear pins: one pin attached to a force transducer (400A, Aurora Scientific, Aurora, Ontario, Canada) and the other pin connected to a length controller (CRK523PMAP, Oriental Motor, Torrance, CA, USA) (See Figure 2-2 and Appendix D on page 244). A single mode fiber-coupled diode laser (660 nm) with collimated beam diameter of 0.8 mm was used to transilluminate the fibers or fiber bundles. The resulting diffraction pattern was scanned using a photodiode array (1280×1 elements, AMS-TAOS USA Inc) to measure the average sarcomere length of the fibers or fiber bundles (with a resolution of ~10nm). The resolution of the photodiode array was validated using two diffraction gratings of sizes 2 µm (Edmond Optics, Barrington, NJ, USA) and 3.33 µm (Thorlabs, Newton, NJ, USA). The force transducer was validated by hanging standard weights of 10 mg, 100 mg, 1 g, and 2 g (ASTM Class II Standard Weights Troemner, NJ, USA) repeated for 12 trials each with no measurement having more than 6%, 4%, 2%, and 1% errors, respectively.

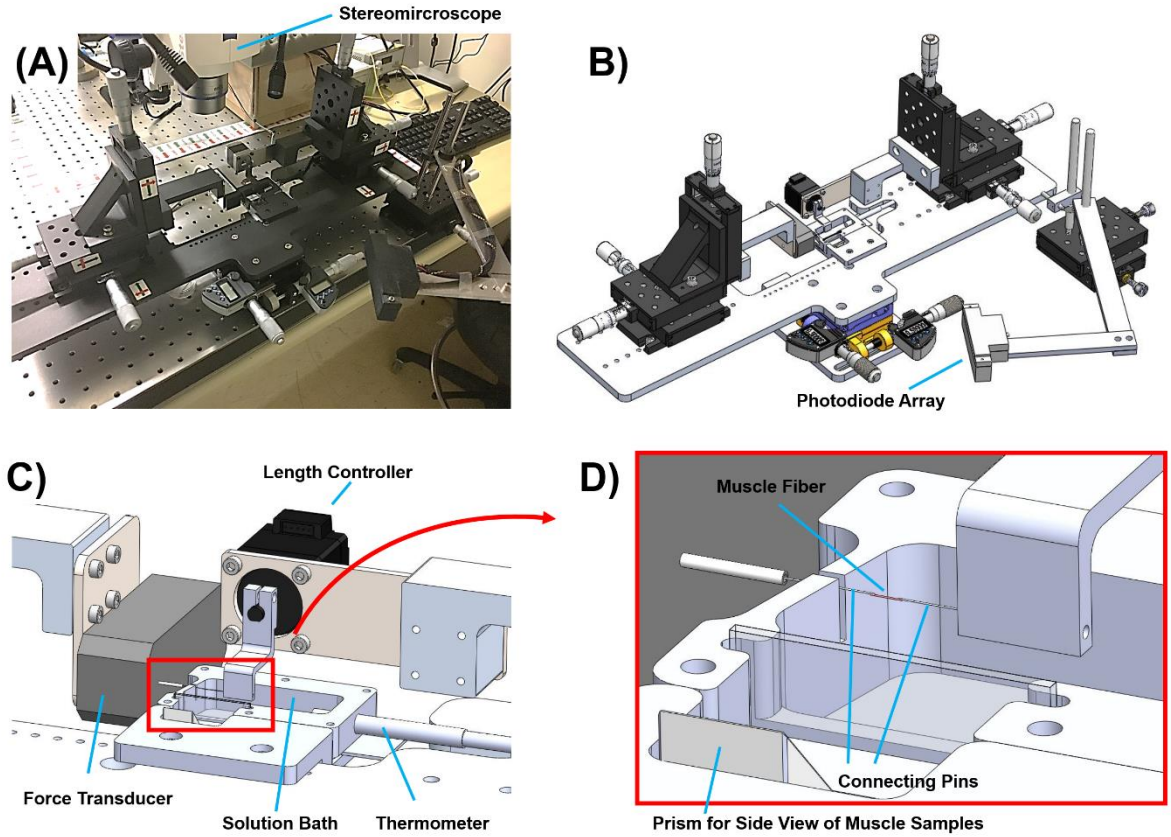

Figure 2-2. The muscle mechanical testing apparatus used for this study (A) and schematics of its components(B-D). For the details of the apparatus refer to Appendix D on page 244.

Each fiber or fiber bundle, after being mounted and secured to the pins of the force transducer and length controller, was stretched manually to reach to its slack sarcomere length. The slack sarcomere length is defined as the sarcomere length after which stretching the fiber or fiber bundle would result in a resisting (passive) force. At slack sarcomere length, using a crosshair reticle inside the eye piece of the stereomicroscope the diameters of each fiber/fiber bundle were measured with resolution of 1 micron at three points across the fiber/fiber bundle length. This measurement was performed from both top and side views (a prism adjacent to the fiber/fiber bundle enabled seeing the side view through the microscope lens). The top and side view diameters were determined as the average of the readings at those three points across the

fiber/fiber bundle length. The cross section of each fiber/fiber bundle was approximated by an ellipse and its area was calculated using the minor and major (i.e. top and side view) diameters.

All tests started from the slack sarcomere length and included four to eight cumulative stretches (i.e. displacement-controlled). Each stretch consisted of 10% strain at a rate of 10% strain per second followed by four minutes relaxation time before the next stretch (Figure 2-3A). At the end of each stretch (i.e. after four minutes) the sarcomere length was measured for calculation of the strain; and the force reading was divided by the CSA calculated at slack length of the fiber/fiber bundle to obtain the engineering stress. An exponential curve was fitted to the resulting stress-strain data for each fiber or fiber bundle and the slope of the tangent at 30% strain was considered as its tangent modulus (Figure 2-3B).

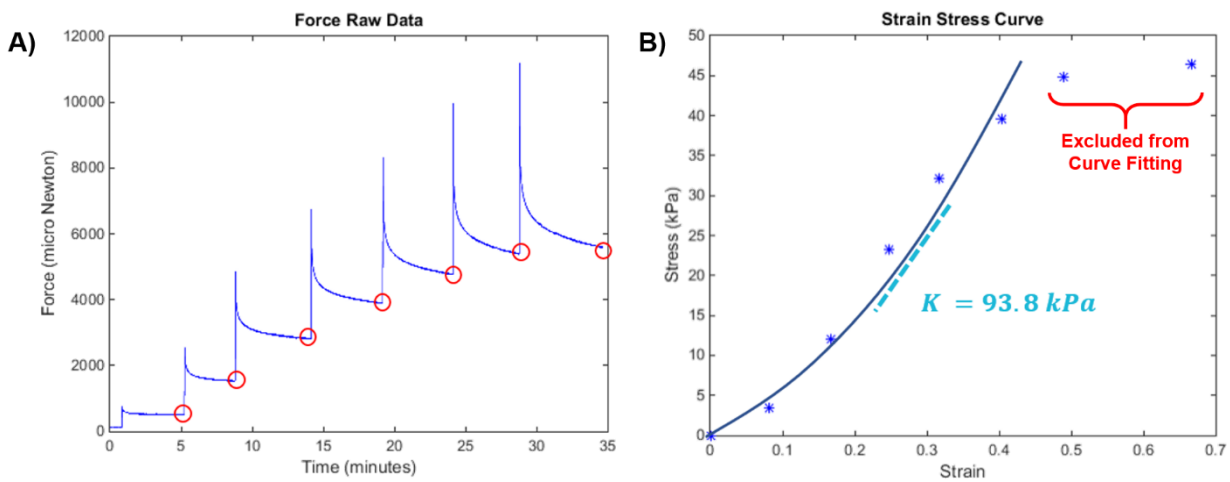

Figure 2-3. Raw data from a sample mechanical test consisting of seven cumulative stretches. All tests consisted of between four and eight cumulative stretches. (A) The force reading at the end of each stretch (i.e. after four minutes relaxation time) (circled in red) was used for calculation of the engineering stress. (B) An exponential curve was fitted to the resulting stress-strain data for each fiber or fiber bundle test and the slope of the tangent at 30% strain was considered as its tangent modulus. The last data points for which a partial rupture or failure was evident were excluded from curve fitting.

2.2.2 Immunohistochemistry

The portion of the muscle biopsy for histological analysis was immediately mounted longitudinally on a cork covered with Tragacanth gel and was frozen in isopentane cooled by liquid nitrogen (all within five minutes after harvest). The frozen samples were stored at -80 °C and later sectioned transversely with a cryostat to 10μm thickness and fixed on two identical slides. The slides were stained for measurement of collagen type I area fraction (as an estimate of the connective tissue) using Mouse IgG against collagen I (Abcam #ab90395 , dilution: 1:100 with Blocking buffer; PBS 0.3% Triton X-100 3% Goat serum) as the primary antibody and Goat against Mouse IgG (Alexa Fluor 488, Thermo Fisher Scientific, Massachusetts, USA dilution 1:200 with Blocking Buffer) as the secondary antibody for Collagen I. Fluorescent images were taken using Zeiss microscope and were analyzed using ImageJ software for measurement of the area fraction (Figure 2-4).

2.2.3 Data Analysis

The fiber tangent modulus and the fiber bundle tangent modulus of each biopsy was represented by the mean tangent modulus of the extracted fibers and fiber bundles from that biopsy, respectively. This led to even samples sizes for each group (e.g. 13 tangent modulus values for multifidus fibers at L1) and normal distribution of all data in this study. One-way repeated measures ANOVAs ($p<0.05$) were used to evaluate the effect of spinal level (as the independent factor) on the tangent modulus values at 30% strain for multifidus fibers, longissimus fibers, multifidus fiber bundles, and longissimus fiber bundles. Furthermore, using one-way repeated measures ANOVAs ($p<0.05$) the effect of spinal level on the mean stresses predicted by the fitted curves at strains of 10%, 20%, 30%, 40%, 50%, 60%, 70%, and 80% was evaluated.

For immunohistochemical analysis at the fascicle level, which was only performed on rats 4-13, the mean of collagen I area fraction measured from the two slides prepared from each biopsy was considered as the representative of that biopsy. Those slides that were not correctly sectioned or too saturated with stains were removed from analysis and therefore due to missing data from them, the linear mixed-models analysis ($p<0.05$) was used to study the effect of spinal level (as the independent factor) on collagen content of multifidus and longissimus muscle fascicles.

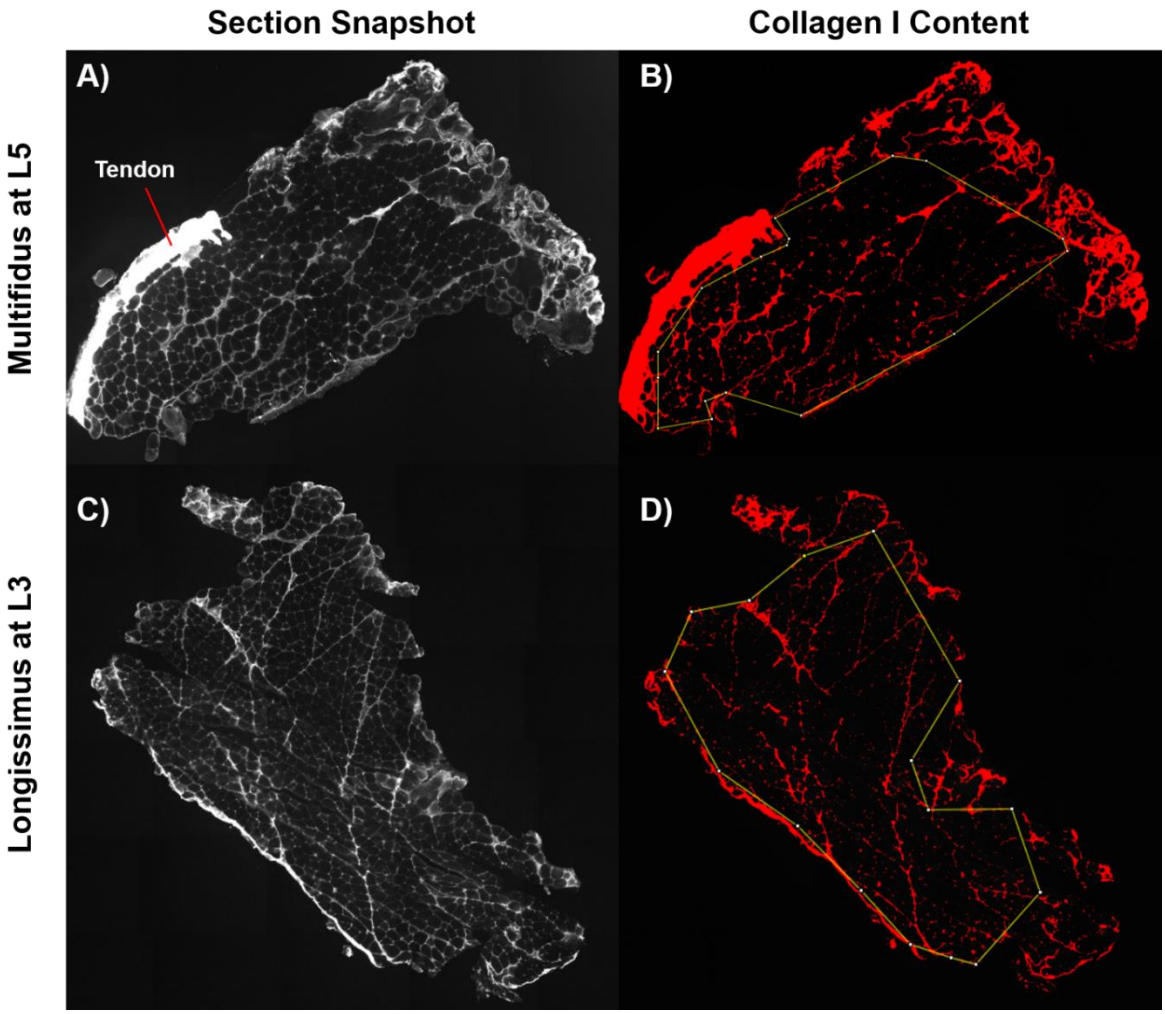

Figure 2-4. Fluorescent Images of stained sections created from a sample biopsy from Multifidus at L5 (A-B) and a sample biopsy from Longissimus at L3 (B-D). For computation of collagen I area fraction, muscle portion of biopsies were segmented using ImageJ software (yellow lines in B and D) such that tendons or low quality parts of the sections (e.g. saturated or folded tissue at the periphery) were excluded. The stained sections contained ~500-1000 fibers.

2.3 Results

2.3.1 Mechanical Testing

In total, 192 fibers and 262 fiber bundles were tested and categorized based on their muscle group and spinal level. Twenty-six outliers were identified and removed from the data set as having values 1.5 times the interquartile range (IQR) above the third quartile of their group (this is equivalent to the data points beyond mean±3std in a normally distributed population, which accounts for only 0.26% of all data). The muscle fiber tangent moduli for multifidus at L1, L3, and L5 spinal levels were 26.4±7.1, 25.1±7.9, and 25.3±8.4 kPa, respectively (mean and standard deviation (SD)), while the corresponding values for longissimus were 27.2±9.6, 20.8±4.9, and 24.1±5.5 kPa (Figure 2-5). The differences in tangent moduli values for fibers among the spinal levels were not statistically significant for multifidus (p=0.92) or longissimus (p=0.22).

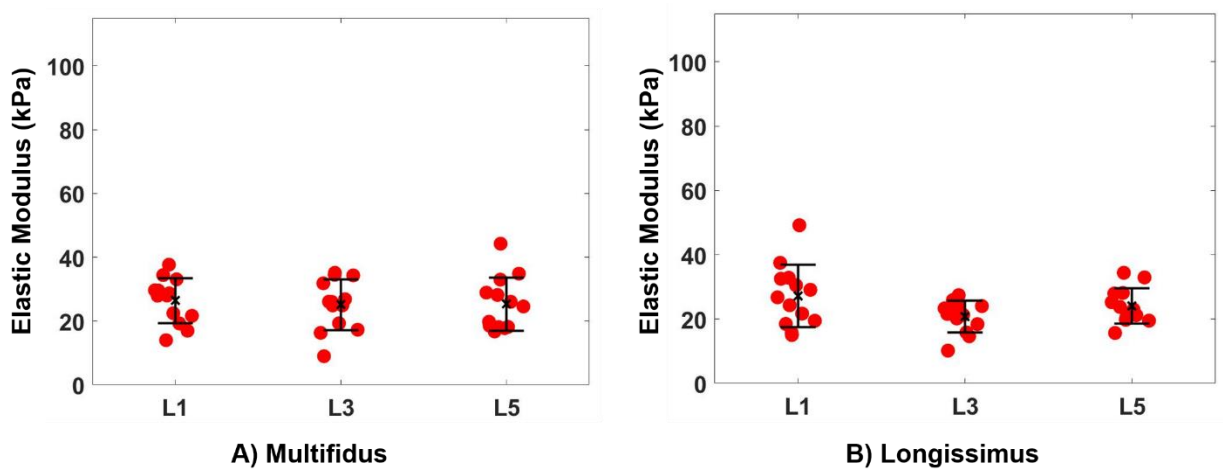

Figure 2-5. Averaged (± SD) tangent modulus of singles fibers at three different spinal levels in (A) Multifidus and (B) Longissimus.

While not statistically tested, fiber bundles exhibited larger tangent moduli compared to single fibers (Figure 2-6). The muscle fiber bundle tangent moduli for multifidus at L1, L3, and L5

were 59.7±25.0, 55.0±19.4, and 42.8±18.9 kPa, respectively (mean and SD), and for longissimus fiber bundles those values were 62.4±25.8, 51.7±24.7, and 51.7±27.6 kPa. In comparison to fibers, fiber bundles showed larger variability in their tangent moduli values for both muscle groups. However, similar to fibers, the differences in tangent modulus values for bundles of fibers among the spinal levels were not statistically significant either for multifidus (p=0.053) or longissimus (p=0.36).

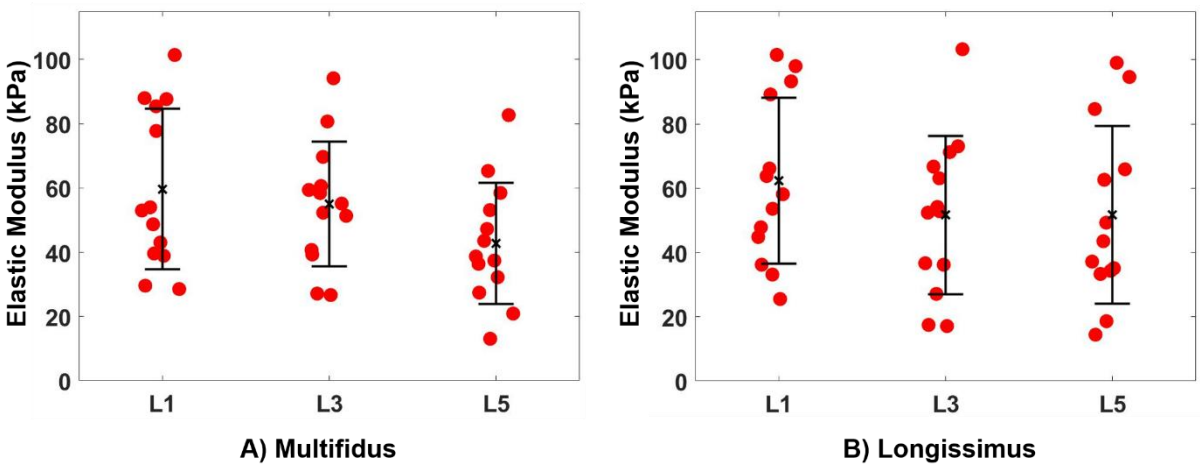

Figure 2-6. Averaged (± SD) tangent modulus of fiber bundles at three different spinal levels in (A) Multifidus and (B) Longissimus.

Furthermore, no significant difference was found between spinal levels when examining the mean stresses at strains from 10% to 80% (Figure 2-7, all p>0.05).

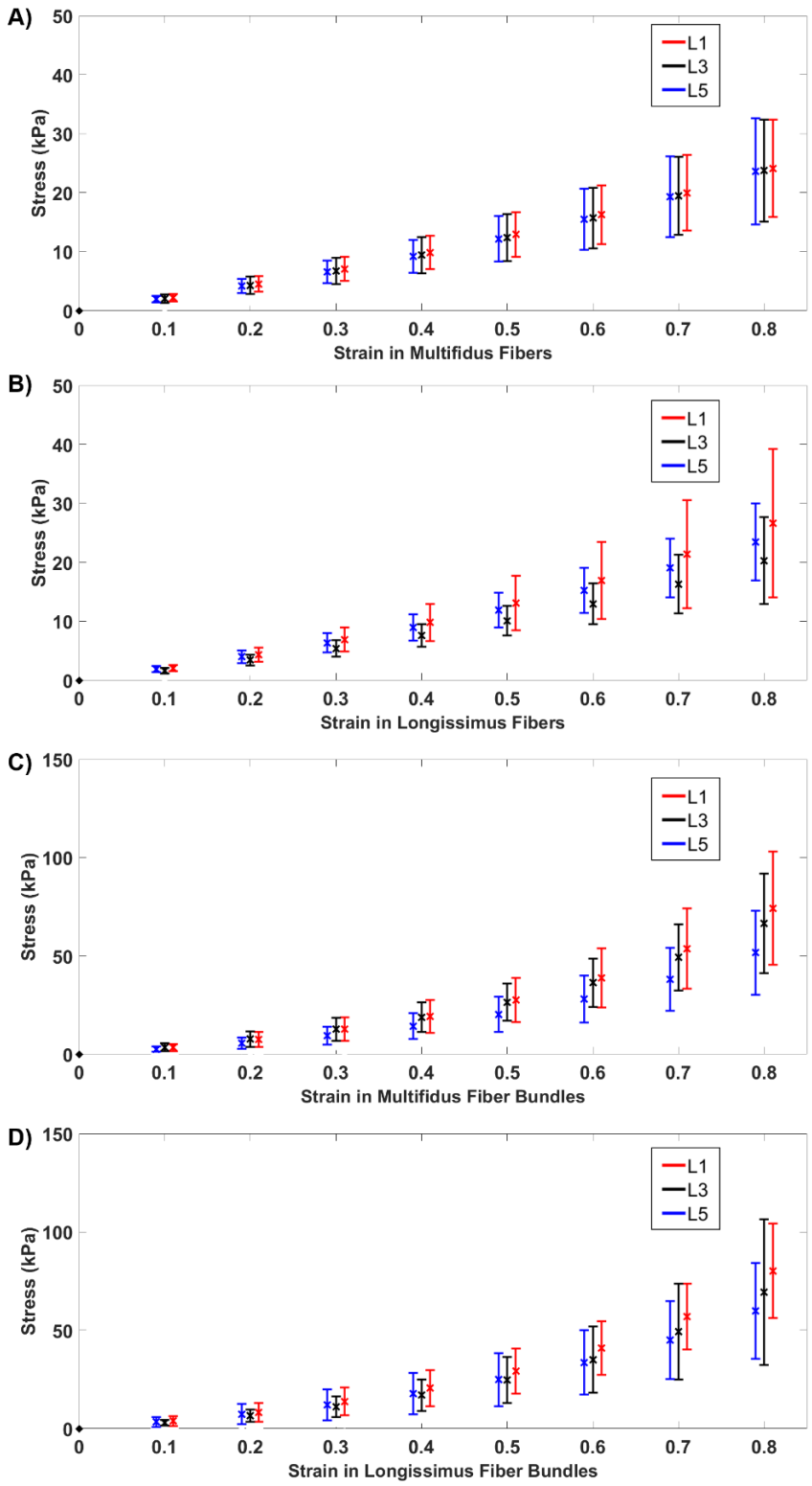

Figure 2-7. Averaged (± SD) stresses precited by the fitted curves for (A) Multifidus fibers, (B) Longissimus fibers, (C) Multifidus fiber bundles, and (D) Longissimus fiber bundles.

The slack sarcomere length was not significantly different between the spinal levels except for multifidus fibers (p = 0. 02 for multifidus and p=0.57 for longissimus fibers; p = 0.57 for multifidus and p=0.33 for longissimus fiber bundles Figure 2-8). The mean±SD slack sarcomere lengths at the L1, L3, and L5 levels were respectively 2.1±0.1, 2.2±0.1, and 2.1±0.1 for multifidus fibers; 2.2±0.2, 2.3±0.2, and 2.3±0.2 for longissimus fibers; 2.1±0.2, 2.1±0.1, and 2.1±0.1 for multifidus fiber bundles; and 2.2±0.2, 2.2±0.1, and 2.2±0.1 for longissimus fiber bundles.

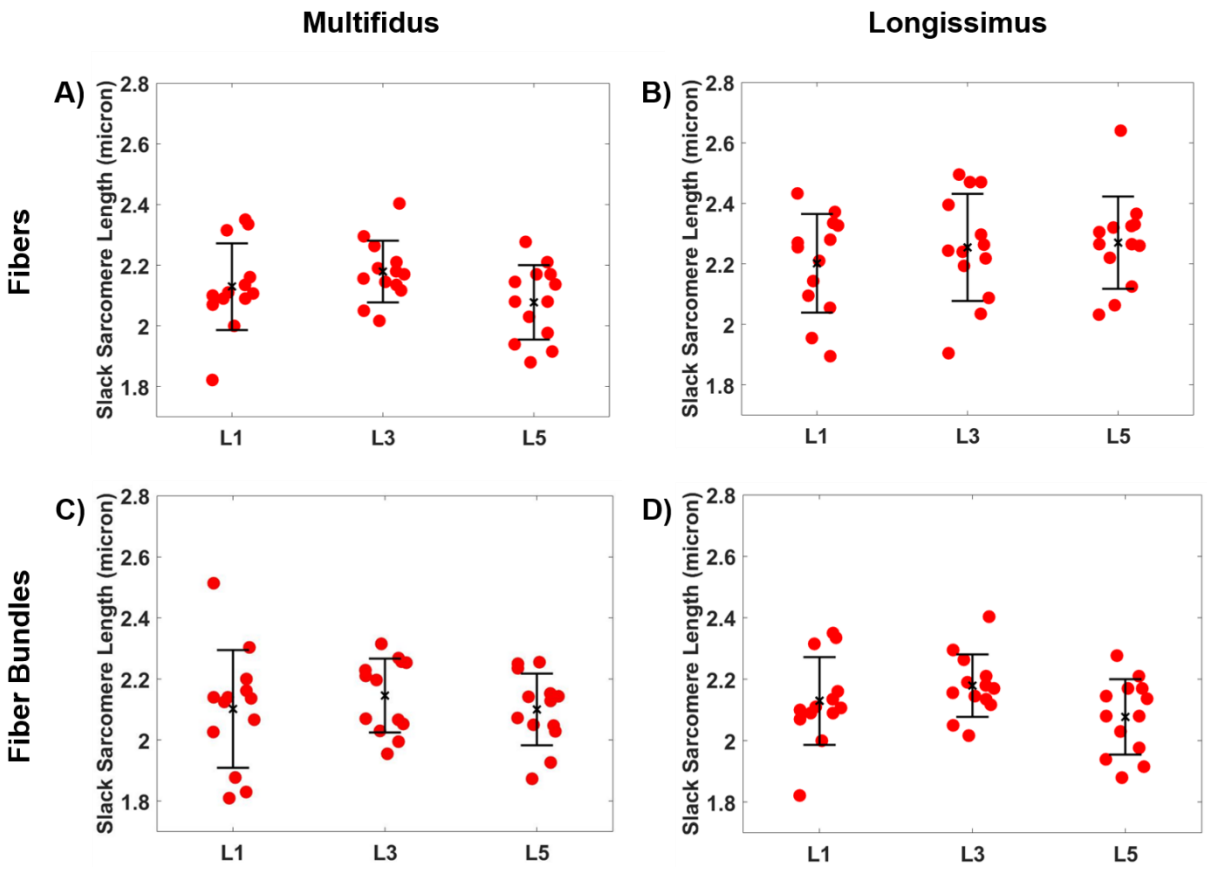

Figure 2-8. Averaged (± SD) slack sarcomere length for (A) Multifidus fibers, (B) Longissimus fibers, (C) Multifidus fiber bundles, and (D) Longissimus fiber bundles.

2.3.2 Immunohistochemistry

Collagen I area fraction revealed no significant difference between the different spinal levels for either muscle type (p=0.26 for Multifidus and p=0.52 for longissimus). Collagen I area fraction measurements for multifidus were 7.5±3.7 (mean±SD) at L1, 5.6±0.7 at L3, and 7.2±4.0 at L5. The corresponding values in longissimus were 6.4±3.5 at L1, 4.6±2.3 at L3, and 4.9±3.8 at L5 (Figure 2-9).

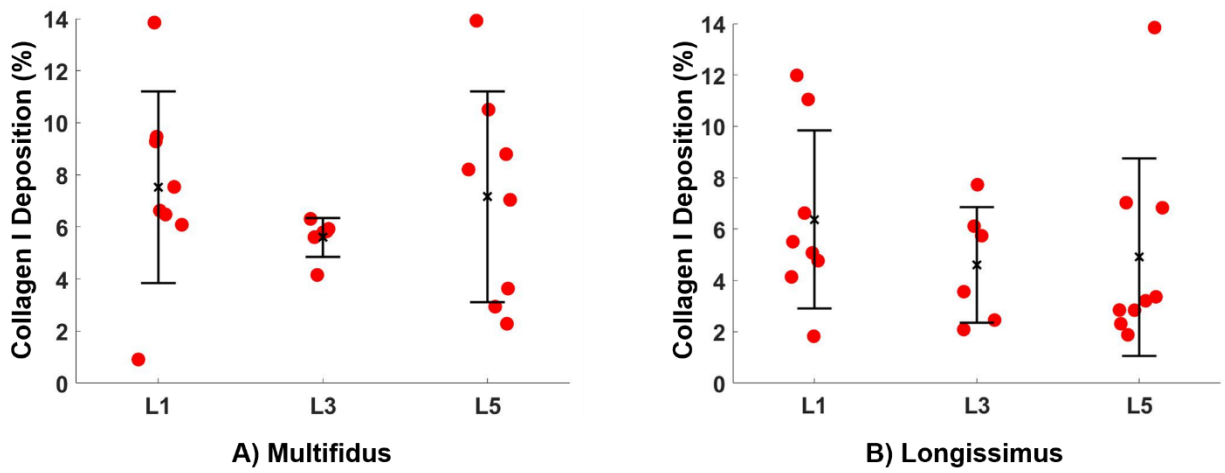

Figure 2-9. Averaged (± SD) collagen I deposition of muscle biopsies taken from three different spinal Levels in (A) Multifidus and (B) Longissimus.

2.4 Discussion

The results of this study highlighted that the tangent modulus, slack sarcomere length, and collagen content of the lumbar paraspinal muscles are independent of spinal level. This finding provides the basis for the assumption of similar mechanical properties for both muscle fibers and fiber bundles along a healthy paraspinal muscle in computational models of the spine. These results are corroborated by the observation of Brown et al. [90] in multifidus of a group of four rabbits, where no effect of spinal level was evident in passive tangent modulus of fibers or bundles of fibers between L3 and L7.

Other muscle properties including the entire muscle CSA and fatty infiltration of paraspinal muscles have shown level dependency in some studies. Studying 80 adults with spinal symptoms, Urrutia et al. [214] found that fat signal fractions increased significantly from L1 to S1 in erector spinae and noted that fatty infiltration and CSA of multifidus were significantly different between all adjacent levels. Similarly, Crawford et al. [216] detected the highest fat infiltration in lower levels of lumbar spine musculature when examining 80 asymptomatic healthy volunteers. These level-dependences have been shown to even differ between ethnicities [215] or groups of different ages [217]. However, no level dependency was observed for the measured biomechanical properties in the current study.

Similar to the study by Brown et al. [91] on rat abdominal muscles and studies in other species [90][102][55], passive behavior of fibers was quite linear in most cases whereas fiber bundles had nonlinear stress strain curves. Nevertheless, there was no difference in slack sarcomere lengths of bundles and single fibers in the current study, while in the study by Brown et al. [91] bundles had shorter slack sarcomere lengths.

Larger tangent modulus in bundles of fibers arise from the extracellular matrix and properties of its constituents [105]. The largest constituents of muscle extracellular matrix are collagen isoforms [106][105], among which fibrillar collagens, specifically type I (~70% of total collagen) and type III, are the most prevalent [107][105][108]. Collagen I is associated with high tensile load-bearing properties [107][109] and is deemed to be a positive predictor of muscle stiffness [108] while collagen III is considered to contribute to tissue-compliance [109][110]. In a recent study by Ward et al. [55] passive stiffness and collagen content at different muscle scales were measured which revealed a nonlinearly increasing pattern for both properties from small bundles of fibers to whole muscle. At the whole muscles level, collagen was the strongest predictor of muscle passive function.

Due to the challenges in direct measurement of elastic modulus at the fascicular or whole muscle level, we measured collagen I content instead, and found no difference between the vertebral levels. With the reported strong correlation between collagen I and collagen content [108], it can be inferred that passive properties at the fascicle and whole muscle level should not differ between the vertebral levels, either. However, it is noteworthy that not just the content, rather the organization and quality of collagen are also important in determining tangent modulus of the muscle. A limitation of the immunostaining method utilized in this study is that it measured the collagen I content across a transverse section of the biopsy, whereas a volumetric measurement approach such as a three dimensional imaging technique or using hydroxyproline assay may have been more appropriate [108]. There was no significant correlation between tangent modulus of a fiber bundle and collagen content of a fascicle in this study (Appendix A, Figure A-1and Figure A-2), which is not surprising as those parameters were measured at different scales: one at the bundle and the other at the fascicle scale. Ward et al. [55] demonstrated for both collagen

content and tangent modulus to increase significantly from the fiber bundle scale to fascicle scale.

Fiber bundles manifested a considerably large variability in their tangent moduli in this study. Such large variability could have resulted in statistically insignificant differences between the levels. In presence of such variability, overall, assumption of similar mechanical properties between the levels appears to be fine.

The source of larger variability in tangent moduli of fiber bundles in this study could stem from the variability in bundle sizes (the number of fibers in the tested bundles averaged 14 fibers with SD of 7 fibers). The tangent modulus of a fiber bundles computed from the stress-strain data is assumed to be independent of the CSA of the bundle (as the measured force has been already divided by CSA to obtain the stress); however, this assumption may not be valid and has never been demonstrated for muscle tissue. To avoid any possible bundle size artifact for comparison of fiber bundles tangent modulus among the levels, we aimed for a relatively even distribution of bundle sizes across levels and muscles. For example, out of six bundles extracted from a biopsy, two would be small (~7 fibers), two medium (~14 fibers), and two large (~21 fibers).

All tangent modulus values in this study were calculated at 30% strain. This should not make a significant difference in tangent modulus of single fibers as they typically show near-linear passive behavior [55]. However, due to the nonlinear behavior of fiber bundles, the tangent modulus would vary depending on where on the stress-strain curve the tangent is applied. While some studies selected a certain sarcomere length to compute the tangent (e.g. 3.2 micron [91] [220] or 4 micron [94]), we selected a certain strain (i.e. 30%) believing it resulted in more standard outcomes as slack sarcomere lengths were not necessarily the same for all bundles

(ranged from 1.8 to 2.6 µm in our study, which would result in tangents at strains ranging from 23% to 77% if 3.2 µm was selected). Also, by 30% strain, bundles have passed their initial toe region while still remaining within their physiological excursion range in both rat [223] and human [224]). It is noteworthy that the stresses at strains between 10% to 80% were also examined in this study but no significant difference in those values was found between the spinal levels.

The current study showed there is no vertebral level effect in passive behavior of paraspinal muscles in rats. This finding can be used as a basis for the assumption of similar mechanical properties along the length of these muscles in a musculoskeletal model. Although rats are mammals and often have similar muscle properties to human [102], daily activities as quadrupeds differ from humans which should be noted when translating the results of this study to humans. Conducting a similar study on humans would be ideal; however there are limiting factors in obtaining muscle biopsies from healthy individuals. Due to the deep nature of paraspinal muscles, non-invasive collection of muscle biopsies from healthy individuals is associated with substantial technical and ethical challenges. Intraoperative access to paraspinal muscles is possible, however those who undergo a surgery typically have a spinal pathology; therefore, any findings related to the effect of vertebral level on their paraspinal muscles could be associated with that pathological condition and may not represent normal muscles of healthy individuals.

2.5 Conclusions

The results of this study highlighted that the tangent modulus, slack sarcomere length, and collagen I content of the lumbar paraspinal muscles are independent of the spinal level. This

finding provides the basis for the assumption of similar mechanical properties along a paraspinal muscle group. It implies that one may reasonably suffice to measurement of paraspinal muscle biomechanical properties at one spinal level and use that to represent the entire muscle group in a musculoskeletal model of a normal spine, with no need for further measurements at other vertebral levels. The results of current study also serve as a baseline for future animal studies where the vertebral effect of a pathology or treatment such as the effect of open fusion surgery on paraspinal muscles is of interest.

Chapter 3 Larger Muscle Fibers and Fiber Bundles Manifest Smaller Elastic Modulus in Paraspinal Muscles of Rats and Humans

In this chapter, another fundamental question on passive properties of the paraspinal muscles is addressed. While most studies assume that the size of a muscle fiber bundle (i.e. a number of muscle fibers ensheathed in their connective tissue) does not influence elastic modulus after normalizing for cross sectional area, elastic modulus of muscle fibers has been shown to be size-dependent. The objectives of this chapter were to determine the degree to which this size effect was evident in muscle fiber bundles and to examine the validity of the frequent assumption of a circular cross section of muscle fiber bundles. These are important considerations in characterization of paraspinal muscle passive properties; and may have considerable implications, especially when contrasting the results of the studies using varying sizes for testing.

3.1 Introduction

Passive stiffness is an important property of skeletal muscles. In particular, the passive elastic modulus of a muscle has a direct impact on the amount of force generated in resistance to lengthening and hence is critical in biomechanical modeling. Elastic modulus also has a pivotal role in cell mechanics and affects function, differentiation, and the proliferation of muscle cells. For example, myofibroblasts have been shown to contract and secrete more extracellular matrix on a stiffer substrate [225], while their differentiation and function are impeded below certain elastic modulus thresholds [226][227][228].

Interestingly, many studies have reported that muscles in individuals with orthopedic pathologies manifest significantly different elastic moduli than muscles of healthy subjects, in both humans [93][96][94][229][95] and animals [90][97][230]. The differences were evident both at the

cellular level (i.e. for a single muscle fiber) [93][96][95][97] and the tissue level (i.e. for a bundle of muscle fibers ensheathed in their connective tissue), with most differences existing at the tissue level [96][94][90][230][231]. In some cases, muscle fiber bundles have been reported to be up to four times stiffer in normal population than compared to the patients with pathology (spasticity)[96]. These observations highlight the importance of elastic modulus in muscle physiology, pathology, and biomechanics and encourage more research to be conducted for better understanding and addressing musculoskeletal conditions.

Researchers characterize the passive stiffness of muscle fibers and fiber bundles with a uniaxial stretch test to determine the elastic modulus. They test fibers and fiber bundles of different sizes and normalize for cross-sectional area (CSA) assuming that this eliminates the effect of size (i.e. CSA). The size of muscle fiber bundles tested to determine elastic modulus varies from 3 to 30 fibers in the literature [96][90][97][98][55][99]. Whether the effect of size on elastic modulus disappears after normalizing for CSA is unknown. A recent study by Noonan et al. suggested that elastic modulus does depend on the size of the muscle fiber [100]. This question has not been solved for bundles of muscle fibers.

Another important point regarding the measurement of elastic modulus is that most studies of single muscle fibers or bundles of muscle fibers assumed a cylindrical shape and only measured diameter of those specimens in one plane [98][55][101][86][91][102]. Other investigators believe measurement of diameters in two different planes (i.e. both top and side views) is necessary [103][99]. Blinks [104] examined 16 frog fibers and found ~20% difference in the calculated CSA when using only one diameter versus two. For humans and rodents, whether the assumption of a cylindrical shape is acceptable and to what extent it influences the measured CSA of a muscle fiber or a bundle of muscle fibers remains unknown.

Therefore, the objectives of this study were (1) to explore whether the size of a single muscle fiber or a bundle of muscle fibers has an influence on its measured elastic modulus; and (2) to examine whether the assumption of a circular shape for the cross section of a muscle fiber or a bundle of fibers is valid. We include samples from two types of paraspinal muscle, multifidus and longissimus, in both rats and humans.

3.2 Methods

3.2.1 Study Groups

Under anesthesia, fresh muscle biopsies from the lumbar paraspinal muscles of two groups of rats and one group of humans were collected (approved by the University of British Columbia animal care committee and clinical research ethics board, Vancouver, Canada). Group 1 consisted of 13 male Sprague Dawley rats ~8 weeks old (330±14g) that had undergone no experimental procedure. Group 2 included six Sprague Dawley rats ~21 weeks old (452±28g) that had undergone a sham surgery with a small midline incision on their thoracolumbar fascia ~13 weeks before collecting biopsies. Group 3 was comprised of nine patients with degenerative spinal deformity undergoing a spinal surgery for the first time. A minimum of two biopsies from multifidus and two biopsies from longissimus were collected from each rat/patient. The biopsies were taken from L1, L3, and L5 in rats and L4/L5 in humans. All fresh biopsies were treated similarly: they were transferred to a physiological storage solution immediately after harvest, and after 24 hours incubation at 4 °C were stored at -20 °C for a minimum of 24 hours. Mechanical properties of muscle tissues stored in this way are expected to remain stable for up to three months [221][222]. Later, the biopsies were transferred to a cold relaxing solution under a dissecting microscope to extract single fibers and bundles of fibers for mechanical testing.

From each biopsy, two to three single fibers and two to six bundles of fibers were extracted for measurement of their geometric dimensions and elastic modulus. While the maintenance of a balance in the size range of extracted bundles of fibers was attempted, more emphasis was placed on taking extreme care to maintain the integrity of the bundles during extraction. For instance, out of six bundles extracted from a biopsy, two would typically be small (~7 fibers), two medium (~14 fibers), and two large (~21 fibers; Figure 3-1). Based on previous work showing no difference between the spinal levels [232], all samples belonging to the same study group and the same muscle group were put into one pool for data analysis. For example, for study group 1 (G1) four types of samples were pooled: G1 Multifidus Fibers, G1 Longissimus Fibers, G1 Multifidus Bundles, and G1 Longissimus Bundles.

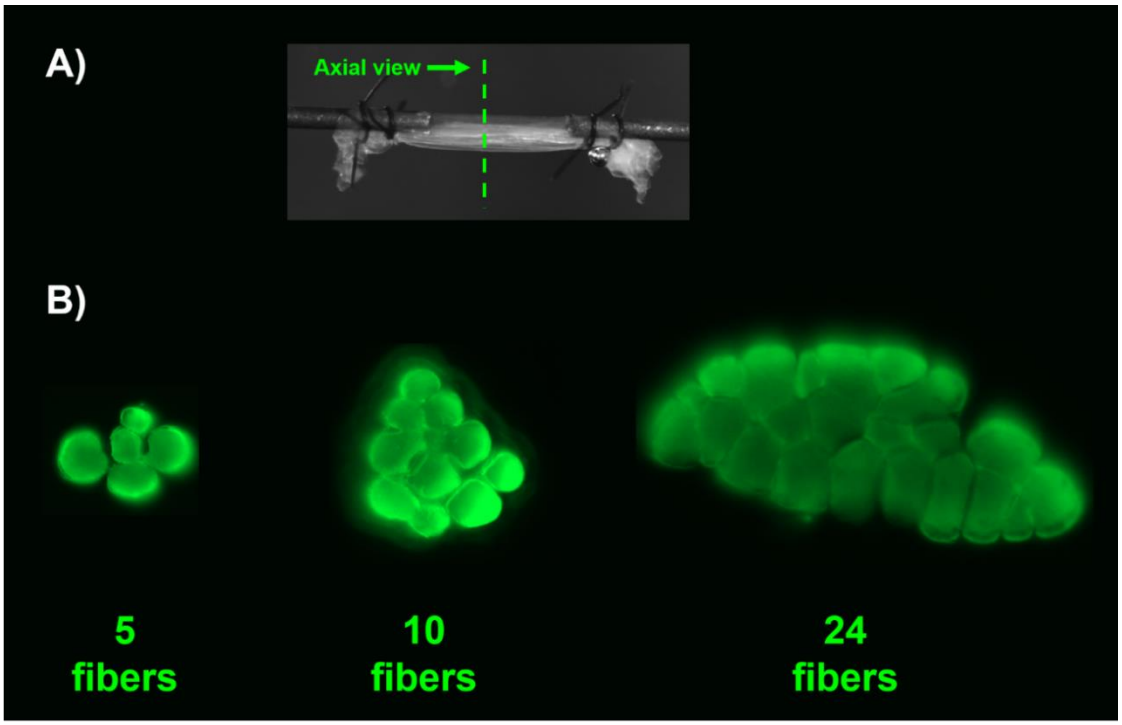

Figure 3-1. Muscle fiber bundle specimen for mechanical testing; (A) The specimens were mounted onto two collinear pins and secured to them via suture loops. (B) Axial view of three tested muscle fiber bundles. Out of six bundles extracted from a biopsy, two would typically be small (~7 fibers), two medium (~14 fibers), and two large (~21 fibers).

3.2.2 Mechanical Testing

The same methodology as described in section 2.2.1 was followed for mechanical testing and measurement of elastic modulus. Briefly, each fiber/fiber bundle was immersed into a bath of physiological relaxing solution and was secured at its ends to two collinear pins with outer diameter of 0.15 mm (No. 26002-15, Fine Science Tools, BC, Canada). One pin was connected to a highly sensitive force transducer (400A, Aurora Scientific, Ontario, Canada) and the other pin was attached to a length controller (CRK523PMAP, Oriental Motor, USA). The fiber or fiber bundle was lengthened until it reached a length beyond which passive force started to develop (known as slack sarcomere length). Using a crosshair reticle inside the eye piece of a stereomicroscope, top and side diameters were measured with a resolution of 1 micron at three different points along the specimen (Figure 3-2). This measurement technique resulted in a precision of 3 micron for each diameter reading. The average of the readings for the top and side diameters at those three points were used to calculate the CSA of each specimen. From the slack length, each specimen underwent cumulative (four to eight) stretches, each of 10% strain at a rate of 10% strain per second followed by 4 minutes relaxation [99]. The force reading at the end of each increment was divided by the CSA to obtain the engineering stress. The specimens were transilluminated by a single mode fiber-coupled diode laser (660 nm) and the resulting diffraction pattern was scanned by a photodiode array to measure (with a resolution of ~10nm) the sarcomere length of the specimen prior to any stretches and at the end of each increment. This enabled calculation of the strain after each increment. Elastic modulus was calculated as tangent at 30% strain from the stress-strain curve. All tests were performed within three weeks after collection of muscle biopsies.

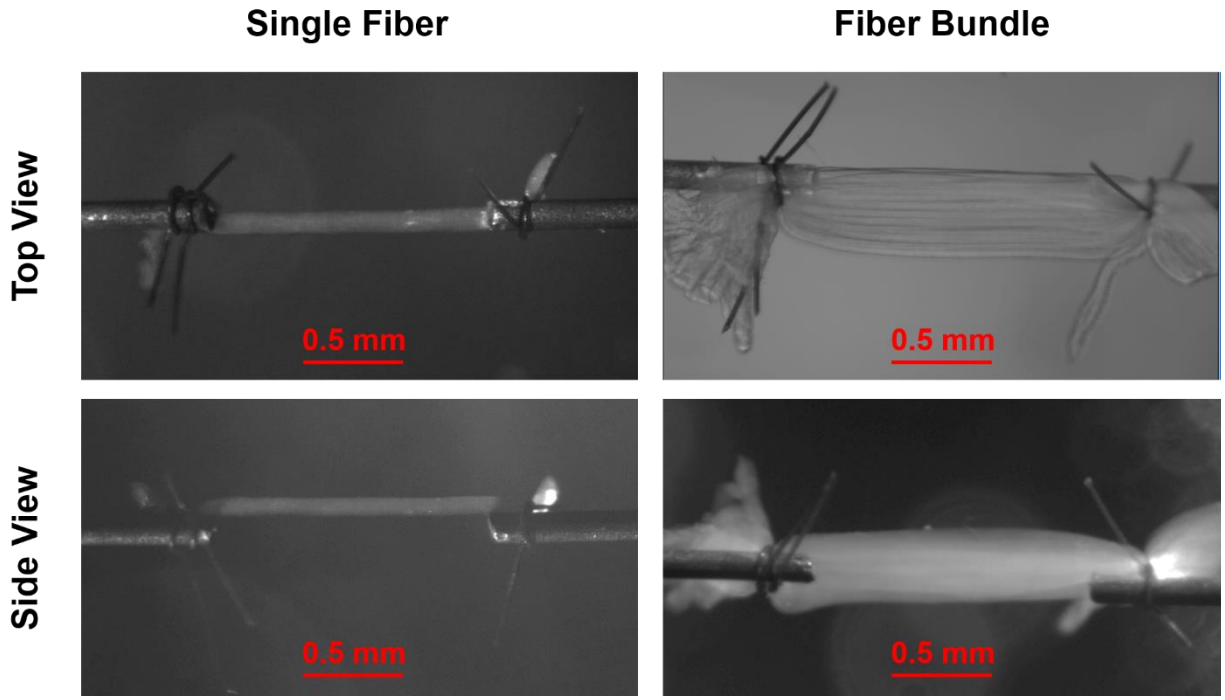

Figure 3-2. Top and side views of a representative single muscle fiber and a fiber bundle. Top and side diameters were measured at three different points along the specimen. The average of the readings for the top and side diameters at those three points were used to calculate the CSA of each specimen.

3.2.3 Statistical Analysis

For each pool of samples (e.g. G3 Longissimus Bundles), a linear regression approach was taken to find a correlation between the CSA (independent variable) of samples and their elastic moduli (dependent variable). The slopes, intercept, and correlation of determination were calculated for each analysis. Also, for each pool of samples the ratios of major over minor axis diameters were calculated and the median and inter quartile range (IQR) were determined. The results were contrasted against the theoretical median of 1 (for cylindrical shape assumption) using Wilcoxon signed rank test.

3.3 Results

In total, 391 fibers (192 in G1, 112 in G2, 87 in G3) and 570 bundles of fibers (262 in G1, 137 in G2, and 171 in G3) were tested. Twenty-six outliers in G1, 19 outliers in G2 and 20 outliers in G3 were removed for having modulus values 1.5 times the interquartile range above the third quartile of their group.

All groups manifested a trend of smaller elastic modulus associated with larger fibers and larger bundles of fibers in the paraspinal muscles (Figure 3-3 and Figure 3-4). The correlation of determination R^2 for all groups ranged between 0.06 and 0.30 for muscle fibers ($p<0.05$, except for G3 multifidus fibers where $p = 0.10$; Figure 3-3). For the six groups of muscle fiber bundles, the correlation of determination ranged between 0.03 and 0.23 ($p<0.05$, except for G2 longissimus bundles where $p = 0.16$; Figure 3-4).

The Wilcoxon signed rank test rejected the cylindrical assumption for the cross section of fibers and fiber bundles (all $P<0.00001$). The ratio of the major axis over minor axis had a median (IQR) of 1.15 (0.23), 1.19 (0.32), and 1.29 (0.41) for multifidus fibers of G1, G2, and G3 respectively; and 1.18 (0.23), 1.15 (0.20), and 1.16 (0.39) for longissimus fibers of G1, G2, and G3 respectively (Figure 3-5). The range of minor axis diameters for multifidus fibers were from 0.060 mm to 0.138 mm for G1; 0.049 mm to 0.162 mm for G2, and from 0.034 mm to 0.110 mm in G3; while for longissimus fibers the range of minor axis diameters were from 0.058 mm to 0.117 mm for G1, 0.078 mm to 0.133 mm for G2, and 0.048 mm to 0.121 mm for G3.

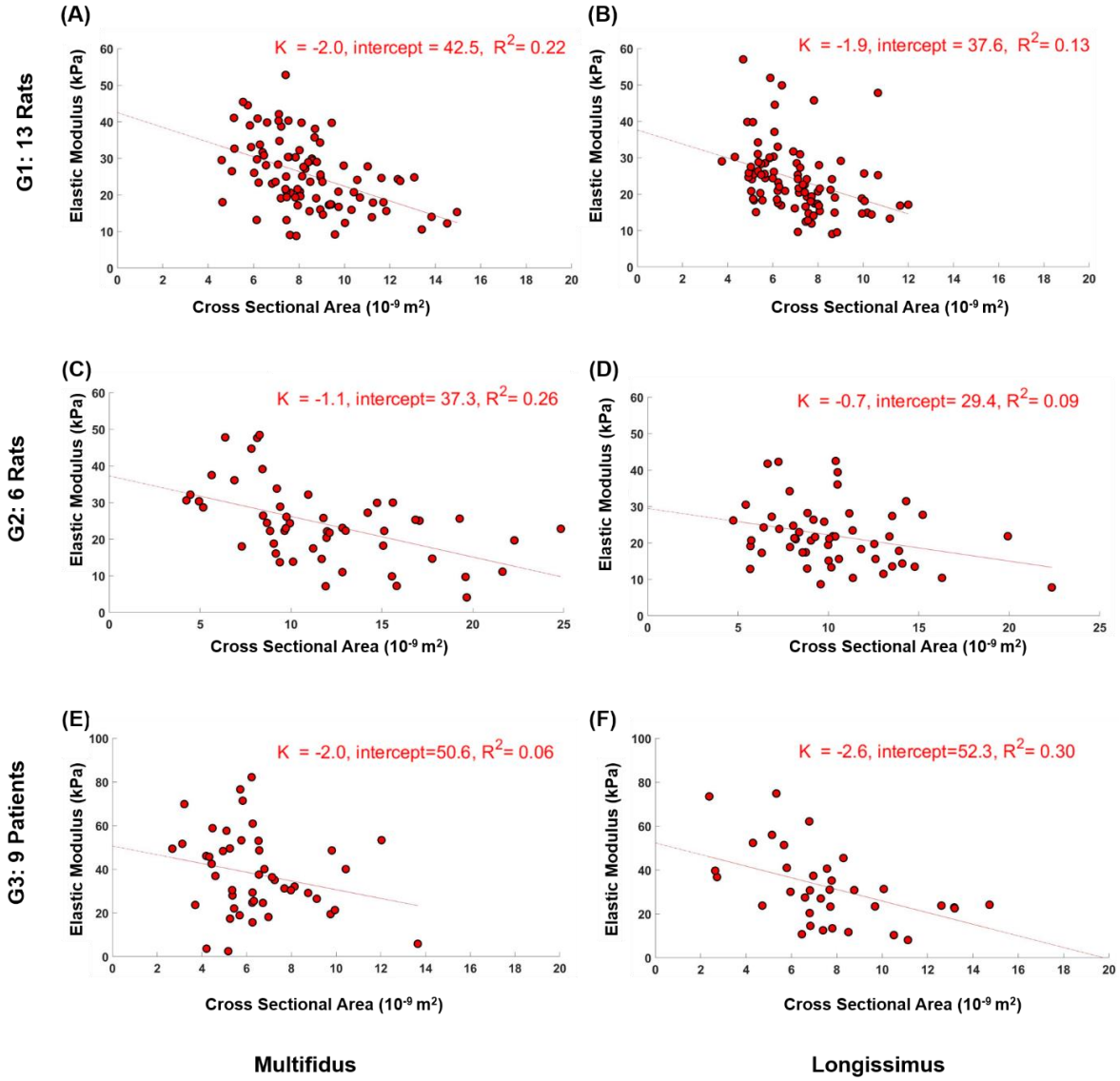

Figure 3-3. Correlation between cross-sectional area and elastic modulus of single fibers from multifidus and longissimus of G1 (A, B), G2 (C, D), and G3 (E, F). All P <0.026 except for G3 multifidus fibers

Bundles of fibers in general had larger ratios compared to fibers. The ratio of the major axis over minor axis had a median (IQR) of 1.44 (0.52), 1.32 (0.39), and 1.27 (0.33) for multifidus fiber bundles of G1, G2, and G3 respectively; and 1.32 (0.55), 1.39 (0.4), and 1.27 (0.35) for longissimus fiber bundles of G1, G2, and G3 respectively (Figure 3-5). The range of minor axis

diameters for multifidus fiber bundles were from 0.121 mm to 0.472 mm for G1; 0.208 mm to 0.703 mm for G2, and from 0.126 mm to 0.622 mm in G3; while for longissimus fibers the range of minor axis diameters were from 0.122 mm to 0.504 mm for G1, 0.198 mm to 0.578 mm for G2, and 0.078 mm to 0.733 mm for G3.

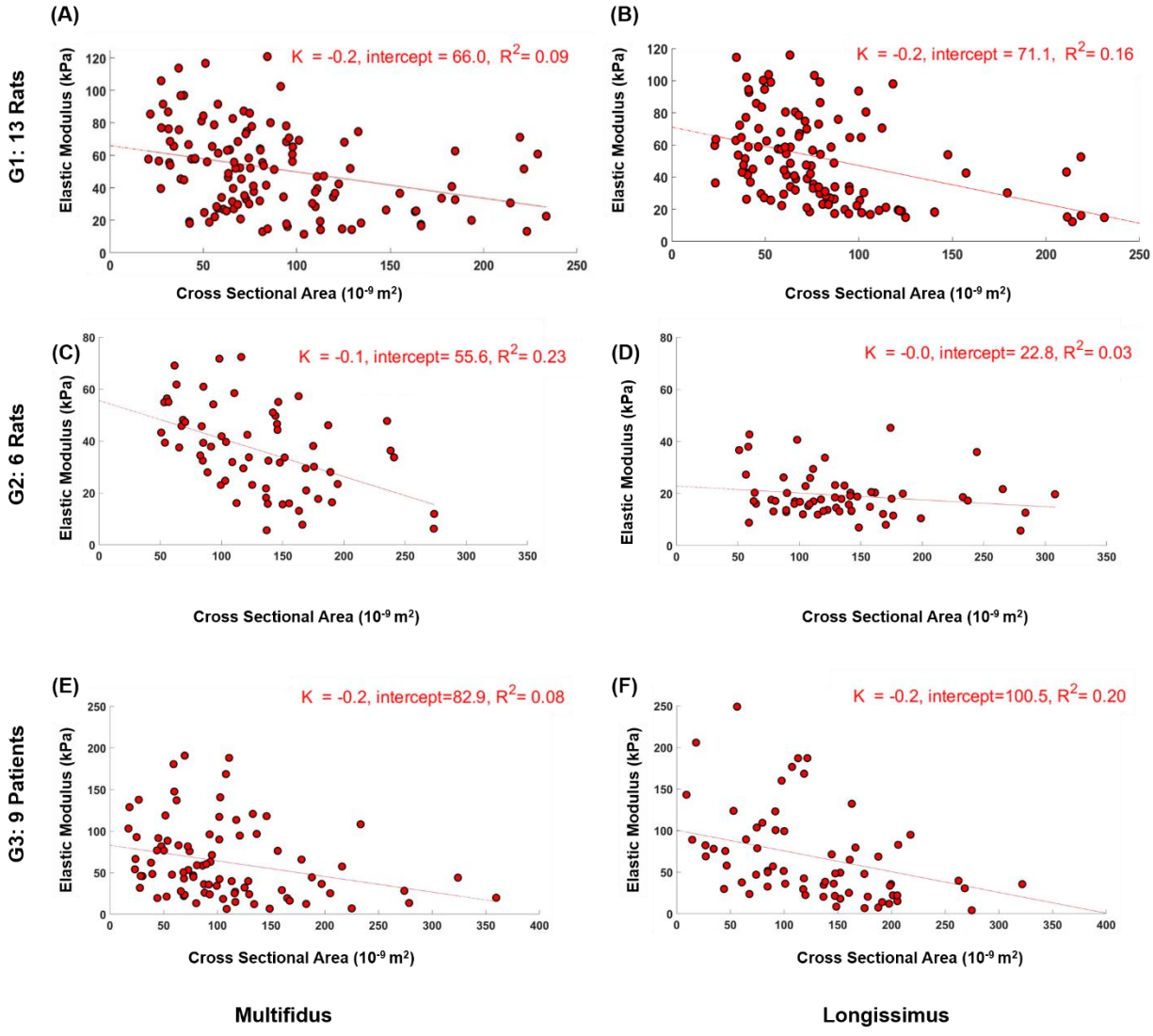

Figure 3-4. Correlation between cross-sectional area and elastic modulus of fiber bundles from multifidus and longissimus of G1 (A, B), G2 (C, D), and G3 (E, F). All P<0.02 except for G2 longissimus bundles that P=0.16 (D)

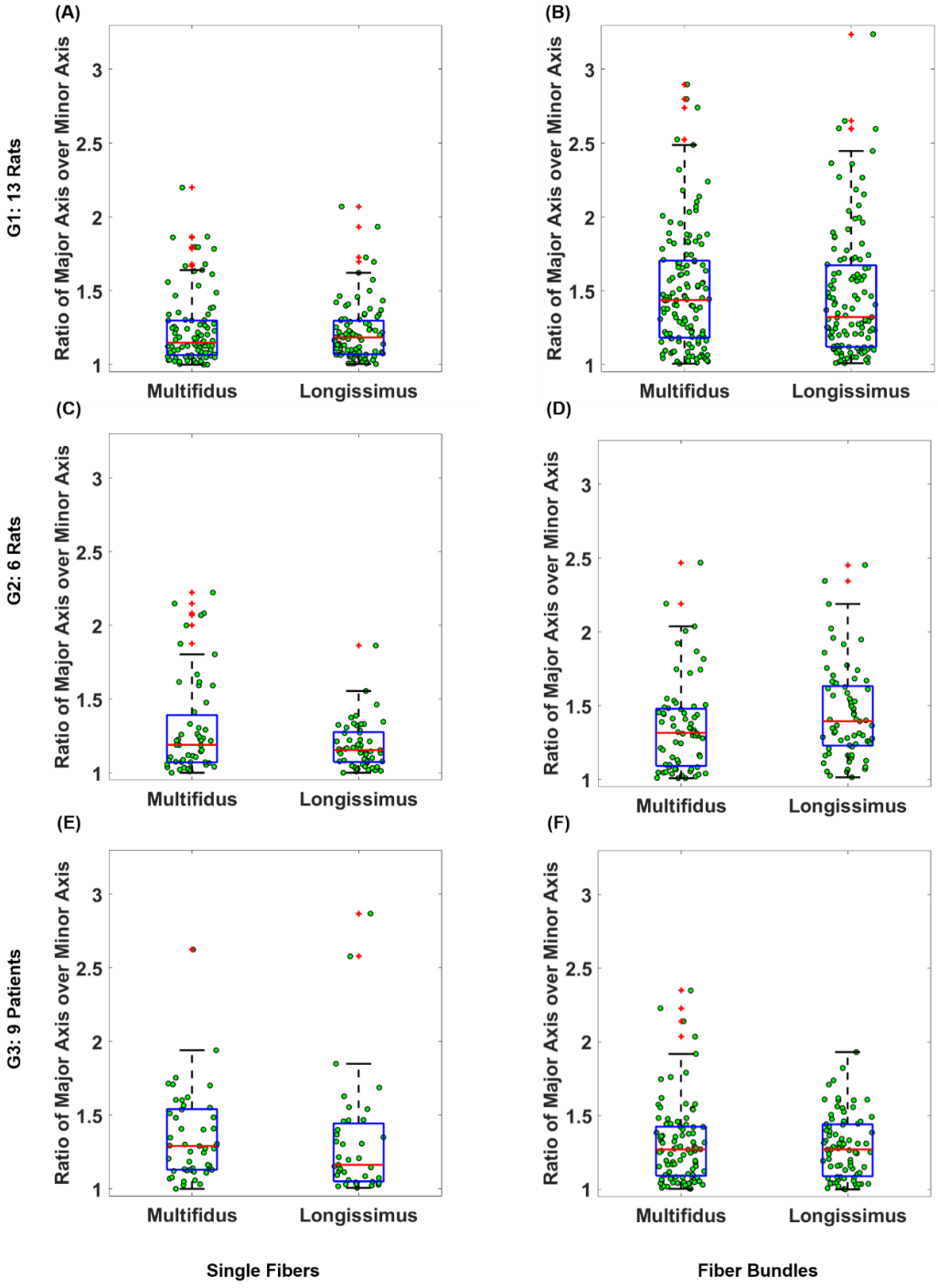

Figure 3-5. Boxplot representation of ratio of major over minor axes of single fibers and fiber bundles tested in G1 (A, B), G2 (C, D), and G3 (E, F). The red lines represent the medians, the heights of the boxes represent the interquartile ranges and red dots identify the outliers

3.4 Discussion

Muscle passive stiffness provides insight into the biomechanical function, physiology, and health of our musculoskeletal system; thus, its accurate measurement is important. Most studies do not differentiate between bundles of muscle fibers with different sizes. Thus, these studies assume that the elastic modulus (i.e. passive stiffness/CSA) of these muscle specimens is independent of size. The same assumption is made for single fibers. The results of our current study demonstrated that the size matters and in general, larger sizes were associated with lower elastic moduli in fibers and bundles of fibers. Therefore, future studies should consider maintaining consistent bundle sizes for measurement of passive properties especially when comparing different groups against each other.

This same finding was observed for single fibers recently by Noonan et al. [100] where larger fibers in vastus laterals of 10 healthy volunteers manifested smaller elastic moduli. They demonstrated that considering a constant thickness and higher elastic modulus for the basement membrane, relative to the modulus of the contractile area of the fiber, results in larger elastic modulus for smaller fibers. The effect is due to the CSA of the basement membrane being proportional to the fiber diameter while the contractile area of a fiber is proportional to its diameter squared. At the fiber bundle level however, no study has examined the effect of size on elastic modulus.

The lower elastic modulus of larger bundles in the current study may arise from their ECM content. It is well established that bundles of fibers have a larger elastic modulus than single fibers due to the high stiffness of ECM [90][86][102][25][92]. Assuming that the ECM and

fibers within a bundle are both homogenous, the elastic modulus of a bundle can be calculated following the rule of mixture for composites as:

$$E_{Bundle} = f_{ECM}E_{ECM} + (1 - f_{ECM})E_{Fiber} \tag{3-1}$$

where E_{Bundle}, E_{ECM}, and E_{Fiber} are the elastic moduli of the bundle, the extracellular matrix, and fibers, respectively; and f_{ECM} denotes the percentage of the extracellular matrix within the bundle. For example, the elastic modulus of a bundle containing 5% ECM (i.e. $f_{ECM} = 0.05$) with a fiber elastic modulus of 20 kPa and ECM elastic modulus of 1MPa [92] is calculated as 69 kPa. The predicted bundle elastic modulus would be 79 kPa or 59 kPa had the ECM percentage been changed to 6% or 4%, respectively.

To further explore this idea, we performed an immunostaining analysis to quantify ECM content in bundles of different sizes from multifidus of one rat in G1 as an example. While the exact relationship between ECM elastic modulus and its constituents is not yet clear, many studies report collagen I as the major contributor to elastic modulus of ECM [55][108]. Therefore, we measured and contrasted collagen I content in bundles of different sizes. A portion of the collected biopsy was separated and immediately snap frozen in isopentane cooled by liquid nitrogen. The biopsy was sectioned, placed on slides, and immune-stained for collagen I. Using Image J software, bundles of different sizes were arbitrarily defined, segmented and their collagen I area fraction (i.e. the ratio of collagen I area over the entire bundle cross-sectional area) was measured. As no collagen I exists inside muscle fibers, the number of fibers within each bundle can easily be counted. However, as the exact border of bundles cannot be determined from the images, two segmentations (types A and B) were performed for each

bundle: the borders of one segmentation (type A) passed internal to the edge of boundary fibers of the bundle (Figure 3-6A&D), while borders of the other segmentation (type B) passed externally, including the boundary edge of the fibers immediately adjacent but external to the bundle (Figure 3-6B&E). The collagen I deposition was measured for these two segmentations and their average was considered for the selected bundle.

Following this approach, collagen I deposition of larger bundles was measured to be smaller for the studied biopsy (Figure 3-7). The three bundles studied had 8, 16, and 25 fibers but their collagen I content was 5.3%, 3.8%, and 3.4% of the area, respectively. Assuming an elastic modulus of ~20 kPa for muscle fibers and ~1 MPa for the ECM [92] and using the rule of mixture, the corresponding elastic moduli of these three bundles are estimated as 72, 57, and 53 kPa, respectively.

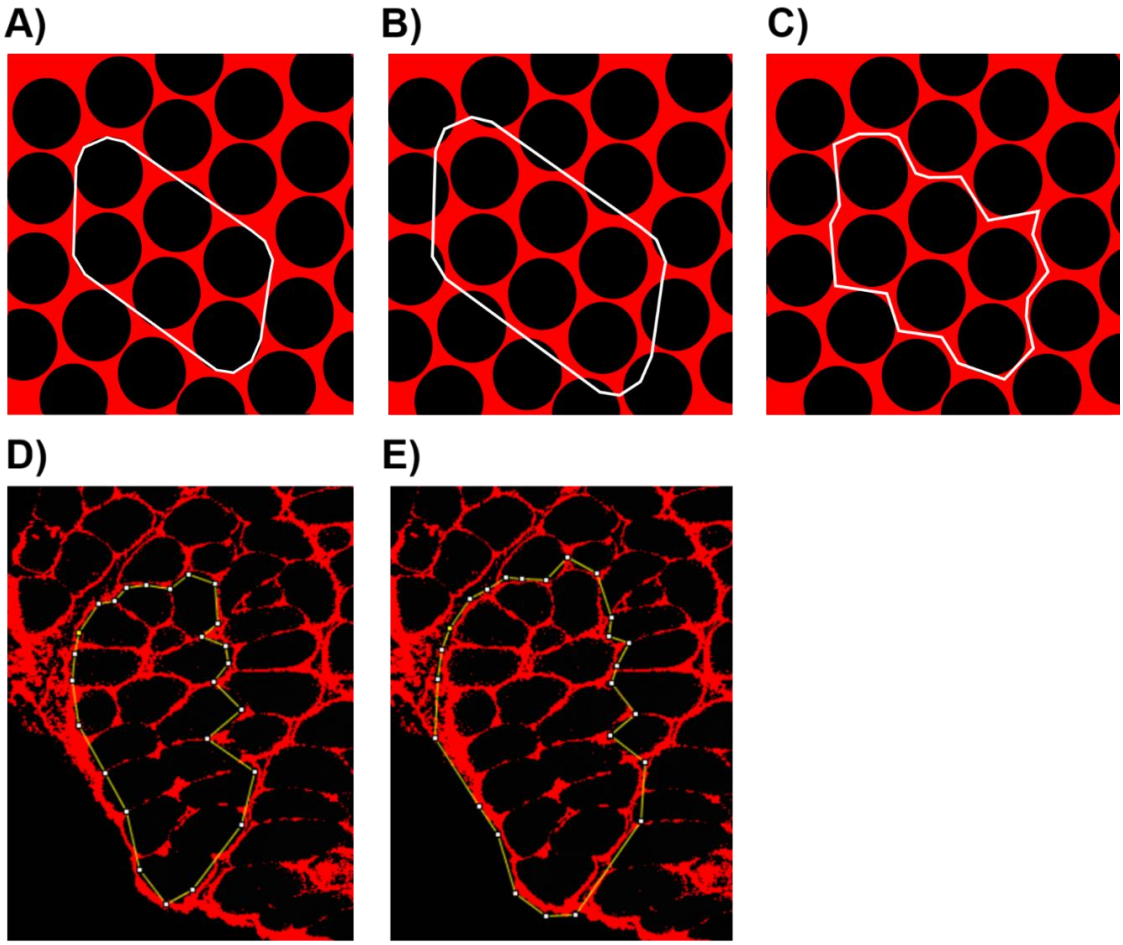

Figure 3-6. Segmentation of fiber bundles from immunohistochemistry images. Two segmentations were performed for each bundle: the borders of one segmentation (type A) passed internal to the edge of boundary fibers of the bundle (A, D), while borders of the other segmentation (type B) passed externally, including the boundary edge of the fibers immediately adjacent but external to the bundle (B, E). Schematic representations for a simulated bundle of 6 fibers, are shown for segmentation type A (A), segmentation type B (B), and how a real bundle may present (C). The collagen I deposition was measured for the two segmentations (D&E) and their average was considered for the selected bundle

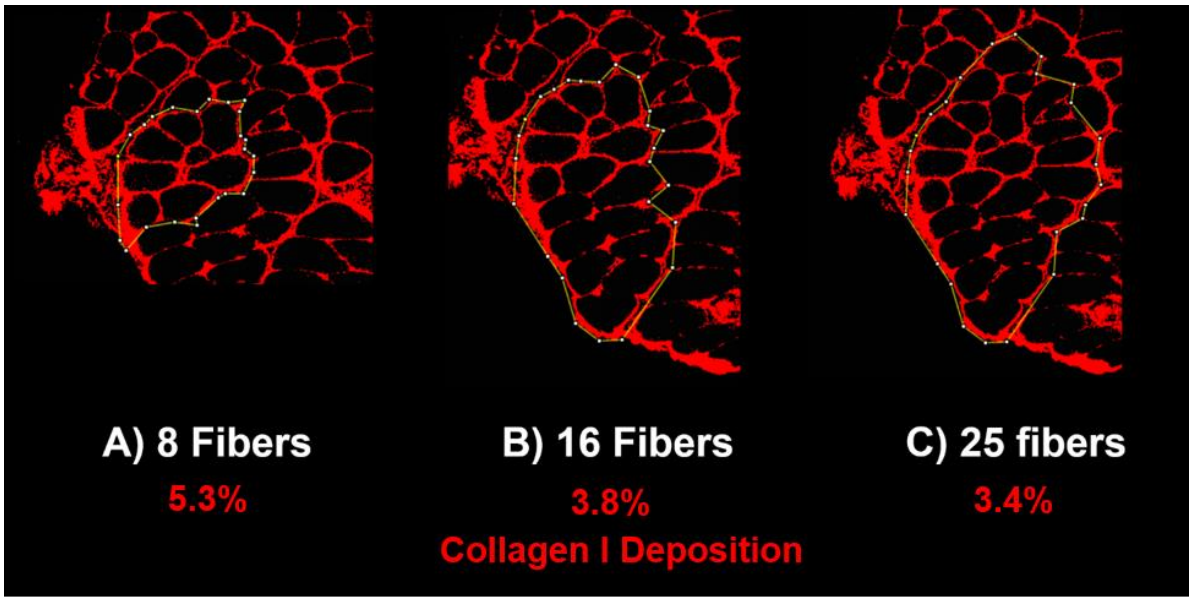

Figure 3-7. Inverse correlation between collagen I deposition and size of three bundles of different sizes from multifidus of one rat in G1. The measured percentage of collagen I deposition for bundles A, B, and C were 5.3%, 3.8%, and 3.4%, respectively.

Another factor contributing to the elastic modulus of a bundle could be the distribution of fiber sizes within that bundle. As our results suggest, larger fibers have a smaller modulus. Therefore, for two muscle bundles with same amount of ECM, the one having more fibers (i.e. consisting of smaller fibers) will have a higher elastic modulus (Figure 3-8).

While both factors, i.e. collagen I deposition and fiber size distribution, could potentially explain the results of our study, further investigation is required to find out their relative effects. Although we reasonably used the average of type A and B segmentations for our sample measurement of collagen I percentage, the actual bundle that was mechanically tested might have a different collagen I content (Figure 3-6C) that could be closer to either segmentation A or B. Notably, for the three bundles in Figure 3-7, segmentation type A would result in larger percentages for larger bundles, while type B segmentation and the average method showed an opposite trend. Therefore, it is quite important to know how much ECM remains on an actual

extracted bundle, for example by measuring the volumetric collagen deposition of a bundle using a three dimensional imaging technique or hydroxyproline assay [108].

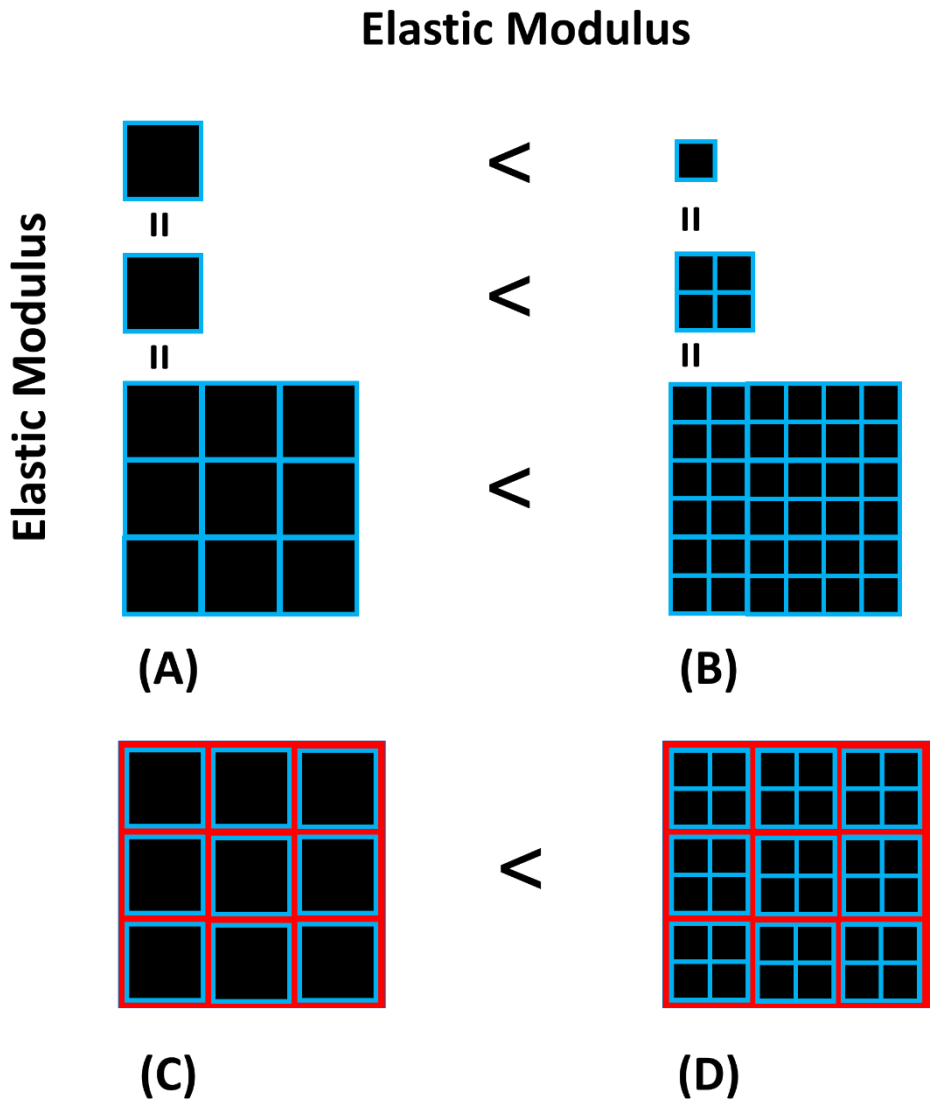

Figure 3-8. Effect of fiber size on bundle elastic modulus. In all images, black color represents the contractile elements of muscle fibers, blue color represents basement membranes of muscle fibers, and red color represents the ECM. Given that larger fibers have smaller elastic moduli (A, B), for two muscle bundles with same ECM content (C, D), the one having more fibers (i.e. consisting of smaller fibers) will have a higher elastic modulus

The linear regression approach in the current study revealed a statistically significant effect of CSA on the elastic modulus of all fibers and fiber bundles (except for G3 multifidus fibers and G2 longissimus bundles). That the R^2 values for this association were relatively low (all $R^2 < 0.30$) is not surprising. The low values for the R^2 could stem from the biological variations in the subjects or from the variations in sites within biopsies from where fibers and fiber bundles were extracted; thus suggesting possible role of other factors that were not studied here. What is noteworthy is the found dependence of elastic modulus on CSA despite being already normalized by the CSA, which means that the size of the fibers and fiber bundles needs to be considered.

For the second objective of this study, the intriguing observation was that muscle fibers and fiber bundles were not cylindrical (all P<0.0001). In contrast to the shape of a single muscle fiber, the shape of a muscle fiber bundle could be somewhat controlled by the person extracting the bundle from the biopsy tissue. However, during extraction to maintain the integrity of a bundle, it may be necessary to avoid separating extra fibers that can result in loss of bundle integrity. This will result in bundle shapes that may not be cylindrical. Many studies only measure fiber and fiber bundle diameter along a single axis typically from the top view [98][55][101][86][91][102]. The cross section of fibers and fiber bundles is then assumed to possess a cylindrical shape. However, measurement of diameters from two orthogonal axes (top and side view) in the current study revealed that such an assumption was not valid in rodents or humans, especially at the bundle level. The ratio of major axis over the minor axis of a cylindrical sample should be equal to 1, whereas the median for ratio of major axis over the minor axis of the samples tested in this study ranged between 1.15 and 1.29 for fibers and 1.27 and 1.44 for fiber bundles. The implication of this finding is that the measurement of elastic modulus values could be off by a factor of 1.15 to

1.29 for fibers and 1.27 to 1.44 for fiber bundles if the diameter along only one axis is measured. Therefore, it is recommended to measure the fiber and bundle diameters from both top and side views.

Muscle is an organized material with several structural levels. In a recent study, Ward et al. [55] measured the elastic modulus of rabbit muscles at multiple levels, i.e. single fibers, fiber bundles (~20 fibers), fascicles (~300 fibers), and whole muscles. They found that elastic modulus increases nonlinearly with these size scales as does the collagen content. The results of the current study demonstrated that larger bundles were associated with lower elastic moduli. These results are not in conflict, but rather they are complementary. Our results suggest that for fiber bundles of less than ~50 fibers larger sizes will be associated with smaller elastic moduli. However, beyond a certain size (e.g. ~300 fibers), bundles will transition to true fascicles, including the presence of perimysium and higher amounts of collagenous tissue, thereby leading to larger elastic moduli compared to bundles. In conclusion, the findings of our study suggest that similar size of bundles should be tested when comparing for differences between groups.

3.5 Conclusions

This study showed that increasing specimen CSA resulted in lower elastic modulus for both rats and humans, muscle fibers and fiber bundles. The lower elastic moduli with increasing size can be explained by relatively less collagenous extracellular matrix in the large fiber bundles. Also, this study exhibited that the assumption of circular CSA is not accurate for single fibers and fiber bundles. Therefore, future studies of passive property measurement should aim for consistent bundle sizes and measuring diameters of two orthogonal axes of the muscle specimens.

Chapter 4 Biomechanical Properties of Paraspinal Muscles in Adult Spinal Deformity Patients – A Preliminary Analysis

Chapters 2 and 3 addressed two fundamental questions on characterization of paraspinal muscles passive behaviour. This chapter investigates if biomechanical properties including the passive behaviour of the paraspinal muscles are different among adult spinal deformity (ASD) patients. Decreased back extensor strength in adult spinal deformity (ASD) patients is well established. While smaller muscle cross-sectional areas have been noted for ASD patients, whether other muscle biomechanical properties including passive elastic modulus, slack sarcomere length (beyond which passive force starts to develop), or in situ sarcomere length (measured inside the body for a certain posture) in these patients leads to decreased strength remains unclear. A reason for lack of data on these paraspinal muscle properties is likely the ethical and technical challenges associated with acquiring fresh muscle biopsies from these patients. The only study measuring elastic modulus of human paraspinal muscles using fresh biopsies was conducted for a mixed group of patients [25]. The objectives of this chapter were therefore, (1) to develop a procedure for acquisition of required human paraspinal muscle biopsies and (2) to evaluate their biomechanical and histological properties for ASD patients. The findings from this study may serve as an invaluable input to musculoskeletal models to help in exploring the etiology of adult spinal deformity or assist in coming up with better treatment strategies for patients suffering from adult spinal deformity.

4.1 Introduction

Adult spinal deformity is prevalent in up to ~30% [2][3][4] and in some cases as high as 68% [30] of people above 65 years old. The exact etiology of adult spinal deformity is not known,

although several risk factors have been identified. Osteoporosis and vertebral fracture, for example, have been deemed to be a common potential cause of adult spinal deformity; however, a recent review article revealed that 60-70% of patients with severe deformity did not have any sign of vertebral fracture [45]. While degenerative disc disease [2][43][6], ligamentous degeneration[44], and proprioceptive deficits [11] have also manifested an association with adult spinal deformity, many believe muscle weakness/dysfunction is playing the key causative role in development of this condition [45][11][46][7][8][9][12][47][48][49][50].

Paraspinal muscle is of fundamental importance to the maintenance of upright posture [50][51]. The weight of the upper body combined with other external forces in daily activities generates a flexion moment on the spine which needs to be counterbalanced by extensor muscles. In addition to preserving the equilibrium, these muscles contribute to maintaining the mechanical stability of the spine [51]. Therefore, it is reasonable that abnormal muscle functioning may be involved in the development of the spine deformity. In fact, multiple studies have reported lower muscle strength in adult deformity patients [46][7][8][9].

A decrease in back extensor strength may arise from changes in different muscle properties including smaller anatomical cross-sectional area, lower level of activation, or shorter muscle moment arm, all of which have been observed to some extent in spinal deformity patients compared to normal population [13][14][15]. However, there are other muscle biomechanical properties that could contribute to force production capacity of a muscle, which include passive elastic modulus, slack sarcomere length (beyond which passive force starts to develop), in situ sarcomere length (measured inside the body for a certain posture), specific tension, fascicle length, or pennation angle. The preponderance of the muscle adaptation literature on in situ sarcomere length, slack sarcomere length, and passive elastic modulus provokes the question

whether these three parameters are different in adult spinal deformity patients compared to normal population.

In situ sarcomere length of human paraspinal muscles varies between different muscle groups. For example, in a prone posture multifidus typically manifests an average in situ sarcomere length of ~2.3 μm [156][224] although an individual value as high as 3.35 μm has been reported [233]; in contrast, psoas typically has an average in situ sarcomere length of ~3.3 µm in a neutral lying posture [224][114] although an individual value as low as 2.60 µm has been measured [233]. While the large variation between these measurements for each muscle group may be an artifact of the postures in which the cadavers were initially embalmed, it may reflect natural differences between humans or their pathologies. It has been shown that in situ sarcomere length of soleus is substantially larger in patients with cerebral palsy (4.07 μm) compared to typically developing children (2.17 μm), although their fascicle lengths were the same [78]. Whether the in situ sarcomere length of paraspinal muscles in adult spinal deformity patients are different compared to normal population is unknown.

Muscle passive elastic modulus has been widely reported to differ between pathologies at both cellular (i.e. for a single muscle fiber) [93][96][95][97] and tissue levels (i.e. for a bundle of muscle fibers ensheathed in their connective tissue) [96][94][90][230][231]. In animal studies, passive elastic modulus of paraspinal muscles has been shown to increase after a disc injury in rabbits [15], or a spinal surgery in rats [234]. In human, up to four times stiffer fiber bundles were measured for upper extremity muscles in control compared to pathologic patients (with spasticity) [96], while for hamstring muscles an opposite observation was made [94]. The passive stiffness of posterior paraspinal muscles has been measured only in one human study [25], which was on a mixed group of patients with degenerative conditions of spine, and it has

never been contrasted among different patient groups. Whether paraspinal muscles in adult spinal deformity patients have different elastic modulus is not known.

Slack sarcomere lengths have also been shown to differ between patient groups. For example, single fibers in upper extremity muscles of cerebral palsy patients had shorter slack sarcomere lengths than normal subjects (1.84±0.05 μm vs. 2.20±0.04 μm)[93]. Differences in slack sarcomere length were noted at the fiber bundle level between human paraspinal muscles [25], which was on a mixed group of patients with degenerative conditions of spine, but it has never been contrasted between different patient groups.

Studying cellular and extracellular structure of muscle fibers can help in better understanding the reason for any observed differences in muscle properties. Histopathological analysis may even provide insight into the underlying mechanism for development of adult spinal deformity. A recent study by Shahidi et al. [235] observed localized fiber degeneration in forms of discontinuous or ragged membrane disruption, adipose replacement, and punctate regions of muscle fiber necrosis for degenerative lumbar spine patients. It is of interest to explore if adult spinal deformity patients present similar or any specific abnormalities.

There are relatively few studies that have measured the biomechanical properties of human paraspinal muscles. A reason for scarce in vivo measurement of these properties in human paraspinal muscles is likely the ethical and technical challenges associated with biopsy acquisition. Ethically, in addition to obtaining consent from the patients undergoing surgery, approval is required from the university ethics board, as well as hospital departments such as anatomy and pathology department, medical devices and reprocessing department, and the operating room management. Technically, biopsy acquisition for in situ sarcomere length

requires specialized biopsy clamps with the ability of preserving the in situ tension such that the biopsies do not contract after collection. Biopsies for passive stiffness testing and biochemical assessment require specific tissue processing methods which should meet the standards of the operating room and the other departments. Step-by-step procedures should be clearly defined and communicated to the clinical team. These challenges need to be addressed in order to obtain the biopsies and measure the desired parameters.

The objectives of this study were, therefore, (1) to develop protocols to acquire biopsies of human multifidus and longissimus from adult spinal deformity patients, and (2) to evaluate them biomechanically and histopathologically.

4.2 Materials and Methods

This study was approved by the University of British Columbia Clinical Research Ethics Board (UBC CREB) and Vancouver Coastal Health Research Institute (VCHRI), Vancouver, Canada. All recruited patients were informed of the study and signed the consent forms (see Appendix B1&2 on pages 215 & 226).

4.2.1 Patient Demographics & Study Design

Patients enrolled for this study were categorized into three groups: I) (DEG) had multilevel degenerative lumbar disease with no sagittal imbalance and no compensatory mechanisms recruited; II) (DEG+COMP) had multilevel degenerative lumbar disease with no sagittal imbalance as multiple compensatory mechanisms were recruited. In other words, the muscle mediated compensatory mechanisms such as pelvic retroversion, segmental hyperlordosis, segmental retrolisthesis and thoracic hypokyphosis were sufficient to maintain a normal sagittal

vertical alignment (SVA), i.e. SVA <5cm; and III) (DEG+COMP+UNBAL) had multilevel degenerative lumbar disease with positive sagittal imbalance despite multiple compensatory mechanisms recruited. The muscle mediated compensatory mechanisms of pelvic retroversion, segmental hyperlordosis, segmental retrolisthesis and thoracic hypokyphosis were insufficient, resulting in abnormal SVA >5cm. As non-invasive muscle biopsy acquisition from healthy individuals was not feasible, group I served as control for groups II and III.

A power analysis suggested that 14 patients were required for detecting 30% difference in passive elastic modulus of the multifidus and longissimus (i.e. 60 kPa vs 80 kPa) based on the data presented in the study by Ward et al. [25]. Smaller number of patients were sufficient for a similar analysis for in situ sarcomere length, but we aimed for 14 patients per group.

In total, nine patients were recruited between September 2019 to March 2020 before the study was halted by COVID-19, among whom four belonged to group I, three to group II, and two to group III. The demographics of the patients, all operated at VGH, are presented in Table 4-1.

Two types of biopsies were required for this study. Type A biopsies needed a special biopsy clamp for measurement of in situ sarcomere length, while Type B biopsies were obtained through a blunt cut and were divided into two halves: one half (Type B1) was used for passive stiffness testing, while the other half (Type B2) was snap frozen for histopathological analysis. Overall, four Type A, four Type B1, and four Type B2 biopsies were collected from each patient, all at L4-L5, and from left longissimus, left multifidus, right multifidus, and right longissimus (Figure 4-1).

Table 4-1. Patient Demographics. All patients recruited for this study were operated at Vancouver General Hospital.

Ptnt #	Gender	Age (yrs)	Diagnosis	Levels Affected	Coronal Deformity		Group
					Severity (Cobb Angle)	Apex (Two-Ends)	
1	F	70	Scoliosis, degenerative, Second, acquired	T10-L4	Severe (58°)	L1 (T11-L3)	III
2	M	64	Spinal stenosis	L4-S1	Moderate (30°)	L2 (L1-L3)	II
3	M	61	Spinal stenosis	L4-L5	Very Mild (8°)	L2 (T12-L4)	I
4	M	75	Spondylosis	L2-S1	Mild (17°)	L2 (L2-L4)	III
5	M	71	Spinal stenosis	L2-L4	Mild (13°)	T12-L1 (T10-L2)	I
6	F	59	Spinal stenosis	L5-S1	Mild (16°)	L3 (L2-L4)	I
7	F	70	Spinal stenosis	L2-S1	Very Mild (4°)	L2 (T12-L4)	II
8	M	73	Spinal stenosis	L3-L5	None (0°)	None	I
9	F	51	Scoliosis, degenerative, Second, acquired	T9-S2 &ILIUM	Severe (57°)	L2 (T12-L3)	II

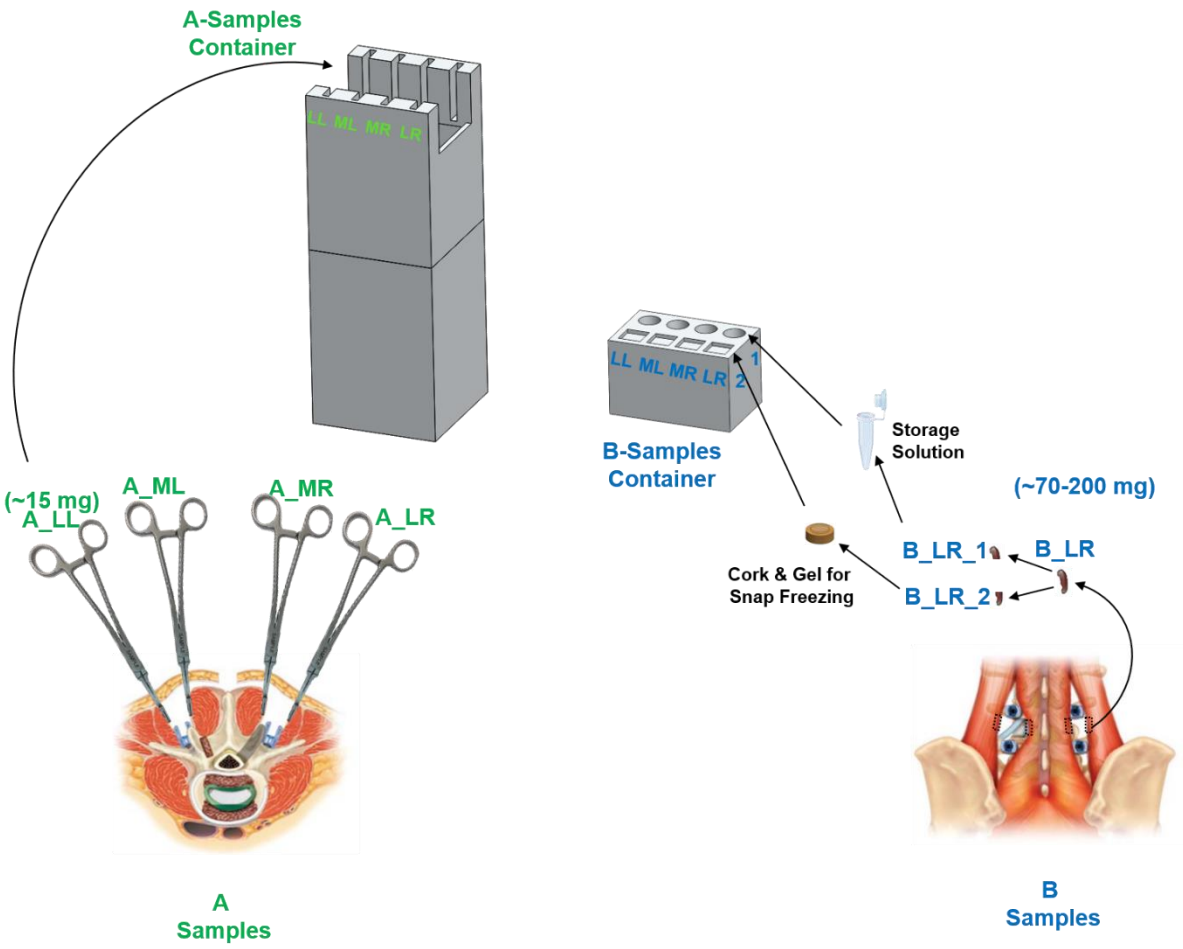

Figure 4-1. Biopsies collected per each patient. Type A biopsies needed a special biopsy clamp for measurement of in situ sarcomere length, while Type B biopsies were obtained through a blunt cut and were divided into two halves: one half (Type B1) was used for passive stiffness testing, while the other half (Type B2) was snap frozen for histopathological analysis. Overall, four Type A, four Type B1, and four Type B2 biopsies were collected from each patient, all at L4-L5, and from left longissimus (LL), left multifidus (ML), right multifidus (MR), and right longissimus (LR).

4.2.2 Logistics for Muscle Biopsy Acquisition

Acquisition and processing of the human biopsies described above and transferring them to the lab required special handling and tools that we developed specifically for this project. Details for some of these items are described in the following sections.

4.2.2.1 Clamp for Type A Biopsies

To measure the in situ sarcomere length, a special muscle biopsy clamp was required to provide firm grip onto the muscle and preserve the in situ tension within the biopsy while not allowing it to shrink. Using medical grade stainless steel 316L, we developed a prototype (Figure 4-2) based on the clamp described by Ward et al. [236]. The functionality of the clamp was validated on a rat rectus femoris where the clamp proved to preserve the in situ sarcomere length successfully (see Appendix B3 on page 233). The clamp was medical grade and ready to use. The policy of Vancouver General Hospital, however, required the clamp to be provided through a commercial biomedical manufacturer. In collaboration with Medtronic engineers, we improved the design of the muscle clamp to have a longer tongue, thinner tips, and narrower width for better accessibility (Figure 4-3). Medtronic generously manufactured five sets of these clamps (20 clamps: three sets of four clamps for usage in Vancouver General Hospital and two sets of four clamps for usage in Toronto Western Hospital). For each patient a set of four clamps was needed to collect biopsies from longissimus left, multifidus left, longissimus right, and multifidus right (Figure 4-1).

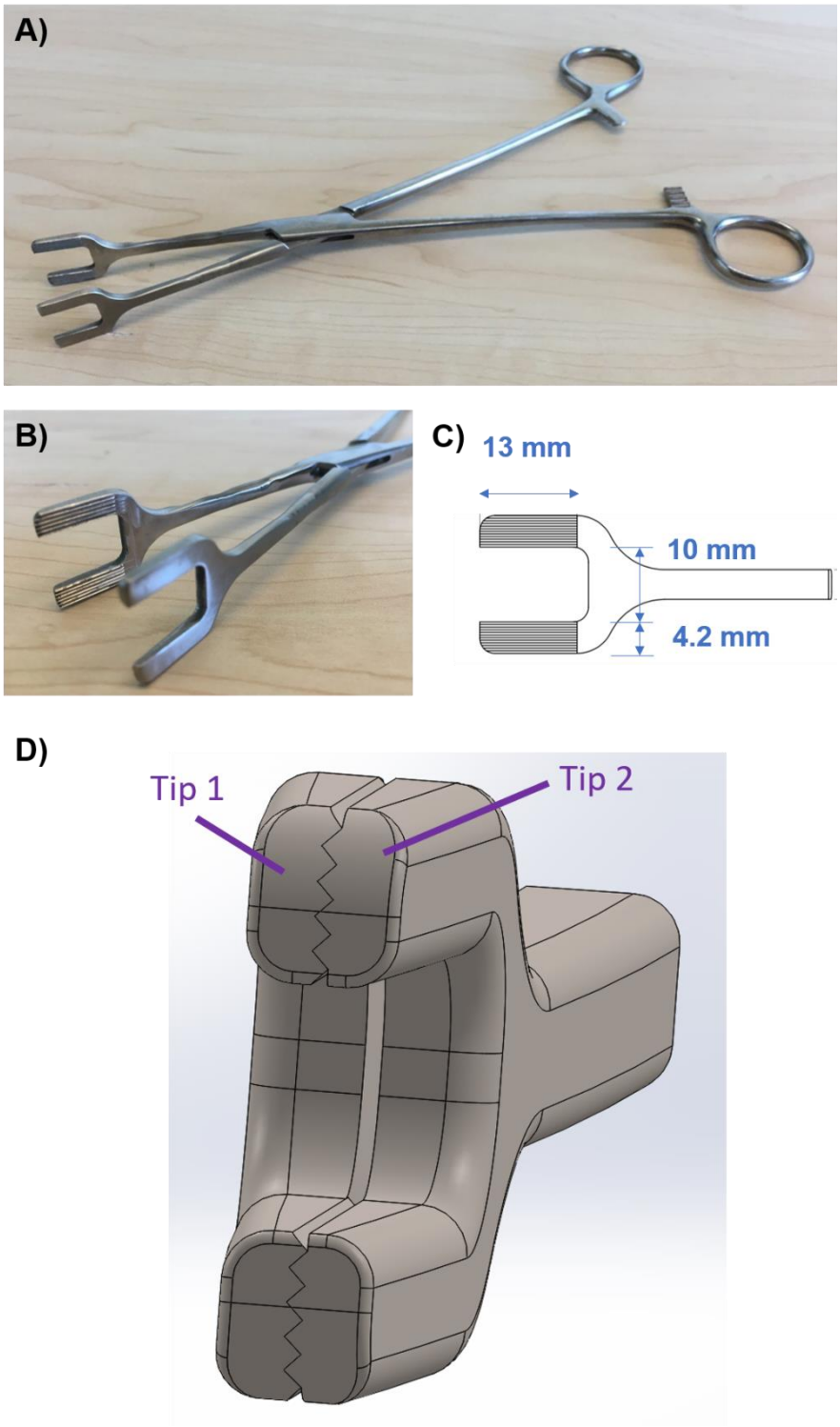

Figure 4-2. House-made clamp developed for measurement of in situ sarcomere length.

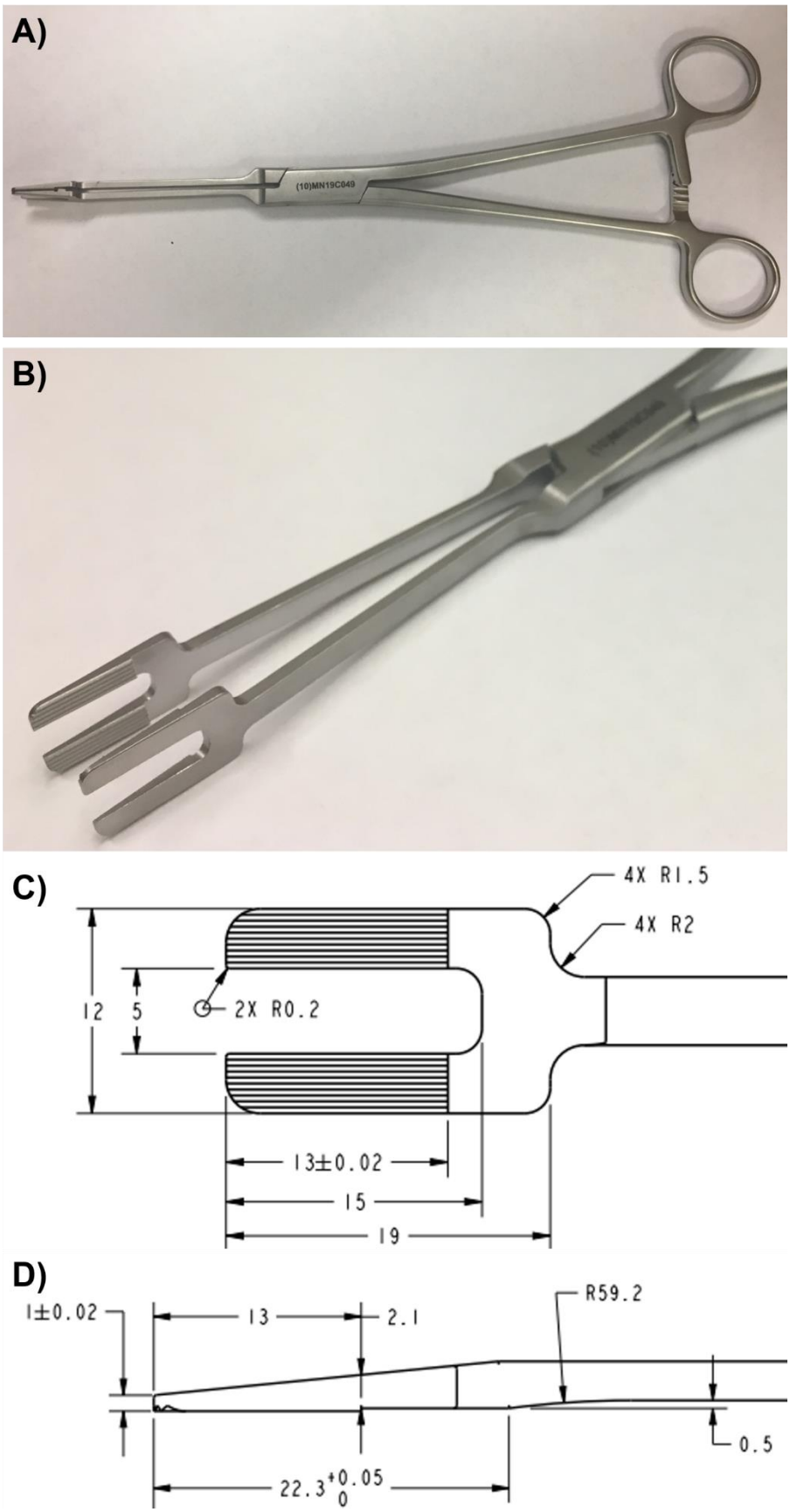

Figure 4-3. The muscle biopsy clamp developed in collaboration with Medtronic engineers and manufactured by Medtronic (A). We made the tongue longer (B) with narrower width (C) and thinner tips (D) for better accessibility and functionality.

4.2.2.2 Primary and Secondary Containers for Type A Biopsies

Immediately after collection of Type A biopsies, the biopsies maintained by the clamps were required to be immersed into formaldehyde for tissue fixation. We designed and manufactured a Type A biopsy container to hold the clamps stable while allowing their tips to float inside tubes filled by formaldehyde (Figure 4-4).

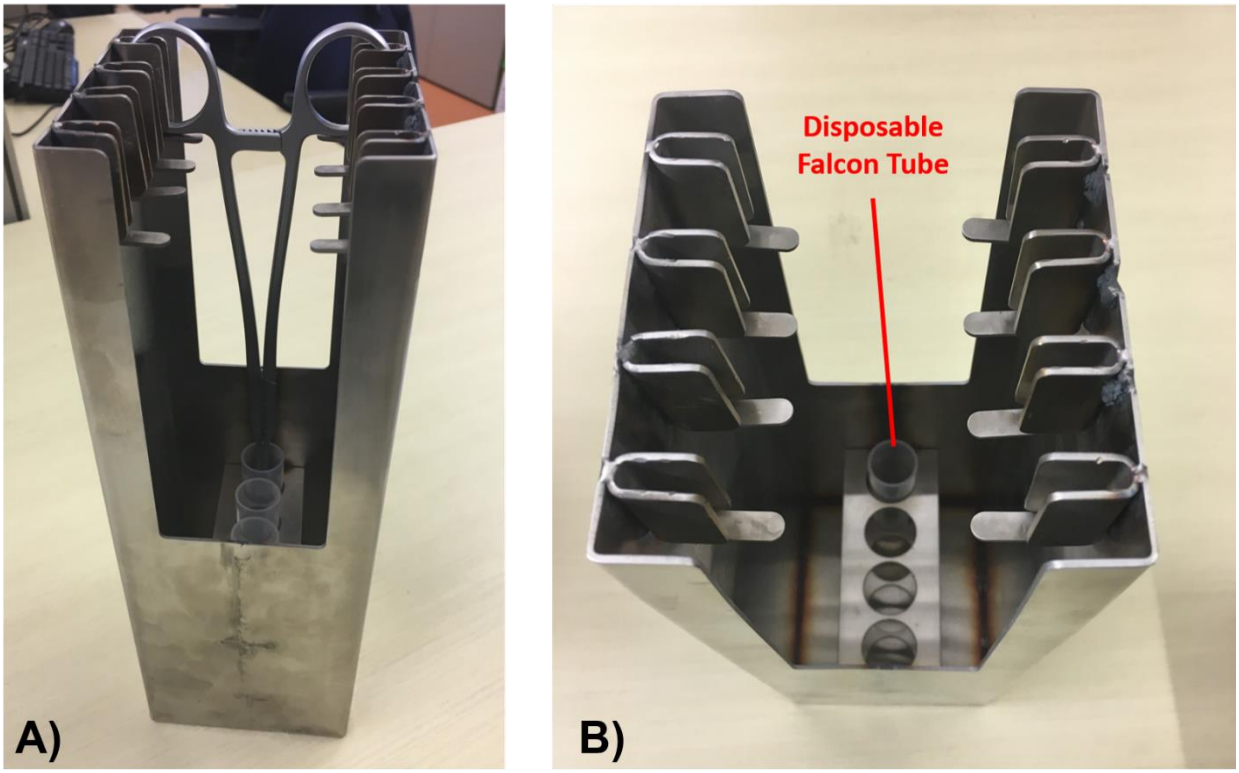

Figure 4-4. Primary Type A biopsy container. It holds the clamps stable (A) while allowing their tips to float inside tubes filled by formaldehyde (B).

Per the operating room policy of the Vancouver General Hospital, the containers needed to be cleaned, sterilized, and brought inside the operating room by the medical device reprocessing department (MDRD). To qualify for their cleaning protocols, all containers were made out of stainless steel 316L. Sheet metal was water cut, bent, and TIG (tungsten inert gas) welded to

make the outside shell. The welding was of high quality to seal the container and to be free from porosity or tiny holes as potential sites of germs. A rack was welded inside to maintain formaldehyde containing tubes in place and stable. Using a customized aluminum comb, a series of hangers were spot welded in parallel for placement of the clamps. Provision of the large openings at the sides was for easier access in placement/removal of the tubes and reduction of the container overall weight (Figure 4-4).

A liquid-tight secondary Type A container was required to encompass the primary Type-A container (Figure 4-5). This added an extra protection layer to protect spillage of the formaldehyde outside the containers on the floor. The tight lid of the secondary container also helped to reduce exposure to formaldehyde vapors. The lid was initially made from polypropylene; however, the high temperature through sterilization made it shrink. Therefore, it was replaced by a 316L stainless steel lid.

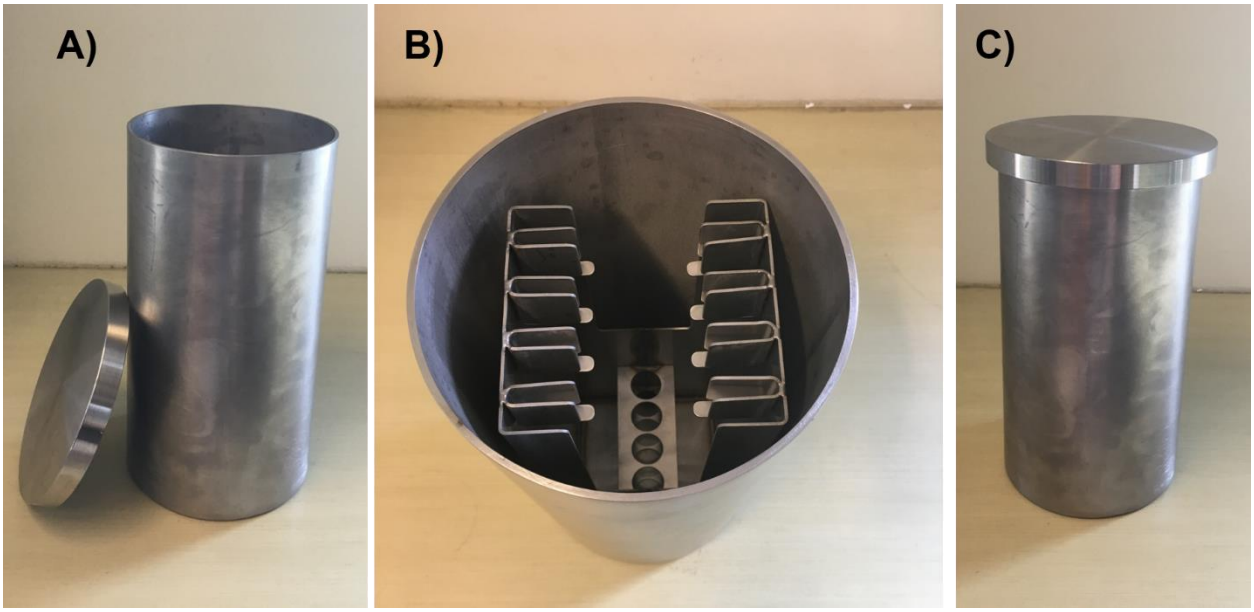

Figure 4-5. Liquid-tight secondary Type A container.

4.2.2.3 Primary and Secondary Containers for Type B Biopsies

Collection of Type B biopsies did not require any clamp. Biopsies with an approximate size of 5mm x 5mm x 10 mm were obtained through blunt cuts, divided in half by the surgeon, and handed to the nurse in the operating room. All eight pieces were placed inside falcon tubes: four containing a dissection solution (Type B1) and four containing phosphate buffered saline (Type B2). A Type B container was necessary for keeping the falcon tubes upright preventing a potential fall and/or spillage (Figure 4-6). The primary Type B container was made as compact as possible to be housed conveniently inside a secondary Type B container filled in half with ice (Figure 4-7).

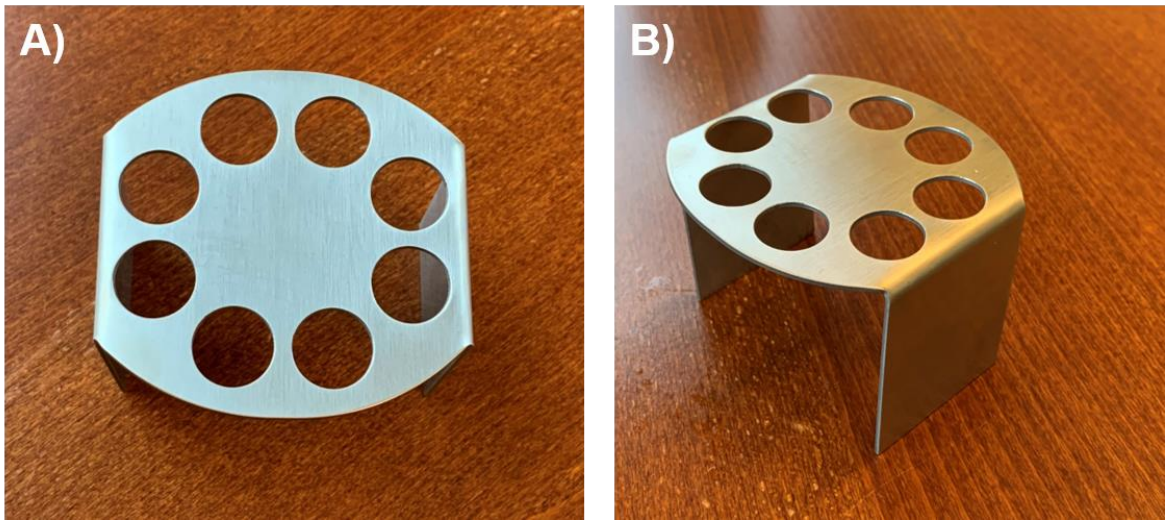

Figure 4-6. Primary Type B biopsy container from top view (A) and isometric view (B).

The secondary Type B container had two functions; first, to add an extra layer of protection in case of spillage; and second, to maintain the inside temperature at 0° C for better preservation of the biopsies until they were transferred to the lab for processing (which took in some cases up to two hours). No commercial insulated container was found to guarantee being safely autoclavable for sterilization purposes. Therefore, we built a customized version entirely out of stainless steel

316L. The container consisted of an outer shell and an inner shell with a gap of half an inch in between (Figure 4-7). The two shells were connected at the top via a donut shape plate with TIG weld. Although a vacuum between the two shells would act as a better insulator, the air itself was sufficient in reducing the rate of heat transfer and preserving the ice inside the container for a couple of hours. As all these containers needed to be carried inside a transport box by the researcher, minimizing their size and weight was constantly considered during the design stage.

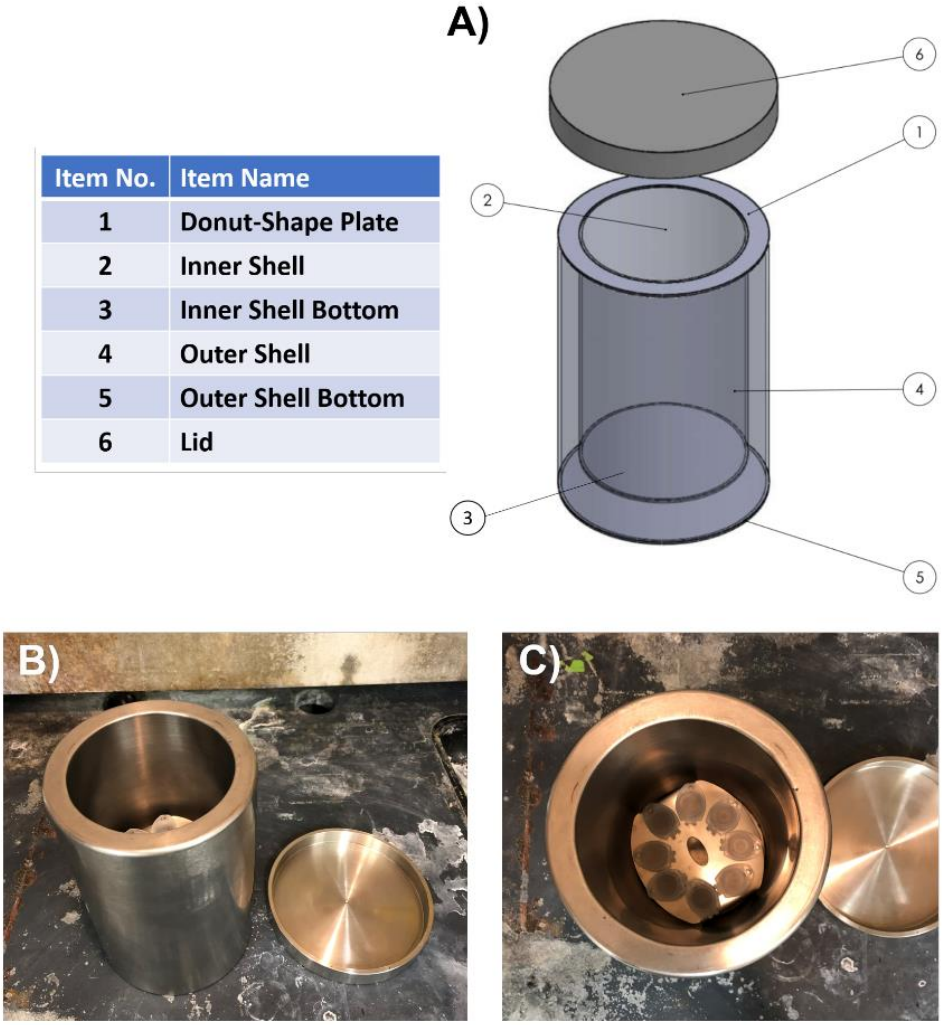

Item No.	Item Name
1	Donut-Shape Plate
2	Inner Shell
3	Inner Shell Bottom
4	Outer Shell
5	Outer Shell Bottom
6	Lid

Figure 4-7. Secondary type B biopsy container. The double layer structure of this container with capsulated air in between the inner and the outer shells acted as a heat insulator.

4.2.2.4 Dewar Support for Isopentane Container

For histopathology, snap freezing the muscle specimens immediately after collection was ideal so as to minimize tissue degradation and loss of biological information. For snap freezing, liquid nitrogen is required to bring down the temperature of isopentane close to its freezing point (~-160 °C). Muscle biopsies were mounted on a cork covered by Tragacanth gel and dropped inside the isopentane for a minute or so and then transferred to a dewar containing dry ice (~-78 °C) until later stored at -80 C° freezers. This method is the gold standard as it is associated with the least freezing artifacts compared to other methods.

Cooling down the isopentane can be achieved by placing a metal cup containing isopentane inside a dewar filled with liquid nitrogen. For safety concerns, this is typically performed in histology labs by hanging isopentane cup via ropes from a stand so hands are not in direct contact with the cold metal cup and also risk of spillage and contamination is minimized (Figure 4-8a). Snap freezing was not allowed inside the operating room, but for performing that outside the operating room the safety regulations of pathology department required us to make a safe and stable replacement for the stand and rope system. Usage of a handle similar to the one shown in Figure 4-8b was not approved for its risk of fall and spillage when placed on a table. We designed and manufactured a dewar support system (Figure 4-9) using stainless steel 316L metal sheets and TIG welding, which successfully passed the required safety standards.

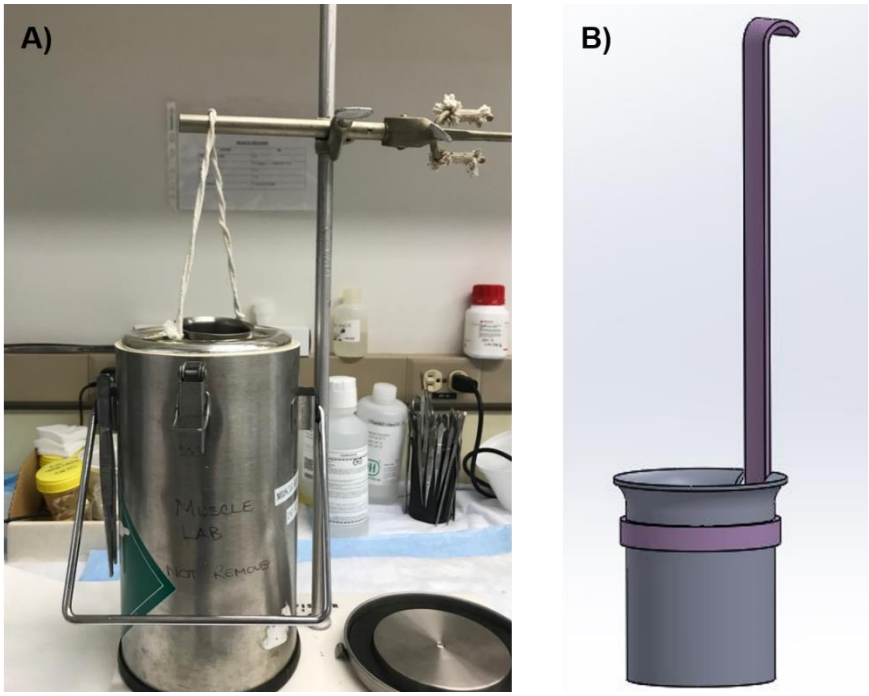

Figure 4-8. Methods for handling the cup filled with isopentane and cold by liquid nitrogen. In muscle labs the stand and rope system is commonly used (A). The proposed alternative method (B) was not approved for its risk of fall and spillage when placed on a table.

Our dewar support system is currently used for snap freezing outside the operating room of Toronto Western Hospital, where we started a parallel study through collaboration with our colleagues at the University of Toronto and the University of Guelph. The operating room policy of Vancouver General Hospital, however, did not approve any tissue processing outside the operating room. Instead, fortunately, they have recently granted a preliminary approval for using the suction tube system which was previously dedicated to clinical specimens only. Through the suction tube system, the biopsies could be transferred directly to the pathology department in less than a couple of minutes. Not only will this fast transferring system allow immediate snap freezing (i.e. less than 10 minutes after harvest), but also it will enable other forms of tissue processing including those required for single cell transcriptomic or mRNA analysis.

Figure 4-9. Dewar support system developed for cooling isopentane inside the dewar filled with liquid nitrogen.

4.2.2.5 Transport Box

All containers and biopsies were required to be transported in a sealed box providing extra level of protection from a potential spillage and contamination (Figure 4-10). As per standard operating room procedures, a member of the operating room staff then ordered a hospital porter to retrieve the specimens (i.e. the entire transport box) and deliver directly to the Anatomic Pathology Department for assigning an accession (tracking) number. Research staff were then allowed to take the transport box to the lab for tissue processing and testing.

Figure 4-10. Transport box for safe transportation of collected muscle biopsies and their containers.

4.2.3 Biopsy Acquisition and Testing

4.2.3.1 Biopsy Type A – In Situ Sarcomere Length

Inside the operating room, immediately after the biopsies were collected, the clamps were transferred into Type-A-Samples container filled with formaldehyde such that the biopsies were thoroughly immersed (see Appendix B4&5 for more details on biopsy acquisition). After more than 48 hours, the fixated biopsies were removed from the clamps and dissected under a stereomicroscope (Nikon, 0.63 X, Japan) to separate muscle fiber bundles. Using a single mode fiber-coupled diode laser (S1FC660, Thorlabs, Newton, NJ,USA) with a wavelength of 660 nm and collimated beam diameter of 0.8 mm, each fiber bundle was transilluminated and the resulting diffraction pattern was used for calculation of its in situ sarcomere length. From each biopsy, three fiber bundles were tested and the average was considered as the in situ sarcomere length of that biopsy.

4.2.3.2 Biopsy Type B1 – Passive Elastic Modulus & Slack Sarcomere Length

One half of Type B biopsies (Type B1), which were provided through a blunt cut, were placed inside falcon tubes filled with a dissecting solution with the same contents as introduced by Noonan et al. [237]. The tubes were immediately placed inside an ice container at 0° C; and within two hours were transferred to a storage solution containing (mmol): KPr (170), Na2ATP (21.2), imidazole (10), MgCl2 (5.3), EGTA (5.0), glutathione (2.5), NaN3 (1), leupeptin (0.05) and 50% (v/v) glycerol and were kept at 4° C for 24 hours. Afterwards, they were preserved at -20° C until they were tested for passive stiffness which took place within two weeks.

The same methodology as described in section 2.2.1 was followed for mechanical testing. Briefly, from each biopsy, a minimum of three fibers and six fiber bundles (14±7 fibers) were

extracted. Each fiber/fiber bundle was mounted and tied onto two pins, one pin attached to a force transducer (400A, Aurora Scientific, Aurora, Ontario, Canada) and the other pin attached to a length controller (CRK523PMAP, Oriental Motor, Torrance, CA, USA)(Figure 2-2). The fibers/fiber bundles were stretched until reaching the slack length, where passive force started to develop. At this point, the slack sarcomere length was measured with a resolution of ~10 nm from the diffraction pattern generated when transilluminating the fibers/fiber bundles using a diode laser. Also, top-view and side-view diameters of the fiber/fiber bundle at three points across the fiber/fiber bundle were measured with a resolution of 1 micron using a cross hair reticle inside the eye piece of a stereo microscope (SteREO Discovery.V8, Zeiss, Plan-Apochromat 0.63x). Hereafter, each fiber/fiber bundle was stretched by 4 to 8 increments, each applying 10% strain at a rate of 10% strain per second, followed by four minutes relaxation (Figure 2-3A). The sarcomere lengths and force readings at the end of each increment were used to calculate the engineering strains and stresses, respectively. A tangent to the strain-stress curve at 30% stain was used to represent the passive elastic modulus of the fiber/fiber bundle (Figure 2-3B).

4.2.3.3 Biopsy Type B2 – Histopathology

The other half of Type B biopsies (Type B2) was placed in falcon tubes containing phosphate buffered saline. The tubes were transferred on ice to the lab and were snap frozen within two hours after harvest by placing them on a cork covered with Tragacanth gel and dropped into isopentane cooled by liquid nitrogen. The samples were stored at -80 °C until they were later sectioned with a cryostat to 10μm thickness and placed on slides for immunostaining.

The staining performed included hematoxylin and eosin (HE), gomori trichrome (GT), nicotinamide adenine dinucleotide hydrogen tetrazonium reductase (NADH), succinic dehydrogenase (SDH), cytochromec oxidase (COX) enzyme histochemistry, fast and slow myosin, and neonatal myosin. The degree and main types of abnormalities were identified for all biopsies. The staining was performed by the pathology department staff in Vancouver General Hospital and were analyzed by an experienced myo-neuropathologist, Dr. Peter Schutz.

4.3 Results

All biopsies were collected as planned in the study design; the only exceptions were Type B2 biopsies for patient 1 (which were used as Type B1 biopsies due to their small size) and longissimus biopsies, Type A and B, for patient 3 (as the surgical exposure was only limited to multifidus muscle).

4.3.1 In Situ Sarcomere Length

In total, 34 type A biopsies were collected. Three biopsies consisted of non-muscle tissue although they were collected by the surgeon from the same anatomical locations that other biopsies were taken. From the remaining 31 biopsies, the average in situ sarcomere length for each patient ranged between 1.94 μm to 3.39 μm for multifidus and 1.99 μm to 3.11 μm for longissimus (Figure 4-11). In general, within each individual the in situ sarcomere lengths of the muscles at the convex side were not necessarily the same as those in the concave side. With the large variability within each group, no salient difference between the three patient groups could be detected. Due to small number of patients recruited per the three specified patient groups, no statistical comparison was made.

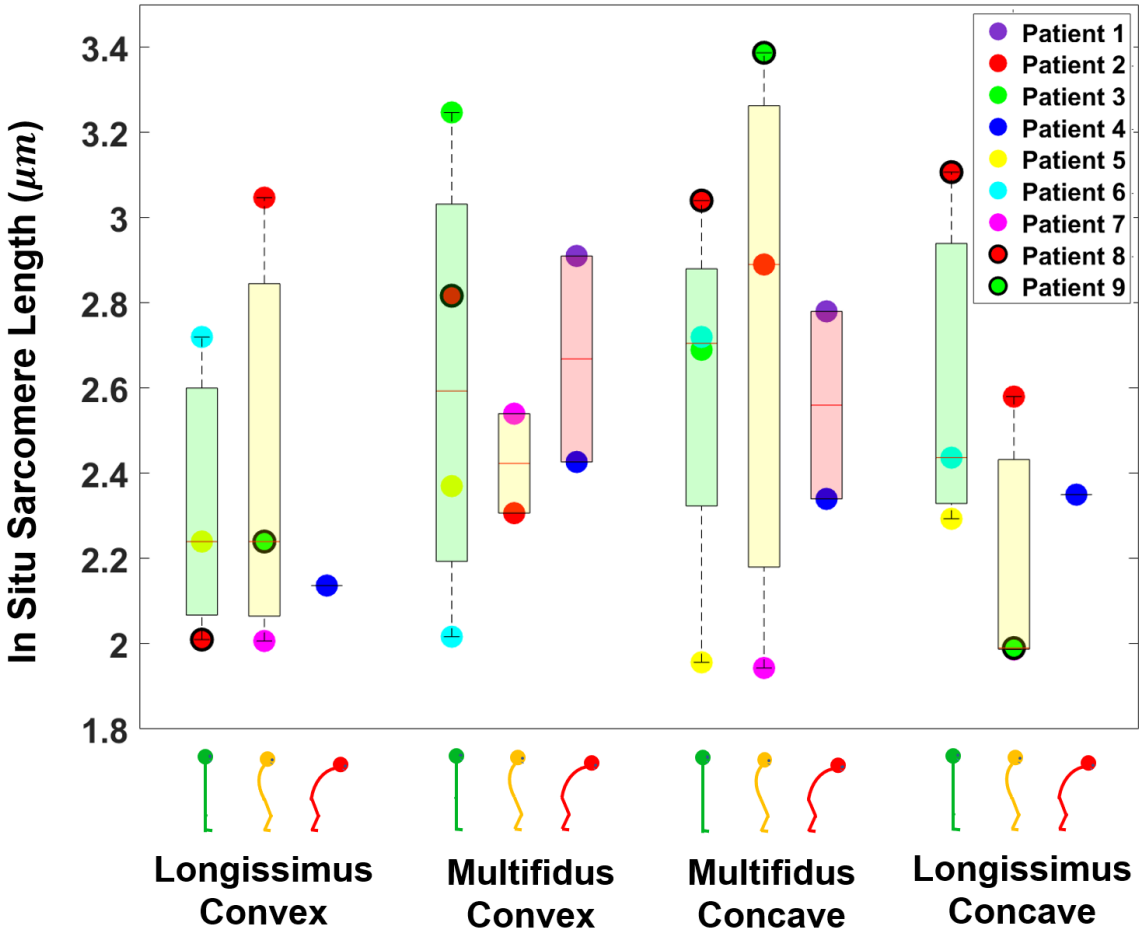

Figure 4-11. In situ sarcomere length represented by boxplots for each patient group. The red lines denote the medians, the heights of the boxes indicate the interquartile ranges and each dot is the average of three measurements for each biopsy (the three measurements were quite close for almost all biopsies). Green, yellow, and red icons represent patient groups I, II, and III, respectively.

4.3.2 Passive Elastic Modulus & Slack Sarcomere Length

In total, 87 fibers and 171 fiber bundles were mechanically tested. The elastic modulus for the single fibers ranged between 2 kPa to 115 kPa for multifidus and 5 kPa to 94 kPa for longissimus. The elastic modulus measured for each single fiber is represented by a dot in Figure 4-12 based on the patient group, muscle group, and the side of the body the fiber belonged to. For multifidus, the concave and convex sides combined, the median(IQR) of single fibers elastic moduli was 37(23) kPa, 32(36) kPa, and 27(25) kPa for patient groups I, II, and III, respectively; while for longissimus, those values were 36(31) kPa, 31(21) kPa, and 13(10) kPa.

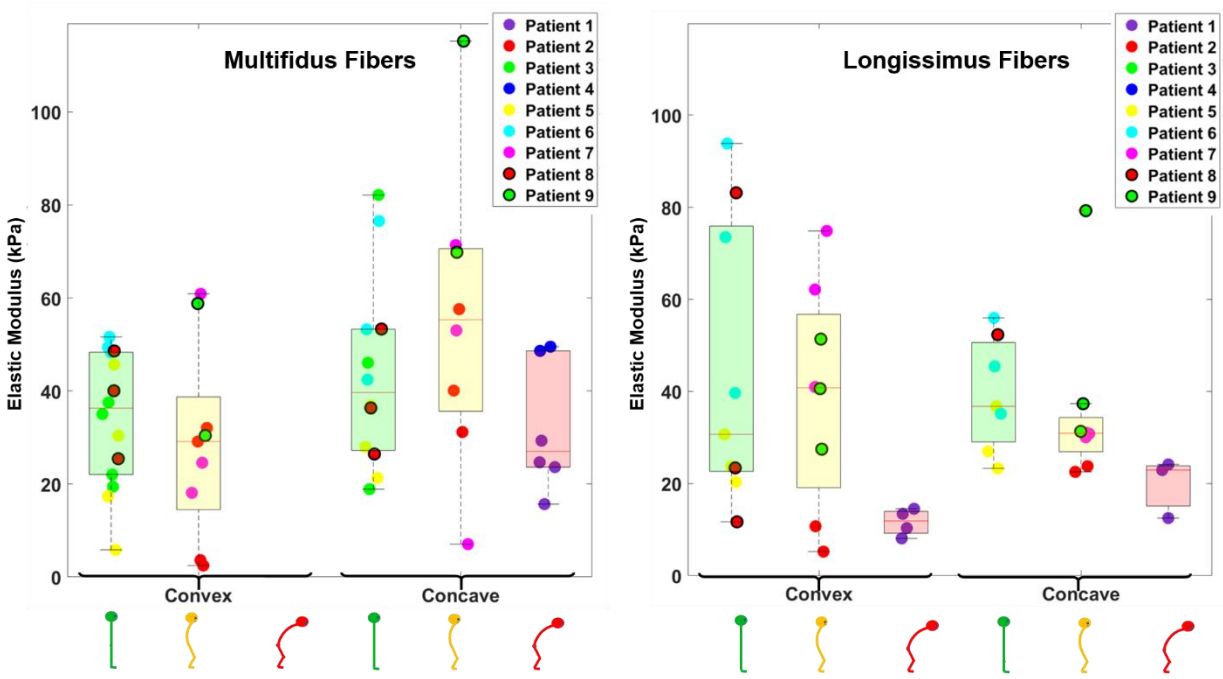

Figure 4-12. Elastic modulus of single fibers represented by boxplots for each patient group. The red lines denote the medians, the heights of the boxes indicate the interquartile ranges and each dot represents elastic modulus value for a tested fiber. Green, yellow, and red icons represent patient groups I, II, and III, respectively.

The elastic modulus for fiber bundles ranged between 6 kPa and 2426 kPa for multifidus and 3 kPa to 2375 kPa for longissimus. The elastic modulus measured for each fiber bundle is represented by a dot in Figure 4-13 based on the patient group, muscle group, and the side of the

body. For multifidus, when the concave and convex sides were combined, the median (IQR) of fiber bundles elastic moduli was 46(89) kPa, 57(61) kPa, and 113(77) kPa for patient groups I, II, and III, respectively; while for longissimus, those values were 38(50) kPa, 102(181) kPa, and 42(89) kPa. Seventeen from 92 tested bundles (18%) in multifidus and 20 from 79 bundles (25%) in longissimus exhibited larger stiffnesses than 120 kPa (an approximate threshold for outliers based on Ward et al.'s data [22]). No statistical comparison was made between the three patient groups due to the small number of patients recruited per each group due to COVID-19.

Slack sarcomere length, defined as the starting point of the passive force-length curve, was recorded for both single fibers and fiber bundles (Figure 4-14). The slack sarcomere length measured for each fiber or fiber bundle is represented by a dot in Figure 4-14 based on the patient group, muscle group, and the side of the body the bundle belonged to. The median (IQR) slack sarcomere length for multifidus fibers, when the concave and convex sides were combined, was 2.10(0.12) μm, 2.08(0.33) μm, and 2.24(0.39) μm for patient groups I, II, and III, respectively; while for longissimus fibers, those values were 2.30(0.24) μm, 2.03(0.17) μm, and 1.95(0.14) μm. Similarly, these values for multifidus fiber bundles were 2.00(0.17) μm, 2.05(0.16) μm, and 2.00(0.34) μm; but for longissimus fiber bundles were 2.07(0.21) μm, 1.98(0.22) μm, and 1.95(0.28) μm. Both fibers and fiber bundles exhibited a large range of 1.8-2.8 μm for the slack sarcomere length.

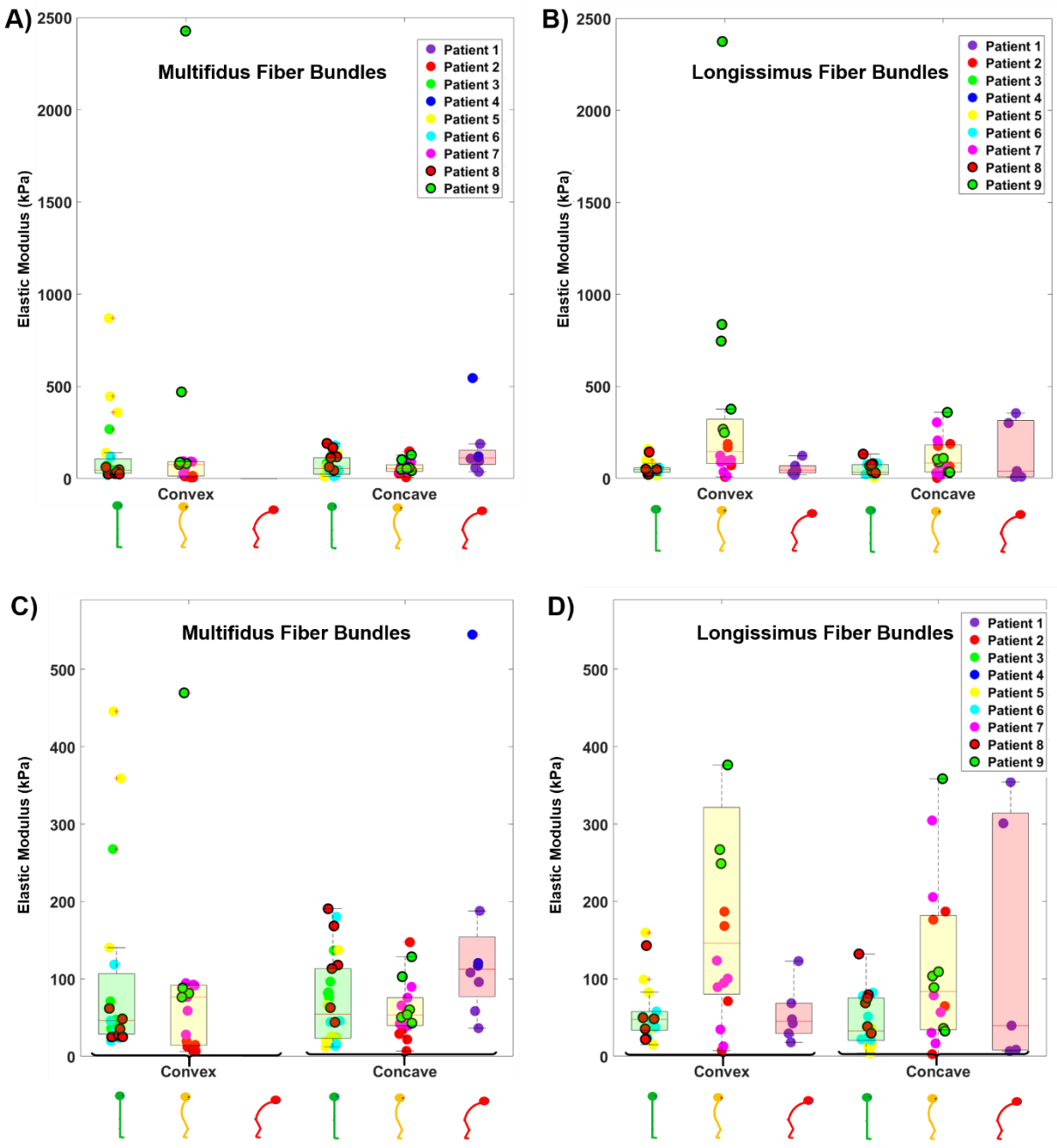

Figure 4-13. Elastic modulus of fiber bundles represented by boxplots for each patient group. (A) and (B) are the same plots as (C) and (D) but with a larger scale on the y-Axis to encompass all data points. The red lines denote the medians, the heights of the boxes indicate the interquartile ranges and each dot represents elastic modulus value for a tested fiber. Green, yellow, and red icons represent patient groups I, II, and III, respectively.

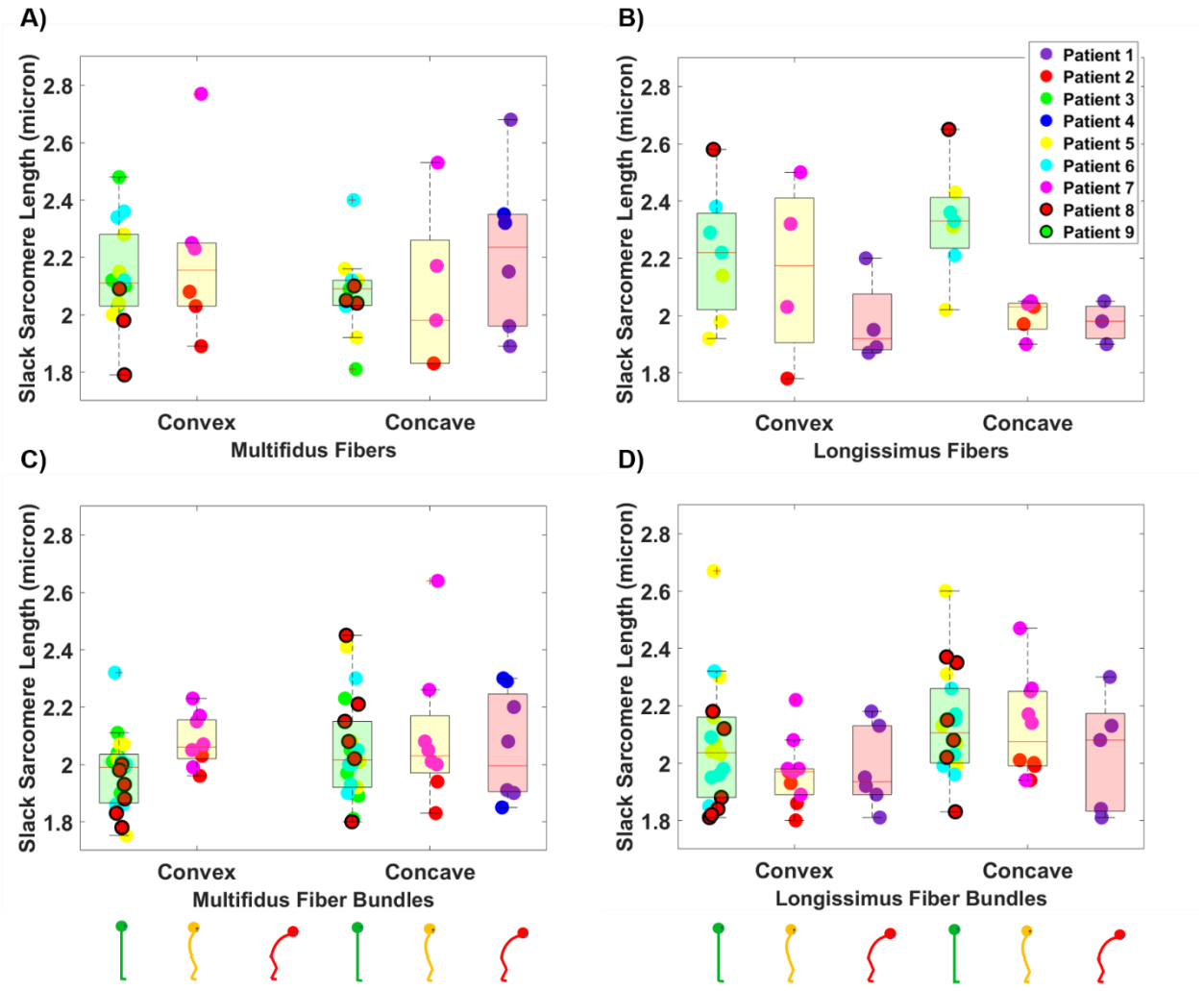

Figure 4-14. Slack sarcomere length represented by boxplots for each patient group. The red lines denote the medians, the heights of the boxes indicate the interquartile ranges and each dot represents elastic modulus value for a tested fiber. Green, yellow, and red icons represent patient groups I, II, and III, respectively.

4.3.3 Histopathology Properties

Twenty-eight biopsies were successfully frozen, sectioned, stained, and reviewed by a myo-neuropathologist blinded to patient demographics. The quality of muscle tissue looked normal for only one patient (patient 6, Figure 4-15). Fibrofatty component varied across biopsies (Figure 4-16). A variety of case-specific abnormalities were observed **(**Table 4-2**)** including core/targets and cox-negative fibers (Patient 2, Figure 4-17), cores and rods (patient 3, Figure 4-18), severe atrophy and fibrosis (patient 4, Figure 4-19), mitochondrial accumulations (patient 5, Figure 4-20), and moth-eaten fibers and pinprick fibers (patient 7, Figure 4-21). In general, the degree of abnormality was more severe in patients of group II and III **(**Table 4-3**).**

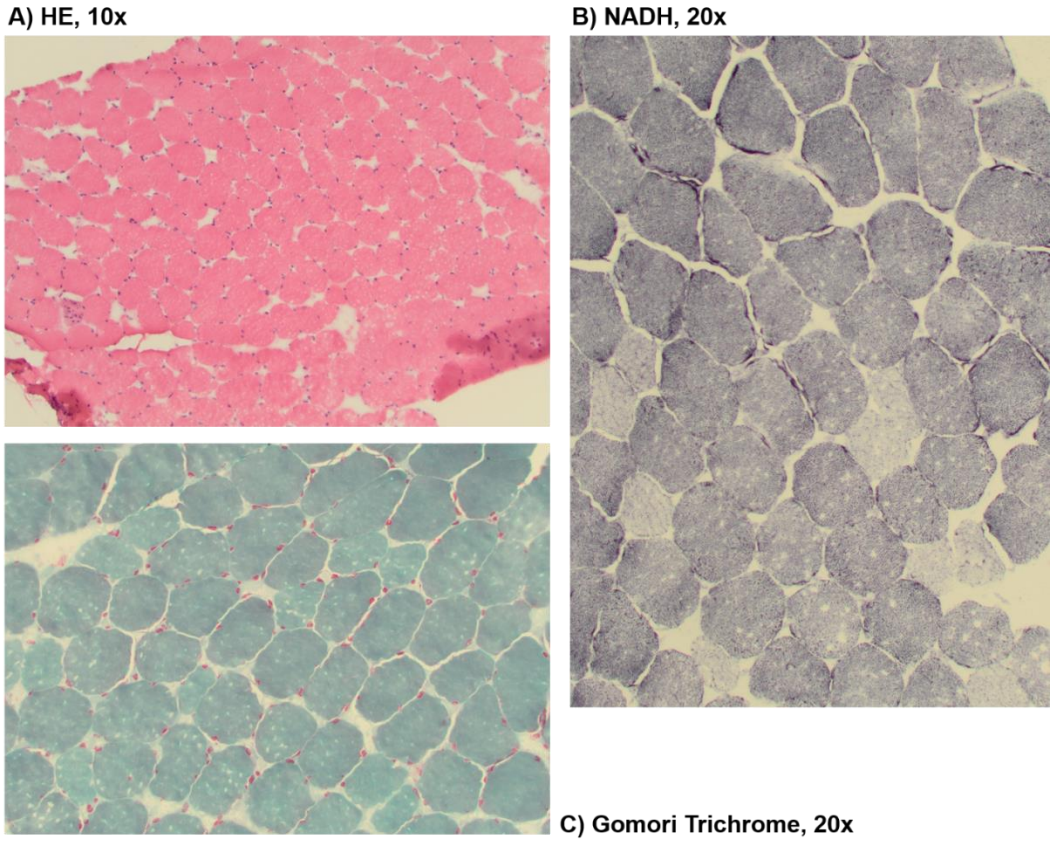

Figure 4-15. Normal muscle tissue in patient 6 as evident through A) HE, B) NADH, and C) Gomori Trichrome staining. The fibers are nicely packed with no irregularities in their shape or cellular structure.

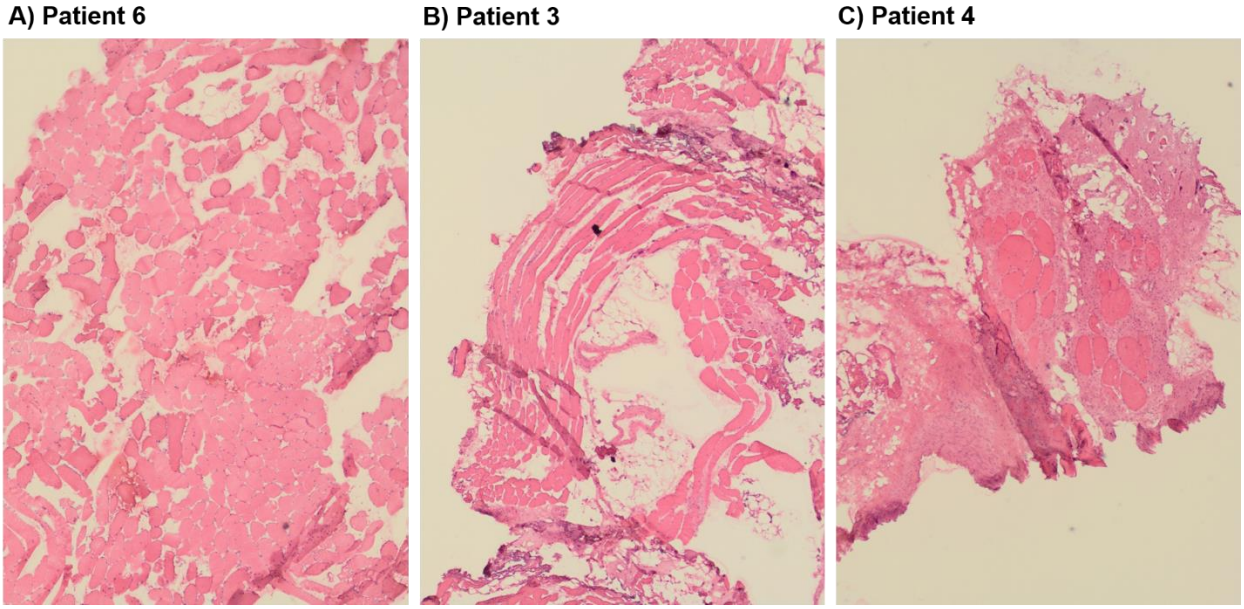

Figure 4-16. Fibrofatty component across different biopsies.

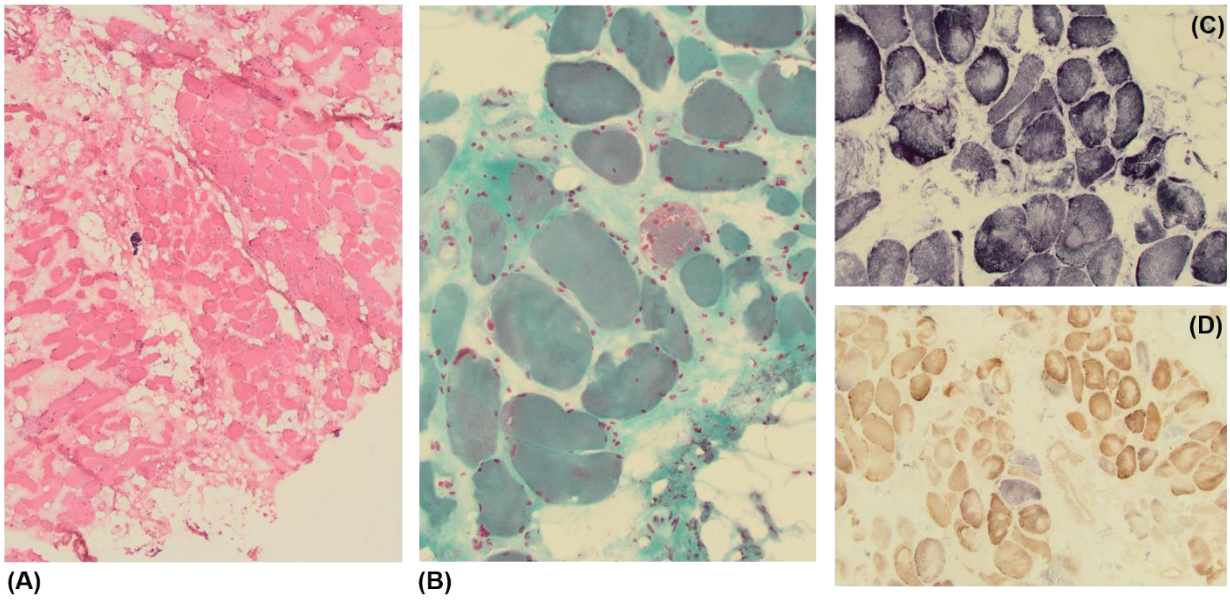

Figure 4-17. Core and targets and cox-negative fibers in convex-side multifidus of patient 2.

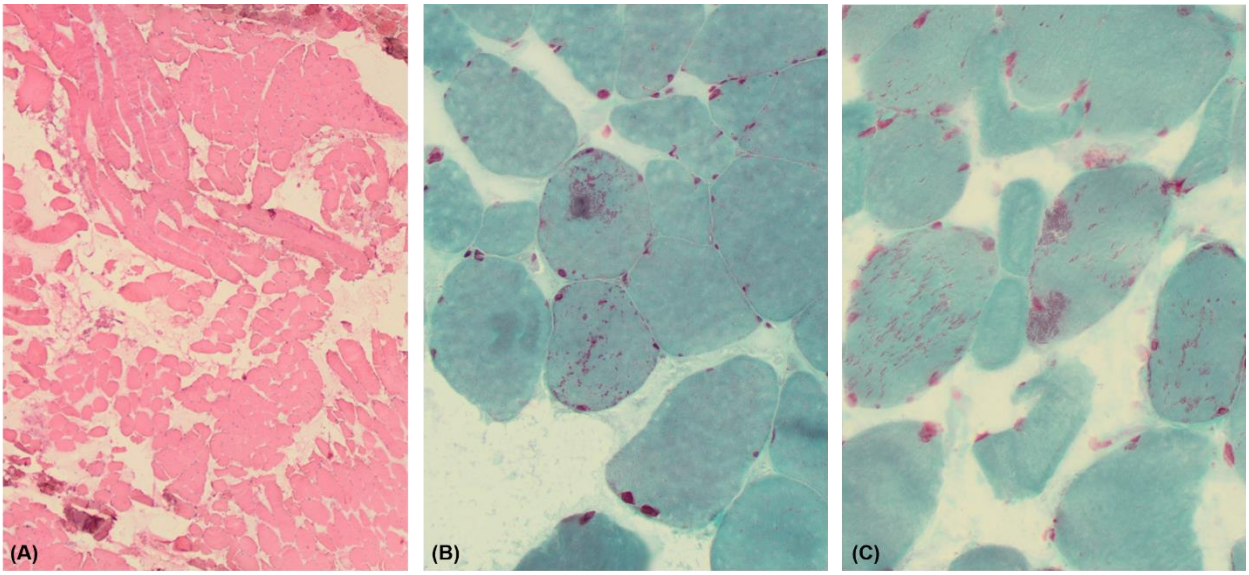

Figure 4-18. Cores and rods in convex multifidus of patient 3.

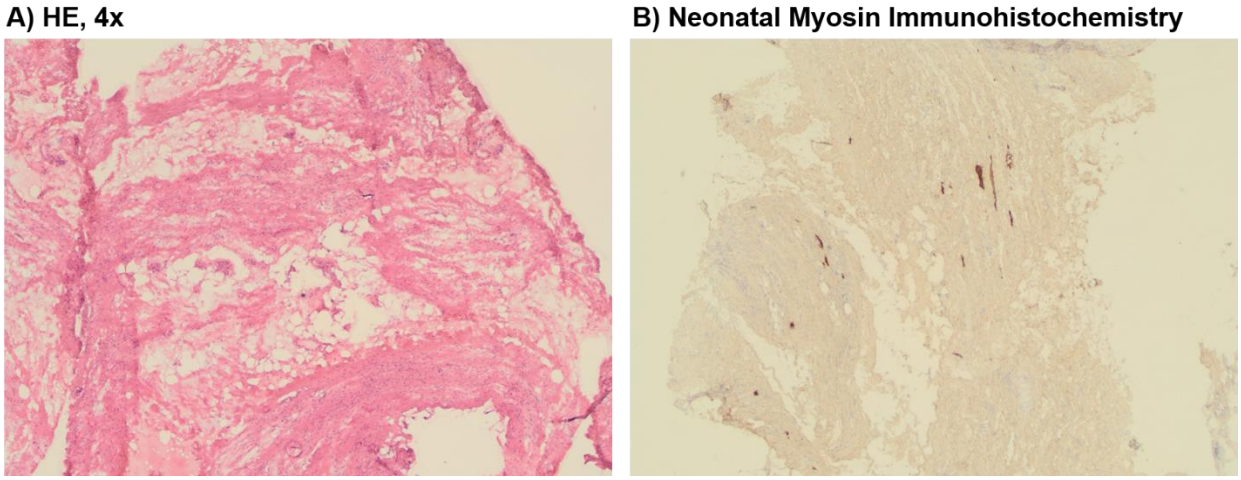

Figure 4-19. Severe Atrophy and Fibrosis in patient 4.

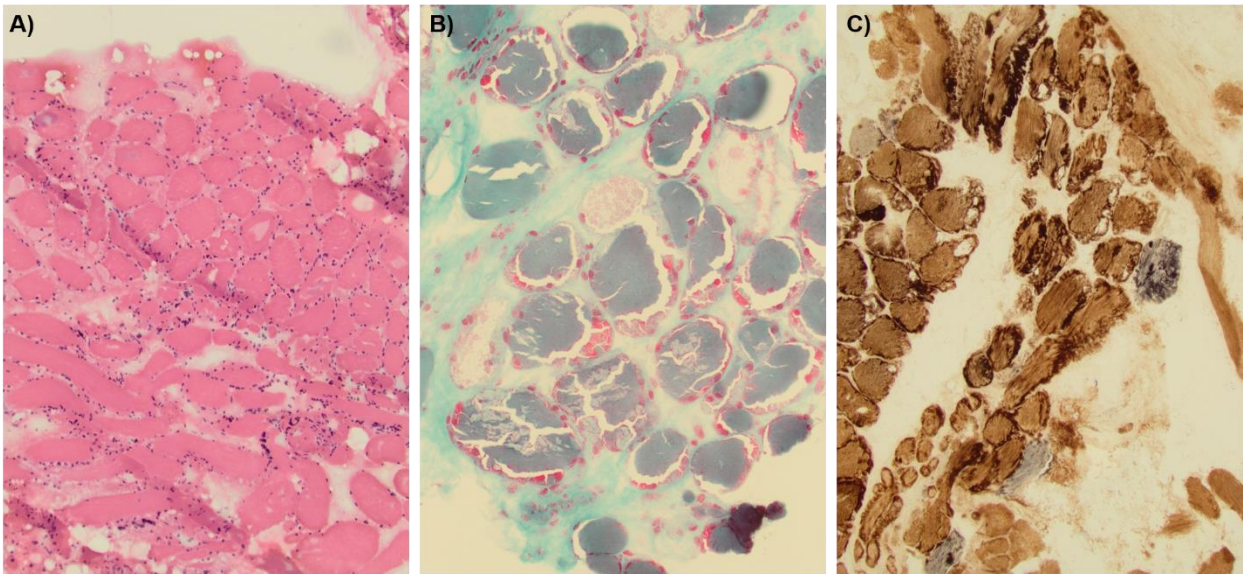

Figure 4-20. Mitochondrial Abnormalities in patient 5.

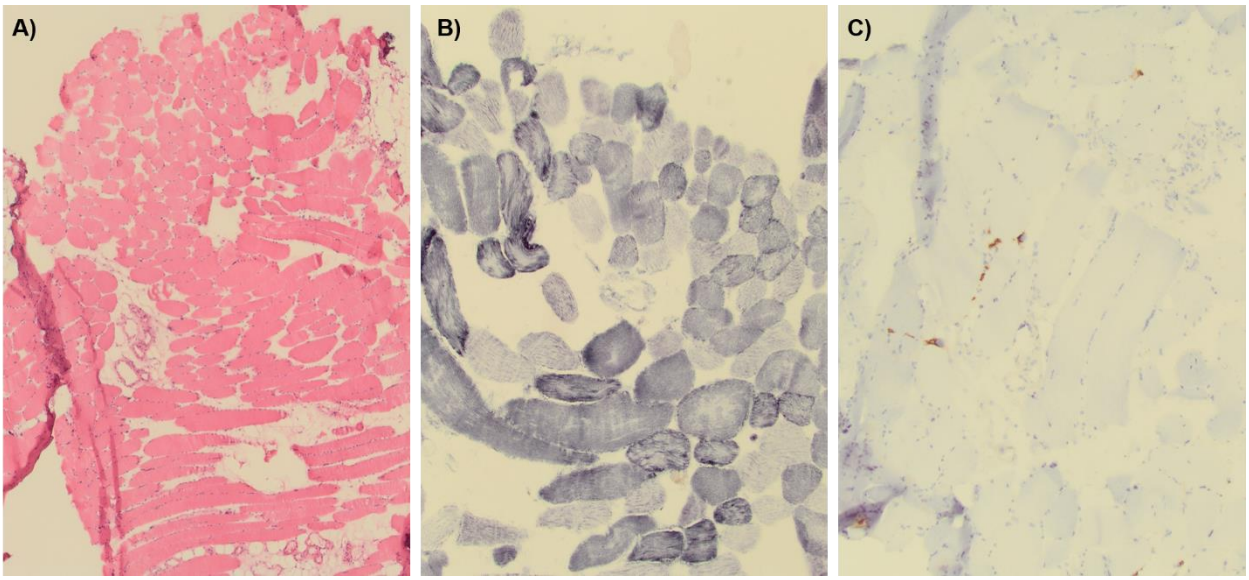

Figure 4-21. Mild moth-eaten fibers and pinprick fibers in convex multifidus of patient 7.

Table 4-2. Main abnormality types identified for each patient through histopathological evaluation.

Group	Patient	Longissimus Convex	Multifidus Convex	Multifidus Concave	Longissimus Concave
I	P3	N/A	Rods Cox-negative Core like	Rods Core like	N/A
	P5	Atrophic-fibers	Mitochondrial	Mitochondrial	Atrophic-fibers
	P6	None	None	None	N/A
	P8	Lobulated	Moth-eaten	Moth-eaten	Lobulated
II	P2	Cores	Cores, Cox-negative	Cores, Cox-negative	Cores
	P7	Moth-eaten Pinprick	Moth-eaten Pinprick	Moth-eaten Pinprick	Moth-eaten Pinprick
	P9	N/A	Rods and Cores	Irregular staining	N/A
III	P4	Fibrotic Replacement	Fibrotic Replacement	Fibrotic Replacement	Fibrotic Replacement

Table 4-3. Degree of histological abnormality for each patient.

Group	Patient	Longissimus Convex	Multifidus Convex	Multifidus Concave	Longissimus Concave
I	P3	N/A	Moderate	Moderate	N/A
	P5	Mild	Moderate	Moderate	Mild
	P6	Normal	Normal	Normal	N/A
	P8	Moderate	Minor	Minor	Moderate
II	P2	Moderate	Severe	Severe	Moderate
	P7	Minor	Minor	Minor	Minor
	P9	No Muscle	Moderate	Minor	Freezing Artifact
III	P4	Severe	Severe	Severe	Severe

4.4 Discussion

Decreased back extensor strength and muscle weakness are well recognized as key risk factors for adult spinal deformity, but it remains unclear what muscle properties are different in those patients that lead to such decreased strength. One reason for lack of our understanding of paraspinal muscles in adult deformity patients is the challenges associated with acquiring fresh human muscle biopsies, which are necessary for measurement of muscle properties including passive stiffness, slack sarcomere length, in situ sarcomere length, and specific tension. This study aimed to address those challenges to obtain the desired biopsies from spinal deformity patients and evaluate them biomechanically and histopathologically. Required tools and protocols were developed for paraspinal muscle biopsy acquisition and were successfully used and implemented at Vancouver General Hospital and Toronto Western Hospital. We were able to measure in situ sarcomere length, slack sarcomere length, and passive stiffness as well as performing histopathological assessments in nine patients. Although research halted due to COVID-19 limited our study to a small number of patients and did not allow a comprehensive comparison between the different categories of spinal deformity patients, some thought-provoking observations were made which provided important insight into the muscles of these patients.

The in situ sarcomere lengths measured in this study unveiled a broad range variation for paraspinal muscles. For example, in multifidus a minimum of 1.9 μm and maximum of 3.4 μm was observed. Such large variation for in situ sarcomere length can result in a substantially different behavior and amount of force a muscle produces, both actively and passively. Based on the well-known force-length curve, at a sarcomere length of ~2.8 for example, the amount of active force a muscle can produce when fully activated is two times larger than when the

sarcomere length is equal to ~1.8 μm or ~3.8 μm. A larger passive force is generated by a muscle whose in situ sarcomere length is 3.4 μm compared to when that is 1.9 μm. The extent of that difference though highly depends on the slack sarcomere length and the body posture. For shorter slack sarcomere lengths, larger passive forces will develop, especially for when the body goes to a flexed posture, where paraspinal extensor muscles experience greater elongation. Investigating the influence of in situ sarcomere length on spinal loading is not trivial with the complicated anatomy of the spine musculature and requires a musculoskeletal model, which is addressed in chapter 5 of the current manuscript.

In situ sarcomere length of paraspinal extensor muscles has been measured previously in live humans only by Ward et al. [156] and that was just for multifidus. In that study, the in situ sarcomere length for eight patients in prone position was 2.0 ± 0.2 μm and for five patients in flexed posture was 2.7 ± 0.1 μm; and the biopsies were taken from patients undergoing surgery with a variety of diagnosis (osseous, disc, or trauma). In our study, the in situ sarcomere lengths were measured for spinal deformity patients, where a large variation in that parameter was measured for both multifidus (1.9 μm - 3.4 μm) and longissimus (2.0 μm - 3.1 μm). Biopsies in the current study were taken from patients in a prone position. When comparing L3-S1 lordosis angles between standing pre-operatively (37 ± 5) and in prone position intra-operatively (38 ± 5, Table 4-4**),** no significant difference was found. Therefore, the large variation of in situ sarcomere length do not appear to be due to differences in postures at which biopsies were obtained. In this study, for the first time in situ sarcomere length of longissimus in live humans was measured. Furthermore, for the first time this parameter was measured for each patient at both convex and concave sides, which presented a difference between the two sides in some patients. Such difference could be from presence of coronal plane deformity in those patients.

Table 4-4. Comparison between lordosis angles of the patients when standing preoperatively and in prone position intraoperatively.

	L3-S1 Lordosis Angle (°)	
	Pre-Operative	**Intra-Operative**
Patient 1	39	N/A
Patient 2	47	43
Patient 3	38	37
Patient 4	33	38
Patient 5	36	41
Patient 6	34	32
Patient 7	36	40
Patient 8	31	31
Patient 9	40	N/A

In situ sarcomere length have also been measured in cadaveric studies. Ward et al. [156], in addition to their in vivo study, examined multifidus of eight cadavers and found an in situ sarcomere length of 2.27 ± 0.06 μm. Zwambag et al. [224] studied seven cadavers and found the in situ sarcomere length for multifidus to be 2.36 ± 0.05 μm, while for longissimus it was 2.41± 0.06 μm. The same measurement was made for longissimus in five cadavers investigated by Delp et al. [115] and a value of 2.31 ± 0.17 μm was reported. In a recent study, Bayoglu et al. [233] measured the in situ sarcomere length of multiple paraspinal muscles in one cadaver and found a value of 3.35 μm for multifidus and 3.57 μm for longissimus. While the cadavers used by Ward et al. [156] and Zwambag et al. [224] were all embalmed in a supine or a neutral anatomical posture, respectively, it is not stated at what posture the cadaver used by Bayoglu et al. [233] was embalmed. Bayoglu et al. noticed L5 was naturally fused to the sacrum in the cadaver they studied. Therefore, while the much larger values reported in their study may be due to the posture at which the cadaver in their study was embalmed (which is unknown), those large values may have a pathologic explanation (especially given that L5 was fused to sacrum in that cadaver) or simply reflect a natural variation. Nevertheless, with all these data, the measurements in our study fell within the range reported in previous studies.

The slack sarcomere length, which pinpoints the start of muscle passive force-length curve, also showed a large range in this study for both single fibers and fiber bundles of paraspinal muscles. This range was between 1.8 μm and 2.8 μm for single fibers and 1.8 μm to 2.7 μm for fiber bundles. Such values could strongly influence the amount of passive forces produced in a muscle and consequently influence the spinal loading. However, the extent of that influence, as stated for in situ sarcomere length, depends on other factors including the body posture, passive stiffness, and in situ sarcomere length, which will be explored by using a musculoskeletal model (chapter 5).

The slack sarcomere length of human posterior paraspinal muscles has been studied previously only by Ward et al. [25]. In multifidus, they found a mean value of 2.08 μm for single fibers and 2.25 μm for fiber bundles. The medians of the different patients in our study were also between 2.08 μm and 2.24 μm for single fibers and 2.00 μm and 2.05 μm for fiber bundles when convex and concave sides were combined. In longissimus, they observed a mean value of 2.25 μm and 2.17 μm for single fibers and fiber bundles, respectively; the medians in our study were between 1.95 μm and 2.30 μm for single fibers and 1.95 μm to 2.07 μm for fiber bundles, when convex and concave sides were combined.

The elastic modulus in this study was evaluated at both single fiber and fiber bundle levels. At the single fiber level, the medians for all groups were between 27 to 37 kPa (except in group III longissimus that exhibited a median of 13 kPa) when convex and concave sides were combined. The only previous study in the literature examining single fiber elastic modulus of human multifidus or/and longissimus also reported a value of 34 ± 2 kPa for multifidus and 33 ± 3 kPa for longissimus single fibers [25]. In their study, multifidus data came from 23 patients, while longissimus biopsies were collected from 7 patients. All biopsies were taken from patients

undergoing a spine surgery, but the diagnosis was not disclosed. The average values in their study and median values of our study are in good agreement for single fibers; however, the variation in our data seemed much greater. While a reason of larger variation could be possible pathological differences in patients between the two studies, another reason is that in our data, an individual test was considered as a data point, whereas in their analysis a data point represented the average of three single fibers tested from each biopsy. This resulted in an standard error of the mean(SEM) of 2 to 3 kPa in their data (which is smaller by its nature than if the standard deviation was reported), as opposed to an IQR of 10-36 kPa observed in our data.

The average value for single fiber elastic modulus measured to date in other human muscles ranges between ~20 to ~70 kPa [96][94][100]. However, for individual tests values as low as ~10 kPa to as high as ~170 kPa have been reported [100]. Noonan et al. [100] obtained these values for vastus lateralis of 10 healthy young humans by passing tangents to the stress-strain curve at ~55% strain as opposed to 30% selected for our study. For a nonlinear behavior, tangents at higher strains are associated with larger values. Nevertheless, in contrast to fiber bundles, the majority of single fibers demonstrated a linear passive behavior [90][93][91][102][55](Chapter 2), as was observed in the current study, and thereby tangents at 30% vs. 55% should not vary considerably. Therefore, the range of elastic modulus values measured in our study (2 kPa to 115 kPa for multifidus and 5 kPa to 94 kPa for longissimus) agree well with the range reported for other muscles of the human body.

Observations for elastic moduli at the fiber bundle level were intriguing. In general, greater values for medians and IQRs were evident for fiber bundles than single fibers. When the results for convex and concave sides were combined, the medians of patient groups ranged between 38 to 113 kPa for fiber bundles (multifidus: 46-113 kPa; and longissimus: 38-102 kPa), whereas for

single fibers this range was 13 to 37 kPa (multifidus: 27-37 kPa; and longissimus: 13-36 kPa). Similarly, IQR ranged between 50 to 181 kPa for fiber bundles, while it varied only between 10 and 36 kPa for single fibers. Ward et al. [25] are the only previous group that measured elastic modulus of fiber bundles in human multifidus or/and longissimus. In their study, larger values were also reported for both the mean and SEM of elastic modulus at the fiber bundle level than single fibers. The mean ± SEM in their study was 91 ± 7 kPa for multifidus and 63 ± 15 kPa for longissimus at the bundle level, while those values were 34 ± 2 kPa and 33 ± 3 kPa for single fibers in multifidus and longissimus, respectively. This refers to the modulating role of the extracellular matrix in determining elastic modulus at the fiber bundle (tissue) level, which has been echoed by multiple studies throughout the literature [90][102][86][92].

Eighteen from 171 bundles (11%) exhibited substantially large elastic moduli for both multifidus and longissimus muscle groups. The elastic moduli for these bundles, which were more prevalent for group II patients, lied mostly between 200 to 1000 kPa but even reached above ~2000 kPa in two cases. Revisiting the strain measurements and raw force data for these tests verified validity of the calculated elastic moduli (Figure 4-22, Figure 4-23, and Figure 4-24). This observation of such large values has never been reported for human paraspinal muscles. This very stiff passive behavior at the bundle level of these muscles is likely due to fibrosis and may have pathologic roots, which should be explored further through histology.

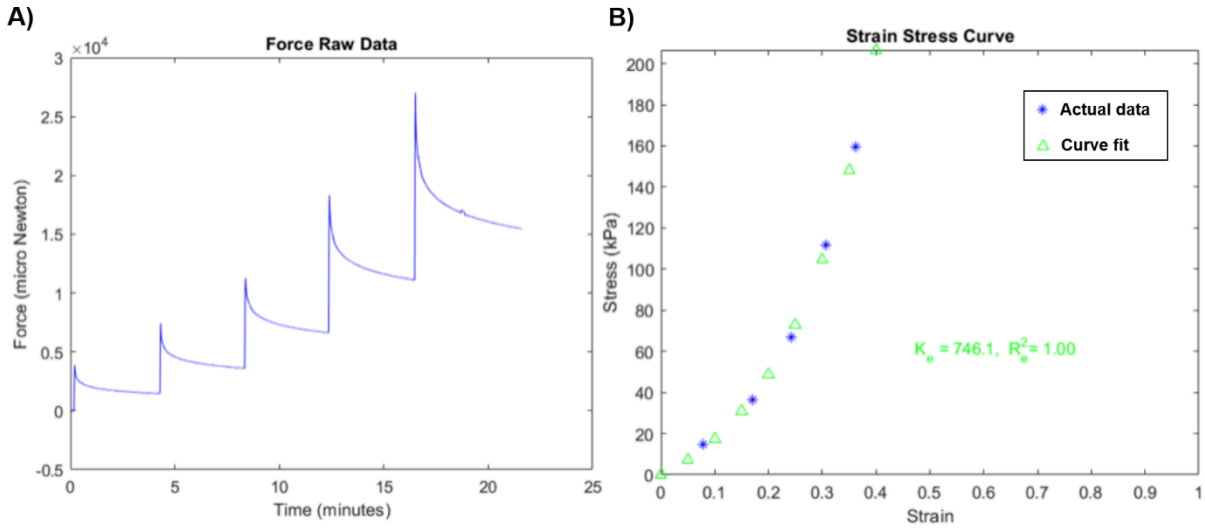

Figure 4-22. Raw force data and stress-strain plot for a muscle fiber bundle with high elastic modulus (746 kPa at 30% strain) collected from longissimus of patient 9 (at the convex-side).

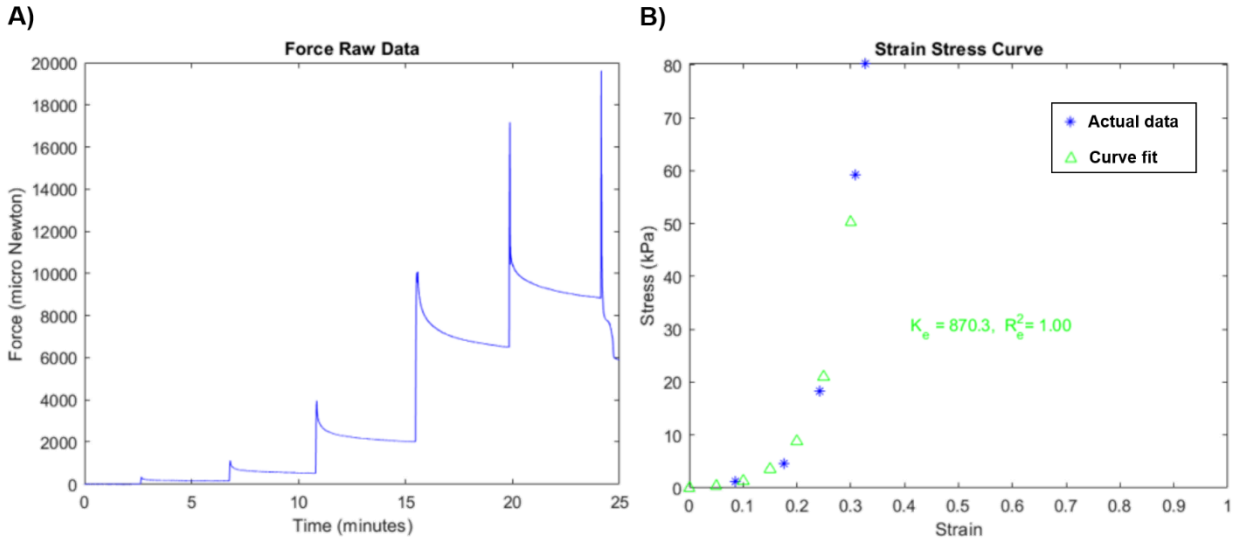

Figure 4-23. Raw force data and stress-strain plot for muscle fiber bundle with high elastic modulus (870 kPa at 30% strain) collected from multifidus of patient 5 (at the convex-side).

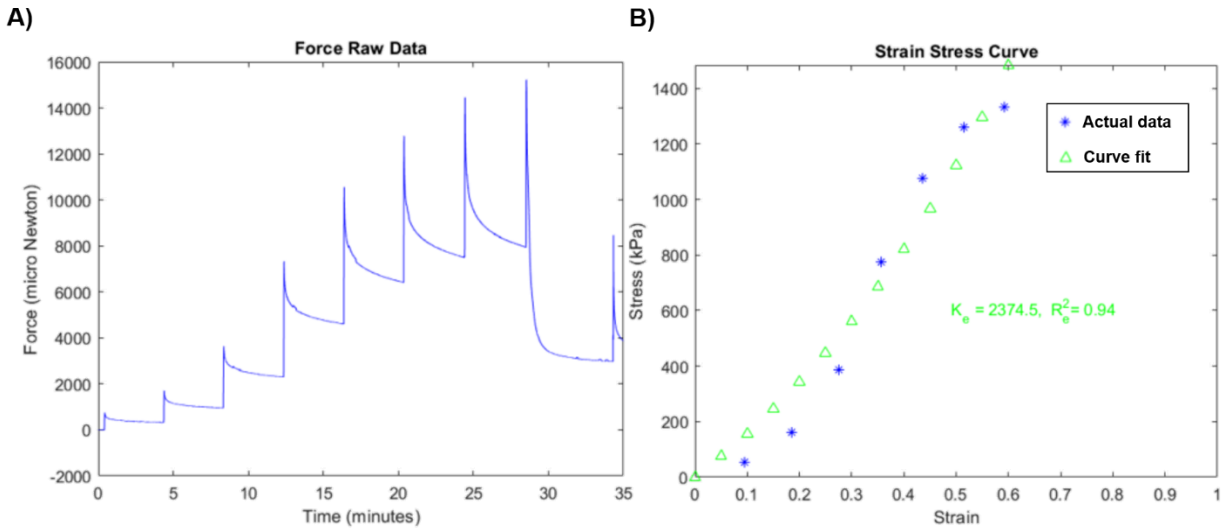

Figure 4-24. Raw force data and stress-strain plot for another muscle fiber bundle with a very high elastic modulus (2375 kPa) from longissimus of patient 9 (at the convex side)

Markedly stiff bundles have been measured for other human muscles or paraspinal muscles of other species. In the study by Lieber et al. [96], fiber bundles from upper extremities of 23 patients with no neuromuscular disorder manifested an average elastic modulus of 463 ± 100 kPa compared to single fibers which had an average elastic modulus of 28 ± 3 kPa. In a recent animal study by our group [234], the effect of surgical muscle damage on passive properties of paravertebral muscles was examined, In this study the lumbodorsal fascia of 12 rats was incised: for six of them posterior paraspinal muscles were detached from the posterior bony elements, while for the other six (sham) those were left intact. Thirteen weeks post-surgery, while single fiber elastic modulus did not show any difference between the two groups, multifidus fiber bundles exhibited significantly larger elastic moduli for the surgical injury group (surgical injury group median 81 kPa, entire range 8-1599 kPa vs. sham median 38, entire range 6-208 kPa, Figure 4-25). Histological assessment revealed an abundance of fibrosis and significantly greater collagen I deposition in multifidus of the surgical injury than the sham group (median(IQR) for surgical injury group was 21%(15%) vs. sham group 6%(4%); Figure 4-26), which could explain

the reason for stiffer bundles observed in the injured muscles. Collagen (especially collagen I) content is recognized as a positive predictor of tissue stiffness by multiple studies [55][108], although its arrangement within the tissue also have shown to influence the stiffness [111].

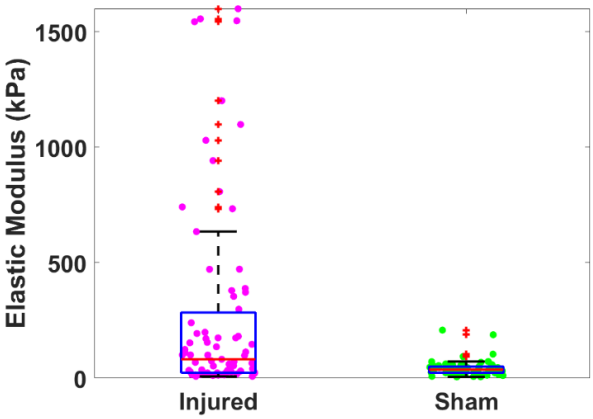

Figure 4-25. Elastic modulus of multifidus fiber bundles in surgical injury vs. sham groups of the study by Yamamoto et al. [234]**. Courtesy of Dr. Yamamoto with permission from Wolters Kluwer Health, Inc.**

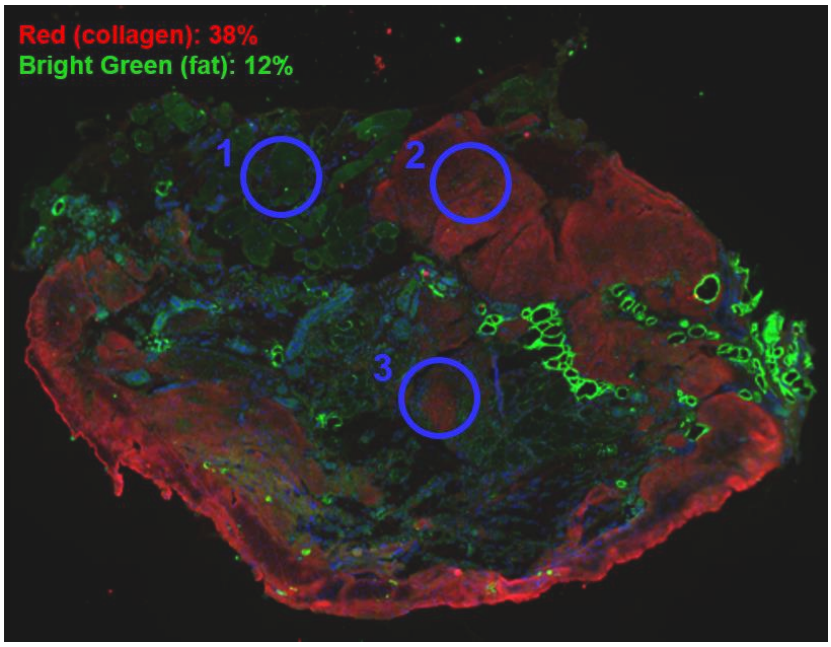

Figure 4-26. Histological structure of multifidus in a rat 13 weeks after surgical injury in the study by Yamamoto et al. [234]**. The constituents of a muscle fiber bundle may vary depending on from where in the muscle biopsy the bundle (represented by blue circles) is extracted. While bundle 1 is mostly comprised of contractile muscle tissue, bundle 2 is mostly occupied by connective tissue, and bundle 3 has a mixture of both. Therefore, their elastic modulus may differ accordingly based on the rule of mixture. See Equation (3-1). Courtesy of Dr. Yamamoto with permission from Wolters Kluwer Health, Inc.**

Large variation in bundle stiffness within same biopsy could be described by the muscle tissue heterogeneity, as evident in multifidus of a rat belonging to surgical injury group in the study by Yamamoto et al. [234] (Figure 4-26). Obviously, bundle 1 has much more collagen than bundles 2 or 3 (Figure 4-26). Therefore, depending on where in the biopsy the fiber bundle is taken from, its stiffness may vary.

The same heterogeneity could be observed at the whole muscle level, especially for pathologic muscles. For instance, while a patient in group I or our study had good quality muscle as observed from their MRI (Figure 4-27), a big portion of paravertebral muscles of a patient in group II consisted of non-muscle tissue (Figure 4-28). Thus, based on where in the whole muscle the biopsy was collected from, the properties could be substantially different. This means for a better assessment of muscle quality and its properties, the measurements should not be limited to a single fiber, a fiber bundle, or a biopsy at the fascicle level. A wholistic view is necessary to assess muscle properties and consequently its functionality.

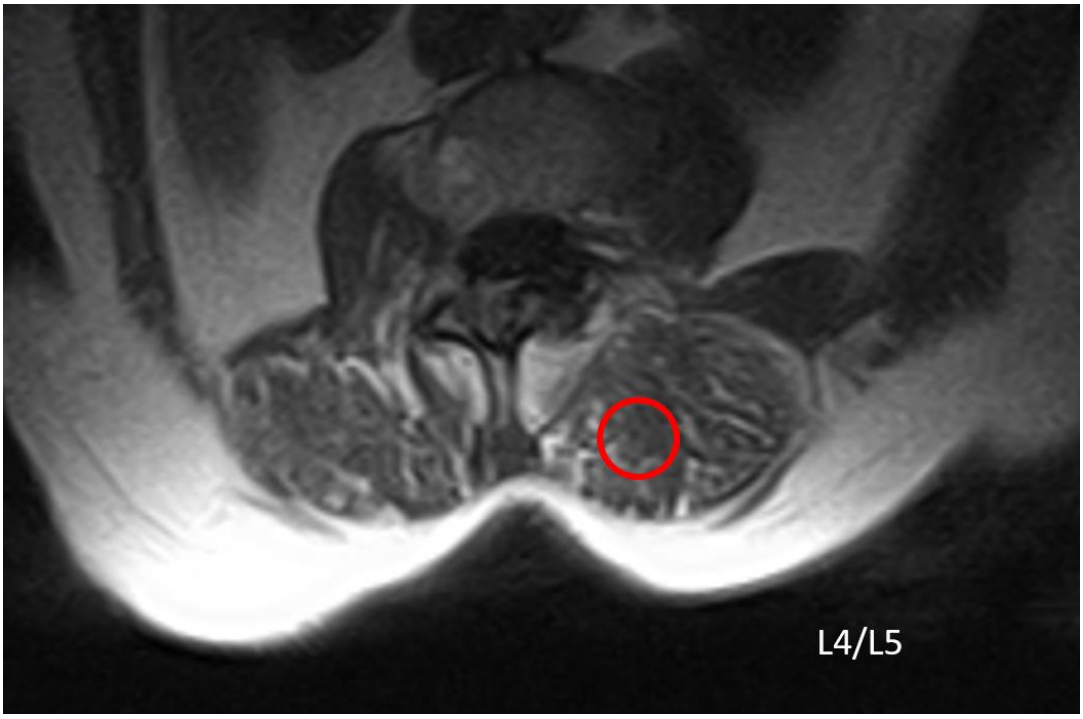

Figure 4-27. Good quality muscle tissue observed through MRI in a patient from group I.

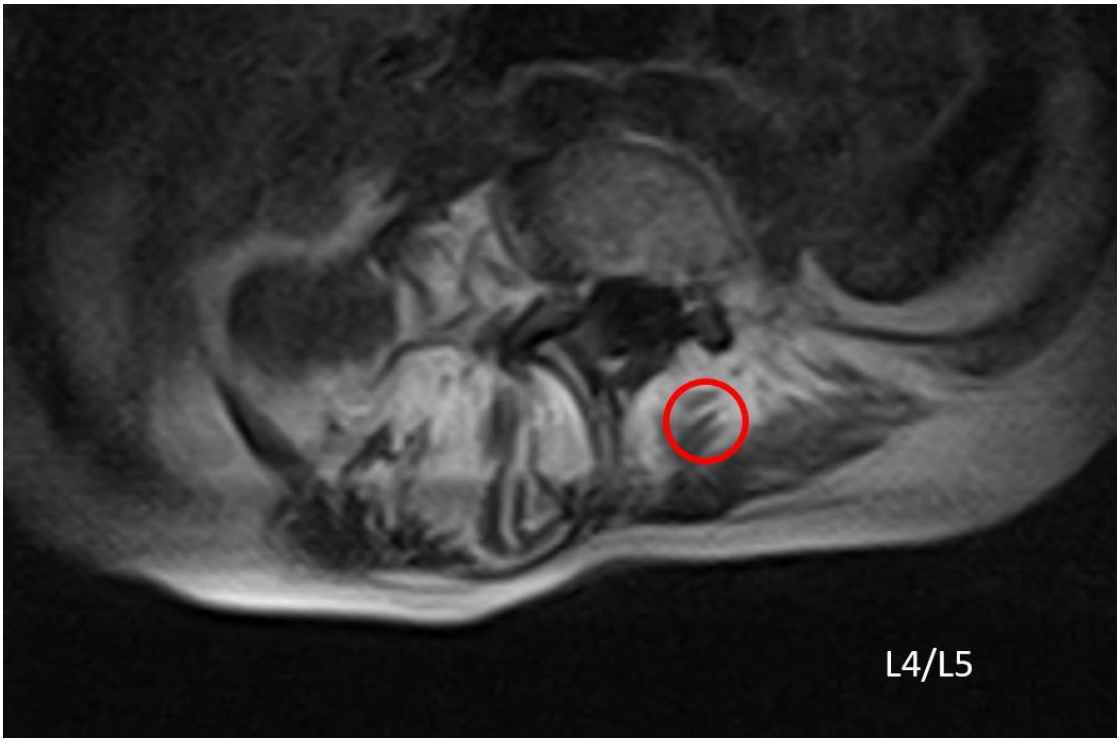

Figure 4-28. Tissue heterogeneity and abundance of non-muscle tissue in paraspinal muscles of a patient from group II observed through MRI.

Direct measurement of all muscle biomechanical properties at the whole muscle level is desired, especially for biomechanical models. However, most of those properties at the whole muscle level has never been measured for human paraspinal muscles as it is not feasible due to its technical and ethical challenges. In fact, the slack sarcomere length or passive stiffness of paraspinal muscles at the whole muscle level has never been measured in any species. In a recent study by Ward et al. [55], examining passive elastic modulus of several lower extremity muscle at fiber, fiber bundle (~20 fibers), fascicle (~300), and whole muscle level for six rabbits manifested a nonlinear increase from smaller scales to larger ones. For example, at 30% strain, the elastic modulus of extensor digitorum was ~30 kPa, ~40kPa, ~260kPa, and ~7500 kPa, at the fiber, fiber bundle, fascicle, and whole muscle levels, respectively. This implies the notion of scale should be considered when assessing the overall muscle functionality using properties measured at the fiber or fiber bundle level only; or when transferring those data to the musculoskeletal models, which typically require whole muscle level information as inputs.

The histopathological analysis of the biopsies in the current study identified a variety of abnormalities at both cellular and tissue levels. At the tissue level, fibrosis was evident in some cases and was greatest for patient 4. At the cellular level, moth-eaten fibers, pinprick fibers, core and targets and cox negative fibers were identified to be prevalent in degenerated muscles. The variety of structural and mitochondrial abnormalities observed in our study is suggestive of diverse causes or mechanisms of potential functional impairment. Interestingly, on average the severity of the abnormalities was qualitatively highest for paraspinal muscles of group III patients, moderate for group II and were somewhat mild to moderate in group I. This is a preliminary analysis though; undoubtedly, more patients are required for finding patterns or making any comparison between the groups.

Our study is the first to document such degenerative observations for human longissimus muscles; and the first to report on multifidus and longissimus in patients with spinal deformity. Multifidus has been recently studied histopathologicaly in detail by two studies marking similar extracellular and intracellular observations to ours. Padwal et al. [238] histologically examined superficial and deep regions of multifidus in 16 patients with lumbar spine pathologies (12 stenosis, 2 spondylolisthesis, and 2 disc herniation) and found an elevated amount of fibrosis and fat in these patients with an overall composition of 11%±9% fat, 49%±16% muscle, and 26%±12% collagen with no difference between the deep and superficial regions. Shahidi et al. also examined multifidus of 10 acute and 22 chronic patients with degenerative lumbar spine pathology and reported a prevalence of regional degenerations and punctate necrosis within muscle fibers with no difference in their amount between the acute and chronic patients. The regional differences were mostly characterized by cellular infiltration, cytoplasmic disruption, and membrane disruption. The most common degenerative phenotype was the increased nuclei number and jagged muscle fiber border; and the most common cell type was the fibro-adipogenic-progenitor (FAP) cells. Given the association of FAP cells with fibrosis [239][240] and with the prevalence of fibrosis in paraspinal muscles of spine pathology patients as also marked by other studies [241][242], further research is required to shed more light on their roles in muscle degeneration and in the etiology of spine pathologies.

There were several limitations to this study that should be considered when interpreting the results. First, due to patient recruitment being halted by COVID-19, the number of patients recruited for this study (four in group I, three in group II and two in group III) were too small for making any comparison between the patient groups. Second, a control group of healthy individuals was desired; however, as non-invasive collection of biopsies from a healthy

population was not feasible, we had to define patient group I, those who did not have any deformity, as the control group for the other two patient groups who had a sagittal deformity (although it was compensated in group II). Further, although presence of a previous spine surgery or a coronal plane deformity were initially set as our exclusion criteria, to increase the number of the patients, those criteria were ignored (for patient 1 & 9). This likely introduced extra factors or variability to the data. Third, given the small size of the biopsies and their poor qualities for some cases due to fibrosis and/or fatty infiltration, extracting three fibers or six fiber bundle was not possible for all biopsies. This led to uneven sample sizes between the biopsies and the patients.

4.5 Conclusions

Despite the aforementioned limitations, the objectives of this study were successfully achieved. We developed the tools and protocols required for acquiring intraoperative biopsies from patients with spinal deformity at Vancouver General Hospital and Toronto Western Hospital. Furthermore, the biopsies from nine patients were collected and evaluated biomechanically and histopathologically. The key findings of those evaluations include observation of substantially stiff fiber bundles in paraspinal muscles of these patients, which links well with the elevated amount of connective tissue/fibrosis observed in their muscles. Finding a variety of cellular and extracellular abnormalities were suggestive of diverse causes or mechanisms of potential functional impairment. Finally, the large variations observed for in situ sarcomere length, slack sarcomere length, and elastic modulus suggest dramatic influences on muscle forces. Given the inter-relationship of these three properties and their dependence on other muscle properties, their influence on spinal forces should be investigated using a musculoskeletal model, which is addressed in the next chapter (Chapter 5). The outcome of this study, once complete, may serve

as an invaluable input to musculoskeletal models to help in exploring the etiology of adult spinal deformity or assist in developing better treatments for patients suffering from adult spinal deformity.

Chapter 5 Biomechanical Properties of Paraspinal Muscles Influence Spinal Loading – A Musculoskeletal Simulation Study

The results of the human study presented in Chapter 4 revealed large variations in biomechanical properties of the paraspinal muscles. To what extent these variations in paraspinal muscle biomechanical properties may affect the spinal loading is what this chapter aims to address. Paraspinal muscles are vital to the functioning of the spine. Changes in muscle physiological cross-sectional area significantly affect spinal loading, but the importance of other muscle biomechanical properties remains unclear. This study explored the changes in spinal loading due to variation in five muscle biomechanical properties: passive stiffness, slack sarcomere length (SSL), in situ sarcomere length, specific tension, and pennation angle. An enhanced version of a musculoskeletal simulation model of the thoracolumbar spine with 210 muscle fascicles was used for this study and its predictions were validated for several tasks and multiple postures. Ranges of physiologically realistic values were selected for all five muscle parameters and their influence on L4-L5 intradiscal pressure (IDP) was investigated in standing and 36°flexion.

5.1 Introduction

Paraspinal muscles are vital to the functionality of the spine and their dysfunction is deemed a major risk factor for a variety of spinal disorders including spinal deformity [7][45], adjacent segment disease [202][185] and lower back pain [203][204][205][206]. To what extent muscle dysfunction is involved in the development of these conditions is unknown. Musculoskeletal models of the spine provide estimates of muscle and spinal loading for various conditions and daily activities and thus provide unique insight into the biomechanical performance of the system, since direct measurement of in vivo spinal forces and moments is not feasible with

current technology. This knowledge could enhance our understanding of the etiology of spinal conditions and help in the development of better treatment or prevention strategies.

Spinal loading depends upon the biomechanical properties of the paraspinal muscles. These properties include physiological cross-sectional area (PCSA), passive stiffness, slack sarcomere length (SSL, beyond which passive force starts to develop), in situ sarcomere length (i.e. sarcomere length measured inside the body for a certain posture), pennation angle, and specific tension (defined as the maximum force per unit area produced by contractile elements)(Figure 5-1). For example, muscle PCSA has been shown to affect both spinal loading magnitudes [184][185] and muscle activation patterns [207]. The importance of many other muscle parameters to the spine remains unknown, even though they have great importance to the biomechanical functioning of the individual muscles.

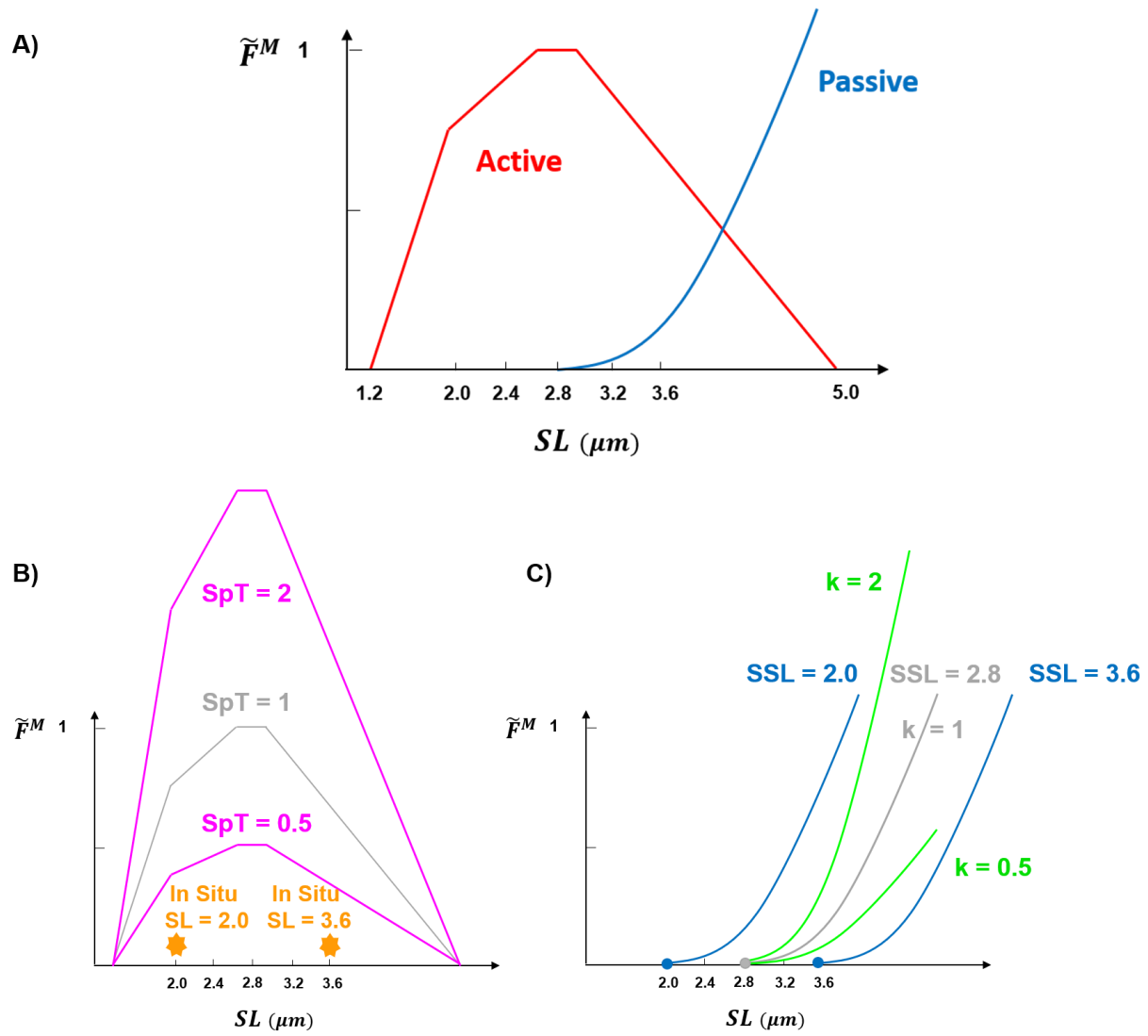

Figure 5-1. Fundamental muscle force-length curve adopted from Millard et al. [212]**. Normalized muscle force $\widetilde{F}^M$ is equal to 1 at optimum sarcomere length which is assumed to be 2.8 μm in human. Multiplying $\widetilde{F}^M$ by the specific tension gives the maximum force per unit area a muscle can produce when fully activated which depends on the sarcomere length (A). The curves may not be the same for all muscles or individuals and could vary with regard to certain parameters including (B) posture specific in situ sarcomere length (SL) and the scaling factor for the specific tension (SpT) or (C) slack sarcomere length (SSL) and stiffness scaling factor (k).**

The well-known force-length relation of muscle (Figure 5-1) is included appropriately in only a relatively few optimization-based biomechanical models of the spine [151][153][152][243]. Even in these models, most of the required muscle parameters are either assumed or taken from cadaveric studies. For example, the passive stiffness, slack sarcomere length, and specific tension

are assumed to be the same for all muscles in these models, while it has been shown to differ between muscle groups or between pathologies [25][96][94][119][237]. Due to the ethical and technical challenges, only few and limited in vivo measurements of these parameters have been made to date (Chapter 4)[25]. This might be because the significance of these parameters in spine modeling is not yet fully understood. In fact, there are no studies that have assessed the effect of these different muscle properties on spinal loading within these different models [151][153][152][243].

Therefore, the objective of this study was to explore changes in spinal loading due to variation in the paraspinal muscle parameters, specifically slack sarcomere length, passive stiffness, in situ sarcomere length, specific tension, and pennation angle.

5.2 Materials and Methods

We used a recent detailed model of the lumbar spine developed by our group [13], which was based on the model introduced by Christophy et al. [11] and used ArtiSynth (www.artisynth.org) [21] for physical simulation. In this study the solution method was enhanced to extend the validation to several activities and postures as described in the following sections.

5.2.1 Geometric Model

The geometry and mechanical properties of the spine model were the same as reported previously [152]. The model consisted of five mobile lumbar vertebrae, L1 to L5, with the entire thorax rigidly fixed to L1. The sacrum and pelvis were fixed to the ground and the segmental weights of the upper body along with the weights of the head, neck, and arms were all incorporated. The adjacent lumbar vertebrae were connected through massless six-dimensional

springs with a 6X6 stiffness matrix for each lumbar functional spinal unit (FSU, defined as a pair of adjacent vertebrae with connecting ligaments, facet joints, and intervertebral disc). Relative displacements and rotations between two adjacent vertebrae generate restoring forces and moments by the six-dimensional springs which are applied equally but in opposite directions at the centers of the two vertebrae. Due to paucity of the data in the literature, only diagonal terms of the stiffness matrix were included: translational terms were taken from one study [244] while the nonlinear formulations for the rotational terms were adopted from another [245]. The effect of the intra-abdominal pressure was modeled as an upward force applied onto the thorax inserted at the center of diaphragm [169] and in all postures remained perpendicular to it.

Muscles in the model comprised 210 fascicles, each modeled as a Hill-type musculotendon actuator. PCSA, supine/prone in situ sarcomere length, pennation angle, and fiber to tendon ratios, were defined for all muscles, as done by Christophy et al. [151]. These anatomic and biomechanical properties are all involved in muscle force computation as:

$$\begin{aligned} F_{muscle} = PCSA \\ \times \Big(activation \times SpT \times SpecificTension \times \tilde{f}_{active}(SL) \\ + k \times K \times \tilde{f}_{passive}(SL) \Big) \times \cos\alpha \end{aligned} \tag{5-1}$$

where K is a constant scaling the normalized passive curve just as does the specific tension for the normalized active curve; SpT and k are the scaling factors for the specific tension and K, respectively, and are both set to 1 by default; SL is the sarcomere length calculated from model fiber length and other anatomic properties (as described in detail in Appendix C1 on page 237);

$\tilde{f}_{active}$ and $\tilde{f}_{passive}$ are force multipliers as functions of SL obtained from the force-length curves (Figure 5-1); and activation of muscle is a decimal varying between 0 and 1.

The normalized force-length and force-velocity curves were taken from the study by Millard et al. [212] and tendons were assumed to be rigid. The baseline value for K was chosen equal to specific tension in our model.

5.2.2 Solution Method

Our spine model in Artisynth uses forward dynamics assisted data tracking and optimization to solve the muscle redundancy problem [152][246][124]. The optimization predicts muscle activations to achieve an input trajectory for one or more target points (Figure 5-2A). In this model, we set the thorax rotation as input to the model, while the other mobile rigid bodies (i.e. L2 to L5) were all able to move freely (B-D). This is a better approach than our previous strategy of prescribing the position of a specific set of target points, as it eliminates the sensitivity of the spinal forces to the translational component of the prescribed trajectory observed in other models [152][247][248][249]. The cost function for the optimization was a weighted summation of four terms: the kinematics tracking error, sum of muscle activations squared, sum of square of difference between the activations of two consecutive time steps, and the sum of FSUs (six-dimensional springs) forces squared. The fourth term was added to the optimization cost function to minimize the intervertebral loads [142][250][131], and was different from our previous model. Quadratic programming was used to solve for the set of muscle activations that would minimize the total cost function.

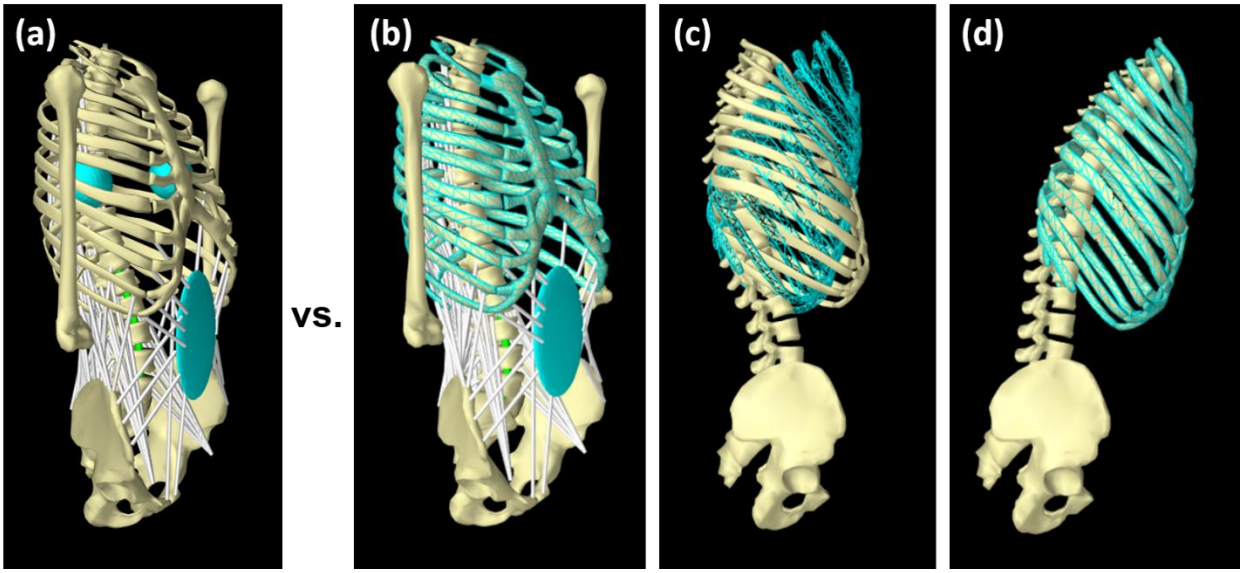

Figure 5-2. Tracking target frames instead of target points in the new solution method. In the previous model, full trajectory of two symmetric target points located at the right and left of the thorax were assigned as input and tracked by the model (a); while in the new solution method, only rotation of the thorax was given as input (b, c) and followed by the model (d).

5.2.3 Calibration

For computation of muscles forces, the normalized force-length curve and force-velocity curve were scaled by the specific tension, which is defined as the maximum contractile force per unit area a muscle can produce at its optimum length; and is typically assumed to be the same for all muscles in a musculoskeletal model. The specific tension along with the weighting terms for the first three cost functions were determined in our previous model through simulation of two postures (10° extension and 10° flexion) of an in vivo study [26]. Adopting the same values, we followed a similar calibration approach including two additional postures (-20° extension, 30° flexion) and determined the weighting term for the new FSU load term in the cost function (see Appendix C2 on page 242 for the details of our calibration approach). Among the three values of 80, 90, and 100 N/cm^2, a specific tension of 100 N/cm^2 was again found to produce model results (including maximum producible extension moments) that were closest to experimentally

reported values[26]. Any simulation with a tracking error of more than 1° from the prescribed thorax position was not considered converged and was rejected in this study (identified as red stars on Figures).

5.2.4 Validation

For validation of the new solution method, we compared the prediction of our model for L4-L5 IDP to the L4-L5 IDP measured in vivo for five symmetric activities [171]: 1) 19° extension, 2) upright standing, 3) and 4) holding a crate of 190N close and far from the chest (25 and 55 cm anterior to the L5-S1 disc), and 5) 36° flexion. The output of our model were the forces and moments on each FSU (six-dimensional spring). We performed a post analysis to compute the IDP values as the sum of IDP resulting from the compressive force and the IDP from the flexion/extension moment. We assumed that shear force did not influence IDP (Frei et al. [251]). The IDP associated with the compressive force, $IDP_{F_{axial}}$, was calculated as:

$$IDP_{F_{axial}} = \frac{F_{axial} \times 0.85}{Disc\ Area \times 0.66} \tag{5-2}$$

where 0.85 is considered as the share of the intervertebral disc from the compressive force on the FSU, F_{axial} [252][253], and 0.66 is the correction factor for the nucleus area [252][254]. For calculation of the IDP associated with the flexion moment, $IDP_{M_{flexion}}$, and extension moment, $IDP_{M_{extension}}$, a linear fit to the data of an in vitro study [255] led to the following relations:

$$IDP_{M_{flexion}} = M_{flexion} \times 0.036 \frac{MPa}{N.m} \tag{5-3}$$

$$IDP_{M_{extension}} = M_{extension} \times 0.018 \frac{MPa}{N.m} \quad (5\text{-}4)$$

where $M_{flexion}$ and $M_{extension}$ were the magnitudes of the flexion and extension moments applied on the FSU.

Two postures of 10° extension and 40° flexion were also simulated to compare the predicted rotations of the vertebrae against those measured for 50 healthy men [160].

5.2.5 Study Design for Investigating Impact of Muscle Parameters

We examined the changes in L4-L5 IDP in response to variation in the following five muscle parameters: slack sarcomere length, passive stiffness, supine/prone in situ sarcomere Length, specific tension, and pennation angle. All simulations were performed for two postures of upright standing and 36° flexion.

The baseline value for the slack sarcomere length in the curves used [212] was the optimum sarcomere length, which is assumed to be 2.8 μm in human [115]. Although a slack sarcomere length value at the whole muscle level is desired, that has never been measured for paraspinal muscles. The slack sarcomere length values measured for human paraspinal muscles ranges between 1.8 μm to 2.8 μm microns for individual muscle fibers and fiber bundles (Chapter 4) and thus for our study we tested 5 different values of 2.0, 2.4, 2.8 (baseline), 3.2, and 3.6 μm. Although larger values of 3.2 and 3.6 μm may not be expected, those were included in case such values are observed in future studies for a certain pathology or when measurements are made at the whole muscle level.

The normalized passive curve was scaled by a constant K of 100 N/cm^2 equal to the selected specific tension for the baseline model. The quintic Bezier splines [212] for the muscle force-length curve-fitting provide high order of continuity and smoothness, but their formulation is not intuitive. To get a sense of how stiff the curve was, the tangent modulus at 10%, 30%, 50%, and 70% strains were 0.26 MPa, 1.01 MPa, 2.45 MPa, and 2.86 MPa, respectively, for the baseline model. To study changes in spinal loading due to variation in muscle stiffness, the entire passive curve was scaled by an additional factor (k) taking values of 0.1, 0.5, 1(baseline), 5, and 10 which resulted in passive stiffnesses close to the ranges reported in the literature for fiber bundles (Chapter 4)[96] and whole muscles [55].

The supine/prone in situ sarcomere length and pennation angle of the muscles in our model were taken from both in vivo and cadaveric studies in the literature and differed between muscle groups. In situ sarcomere length for human paraspinal samples measured in supine/prone posture exhibits values between 1.9 μm to 3.6 μm (Chapter 4)[114][233]; thus, we tested five different values of 2.0, 2.4, 2.8, 3.2, 3.6 μm. For pennation angle, the values ranged between 0° to 14° for the paraspinal muscles. To get a better understanding of its impact on IDP, especially given the measured values of up to 30° for some other muscles of human body [114], we tested a set of values 0°, 7.5°, 15°, 22.5°, and 30°. For supine/prone in situ sarcomere length and passive stiffness in particular, we ran all the simulations once with slack sarcomere length equal to 2.8 μm (baseline) and the other time with setting the slack sarcomere length of the targeted muscles to 2.4 μm, to explore possible interplay between these parameters.

The specific tension measured experimentally for human single fibers rarely exceeds an average value of ~40 N/cm^2 [120]. However, the majority of biomechanical models have chosen values of 80 to 100 N/cm^2 to be able to perform heavy work activities requiring large muscle forces

and to be validated against the in vivo data [142][256][160][207][153][175][122]. We multiplied the baseline specific tension (i.e. 100 N/cm^2) by an additional factor (SpT) taking values of 0.05, 0.1, 0.25, 0.5, 1, and 1.5, to investigate their influence on the L4-L5 IDP. The range of 0.05 to 0.5 has been measured biologically [120], but 1 and 1.5 have been used only in biomechanical models [153][173].

The changes in each muscle parameter were applied in four different scenarios: scenario 1, MUL, involved changes only applied to the multifidus; scenario 2, EXT, involved changes applied to extensor muscles including multifidus, longissimus thoracis, iliocostalis lumborum, and quadratus lumborum; scenario 3, EXT+PS, involved changes applied to extensor muscles as well as psoas; and scenario 4, ALL, involved changes made to all 210 muscle fascicles in the model. These scenarios were defined as to simulate plausible scenarios related to a certain pathology or surgical intervention. For example with genetic pathologies, all muscles may be affected and present higher stiffness values; while for changes after spinal surgeries only multifidus or all those directly attached to the spine (i.e. extensors and psoas) may be involved.

5.3 Results

5.3.1 Validation

The resultant compressive and shear forces along with the flexion moments for all lumbar vertebral levels are presented for the five symmetric activities performed by the baseline model (Table 5-1). The corresponding IDP with forces and moments at the level L4-L5 compared well with the in vivo IDPs (Figure 5-3), such that a linear fit to the predicted L4-L5 IDPs by the model and those measured in vivo resulted in a coefficient of determination of 0.98.

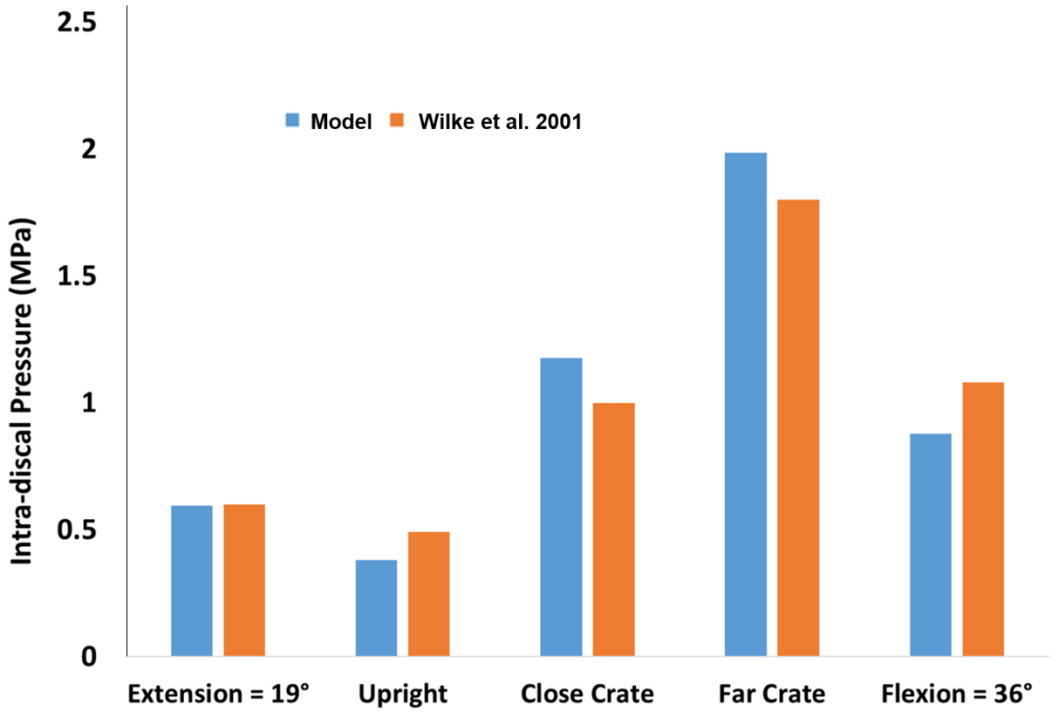

Figure 5-3. Comparison between the predicted L4-L5 IDP by the model and those measured in vivo for five different activities (Wilke et al. 2001)[171]**.**

The rotation of the thorax was dictated by the user but the trajectories of the other vertebrae were free (i.e. were not determined with a predefined function). The intervertebral rotations from upright standing for both 10° extension and 40° flexion fell within the range observed for 50 healthy men [257](Figure 5-4).

Table 5-1 Predicted compressive forces, shear forces, and sagittal plane moments at all vertebral levels by the model for the five different activities performed by the subject of the in vivo study [171]. The crate weighed 190 N. An anterior shear force with a negative value was directed posteriorly. A negative value for sagittal plane moment causes the upper vertebra of the FSU to flex.

Spinal Level	Activity	Compressive force (N)	Anterior Shear Force (N)	Sagittal Plane Moment (N.m)
L1-L2	1- 19° Extension	355	-351	-6.35
	2- Upright Standing	467	-105	-1.17
	3- Holding Crate Close	1456	-163	-1.11
	4- Holding Crate Far	2652	-240	-8.53
	5- 36° Flexion	396	462	13.59
L2-L3	1- 19° Extension	456	-289	-6.01
	2- Upright Standing	514	-60	-0.99
	3- Holding Crate Close	1841	63	-5.06
	4- Holding Crate Far	2976	-130	-7.96
	5- 36° Flexion	568	430	11.53
L3-L4	1- 19° Extension	549	-183	-6.12
	2- Upright Standing	533	-2	-0.56
	3- Holding Crate Close	1802	350	-2.8
	4- Holding Crate Far	2998	318	-5.25
	5- 36° Flexion	729	341	9.56
L4-L5	1- 19° Extension	670	57	-6.98
	2- Upright Standing	529	107	0.26
	3- Holding Crate Close	1646	653	0.65
	4- Holding Crate Far	2798	763	0.71
	5- 36° Flexion	797	324	8.88
L5-S1	1- 19° Extension	671	524	-7.38
	2- Upright Standing	469	235	1.73
	3- Holding Crate Close	1432	803	6.15
	4- Holding Crate Far	2571	1042	6.57
	5- 36° Flexion	813	403	8.41

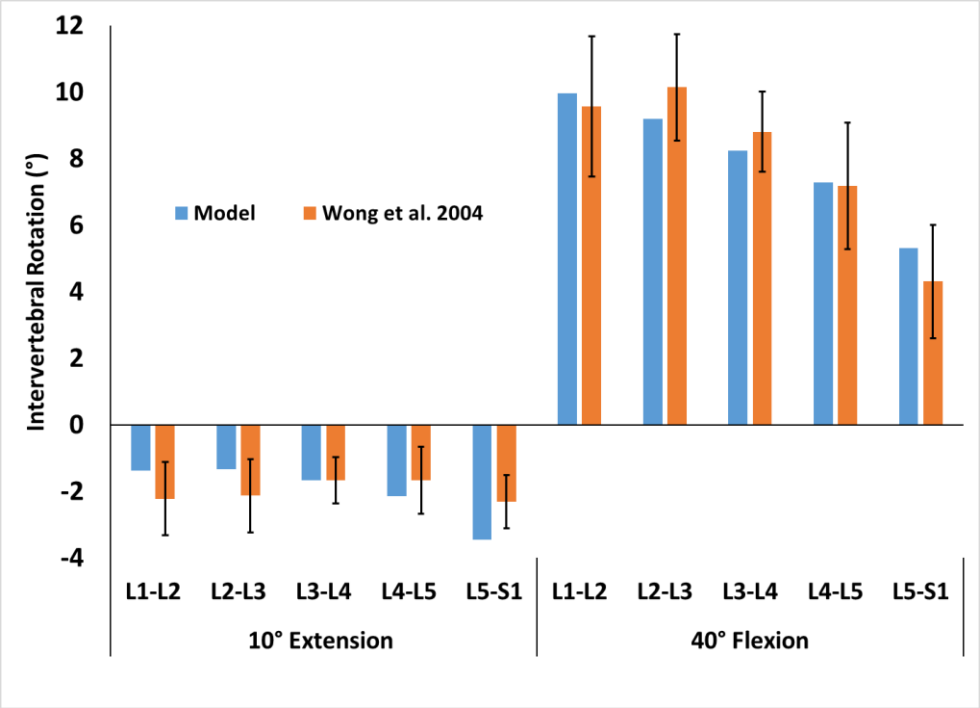

Figure 5-4. Intervertebral rotations for two activities of 10° extension and 40° flexion predicted by the model (blue) and observed in 50 male subjects (orange, Wong et al. 2004 [160]**). The error bars represent the standard deviations.**

5.3.2 Impact of Muscle Parameters on L4-L5 IDP

All muscle parameters except the pennation angle had a dramatic impact on the predicted L4-L5 IDP in both standing and flexion activities.

The influence of slack sarcomere length on the IDP was greatest when it was set to 2.0 μm or 2.4 μm (Figure 5-5, note that slack sarcomere length of 2.8 μm is the baseline value). For example, changing slack sarcomere length of the multifidus to 2.0 μm and keeping the slack sarcomere length equal to 2.8 μm for the other muscles, doubled the IDP in standing. This occurrence was due to development of passive forces in the multifidus, whose sarcomere length was 2.27 μm in standing. The IDP was 7 times and 10 times larger in standing when the slack sarcomere length of EXT and EXT+PS were also set to 2.0 μm, respectively. The model was not able to reach 36° flexion for any of these cases due to substantial passive forces that would have been developed in

that posture. The same but milder trend was observed for when slack sarcomere length was set to 2.4 μm in standing; while in flexion, the IDP even tripled (increased from baseline value of 0.88 MPa to 2.6 MPa). For slack sarcomere length values larger than 2.8 μm, the total IDP did not change, although the distribution between the IDP from the compressive force and the IDP from flexion/extension moment changed somewhat.

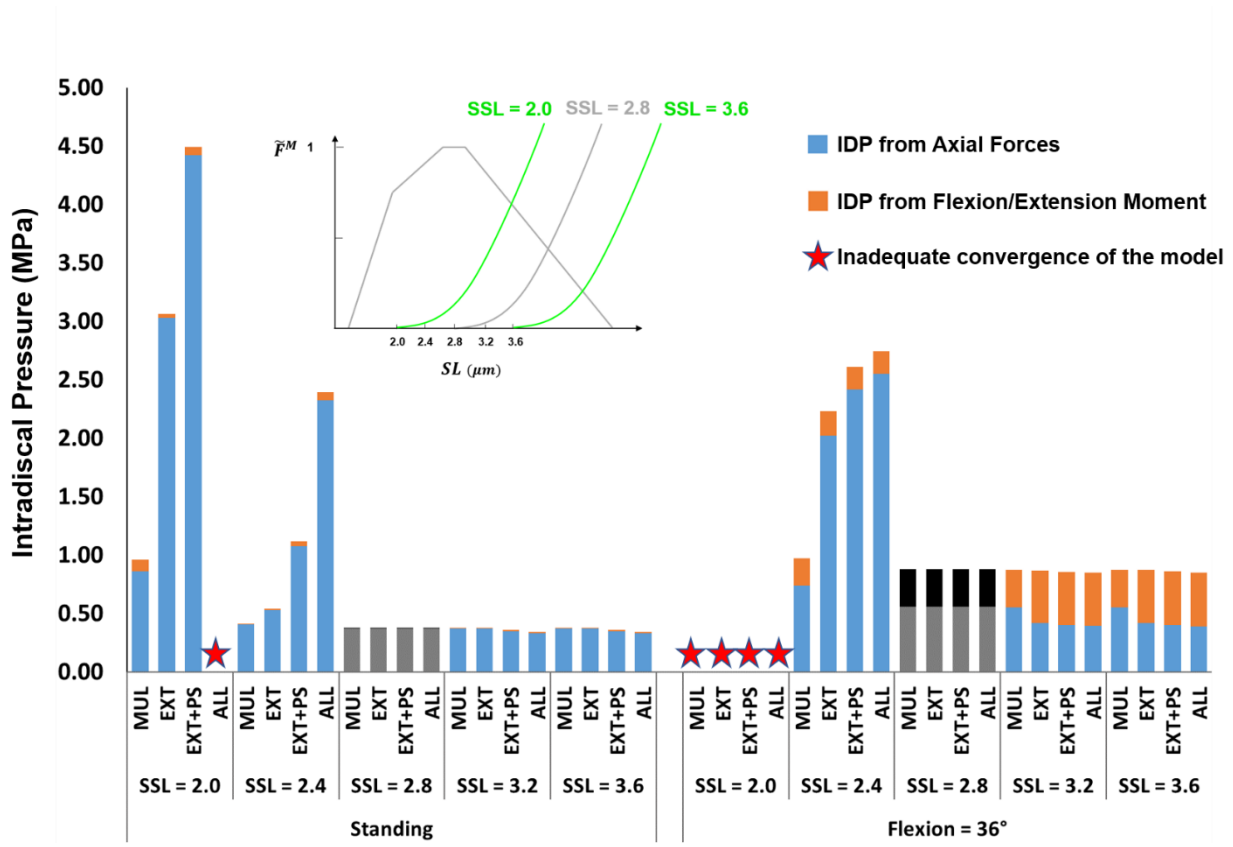

Figure 5-5. The effect of different slack sarcomere length (SSL) values on L4-L5 IDP in upright standing and 36° flexion for four scenarios: changes applied to multifidus (MUL), extensor muscles (EXT), extensor muscles and psoas (EXT+PS), and all 210 muscles in the model (ALL). Grey/black bars represent the baseline values.

The effects of passive stiffness and supine/prone in situ sarcomere length on IDP were both dependent on the slack sarcomere length. When slack sarcomere length was 2.8 μm, reducing the passive stiffness to half or even one tenth of the baseline value did not change the IDP by more than 20% (Figure 5-6). However, when passive stiffnesses was increased to five times or 10

times greater than the baseline, the IDP increased considerably for most scenarios, especially in flexion (Figure 5-6). When slack sarcomere length was set to 2.4 μm for the targeted muscles whose stiffness also changed, for all stiffness scaling factors the IDP changed dramatically both in standing and flexion and its extent depended on what muscles were manipulated (Figure 5-7). For example, a 5 or 10 fold increase in multifidus stiffness combined with setting its slack sarcomere length to 2.4 μm, elevated the IDP in flexion from ~1 MPa to ~2 or ~3 MPa. This IDP increase was a result of multifidus passive forces developed after its sarcomeres lengthened from 2.27 μm (on average) in standing, passed the slack sarcomere length (i.e. 2.4 μm) in 11° flexion and reached 3.01 μm (leading to ~25% strain in multifidus) in 36° flexion.

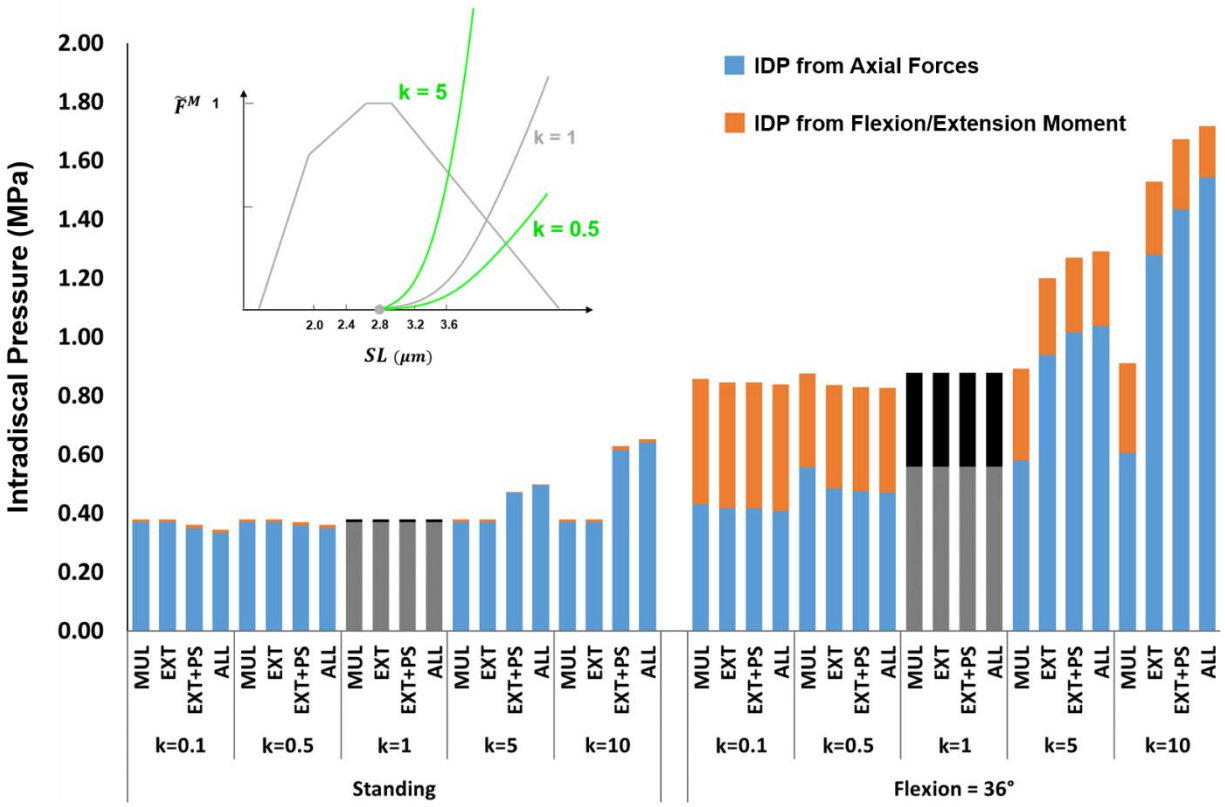

Figure 5-6. The effect of different stiffness scaling factors (k) on L4-L5 IDP in upright standing and 36° flexion for four scenarios: changes applied to multifidus (MUL), extensor muscles (EXT), extensor muscles and psoas (EXT+PS), and all 210 muscles in the model (ALL). Grey/black bars represent the baseline values.

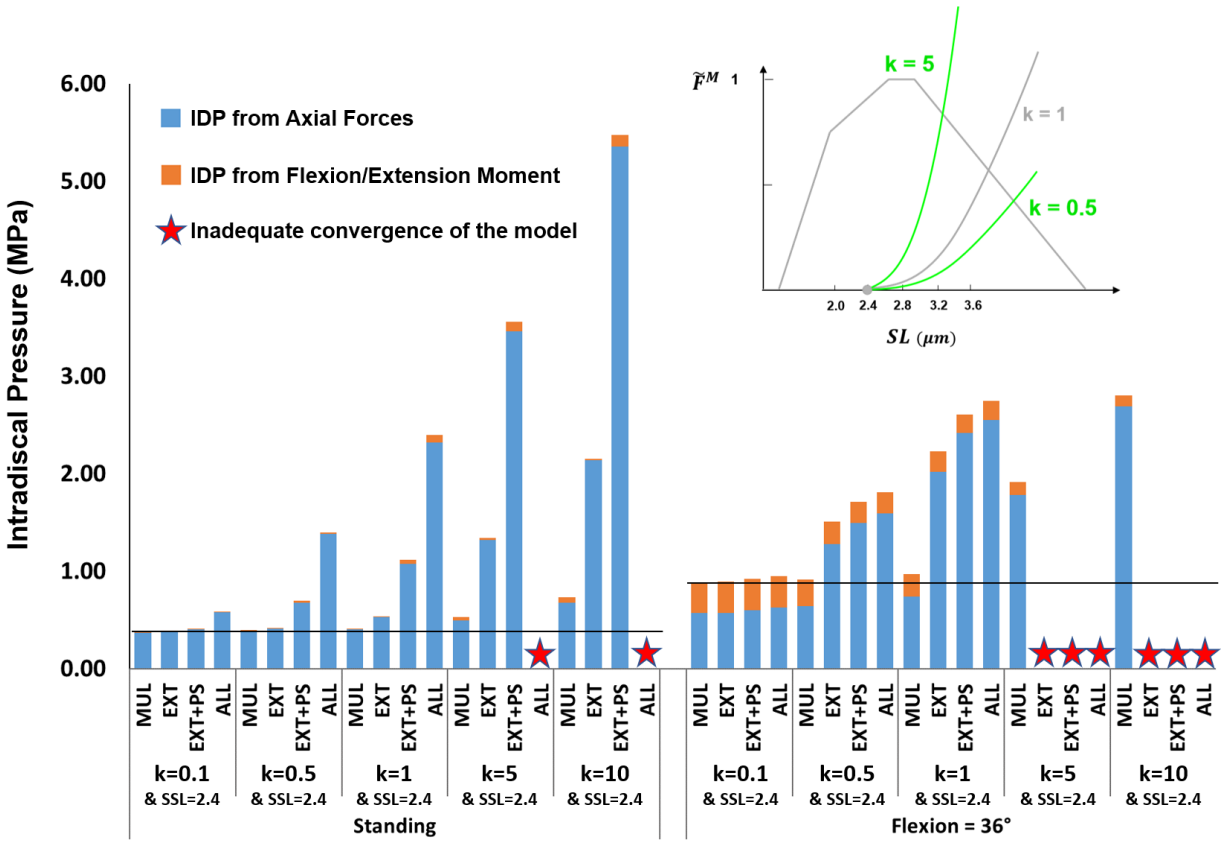

Figure 5-7. The effect of different stiffness scaling factors (k) combined with a slack sarcomere length (SSL) of 2.4 μm to the targeted muscles on L4-L5 IDP in upright standing and 36° flexion for four scenarios: changes applied to multifidus (MUL), extensor muscles (EXT), extensor muscles and psoas (EXT+PS), and all 210 muscles in the model (ALL). The black horizontal lines represent the baseline values.

For the supine/prone in situ sarcomere length values of 2.0 μm and 2.4 μm when slack sarcomere length was 2.8 μm, only small differences in IDP were observed (Figure 5-8). For greater supine/prone in situ sarcomere lengths, however, the increase in the IDP was large, especially in flexion, where sarcomere lengths exceeded the slack sarcomere length. For example, when the supine/prone in situ sarcomere length of the entire group of extensor muscles was 3.6 μm, the IDP increased by 79% (reaching 0.68 MPa from 0.38 MPa) in standing and by 380% (reaching 3.34 MPa from 0.88 MPa) in flexion. When slack sarcomere length was set to 2.4 μm for the targeted muscles whose supine/prone in situ sarcomere length was also changed, much larger increases in IDP occurred for all supine/prone in situ sarcomere length values (Figure 5-9). For

example, when multifidus was manipulated alone to a slack sarcomere length of 2.4 μm and a supine/prone in situ sarcomere length of 3.6 μm compared to when it is set to 2.0 μm, the IDP doubles in both standing and flexion.

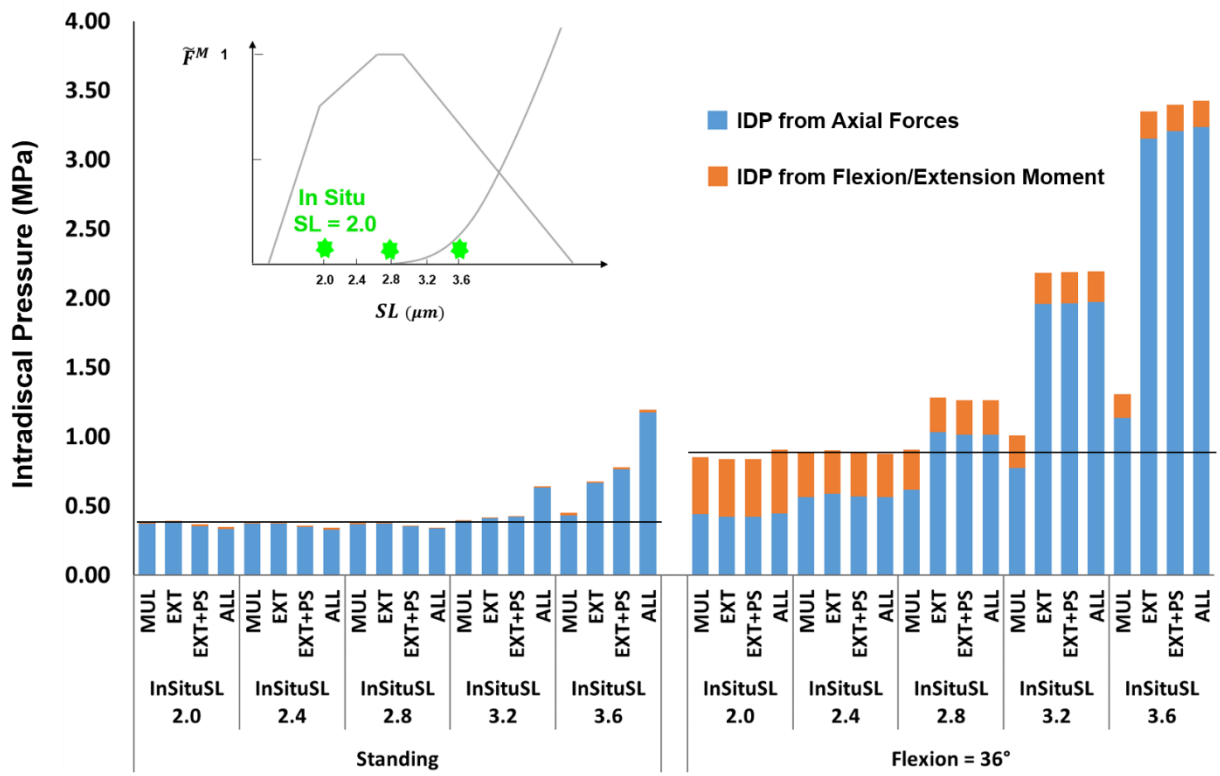

Figure 5-8. The effect of different supine/prone in situ sarcomere length on L4-L5 IDP in upright standing and 36° flexion for four scenarios: changes applied to multifidus (MUL), extensor muscles (EXT), extensor muscles and psoas (EXT+PS), and all 210 muscles in the model (ALL). The black horizontal lines represent the baseline values.

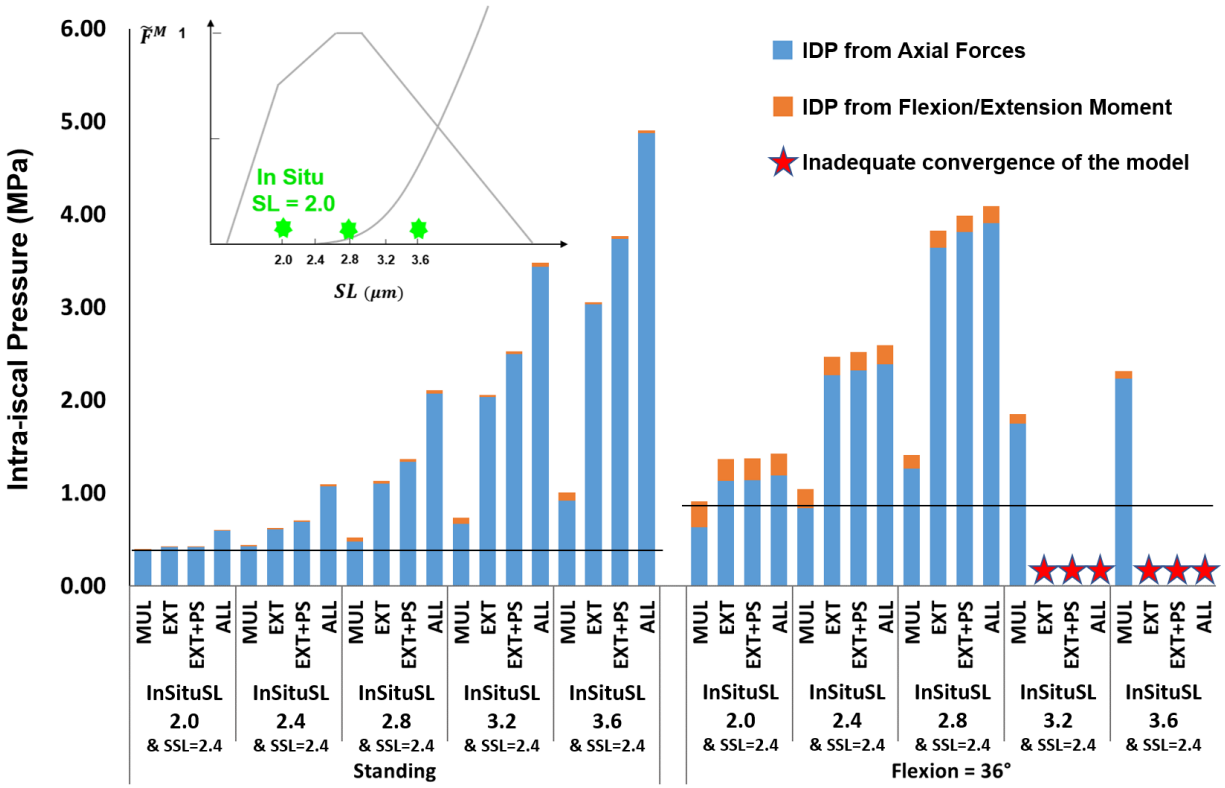

Figure 5-9. The effect of different supine/prone in situ sarcomere lengths combined with a slack sarcomere length (SSL) of 2.4 µm to the targeted muscles on L4-L5 IDP in upright standing and 36° flexion for four scenarios: changes applied to multifidus (MUL), extensor muscles (EXT), extensor muscles and psoas (EXT+PS), and all 210 muscles in the model (ALL). The black horizontal lines represent the baseline values.

The studied values for the specific tension had a minimal influence on the IDP in flexion, except for the scenario where the changes were applied to all muscles, which increased the IDP by 39% when the specific tension was set to one tenth of its baseline value (Figure 5-10). For upright standing, the increase in specific tension also had little effect on the IDP. However, when the specific tension was reduced to half or a quarter of its baseline value, the IDP manifested an increasing trend, with the largest increases occurring when the changes were made to the extensor muscles only. The model was not able to achieve the upright posture when the specific tension was decreased for the extensor muscles to 10% of the baseline value, or 5% of the baseline value for all scenarios, except for when the change was made to multifidus only.

The influence of pennation angle on the overall IDP for both standing and flexion was negligible (Figure 5-11).

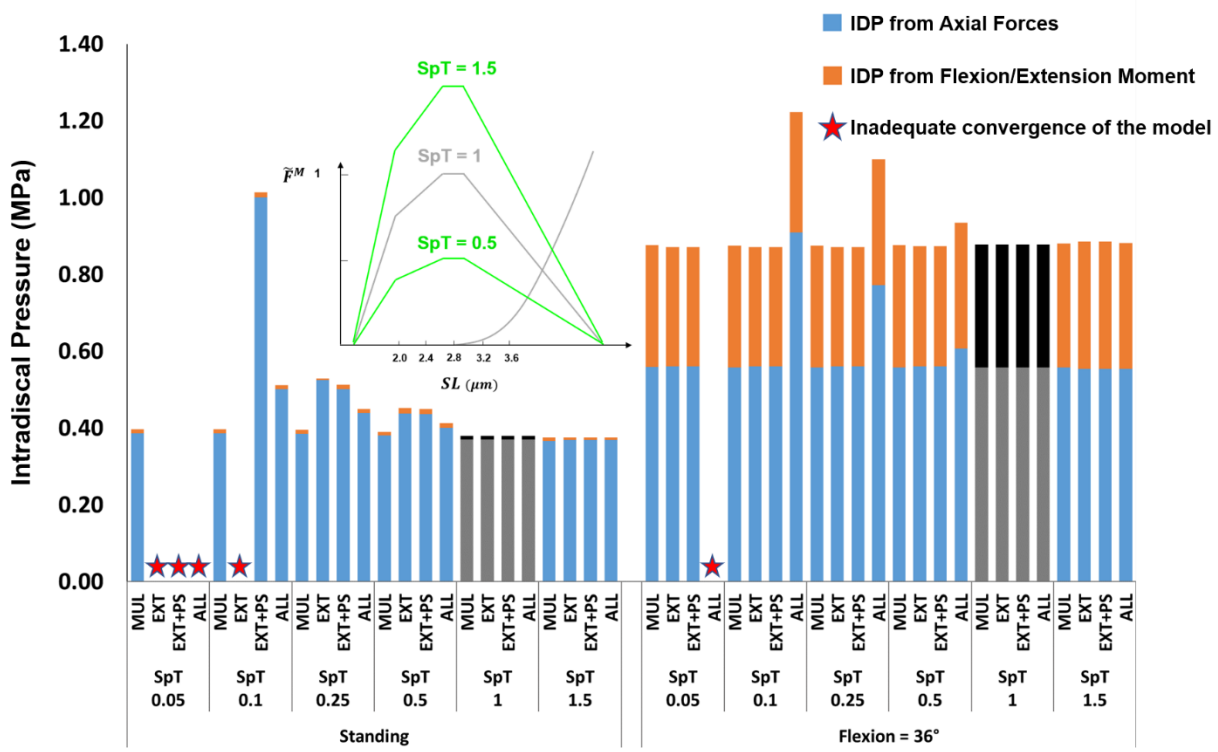

Figure 5-10. The effect of different specific tension scaling factors (SpT) on L4-L5 IDP in upright standing and 36° flexion for four scenarios: changes applied to multifidus (MUL), extensor muscles (EXT), extensor muscles and psoas (EXT+PS), and all 210 muscles in the model (ALL). Grey bars represent the baseline values.

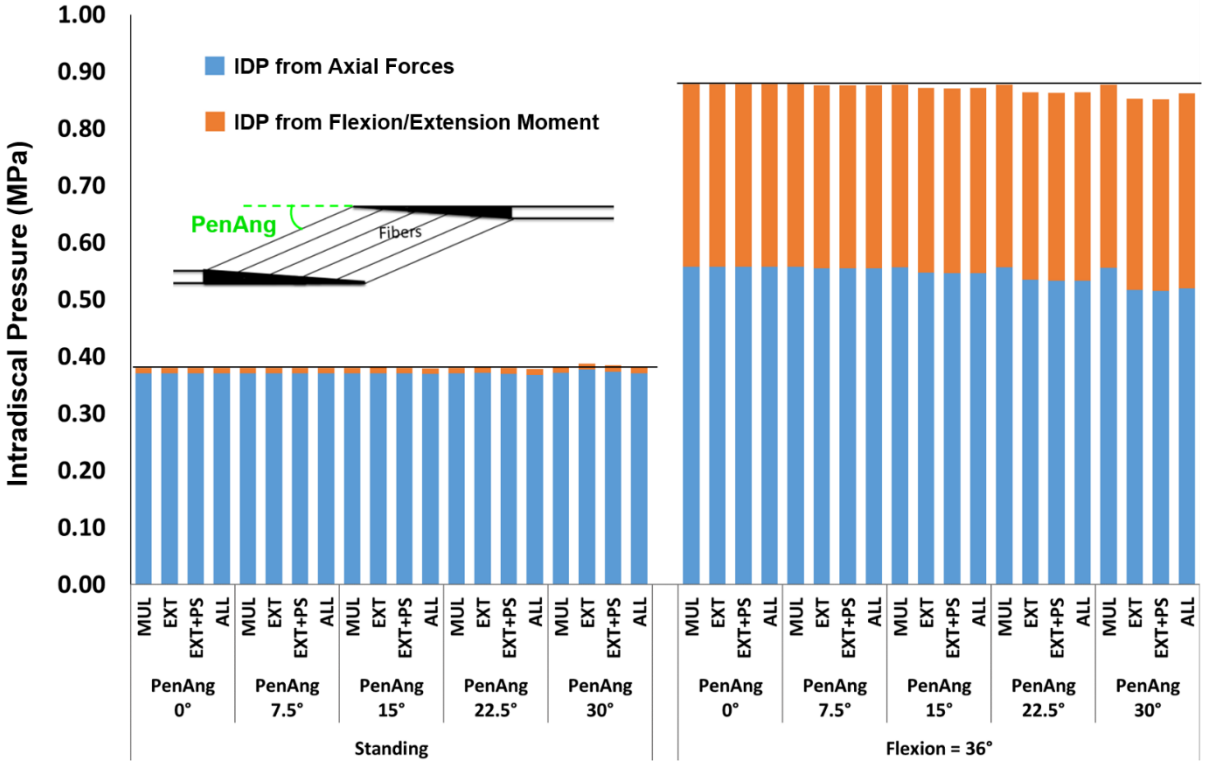

Figure 5-11. The effect of different pennation angles on L4-L5 IDP in upright standing and 36° flexion for four scenarios: changes applied to multifidus (MUL), extensor muscles (EXT), extensor muscles and psoas (EXT+PS), and all 210 muscles in the model (ALL). The black horizontal lines represent the baseline values.

5.4 Discussion

Musculoskeletal models serve as promising tools for gaining knowledge of the spinal loading during various daily activities. The accuracy of their predictions, however, rely on the input variables, including the biomechanical properties of the muscle. The significance of the muscle force-length curve and the parameters associated with it is not yet clearly known for spinal loading, which is probably why only a relatively few optimization-based models have included that appropriately in their solution method [151][153][152][243]. The predicted intervertebral rotations and the L4-L5 IDP in our improved model were in excellent agreement with the

corresponding in vivo measurements [171][257]. The validated model was used to investigate variation of the L4-L5 IDP to a range of muscle parameters. The predictions revealed the strong influence of the slack sarcomere length, passive stiffness, in situ sarcomere length, and specific tension on spinal loading. The reasons for these observations and implications will be explored in the following paragraphs.

The analysis performed in this study revealed the importance of the muscle force-length curve, including both passive and active components, on spinal loading. We observed a substantial influence of slack sarcomere length, passive stiffness, supine/prone in situ sarcomere length, and specific tension on spinal loading, often with interesting interplays between the parameters. For example, in upright standing the passive stiffness scaling factors less than 1 did not make any difference to the prediction of the L4-L5 IDP for the baseline slack sarcomere length (i.e. 2.8 μm). However, for the shorter slack sarcomere length (i.e. 2.4 μm), an increase in passive stiffness from k=0.1 to 0.5 and 1, increased the IDPs due to passive forces being generated in those muscles and thereby increasing joint forces (Figure 5-6 and Figure 5-7). A similar intertwined relationship was evident for slack sarcomere length and supine/prone in situ sarcomere length (Figure 5-8 and Figure 5-9) and is expected for passive stiffness and supine/prone in situ sarcomere length. This is because for shorter supine/prone in situ sarcomere lengths the passive curve does not get involved, therefore changing the stiffness does not make any difference; while for larger supine/prone in situ sarcomere lengths passive forces have already developed thus their values depend on the passive stiffness. Despite the critical importance of these parameters, not enough is known about them in the literature, especially on how they change/adapt together under different conditions (e.g. in different spine pathologies).

The simulated values for all muscle parameters studied herein - slack sarcomere length, supine/prone in situ sarcomere length, passive stiffness, specific tension, and pennation angle were relevant based upon the limited human muscle measurements and the biomechanical models in the literature. For example, the supine/prone in situ sarcomere lengths for most paraspinal muscles in spine models are taken from cadaveric studies [114][115][233]. While the large variation between these measurements in individuals **(**Table 5-2) may be an artifact of the postures in which the cadavers were embalmed, it may reflect natural differences between humans or their pathologies. Prone in situ sarcomere length of multifidus and longissimus have been measured in vivo with observed ranges for individual measurements between 1.9 μm and 3.4 µm (Chapter 4)[156]. Those measurements were obtained through specialized biopsy clamps and were taken from patients undergoing spinal surgery. Less invasive measurement of this parameter in healthy individuals has become feasible recently [258] but has not yet been used for paraspinal muscles.

Table 5-2 Difference in lumbar spine models with regard to the sources of supine/prone in situ sarcomere length values taken from the literature.

	Supine/prone in situ sarcomere length (μm)							
Models	MF	IL	LT	QL	Ps	EO	IO	RA
Christophy et al. 2012 [151]	2.27	2.37	2.31	2.38	3.11	2.83	2.83	2.83
Bruno et al. 2015 [153]	[W-MF]	[D]	[D]	[D]	[W]	[D]	[D]	[D]
Malakoutian et al. 2016 [152]								
Bayoglu et al. 2017 [233]	3.35	2.81	3.57	2.84	2.6	2.82	2.14	2.72
	[B]	[B]	[B]	[B]	[B]	[B]	[B]	[B]

Key:
[W-MF]: Ward et al. 2009b [156]; [W]: Ward et al. 2009a [114]; [D]: Delp et al. 2001 [115]; [B]: Bayoglu et al. 2017 [233]
MF: multifidus; IL: Iliocostalis Lumborum; LT: Longissimus Thoracis; QL: Quadratus Lumborum; Ps: Psoas; EO: External Oblique; IO: Internal Oblique; RA: Rectus Abdominis.

Experimental measurement of slack sarcomere length, passive stiffness, and specific tension requires fresh muscle tissue. slack sarcomere length and passive stiffness of human paraspinal muscles were measured through biopsies collected intraoperatively (Chapter 4)[25]. Those measurements were performed on muscle single fibers and fiber bundles (~10-20 fibers ensheathed in their connective tissue), with the slack sarcomere length exhibiting a range between 1.8 μm to 2.8 μm for the individual data points. The slack sarcomere length of interest for modeling studies should be measured at the fascicle (~500 fibers) or whole muscle level. Due to technical challenges, measurement of slack sarcomere length or even passive stiffness and specific tension in spine muscles has never been done for humans or any other species at the fascicle or whole muscle level. Given these data, the slack sarcomere length range studied herein of 2.0 μm through 3.6 μm seems relevant when considering possibility of larger values if measurements were made at the whole muscle level or for spine pathologic patients.

A similar argument can be made for the passive stiffness. In a recent study on rabbits [55], it was demonstrated for passive stiffness of lower extremity muscles to nonlinearly increase from smaller scales to larger ones. For example, at 30% strain, the stiffness of extensor digitorum was ~30 kPa, ~40kPa, ~260kPa, and ~7500 kPa, at the fiber, fiber bundle, fascicle, and whole muscle levels, respectively. No study to date has measured the whole muscle stiffness of paraspinal muscles. Interestingly, however, it was observed that at the bundle level for human (Chapter 4) individual measurements for stiffness varied between 6 kPa to above ~2000 kPa.

Measurement of specific tension is less challenging as it may suffice to be measured at the fiber level only [259][237], but it has never been done for human paraspinal muscles. The specific tension for human single fibers in muscles tested to date ranges between ~10 to ~40 N/cm^2 [119][120], with the higher value measured in vastus lateralis of world-class sprinters [120].

Surprisingly, most lumbar spine models required a specific tension of between 80 to 100 to be able to perform the heavy work activities requiring large muscle forces [142][256][160][207][153][175][122]. Why physiological values for specific tension are not sufficient for biomechanical models remains unanswered.

Inclusion of muscle dynamics and force-length properties is more straightforward for optimization-based models using a forward dynamics approach [124], but it can be done for those using inverse dynamics also, through addition of further constraints on muscle forces [260]. Using the inverse dynamics approach, input kinematics and external forces are used to calculate the moments at each vertebral level. The moment at each level is distributed between the muscles crossing that level commonly through an optimization technique where sum of muscle forces/stresses to a certain power is minimized. While passive muscle forces are ignored by some models, those including them subtract the passive component of muscle force (generated depending on model position) from the predicted muscle force to obtain the active force component. These active forces should never exceed the maximum force that a given muscle can generate. This maximum active force is dependent on the length of the muscle. For low moment-demand activities (e.g. upright standing), where muscle activations do not approach their maximum, there is little risk of a model predicting a muscle force to exceed its maximum. However, for activities with larger moment-demands, not constraining the force values to within their length-dependent maximum could lead to unrealistic predictions [124]. Without knowledge of the in situ sarcomere length for a certain posture, the normalized force-length curve cannot be used appropriately to obtain the length-dependent muscle maximum isometric force (see Appendix C1 on page 237). Those models that incorporated the force-length curve without knowledge of the in situ sarcomere length had to make assumptions, usually implying that the in

situ sarcomere length at a certain neutral posture (supine, prone or upright standing) for all muscles were the same or equal to the slack length, while recent cadaveric and in vivo studies have revealed large variations for supine/prone in situ sarcomere length between spine muscles, and also that optimal length does not correspond to the passive slack sarcomere length.

For most models of the lumbar spine the kinematics are an input to the model either from subject specific vertebral motion measurements [159][248], or as predefined functions that distribute the overall lumbar spine rotation between the moving vertebrae [151][153][175]. This approach may not be ideal as the spinal forces and moments have been shown to be highly sensitive to input trajectories [152][247][248][249]. For translation specifically, even an error of 0.1 mm is considered too large [247], whereas such level of accuracy is not feasible with the current modalities [261]. Even models that neglect translation and use a predefined, rhythm-based, function for rotation of the vertebrae have been shown to over-predict the joint forces by up to ~40% [249]. In our model, only the rotation (and not the translation) of the thorax was assigned while the other rigid bodies were allowed to move freely with no predefined function. Therefore, the spinal forces/moments in our model were not affected by subjectivity or inaccuracies of the intervertebral input kinematics.

The IDP in this study was calculated as the sum of the IDP resulting from the compressive force and the IDP from the flexion-extension moment both borne by the FSU. Surprisingly, most studies in the literature only relate the compressive forces to IDP and do not consider the IDP from flexion-extension moments [142][169][153][243][175][122]. Pure flexion and extension moments applied to FSUs increases the IDP such that a 10 N.m moment leads to an IDP of ~0.36 MPa in flexion and 0.18 MPa in extension [255][262]. Addition of a compressive load to a pure flexion/extension moment has been shown to result in an IDP equal to summation of the IDPs

from each load when applied separately [263]. In our model for 36° flexion, the contribution of IDP from the sagittal plane moment was 36% of total IDP when baseline muscle parameters were chosen but reached 54% when muscle parameters were changed. Therefore, the predictions of those models that ignore the IDP from flexion-extension moments should be reconsidered particularly for activities simulating a flexed posture.

There was a number of limitations in this study. The load sharing between the intervertebral disc and the posterior elements under a compressive force was considered to be 85% for all postures. However, this value has been shown to vary between postures and to be greater in flexion compared to upright standing or extension [252][253]. The effect of intra-abdominal pressure was modeled as an upward force on the thorax, which was a simplification. Mechanical stability of the spine was not considered in our solution method. Inclusion of that criterion leads to co-contraction of abdominal muscles, which most optimization models fail to predict [163]. Although inclusion of stability criterion results in higher forces for upright standing or other light activities, for heavy work activities or postures like flexion where passive structures are more involved, inclusion of stability criterion appears not to make a difference [250][264]. Adding the stability criterion to our solution method remains as a future step. However, even without such criterion, it is noteworthy that co-contraction of abdominal muscles was evident in our model, especially when passive properties of more muscles (i.e. beyond multifidus) were varied and changed to shorter slack sarcomere lengths or larger stiffness values.

The validation of the model in this study was limited to symmetric tasks and positions within the sagittal plane. In addition, to explore influence of variation in muscle properties on IDP only two tasks of upright standing and flexing to 36° were simulated. While such analysis on asymmetric tasks would also be of interest, the two tasks considered for this study clearly demonstrated the

significant effect of muscle parameters on predicted spinal loading and hence were sufficient for serving the purpose of this study.

5.5 Conclusions

The results of this study highlighted the significance of muscle force-length curve and the parameters associated with it in prediction of spinal loading; therefore, motivating future models to incorporate those parameters in their model for more accurate results. The results also encourage further experimental studies for measurement of these parameters in vivo, especially given the reported wide variations in these parameters.

For adult spinal deformity patients, in particular, more experimental data on paraspinal muscle biomechanical properties can help identify differences and patterns (if any) among these patients. The variations in spinal loading due to the identified patterns and differences in these patients' muscle properties may provide insight into initiation/progression of adult spinal deformity. For example, if further experimental studies reveal larger elastic modulus and shorter slack sarcomere length for paraspinal muscles of adult deformity patients, it can be inferred based on the results of the current study that the spinal loading at L4-L5 is higher in those patients. Given that increased loading results in accelerated degeneration of the intervertebral disc, a lumbar hypolordosis may ensue and lead to a sagittal imbalance. Even in that case, whether the larger elastic modulus and shorter slack sarcomere length were primary or secondary to the deformity remains unclear, and demands further research.

Chapter 6 Discussion and Conclusion

The etiology of adult spinal deformity, similar to many other spinal conditions [265][27], is complicated and likely multifactorial. The preponderance of evidence throughout the literature suggests a consensus on muscle dysfunction as a key player in progression of adult spinal deformity [45][11][46][7][8][9][12][47][48][49][50]. While decreased back extensor strength in these patients has been documented by multiple studies [46][7][8][9], it remains unclear what muscle properties in these patients underlie these observations. In an attempt to address this question and thereby shed light on the etiology of adult spinal deformity, four studies were conducted and presented in this dissertation.

The first two studies aimed to answer two foundational questions on muscle properties in general: one on the effect of vertebral level on muscle biomechanical properties, and the other one on the effect of size of a fiber or fiber bundle on its elastic modulus. The third study assessed biomechanical properties of paraspinal muscles in adult spinal deformity patients. And finally, the fourth study used those muscle properties as input into a musculoskeletal model of the lumbar spine to explore the significance of their influence on the spinal forces.

6.1 Summary of Thesis Results

The first study was conducted on lumbar paraspinal muscles of 13 healthy rats, in which neither single fibers nor the fiber bundles exhibited any significant difference in their elastic moduli or slack sarcomere lengths between the spinal levels. The collagen content was also examined at the fascicle level and no significant difference was evident between the spinal levels. The results of

this study suggested that the assumption of similar biomechanical properties within a paraspinal muscle group existing at multiple spinal levels is valid.

The second study investigated paraspinal muscles of two groups of rats and one group of human subjects. In this study, smaller single fibers and fiber bundles manifested larger elastic moduli, recommending consistent sizes of fiber bundles to be selected for measurement of elastic modulus. This is very important especially when the results are meant to be compared between different groups. Furthermore, this study demonstrated that measuring dimensions of fibers and fiber bundles at least from two orthogonal views is necessary for higher accuracy of results, otherwise on average an error of up to ~44% in measured elastic moduli may be expected.

In the third study, all technical and ethical requirements for intraoperative collection of human paraspinal muscle biopsies were addressed. Biomechanical properties of paraspinal muscles were assessed in a cohort of nine adult spinal deformity patients: four patients with no sagittal imbalance and no usage of compensatory mechanisms (Group I); three patients with no sagittal imbalance through usage of compensatory mechanisms (Group II); and two patients with sagittal imbalance despite usage of compensatory mechanisms (Group III). No statistical comparison could be made between the groups due to small number of patients (because of patient recruitment halted in March 2020 by COVID-19) but interesting observations were made for individual data points. In situ sarcomere lengths exhibited large variations (1.9 μm - 3.4 μm). Similarly, slack sarcomere lengths varied between 1.8 μm to 2.8 μm. Finally, while single fibers manifested stiffness values up to 119 kPa, several fiber bundles had stiffnesses as high as 2000 kPa. Histopathological analysis unveiled a variety of case-specific abnormalities, including extensive fibrosis and fatty infiltration at the extracellular level, and mitochondrial dysfunction at the intracellular level.

In the fourth study, the validation of an existing musculoskeletal model of the thoracolumbar spine was enhanced to multiple postures and activities within the sagittal plane. The variations observed for the biomechanical properties, specifically for in situ sarcomere length, elastic modulus, slack sarcomere length, along with the values in the literature for specific tension and pennation angle were input to the model. The ranges selected for all parameters except the pennation angle led to substantial variations in spinal forces. This study highlighted the importance of these parameters along with the muscle force-length curve to the spinal forces. Therefore, they should be considered in the solution method of the musculoskeletal models. Notably, more experimental data are needed to examine these parameters in different groups of patients, specifically those with adult spinal deformity.

6.2 Spinal Deformity Biomechanics

6.2.1 Geometric Properties

Several recent modeling studies have examined the effect of spinal deformity on spinal forces and moments. Almost all found altered muscle activation patterns and increased loading on the spine.

6.2.1.1 Coronal-Plane Deformity

Using a musculoskeletal model of the lumbar spine [266], Stokes [267] simulated a lumbar scoliosis (average of 15 patients) with an apex at L2 to the left of the spine but varying Cobb angles from 0°, to 13°, 26°, 38°, and 51°. Maximum effort opposing moments on T12 was applied along the three principal axes. Asymmetrical spinal loading was noted with an increasing lateral shear force associated with greater scoliosis (i.e. larger Cobb angles). In contrast to the lateral shear force, the compressive forces did not follow any specific trend: in some cases they

were applied with an offset from the symmetry plane of the vertebra toward the convex side, while in other cases the offset was on the concave sides.

Recently, advances in subject-specific modeling has enabled more realistic three-dimensional representation of scoliotic spines. Although almost all those studies have simulated idiopathic adolescent scoliosis, their findings can be insightful in studying adult scoliosis.

Bassani et al. [192] reconstructed subject-specific musculoskeletal models from the biplanar radiographs taken by EOS system for 38 adolescent patients with mild idiopathic scoliosis. Using AnyBody, they examined the spinal forces at the apex of the scoliotic curve as well as at L4-L5 and L5-S1 for the upright standing posture and found significant correlations between the forces and the geometric parameters. Interestingly, only sagittal plane geometric parameters including sacral slope, pelvic incidence, lumbar lordosis, and thoracic kyphosis exhibited significant correlations with spinal forces, and that was with the posteroanterior shear forces. The coronal plane parameters including Cobb angle appeared not to have a significant correlation with any of the force components. This lack of correlation can be due to inclusion of patients with only mild and not severe scoliosis.

Also using AnyBody model, Barba et al. [194] created subject specific models for 132 adolescent patients with idiopathic scoliosis. The scoliotic severity in each patient was described as mild, moderate, and severe if the Cobb angle was between 10° to 25°, 25° to 45°, and greater than 45°, respectively. They also adjusted PCSA of the paraspinal muscles at the convex and concave sides to represent the asymmetry reported by other studies in the literature [268][269]. The predicted muscle activations for the paraspinal muscles were in fair agreement with EMG studies [270][271] observing larger activations at the convex sides for the scoliotic curves in the

thoracic region. For upright standing, which was the only posture studied in this study, the lateral shear force was found to be proportional to the severity of the scoliosis and peaking at the apex and its immediately adjacent vertebrae.

Using OpenSim, Schmid et al. [196] analyzed the spinal forces in 24 adolescent patients with mild to moderate idiopathic scoliosis for the upright standing posture. In comparison with a model with no deformity, median of compressive forces predicted for these scoliosis patients were greater by 3%, 10%, and 18% at two levels above the apex, at the apex, and at two levels below the apex, respectively. They also examined the compressive spinal forces when carrying loads having 10%, 15%, and 20% of the body weight. The loads were carried at different positions including front (front pack), back (backpack), convex, and concave sides. Highest apical compressive forces were observed when the loads were carried on the convex side or at the front than at the concave side or at the back.

6.2.1.2 Sagittal Plane Deformity

Briggs et al. [191] digitized lateral radiographs of 44 patients and split them into high kyphosis (21 patients) and low kyphosis (23 patients) groups based on the median value of their T2-T9 kyphosis angles (which was 31.5°). By adjusting the position of the vertebrae for each patient in a model with 180 muscle fascicles [150], Briggs et al. studied the spinal forces and moments for standing. They found strong positive correlation between thoracic kyphosis curvature and the net segmental loads; and observed larger muscle forces and lumbar spinal forces. The main reason was an anterior shift in the center of mass, which led to larger moments on the spine. Muscles took the majority of that moment and resulted in an increase in compressive forces in the lumbar spine region. In another study, Briggs et al. [272] investigated the effect of a vertebral fracture in

the thoracic region on spinal forces, which also resulted in similar findings, i.e. an increase in spinal loads.

In a musculoskeletal model with the same muscles as simulated by Arjmand and Shirazi-Adl [159], Galbusera et al. [273] represented the spine geometry by three circular arcs and examined the effect of sagittal plane geometric parameters on the lumbar spinal loads. One thousand randomized models were created by varying the sagittal plane parameters, among which C7 plumb line, lumbar lordosis, and sacral slope were found to be the most influential. While C7 plumb line was more associated with the compressive force, lumbar parameters were more linked with the shear forces.

Using AnyBody, Bassani et al. [199] have recently generated 2770 artificial configurations of the upper body by varying the spinopelvic parameters. Except pelvic incidence, the other parameters including the C7 plumb line, sacral slope and lumbar lordosis (described based on Roussouly classification [274]) played a determining role in the spinal compressive and shear forces at L4-L5 or/and L5-S1 levels.

As can be inferred from this body of literature, geometric parameters, particularly those in the sagittal plane do influence the spinal loading and therefore should be considered when studying adult spinal deformity patients. Some geometric parameters including pelvic incidence remain constant through a patient's life, while the others could change. Whether that change starts on its own, or takes place to compensate for the spinal malalignment in response to a change in another geometric/muscle parameter is not clear but is important for discovering the etiology of adult spinal deformity. That knowledge can help in providing better treatments or introducing effective preventative strategies.

6.2.2 Muscle Properties

Relatively few modeling studies have investigated the effect of muscle properties on spinal deformity. However, those investigating them found interesting results.

Stokes and Gardner-Morse [275] examined the effect of different strategies for determining muscle forces in patients with scoliosis. They used the same scoliosis model developed by Stokes [267], but each time adopted one of the following three cost functions: 1) minimizing muscles stresses cubed; 2) minimizing lateral bending moments at each intervertebral joint in addition to muscle stresses cubed; and 3) reversing the spinal load asymmetry by maximizing self-correcting lateral bending moments at the joints immediately above and below the apex in addition to minimizing muscle stresses cubed. While the first cost function predicted spinal loading that would promote progression of deformity, the other two cost functions resulted in muscle activation patterns and spinal loads that would resist that. The magnitude of muscle stresses (physiological cost) was higher for the latter two strategies.

This is an important consideration when interpreting the results of modeling studies. For example, in the studies by Barba et al. [194] and Schmid et al. [196], which used AnyBody and OpenSim models, respectively, minimum muscle activations squared was adopted for the cost function. Both studies predicted greater paraspinal activations on the convex side of the thoracic scoliosis curves, which was in harmony with the findings of the EMG studies in the literature [268][269]. For the thoracolumbar curves, however, EMG studies observed larger activations at the concave side, whereas the modeling studies suggested an opposite trend. This could be due to a different strategy adopted by the central nervous system than just minimizing muscle

activations squared. Therefore, further studies on identification of neuro-control strategies of the human body will help in more accurate modeling results.

In an intriguing study, Kamal et al. [195] recently examined the effect of unilateral muscle weakening on the spinal loads in an adolescent patient with idiopathic scoliosis. Using ABAQUS and MATLAB, they created a hybrid finite element and musculoskeletal model of the growing spine based on subject-specific EOS images [209]. The muscle forces for upright standing posture were determined by minimizing the reaction moments and the sum of muscle stresses cubed while guaranteeing mechanical stability of the system. They simulated muscle weakening by 95% reduction in the PCSA of the targeted muscles. It was observed by decreasing the size of longissimus and multifidus on the concave side, the compressive forces on the concave side decreased, as did the concave-side over convex-side ratio of Von Mises stresses in the growth plates. Muscle weakening, therefore, suggested a deceleration in progression of the scoliosis curvature in their study. Their results corroborated the observation by Wong et al. [276] in nine adolescent patients with idiopathic scoliosis whose paravertebral muscles (psoas major) on the concave-side were temporally paralyzed through botulinum toxin injection. Interestingly, the radiographical measurements including the Cobb angles significantly improved six weeks after the injection.

As stated, few modeling studies have explored the effect of muscle properties on spinal deformity. Other than PCSA, properties such as in situ sarcomere length, passive elastic modulus, slack sarcomere length, or specific tension may be involved in initiation or progression of a spinal deformity. Our modeling study (Chapter 5), demonstrated the significant influence these muscle properties can have on spinal loading, but that was in a model with no deformity. Given that geometric parameters also exhibit a determining effect on the spinal loads, geometric

parameters and muscle properties should both be considered together in a model. This suggests moving toward subject-specific models, where not just the bony geometry but also the muscle properties are personalized for the patient. Obviously, more advances in experimental studies are required to obtain such data.

6.3 Clinical Correlations for Adult Spinal Deformity

6.3.1 Geometric Properties

Global spinal deformities typically involve more than one regional deformity. These regional changes may develop to compensate for an initial deformity. For example, loss of lumbar lordosis may initiate due to multi-level disc degeneration at the caudal site of the lumbar spine [32][277]. Loss of lumbar lordosis causes an anterior shift of the C7 plumb line. To compensate for the loss of lumbar lordosis and achieve global sagittal alignment, a decrease in thoracic kyphosis or increase in cervical lordosis may ensue. Such compensation may even extend to the hip and lower extremities in forms of pelvic tilt, knee flexion, or pelvic shift (Figure 6-1). All these mechanisms can be recruited by a patient to bring the sagittal vertical axis to its original place. However, the sequence and order of these changes are not well-understood and seem to vary between patients based on their age, pain level, or region of the deformity [278].

Recent classifications of sagittal alignment emphasize the need for a full analysis of the pelvis, due to its important role at the base of the spine [279][280]. Pelvic incidence describes the morphology of the pelvis and remains constant for a patient, while pelvic tilt represents the amount of pelvic rotation about the hip joint. The latter can mask the true spinal alignment, and therefore should be measured [32]. Maintaining the global sagittal alignment for people with small pelvic incidence necessitates small lumbar lordosis, while for those with a large pelvic

incidence requires large lumbar lordosis. Therefore, spinopelvic mismatch is defined as the subtraction of lumbar lordosis from the pelvic incidence. A clinical rule of thumb is to keep this parameter less than 10°[281]. However, for those with hyperkyphosis this value is recommended to be less than -10° [282]. According to a multi-center study, most clinically relevant parameters for sagittal alignment are sagittal vertical axis, spinopelvic mismatch, and pelvic tilt [279]. Ideal values for these parameters are less than 40 mm, less than 10°, and less than 20°, respectively [280].

While research on the extent of the compensatory mechanisms, their sequences, and the reasons behind them is ongoing, what seems to be a point of consensus for clinicians is that the full-body x-rays are necessary for better assessment and treatment of these patients. A full head-to-toe image assist in unmasking the compensatory mechanisms utilized by a patient to maintain their sagittal alignment. Sagittal vertical axis alone is not sufficient, as a patient may stay erect by flexing their knees, while suffering from an extreme lumbar lordosis. An important implication of these clinical findings is that musculoskeletal models should move toward full-body simulations for a more comprehensive understanding of adult spinal deformity and addressing clinical questions related to them.

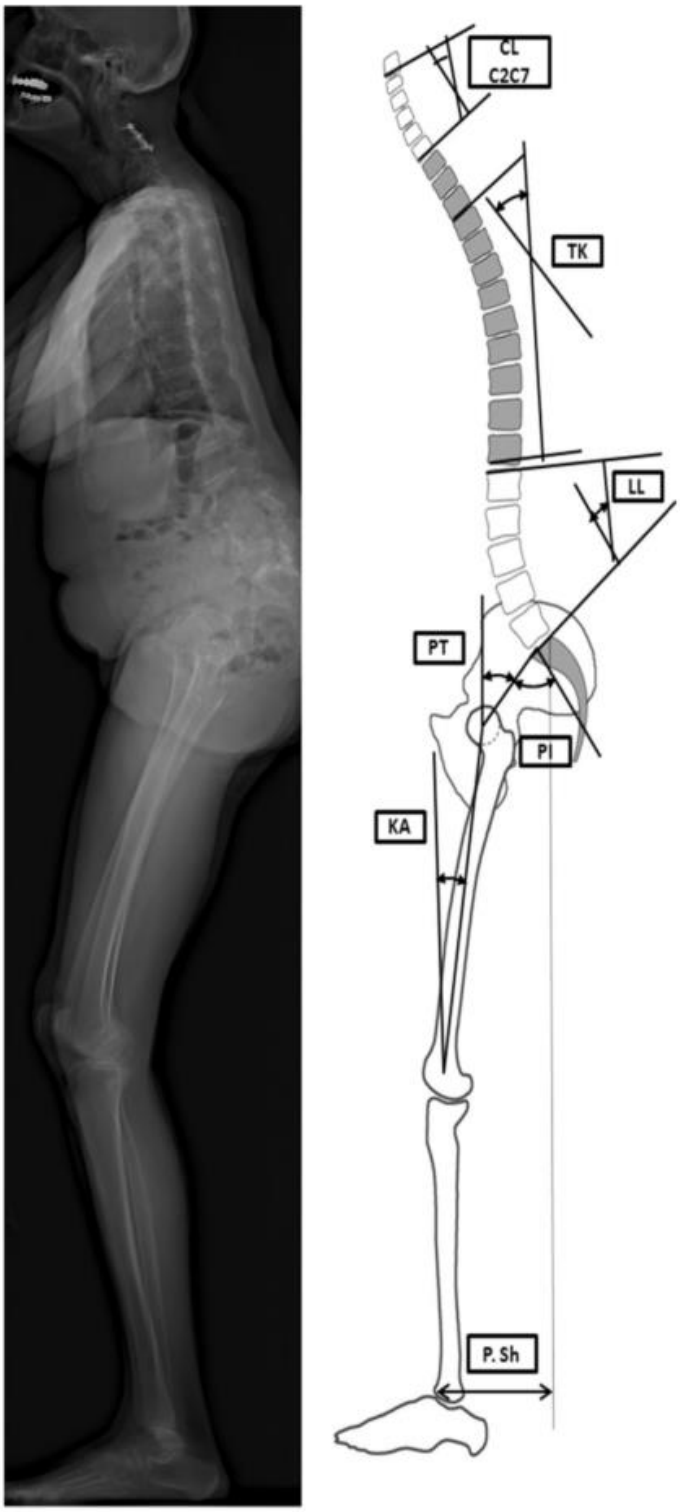

Figure 6-1. Geometric parameters associated with sagittal alignment and compensatory mechanisms. The parameters include CL: cervical lordosis; TK: thoracic kyphosis; LL: lumbar lordosis; PT: pelvic tilt; PI: pelvic incidence; KA: knee angle; P.Sh: pelvic shift. Adapted from [32] with permission from Springer Nature.

6.3.2 Muscle Properties

Multiple recent studies have explored the association of muscle properties and adult spinal deformity. Jun et al. [283] investigated the effect of lumbar (L3) paraspinal muscle quantity (cross-sectional area) and quality (fatty degeneration ratio) in 50 elderly patients (60-80 years old) on sagittal alignment of their spines. They found for muscle fatty degeneration to correlate significantly with thoracic kyphosis, pelvic tilt, sagittal vertical axis, and pelvic mismatch. The cross-sectional area of the muscles also exhibited a significant correlation with lumbar lordosis and pelvic mismatch.

Shafaq et al. [284] measured fatty infiltration and cross-sectional area of multifidus and longissimus from L1-S1 in 57 patients with degenerative lumbar scoliosis. They found that cross-sectional area and fatty infiltration of both muscles were larger on the concave than convex side at all studied vertebral levels (except for longissimus cross-sectional area which was only significant at L4-L5 and L5-S1). A histological assessment in four of these patients also reflected more degeneration on the concave than convex side. Several other studies have reported asymmetric muscle properties for patients with deformity in the coronal plane, although most of them were in adolescents with idiopathic scoliosis [285][286][287].

In a recent study published in 2021, Elysee et al. [288] examined the association of global sagittal alignment with fatty infiltration and cross-sectional area of paravertebral muscles in 107 adult spinal deformity patients. The measurements were made for multifidus, erector spinae, and psoas at T2 (49 patients), T10 (39 patients), and L3 (81 patients). In contrast to cross-sectional areas, fatty infiltration at all these levels was positively correlated with global deformity, anterior malalignment, and pelvic retroversion. The authors concluded that “In ASD patients, global

sagittal malalignment is related to FI of the PVM throughout the lumbar and thoracic spine, as identified through CT. Future research should investigate how FI relates to ASD pathogenesis" (ASD: adult spinal deformity; FI: fatty infiltration; PVM: paravertebral muscles; and CT: computed tomography). Similar messages have been noted by others [289][290][291].

It seems clear that muscle properties are gaining attention among biomechanical and clinical studies as important risk factors involved in the initiation/progression of adult spinal deformity. Our modeling study demonstrated the importance of muscle properties on spinal loading. Our preliminary histological analysis of human paravertebral muscles in adult deformity patients also revealed a variety of case-specific abnormalities at both the cellular and tissue level. However, further studies are needed to shed more light on pathogenical role of these factors. Whether the spinal deformity initiates with a geometric abnormality and muscle changes occur secondary to that or vice versa is not yet known. But what is clear is that both muscle and geometric properties are important, suggesting adoption of a holistic approach toward identifying the etiology of adult spinal deformity.

6.4 Limitations and Recommendations

For each of the four studies presented in this thesis, there were a number of limitations in the methodologies that should be considered when interpreting the results. Some of these limitations are reviewed in further details in this section and a number of recommendations are proposed accordingly for future studies.

6.4.1.1 Studying the Effect of Vertebral Level

The effect of vertebral level on paraspinal muscle biomechanical properties was examined in rats instead of humans. Although rats are also mammals and have shown similar muscle properties to humans [102], they are quadrupeds with different daily activities than humans. That should be considered when transferring the results of this study to human musculoskeletal models.

Studying the effect of vertebral levels in the human body would be ideal but that is limited by several ethical and technical challenges. Paraspinal muscles, particularly multifidus and erector spinae, are deep and close to the nerve roots making a safe non-invasive biopsy collection quite challenging. Human biopsies can be accessed intraoperatively; however, those who undergo a surgery typically have a spinal condition that may have already affected the paraspinal muscle properties [90].

Future studies interested in the effect of vertebral level may use biped animals such as primates, but that comes with substantial expenses. An alternative is to improve non-invasive biopsy collection methods [280] to warrant a safe acquisition when aiming for human paraspinal muscles. This may be possible by utilizing assistive imaging modalities (e.g. ultrasound) to guide the biopsy-collecting tool directly into the targeted muscle.

For musculoskeletal models, the stiffness at the fascicle/whole muscle level is desired. Since passive behaviour of muscles increases nonlinearly from the fiber bundle to the fascicle and whole muscle scales, an ideal study would measure the muscle stiffness directly at the whole muscle level. Such direct measurement requires detachment of one end of the whole muscle from the bone, which is not ethical in humans, especially at multiple spinal levels. Furthermore, such measurement requires an apparatus that must be sterilized, which is quite challenging to meet

operating room standards. Measuring the passive stiffness at the whole muscle level is less challenging in animals, but still difficult in rat paraspinal muscles due to their short lengths. To date, paraspinal muscle stiffness at the fascicle/whole muscle level has not been directly measured in any species.

In the current study an indirect approach was selected to contrast the biomechanical properties of the paraspinal muscles between the vertebral levels at the fascicle/whole muscle level. We investigated collagen I content of the muscle fascicles as a measure for estimation of their elastic modulus. While at the whole muscle level collagen has been observed to be a strong predictor of muscle stiffness [90], the role of other constituents in determining its stiffness at the whole muscle level has not been examined. At the fiber bundle level, several other factors such as collagen IV, collagen III, total proteoglycan, and biglycan have been shown to contribute to prediction of the bundle stiffness. Therefore, further studies at the whole muscle level should be conducted to identify those determining constituents and their weightings in predicting the stiffness. With that, indirect approaches can be adopted confidently for evaluating muscle properties. It is noteworthy that not just the content but the architecture of those constituents may influence the stiffness and should be considered.

6.4.1.2 Studying the Effect of Fiber Bundle Size

In this study larger fiber bundles exhibited a smaller elastic modulus. With the determining role of ECM in modulating the stiffness of fiber bundles, we demonstrated in an example that a smaller bundle may include larger area fraction of ECM, and hence manifest larger stiffness. From a transverse section of a muscle biopsy (at the fascicle/whole muscle level), however, one cannot determine the exact boundary of a bundle. We used the average of two segmentations,

type A (Figure 3-6A&D) and type B (Figure 3-6B&E) as an estimate of the ECM area fraction in a bundle; but the actual bundle tested mechanically for passive stiffness, may have had an area fraction closer to type A or type B. While type B segmentation and the average method suggested a larger estimate of ECM area fraction for smaller bundles, type A segmentation showed an opposite trend. Therefore, other alternatives should be sought in future studies for determining the ECM content of a bundle.

An alternative is to use the mechanically tested bundle for determining its ECM content through immunostaining. We attempted this (not included in the methodology of Chapter 3) by fixing ~20 tested bundles in formaldehyde for a day, keeping them in a sucrose solution for another two days, and placing them into O.C.T. (optimal cutting temperature) compound for sectioning them transversely. However, due to the tiny size of the bundles, achieving a transverse section perpendicular to the fiber direction was not possible in some cases. In many cases the fibers within the bundle deteriorated or became separated (Figure 6-2). Therefore, if this approach is selected by a future study, fine tuning the methodology to avoid those artifacts is essential.

Another alternative is to measure the constituents of the mechanically tested bundles through biochemical processing. For example, a hydroxyproline assay can be used to measure the collagen content of a fiber bundle. By knowing the volume of the bundle, the collagen volume fraction can be determined [108].

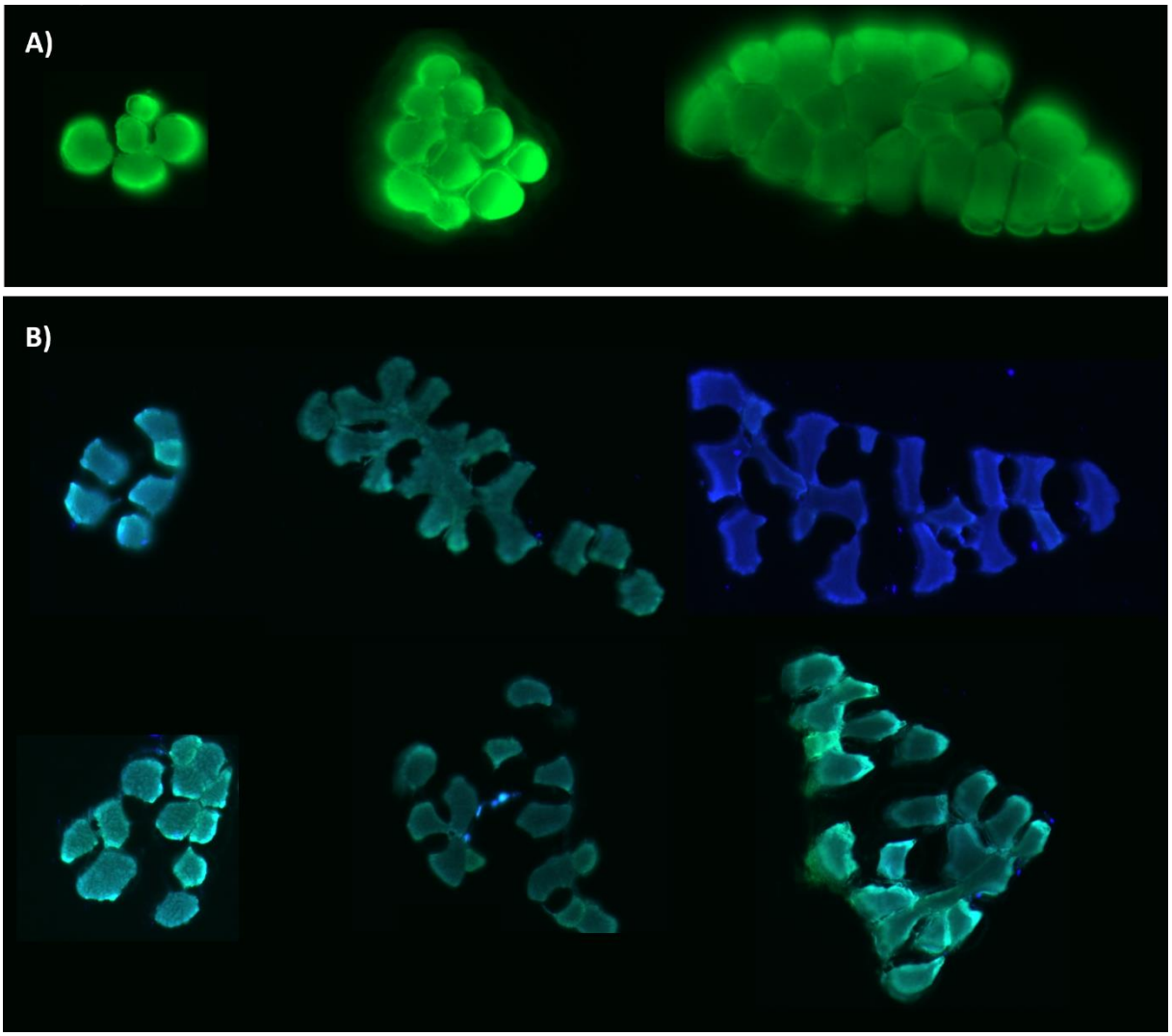

Figure 6-2. Transverse cross section of the tested fiber bundles. Bundles were placed in formaldehyde for a day, transferred to a sucrose solution for another two days, and finally placed in into O.C.T. compound for sectioning. Due to the tiny size of the bundles, achieving an intact non-deteriorated cross section of the fiber bundles (A), was not always possible following this methodology (B).

Another limitation of our study was only measuring collagen I content to approximate the ECM content. As discussed in section 6.4.1.1, other constituents of the ECM may be involved in determining its stiffness. Therefore, future studies should measure the content of other constituents along with collagen for a more accurate estimation of ECM content.

6.4.1.3 Human Study

The main limitation of our human study was the small number of patients recruited due to restrictions imposed because of COVID-19. Based on our power analysis, we aimed for 16 patients in each of the three groups, but we were able to recruit only four patients for group I, three for group II, and two for group III. This prevented us from a statistical comparison between the patient groups, although several intriguing observations were made biomechanically and histopathologically. Once restrictions are lifted, the study should continue in search for patterns and differences between the patient groups.

Non-invasive measurement of the muscle properties investigated in this study was not feasible, which prevented us from recruiting a healthy population as control. Therefore, we defined patient group I (with no deformity) as the control group for the other two patient groups who had a sagittal deformity (although it was compensated in group II). Considerable changes in paraspinal muscle passive properties in response to intervertebral disc injuries have been shown by animal studies [90]. Also, various morphological and biochemical changes in paraspinal muscles have been documented for patients with low back pain. Therefore, the muscle properties measured in patient group I may be different than the healthy population. Yet, once the study is complete, clear differences might be observed in muscle properties due to different nature of the pathology of these patients.

To include a healthy control group, future studies should move toward non/minimally invasive techniques for measurement of in situ sarcomere length and passive properties. Using the second harmonic generation of the light beam and specialized needles equipped with two tiny prisms, a minimally invasive measurement of in situ sarcomere length in healthy individuals has become

feasible recently [258] but has not yet been used for paraspinal muscles. Similar tools used for biopsy acquisition from lower extremity muscles can be equipped with imaging-guided techniques to provide a safe acquisition of muscle biopsies from the deep paraspinal muscles. Those biopsies can be used for assessing muscle passive properties.

A major shortcoming, which is not just limited to this study, relates to determining muscle passive properties at the whole muscle level. Musculoskeletal models require such information, but direct measurement of that in human is not ethically/technically feasible (for the reasons described in section 6.4.1.1). Therefore, an indirect method should be adopted.

To determine the paraspinal muscle stiffness at the whole muscle level indirectly, more than one measurement technique is required. Mechanical testing of fiber bundle stiffness encompasses the stiffness of muscle fibers and to some extent the extracellular matrix but excludes the stiffness contribution from some other important constituents of the muscle. At the fascicle and whole muscle level, there are other tissues including perimysium and epimysium that are ignored if one suffices to the bundle level measurements. In addition, most of the human biopsies tested in our study included fibrosis and fatty infiltration, which were heterogeneously distributed across a collected muscle biopsy. When extracting fiber bundles, we would aim for muscle bundles that mainly were comprised of muscle fibers. The reason was that our strain measurements were based on laser diffraction technique, which only functions properly on bundles containing muscle fibers. Therefore, our data on bundle elastic modulus is biased toward the portion of a muscle biopsy that contains muscle fibers and may not represent the entire biopsy. This means a muscle fascicle in a patient might have had a very high elastic modulus due to the abundance of connective tissues, but the fiber bundle tested in our study reported a small value, as it was extracted from the portion of the biopsy that was mostly occupied by the contractile tissues.

MRI can provide a whole picture of muscles, where fatty infiltration can be differentiated from muscle tissue. However, current clinical MR techniques are not able to detect fibrosis. Histological assessments, on the other hand, offer valuable information on the entire biopsy structure and clearly differentiate between the contractile muscle tissue and fibrosis or other non-muscle tissues. However, biopsies collected from the same muscle have shown to differ depending on where in that muscle they were collected. In the study by Padwal et al. [238], although the collagen content of the biopsies from superficial versus deep regions of human multifidus were the same, the superficial biopsies had less loose and denser collagen in contrast to those taken from the deep region.

These observations suggest that MRI, histology, and mechanical testing of fiber bundles can each provide information on only certain part of the whole muscle stiffness. Therefore, a summation of those information is required to provide a holistic estimation of the passive properties at the whole muscle level.

Future studies at all three fronts including MRI, histology, and fiber bundle mechanical testing should be conducted to facilitate estimation of whole muscle stiffness. We have recently added the ability of measuring strains using image processing techniques to our apparatus, therefore our mechanical testing will not be limited to the bundles from the contractile portion of the biopsies; rather the stiffness of specimens mostly consisted of connective tissues can also be quantified.

Further histological and biochemical analysis of the mechanically tested fiber bundles should be performed to discover correlations between muscle tissue constituents and a bundle stiffness. With such correlations, one can suffice to histological assessment of a biopsy and estimate its stiffness without needing to test them mechanically.

Future imaging studies may focus on finding biomarkers with which fibrosis and other relevant constituents of muscle tissues can be detected and quantified. Using the correlations obtained from histological studies and with improvements in machine learning algorithms, in the future one may only use the MR image to estimate the whole muscle stiffness non-invasively, without any need for mechanical testing or histological assessment.

6.4.1.4 Musculoskeletal Modeling

Our musculoskeletal modeling study demonstrated the significance of biomechanical muscle properties on spinal loading. Although the analysis was conducted only for two static activities, that sufficiently served our purpose of highlighting their importance. However, it would be interesting to explore the effect of those properties in other asymmetric and dynamic daily activities, which remains to be addressed in future studies.

The share of the intervertebral disc from the axial force was considered 85% for all postures in this study. However, this value has been shown to vary between postures and to be greater in flexion compared to upright standing or extension [252][253]. For example, the percentage of a 700N axial force taken by facet joints in 9 human FSUs had a range of 8% to 25% in 5° extension as opposed to 2% to 9% in 5° flexion [292]. For higher compressive forces however, a wider range of data is presented in the literature: for flexion and extension, respectively, values as low as 2% and 8% [293] and as high as 22% and 30% [294] are reported for facet joints. Therefore, assuming 85% load-carriage by the disc is reasonable but adjusting this value in the model based on postures and the amount of compressive force is ideal and should be considered in future studies.

The effect of intra-abdominal pressure was modeled as an upward force on thorax. This is an under representation of intra-abdominal pressure as is it exerts forces in all directions especially onto the spinal column and supports the vertebrae against shear forces. This implies the shear forces in our study, especially those directed anteriorly may have been overestimated.

Mechanical stability of the spine was not considered in our solution method. Inclusion of that criterion leads to co-contraction of abdominal muscles, which most optimization models fail to predict [163]. This results in higher forces in upright standing or other light activities, but for heavy work activities or postures like flexion where passive structures are more involved, inclusion of stability criterion appears not to make a difference [250][264]. Adding the stability criterion to our solution method remains as a future step.

The next version of our model should address the limitations listed above. This includes adding a mechanical stability criterion to the solution method, incorporating a more realistic representation of the effect of the intra abdominal pressure, and considering posture-specific ratios for sharing the axial forces between the intervertebral disc and the posterior elements. In addition, the validation of the model should be extended to asymmetric postures and activities.

Another shortcoming, which was not just limited to this study, was the paucity of the data in the literature on human paraspinal muscle properties. Our musculoskeletal modeling study demonstrated the pivotal role of the slack sarcomere length and elastic modulus in spinal loading; nevertheless, no study to the best of author's knowledge has measured them at the whole muscle level for the paraspinal muscles. Further experimental studies are required to enhance our knowledge of these parameters. Given the tissue heterogeneity observed for patients at the whole muscle level, the muscle properties in the models should be adjusted to account for

such heterogeneity. This can be done by using the rule of mixture, i.e. Equation (3-1), but at the whole muscle level.

In line with the overall goal of this PhD project, we aimed to develop patient specific models of the spine based on the data we collected from our human study. In addition to the muscle properties, we have standing x-rays of our patients in addition to their supine MRI and standing Open MRI in several postures. Using these data, a set of musculoskeletal models with personalized muscle properties and geometric parameters can be developed in future studies. Such models can serve a variety of purposes including studying etiology of adult spinal deformity or assisting in planning surgeries.

6.5 Contributions

The overall goal of this research project was to investigate if biomechanical properties of the paraspinal muscles are different in adult spinal deformity patients; and whether those differences could influence spinal loading and be associated with initiation/progression of adult spinal deformity. To achieve that overall goal, this thesis made the following specific contributions:

1. Developed and validated an apparatus for measuring passive stiffness of muscle fibers and fiber bundles. This included a temperature-controlled solution bath, a precise length controller, and a photodiode array system for measurement of muscle sarcomere lengths using the laesr diffraction technique.
2. Designed a specialized muscle biopsy clamp in collaboration with Medtronic engineers to collect human muscle biopsies intraoperatively. Manufactured the first prototype of the clamp and validated its functionality in a rat study.
3. Developed the tools and protocols required for acquiring intraoperative biopsies from patients with spinal deformity at Vancouver General Hospital and Toronto Western Hospital.

4. Developed and received animal and human ethics approval for intraoperative muscle biopsy acquisition from rats and humans, respectively.
5. Collected intraoperative biopsies from nine patients and evaluated them biomechanically and histopathologically.
6. Tested extensively the passive properties of rat and human skeletal muscle fibers and fiber bundles (more than 500 fibers/fiber bundles).
7. Investigated the effect of vertebral level on biomechanical properties of paraspinal muscles in 13 healthy rats.
8. Investigated the effect of fiber and fiber bundle size on the elastic modulus of rats and humans.
9. Improved the solution method of a musculoskeletal model of the lumbar spine (previously developed by the author during his Matser's studies) and enhanced its validation to several other postures and activities.
10. Investigated the influence of biomechanical properties of paraspinal muscles on spinal loading. The properties included the passive elastic modulus, slack sarcomere length, in situ sarcomere length, specific tension and pennation angle.

6.6 Conclusions

With reference to the objectives of this thesis, it can be concluded that:

1a) Biomechanical properties of the paraspinal muscles including the elastic modulus and slack sarcomere length are independent of the vertebral level at the fiber and fiber bundle levels;

1b) Collagen content of paraspinal muscles at the fascicle/whole muscle level is independent of the spinal level; therefore, within a muscle group, assumption of similar biomechanical properties between the vertebral levels appears to be fine.

2a) Larger fibers and fiber bundle sizes manifest smaller elastic moduli; therefore, future studies of passive property measurement should aim for consistent bundle sizes, especially when making comparison between different groups.

2b) Measuring diameters of fibers and fiber bundles at least from two orthogonal views is necessary for higher accuracy of calculating their elastic modulus.

3a) Paraspinal muscles in adult spinal deformity patients present with large variations in their biomechanical properties including the in situ sarcomere length, elastic modulus, and slack sarcomere length.

3b) Substantially stiffer fiber bundles in some patients have biomechanical implications and reflects the importance of extracellular matrix.

3c) Presence of a variety of case-specific cellular and extracellular abnormalities in paraspinal muscles of adult spinal deformity patients are suggestive of diverse causes or mechanisms of potential functional impairment.

4a) Paraspinal muscle properties, specifically slack sarcomere length, passive stiffness, in situ sarcomere length, and specific tension dramatically influence the spinal forces. Therefore, future modeling studies should incorporate those parameters in their model for more accurate and physiological results. Given the paucity of data in the literature, further experimental studies for measurement of these parameters in vivo should be conducted.

The results of this line of research in the long term will provide insight into the significance of muscle functional properties in the development of spinal disorders and may suggest shifting the focus of future treatments toward muscle-preserving strategies, pharmaceutical approaches such

as botulinum toxin injections, or advent of muscle remodeling techniques to prevent progression of such spinal conditions.

Bibliography

[1] United Nations Department of Economic and Social Affairs, P. D., 2020, "World Population Ageing 2020 Highlights: Living Arrangements of Older Persons Ageing 2020."

[2] Kado, D. M., Prenovost, K., and Crandall, C., 2007, "Narrative Review: Hyperkyphosis in Older Persons," Ann. Intern. Med., **147**(5), pp. 330–338.

[3] Perennou, D., Marcelli, C., Herisson, C., and Simon, L., 1994, "Adult Lumbar Scoliosis: Epidemiologic Aspects in a Low-Back Pain Population," Spine (Phila. Pa. 1976)., **19**(2), pp. 123–128.

[4] Kebaish, K. M., Neubauer, P. R., Voros, G. D., Khoshnevisan, M. A., and Skolasky, R. L., 2011, "Scoliosis in Adults Aged Forty Years and Older: Prevalence and Relationship to Age, Race, and Gender," Spine (Phila. Pa. 1976)., **36**(9), pp. 731–736.

[5] Imagama, S., Matsuyama, Y., Hasegawa, Y., Sakai, Y., Ito, Z., Ishiguro, N., and Hamajima, N., 2011, "Back Muscle Strength and Spinal Mobility Are Predictors of Quality of Life in Middle-Aged and Elderly Males," Eur. Spine J., **20**(6), pp. 954–961.

[6] Katzman, W. B., Wanek, L., Shepherd, J. A., and Sellmeyer, D. E., 2010, "Age-Related Hyperkyphosis: Its Causes, Consequences, and Management," J. Orthop. Sport. Phys. Ther., **40**(6), pp. 352–360.

[7] Sinaki, M., Itoi, E., Rogers, J. W., Bergstralh, E. J., and Wahner, H. W., 1996, "Correlation of Back Extensor Strength with Thoracic Kyphosis and Lumbar Lordosis in Estrogen-Deficient Women," Am. J. Phys. Med. Rehabil., **75**(5), pp. 370–374.

[8] Sinaki, M., Brey, R. H., Hughes, C. A., Larson, D. R., and Kaufman, K. R., 2005, "Balance Disorder and Increased Risk of Falls in Osteoporosis and Kyphosis: Significance of Kyphotic Posture and Muscle Strength," Osteoporos. Int., **16**(8), pp. 1004–1010.

[9] Mika, A., Unnithan, V. B., and Mika, P., 2005, "Differences in Thoracic Kyphosis and in Back Muscle Strength in Women with Bone Loss Due to Osteoporosis," Spine (Phila. Pa. 1976)., **30**(2), pp. 241–246.

[10] Sinaki, M., Wollan, P. C., Scott, R. W., and Gelczer, R. K., 1996, "Can Strong Back Extensors Prevent Vertebral Fractures in Women with Osteoporosis?," *Mayo Clinic Proceedings*, Elsevier, pp. 951–956.

[11] Granito, R. N., Aveiro, M. C., Renno, A. C. M., Oishi, J., and Driusso, P., 2012, "Comparison of Thoracic Kyphosis Degree, Trunk Muscle Strength and Joint Position Sense among Healthy and Osteoporotic Elderly Women: A Cross-Sectional Preliminary Study," Arch. Gerontol. Geriatr., **54**(2), pp. e199–e202.

[12] Weale, R., and Weale, M., 2012, "The Dowager's Hump: An Early Start?," Gerontology, **58**(3), pp. 212–215.

[13] Kang, C. H., Shin, M. J., Kim, S. M., Lee, S. H., and Lee, C. S., 2007, "MRI of Paraspinal Muscles in Lumbar Degenerative Kyphosis Patients and Control Patients with Chronic Low Back Pain," Clin. Radiol., **62**(5), pp. 479–486.

[14] Hyun, S. J., Kim, Y. J., and Rhim, S. C., 2016, "Patients with Proximal Junctional Kyphosis after Stopping at Thoracolumbar Junction Have Lower Muscularity, Fatty Degeneration at the Thoracolumbar Area," Spine J., **16**(9), pp. 1095–1101.

[15] Park, K. hee, Oh, J. seop, An, D. hyun, Yoo, W. gyu, Kim, J. man, Kim, T. ho, and Kang, M. hyeok, 2015, "Difference in Selective Muscle Activity of Thoracic Erector Spinae During Prone Trunk Extension Exercise in Subjects With Slouched Thoracic Posture," PM R, **7**(5), pp. 479–484.

[16] White, A. A., and Panjabi, M. M., 1990, "Clinical Biomechanics of the Spine," Lippincott Philadelphia, PA, **446**.

[17] Netter, F. H., 2014, *Atlas of Human Anatomy, Professional Edition: Including NetterReference.Com Access with Full Downloadable Image Bank (Google EBook)*, Elsevier health sciences.

[18] Schmidt, H., 2006, "Finite-Elemente-Analyse Zur Bestimmung Des Mechanischen Verhaltens Der Gesunden Und Degenerierten Bandscheibe Unter Komplexer Belastung."

[19] Adams, M. A., and Roughley, P. J., 2006, "What Is Intervertebral Disc Degeneration, and What Causes It?," Spine (Phila. Pa. 1976)., **31**(18), pp. 2151–2161.

[20] Broom, N. D., and Thambyah, A., 2018, "The Intervertebral Disc–Endplate System," *The Soft–Hard Tissue Junction: Structure, Mechanics and Function*, Cambridge University Press, pp. 155–282.

[21] Wallner-Schlotfeldt, T., 2000, *Clinical Anatomy of the Lumbar Spine and Sacrum*, Elsevier Health Sciences.

[22] Catalyst University, 2020, "The Major Ligaments of the Spine" [Online]. Available: https://www.youtube.com/watch?app=desktop&v=_GHzD4ZDM6A. [Accessed: 03-Feb-2021].

[23] Skandalakis, J. E., 1999, *Clinically Oriented Anatomy*, Lippincott Williams & Wilkins.

[24] Horan, F., 2009, "Gray's Anatomy: The Anatomical Basis of Clinical Practice," J. Bone Joint Surg. Br., **91-B**(7), pp. 983–983.

[25] Ward, S. R., Tomiya, A., Regev, G. J., Thacker, B. E., Benzl, R. C., Kim, C. W., and Lieber, R. L., 2009, "Passive Mechanical Properties of the Lumbar Multifidus Muscle Support Its Role as a Stabilizer," J. Biomech., **42**(10), pp. 1384–1389.

[26] Daggfeldt, K., and Thorstensson, A., 2003, "The Mechanics of Back-Extensor Torque Production about the Lumbar Spine," J. Biomech., **36**(6), pp. 815–825.

[27] Malakoutian, M., 2014, "Degeneration and Mechanics of the Segment Adjacent to a Lumbar Spine Fusion : A Biomechanical Analysis," University of British Columbia.

[28] Bogduk, N., Pearcy, M., and Hadfield, G., 1992, "Anatomy and Biomechanics of Psoas Major," Clin. Biomech., **7**(2), pp. 109–119.

[29] O'Lynnger, T. M., Zuckerman, S. L., Morone, P. J., Dewan, M. C., Vasquez-Castellanos, R. A., and Cheng, J. S., 2015, "Trends for Spine Surgery for the Elderly: Implications for Access to Healthcare in North America," Neurosurgery, **77**(4), pp. S136–S141.

[30] Schwab, F., Dubey, A., Gamez, L., El Fegoun, A. B., Hwang, K., Pagala, M., and Farcy, J. P., 2005, "Adult Scoliosis: Prevalence, SF-36, and Nutritional Parameters in an Elderly

Volunteer Population," Spine (Phila. Pa. 1976)., **30**(9), pp. 1082–1085.

[31] Ames, C. P., Scheer, J. K., Lafage, V., Smith, J. S., Bess, S., Berven, S. H., Mundis, G. M., Sethi, R. K., Deinlein, D. A., Coe, J. D., Hey, L. A., and Daubs, M. D., 2016, "Adult Spinal Deformity: Epidemiology, Health Impact, Evaluation, and Management," Spine Deform., **4**(4), pp. 310–322.

[32] Diebo, B. G., Henry, J., Lafage, V., and Berjano, P., 2014, "Sagittal Deformities of the Spine: Factors Influencing the Outcomes and Complications," Eur. Spine J., **24**(1), pp. 3–15.

[33] Youssef, J. A., Orndorff, D. O., Patty, C. A., Scott, M. A., Price, H. L., Hamlin, L. F., Williams, T. L., Uribe, J. S., and Deviren, V., 2013, "Current Status of Adult Spinal Deformity," Glob. Spine J., **3**(1), pp. 051–062.

[34] Ailon, T., Smith, J. S., Shaffrey, C. I., Lenke, L. G., Brodke, D., Harrop, J. S., Fehlings, M., and Ames, C. P., 2015, "Degenerative Spinal Deformity," Neurosurgery, **77**(4), pp. S75–S91.

[35] Cho, K.-J., Kim, Y.-T., Seo, B., and Shin, J., 2016, "Radiological Evaluation and Classification of Adult Spinal Deformity," J. Korean Orthop. Assoc., **51**(1), p. 1.

[36] Ailon, T., Shaffrey, C. I., Lenke, L. G., Harrop, J. S., and Smith, J. S., 2015, "Progressive Spinal Kyphosis in the Aging Population," Neurosurgery, **77**(4), pp. S164–S172.

[37] Diebo, B. G., Shah, N. V., Boachie-Adjei, O., Zhu, F., Rothenfluh, D. A., Paulino, C. B., Schwab, F. J., and Lafage, V., 2019, "Adult Spinal Deformity," Lancet, **394**(10193), pp. 160–172.

[38] Kim, H., Kim, H. S., Moon, E. S., Yoon, C. S., Chung, T. S., Song, H. T., Suh, J. S., Lee, Y. H., and Kim, S., 2010, "Scoliosis Imaging: What Radiologists Should Know," Radiographics, **30**(7), pp. 1823–1842.

[39] Good, C. R., Auerbach, J. D., O'Leary, P. T., and Schuler, T. C., 2011, "Adult Spine Deformity," Curr. Rev. Musculoskelet. Med., **4**(4), pp. 159–167.

[40] Šarčević, Z., Savić, D., and Tepavčević, A., 2020, "Correlation between Isometric Strength in Five Muscle Groups and Inclination Angles of Spine," Eur. Spine J., **29**(1), pp. 161–168.

[41] Ensrud, K. E., Black, D. M., Harris, F., Ettinger, B., and Cummings, S. R., 1997, "Correlates of Kyphosis in Older Women," J. Am. Geriatr. Soc., **45**(6), pp. 682–687.

[42] Kado, D. M., Huang, M. H., Karlamangla, A. S., Cawthon, P., Katzman, W., Hillier, T. A., Ensrud, K., and Cummings, S. R., 2013, "Factors Associated with Kyphosis Progression in Older Women: 15 Years' Experience in the Study of Osteoporotic Fractures," J. Bone Miner. Res., **28**(1), pp. 179–187.

[43] Schneider, D. L., Von Mühlen, D. G., Barrett-Connor, E., and Sartoris, D. J., 2004, "Kyphosis Does Not Equal Vertebral Fractures: The Rancho Bernardo Study," J. Rheumatol., **31**(4), pp. 747–752.

[44] Nardo, L., Lane, N. E., Parimi, N., Cawthon, P. M., Fan, B., Shepherd, J., Cauley, J., Zucker-Levin, A., Murphy, R. A., and Katzman, W. B., 2014, "Diffuse Idiopathic Skeletal Hyperostosis Association with Thoracic Spine Kyphosis: A Cross-Sectional Study for the

Health Aging and Body Composition Study," Spine (Phila. Pa. 1976)., **39**(24), pp. E1418–E1424.

[45] Roghani, T., Zavieh, M. K., Manshadi, F. D., King, N., and Katzman, W., 2017, "Age-Related Hyperkyphosis: Update of Its Potential Causes and Clinical Impacts—Narrative Review," Aging Clin. Exp. Res., **29**(4), pp. 567–577.

[46] Roghani, T., Khalkhali Zavieh, M., Talebian, S., Akbarzadeh Baghban, A., and Katzman, W., 2019, "Back Muscle Function in Older Women With Age-Related Hyperkyphosis: A Comparative Study," J. Manipulative Physiol. Ther., **42**(4), pp. 284–294.

[47] Balzini, L., Vannucchi, L., Benvenuti, F., Benucci, M., Monni, M., Cappozzo, A., and Stanhope, S. J., 2003, "Clinical Characteristics of Flexed Posture in Elderly Women," J. Am. Geriatr. Soc., **51**(10), pp. 1419–1426.

[48] Sugai, K., Michikawa, T., Takebayashi, T., and Nishiwaki, Y., 2019, "Association Between Muscle Strength, Mobility, and the Progression of Hyperkyphosis in the Elderly: The Kurabuchi Cohort Study," Journals Gerontol. - Ser. A Biol. Sci. Med. Sci., **74**(12), pp. 1987–1992.

[49] Cangussu-Oliveira, L. M., Porto, J. M., Freire Junior, R. C., Capato, L. L., Gomes, J. M., Herrero, C. F. P. da S., Nogueira-Barbosa, M. H., de Paula, F. J. A., and de Abreu, D. C. C., 2020, "Association between the Trunk Muscle Function Performance and the Presence of Vertebral Fracture in Older Women with Low Bone Mass," Aging Clin. Exp. Res., **32**(6), pp. 1067–1076.

[50] Banno, T., Arima, H., Hasegawa, T., Yamato, Y., Togawa, D., Yoshida, G., Yasuda, T., Oe, S., Mihara, Y., Ushirozako, H., and Matsuyama, Y., 2019, "The Effect of Paravertebral Muscle on the Maintenance of Upright Posture in Patients With Adult Spinal Deformity," Spine Deform., **7**(1), pp. 125–131.

[51] Cholewicki, J., and McGill, S. M., 1996, "Mechanical Stability of the in Vivo Lumbar Spine: Implications for Injury and Chronic Low Back Pain," Clin. Biomech., **11**(1), pp. 1–15.

[52] Lieber, R. L., 2011, *Skeletal Muscle Structure, Function, and Plasticity*, Lippincott Williams & Wilkins.

[53] Borg, T. K., and Caulfield, J. B., 1980, "Morphology of Connective Tissue in Skeletal Muscle," Tissue Cell, **12**(1), pp. 197–207.

[54] Lieber, R. L., 2008, *Skeletal Muscle Structure, Function, and Plasticity*, Lippincott Williams & Wilkins.

[55] Ward, S. R., Winters, T. M., O'Connor, S. M., and Lieber, R. L., 2020, "Non-Linear Scaling of Passive Mechanical Properties in Fibers, Bundles, Fascicles and Whole Rabbit Muscles," Front. Physiol., **11**.

[56] Marieb, E. N., 2000, *Essentials of Human Anatomy & Physiology*, Benjamin Cummings.

[57] Shishmarev, D., 2020, "Excitation-Contraction Coupling in Skeletal Muscle: Recent Progress and Unanswered Questions," Biophys. Rev., **12**(1), pp. 143–153.

[58] Wikipedia, "Sarcoplasmic Reticulum," Wikipedia [Online]. Available: https://en.wikipedia.org/wiki/Sarcoplasmic_reticulum. [Accessed: 03-Feb-2021].

[59] Bottinelli, R., Canepari, M., Pellegrino, M. A., and Reggiani, C., 1996, "Force-Velocity Properties of Human Skeletal Muscle Fibres: Myosin Heavy Chain Isoform and Temperature Dependence," J. Physiol., **495**(2), pp. 573–586.

[60] De Deyne, P. G., Hayatsu, K., Meyer, R., Paley, D., and Herzenberg, J. E., 1999, "Muscle Regeneration and Fiber-type Transformation during Distraction Osteogenesis," J. Orthop. Res., **17**(4), pp. 560–570.

[61] Goldspink, G., Scutt, A., Loughna, P. T., Wells, D. J., Jaenicke, T., and Gerlach, G. F., 1992, "Gene Expression in Skeletal Muscle in Response to Stretch and Force Generation," Am. J. Physiol. Integr. Comp. Physiol., **262**(3), pp. R356–R363.

[62] Andersen, J. L., and Aagaard, P., 2000, "Myosin Heavy Chain IIX Overshoot in Human Skeletal Muscle," Muscle and Nerve, **23**(7), pp. 1095–1104.

[63] Fry, A. C., 2004, "The Role of Resistance Exercise Intensity on Muscle Fibre Adaptations," Sport. Med., **34**(10), pp. 663–679.

[64] Pansarasa, O., Rinaldi, C., Parente, V., Miotti, D., Capodaglio, P., and Bottinelli, R., 2009, "Resistance Training of Long Duration Modulates Force and Unloaded Shortening Velocity of Single Muscle Fibres of Young Women," J. Electromyogr. Kinesiol., **19**(5), pp. e290–e300.

[65] Aagaard, P., Andersen, J. L., Dyhre-Poulsen, P., Leffers, A. M., Wagner, A., Peter Magnusson, S., Halkjær-Kristensen, J., and Simonsen, E. B., 2001, "A Mechanism for Increased Contractile Strength of Human Pennate Muscle in Response to Strength Training: Changes in Muscle Architecture," J. Physiol., **534**(2), pp. 613–623.

[66] Makarov, M., Birch, J., and Samchukov, M., 2009, "The Role of Variable Muscle Adaptation to Limb Lengthening in the Development of Joint Contractures: An Experimental Study in the Goat," J. Pediatr. Orthop., **29**(2), pp. 175–181.

[67] Elsalanty, M., Makarov, M., Cherkashin, A., Birch, J., and Samchukov, M., 2007, "Changes in Pennate Muscle Architecture after Gradual Tibial Lengthening in Goats," Anat. Rec., **290**(5), pp. 461–467.

[68] Williams, P., Kyberd, P., Simpson, H., Kenwright, J., and Goldspink, G., 1998, "The Morphological Basis of Increased Stiffness of Rabbit Tibialis Anterior Muscles during Surgical Limb-Lengthening," J. Anat., **193**(1), pp. 131–138.

[69] Lindsey, C. A., Makarov, M. R., Shoemaker, S., Birch, J. G., Buschang, P. H., Cherkashin, A. M., Welch, R. D., and Samchukov, M. L., 2002, "The Effect of the Amount of Limb Lengthening on Skeletal Muscle," Clin. Orthop. Relat. Res., **402**(402), pp. 278–287.

[70] Boakes, J. L., Foran, J., Ward, S. R., and Lieber, R. L., 2007, "Case Report: Muscle Adaptation by Serial Sarcomere Addition 1 Year after Femoral Lengthening," Clin. Orthop. Relat. Res., **456**(456), pp. 250–253.

[71] Tabary, J. C., Tabary, C., Tardieu, C., Tardieu, G., and Goldspink, G., 1972, "Physiological and Structural Changes in the Cat's Soleus Muscle Due to Immobilization at Different Lengths by Plaster Casts," J. Physiol., **224**(1), pp. 231–244.

[72] Griffin, G. E., Williams, P. E., and Goldspink, G., 1971, "Region of Longitudinal Growth in Striated Muscle Fibres," Nat. New Biol., **232**(27), pp. 28–29.

[73] Williams, P. E., and Goldspink, G., 1971, "Longitudinal Growth of Striated Muscle Fibres.," J. Cell Sci., **9**(3), pp. 751–767.

[74] Heslinga, J. W., te Kronnie, G., and Huijing, P. A., 1995, "Growth and Immobilization Effects on Sarcomeres: A Comparison between Gastrocnemius and Soleus Muscles of the Adult Rat," Eur. J. Appl. Physiol. Occup. Physiol., **70**(1), pp. 49–57.

[75] Csapo, R., Maganaris, C. N., Seynnes, O. R., and Narici, M. V, 2010, "On Muscle, Tendon and High Heels," J. Exp. Biol., **213**(15), pp. 2582–2588.

[76] Seynnes, O. R., De Boer, M., and Narici, M. V., 2007, "Early Skeletal Muscle Hypertrophy and Architectural Changes in Response to High-Intensity Resistance Training," J. Appl. Physiol., **102**(1), pp. 368–373.

[77] Burkholder, T. J., and Lieber, R. L., 1998, "Sarcomere Number Adaptation after Retinaculum Transection in Adult Mice.," J. Exp. Biol., **201**(Pt 3), pp. 309–316.

[78] Mathewson, M. A., Ward, S. R., Chambers, H. G., and Lieber, R. L., 2015, "High Resolution Muscle Measurements Provide Insights into Equinus Contractures in Patients with Cerebral Palsy," J. Orthop. Res., **33**(1), pp. 33–39.

[79] Narici, M. V, and Maganaris, C. N., 2007, "Plasticity of the Muscle-Tendon Complex with Disuse and Aging," Exerc. Sport Sci. Rev., **35**(3), pp. 126–134.

[80] Farup, J., Kjølhede, T., Sørensen, H., Dalgas, U., MØller, A. B., Vestergaard, P. F., Ringgaard, S., Bojsen-Møller, J., and Vissing, K., 2012, "Muscle Morphological and Strength Adaptations to Endurance vs. Resistance Training," J. Strength Cond. Res., **26**(2), pp. 398–407.

[81] D'Antona, G., Pellegrino, M. A., Adami, R., Rossi, R., Carlizzi, C. N., Canepari, M., Saltin, B., and Bottinelli, R., 2003, "The Effect of Ageing and Immobilization on Structure and Function of Human Skeletal Muscle Fibres," J. Physiol., **552**(2), pp. 499–511.

[82] Trappe, S., Trappe, T., Gallagher, P., Harber, M., Alkner, B., and Tesch, P., 2004, "Human Single Muscle Fibre Function with 84 Day Bed-Rest and Resistance Exercise," J. Physiol., **557**(2), pp. 501–513.

[83] Kjaer, M., 2004, "Role of Extracellular Matrix in Adaptation of Tendon and Skeletal Muscle to Mechanical Loading," Physiol. Rev., **84**(2), pp. 649–698.

[84] Regev, G. J., Kim, C. W., Tomiya, A., Lee, Y. P., Ghofrani, H., Garfin, S. R., Lieber, R. L., and Ward, S. R., 2011, "Psoas Muscle Architectural Design, in Vivo Sarcomere Length Range, and Passive Tensile Properties Support Its Role as a Lumbar Spine Stabilizer," Spine (Phila. Pa. 1976)., **36**(26), pp. E1666–E1674.

[85] Gajdosik, R. L., 2001, "Passive Extensibility of Skeletal Muscle: Review of the Literature with Clinical Implications," Clin. Biomech., **16**(2), pp. 87–101.

[86] Prado, L. G., Makarenko, I., Andresen, C., Krüger, M., Opitz, C. A., and Linke, W. A., 2005, "Isoform Diversity of Giant Proteins in Relation to Passive and Active Contractile Properties of Rabbit Skeletal Muscles," J. Gen. Physiol., **126**(5), pp. 461–480.

[87] Patel, T. J., and Lieber, R. L., 1996, "Force Transmission in Skeletal Muscle: From Actomyosin to External Tendons.," Exerc. Sport Sci. Rev., **25**, pp. 321–363.

[88] Horowits, R., 1992, “Passive Force Generation and Titin Isoforms in Mammalian Skeletal Muscle,” Biophys. J., **61**(2), pp. 392–398.

[89] Granzier, H., Helmes, M., Cazorla, O., McNabb, M., Labeit, D., Wu, Y., Yamasaki, R., Redkar, A., Kellermayer, M., and Labeit, S., 2000, “Mechanical Properties of Titin Isoforms,” *Elastic Filaments of the Cell*, Springer, pp. 283–304.

[90] Brown, S. H. M., Gregory, D. E., Carr, J. A., Ward, S. R., Masuda, K., and Lieber, R. L., 2011, “ISSLS Prize Winner: Adaptations to the Multifidus Muscle in Response to Experimentally Induced Intervertebral Disc Degeneration,” Spine (Phila. Pa. 1976)., **36**(21), pp. 1728–1736.

[91] Brown, S. H. M., Carr, J. A., Ward, S. R., and Lieber, R. L., 2012, “Passive Mechanical Properties of Rat Abdominal Wall Muscles Suggest an Important Role of the Extracellular Connective Tissue Matrix,” J. Orthop. Res., **30**(8), pp. 1321–1326.

[92] Meyer, G. A., and Lieber, R. L., 2011, “Elucidation of Extracellular Matrix Mechanics from Muscle Fibers and Fiber Bundles,” J. Biomech., **44**(4), pp. 771–773.

[93] Fridén, J., and Lieber, R. L., 2003, “Spastic Muscle Cells Are Shorter and Stiffer than Normal Cells,” Muscle and Nerve, **27**(2), pp. 157–164.

[94] Smith, L. R., Lee, K. S., Ward, S. R., Chambers, H. G., and Lieber, R. L., 2011, “Hamstring Contractures in Children with Spastic Cerebral Palsy Result from a Stiffer Extracellular Matrix and Increased in Vivo Sarcomere Length,” J. Physiol., **589**(10), pp. 2625–2639.

[95] Mathewson, M. A., Chambers, H. G., Girard, P. J., Tenenhaus, M., Schwartz, A. K., and Lieber, R. L., 2014, “Stiff Muscle Fibers in Calf Muscles of Patients with Cerebral Palsy Lead to High Passive Muscle Stiffness,” J. Orthop. Res., **32**(12), pp. 1667–1674.

[96] Lieber, R. L., Runesson, E., Einarsson, F., and Fridén, J., 2003, “Inferior Mechanical Properties of Spastic Muscle Bundles Due to Hypertrophic but Compromised Extracellular Matrix Material,” Muscle and Nerve, **28**(4), pp. 464–471.

[97] Gsell, K. Y., Zwambag, D. P., Fournier, D. E., Séguin, C. A., and Brown, S. H. M., 2017, “Paraspinal Muscle Passive Stiffness Remodels in Direct Response to Spine Stiffness: A Study Using the ENT1-Deficient Mouse,” Spine (Phila. Pa. 1976)., **42**(19), pp. 1440–1446.

[98] Marcucci, L., Bondì, M., Randazzo, G., Reggiani, C., Natali, A. N., and Pavan, P. G., 2019, “Fibre and Extracellular Matrix Contributions to Passive Forces in Human Skeletal Muscles: An Experimental Based Constitutive Law for Numerical Modelling of the Passive Element in the Classical Hill-Type Three Element Model,” PLoS One, **14**(11), p. e0224232.

[99] De Bruin, M., Smeulders, M. J., Kreulen, M., Huijing, P. A., and Jaspers, R. T., 2014, “Intramuscular Connective Tissue Differences in Spastic and Control Muscle: A Mechanical and Histological Study,” PLoS One, **9**(6), p. e101038.

[100] Noonan, A. M., Zwambag, D. P., Mazara, N., Weersink, E., Power, G. A., and Brown, S. H. M., 2020, “Fiber Type and Size as Sources of Variation in Human Single Muscle Fiber Passive Elasticity,” J. Biomech. Eng., **142**(8).

[101] Toursel, T., Stevens, L., Granzier, H., and Mounier, Y., 2002, “Passive Tension of Rat

Skeletal Soleus Muscle Fibers: Effects of Unloading Conditions," J. Appl. Physiol., **92**(4), pp. 1465–1472.

[102] Zwambag, D. P., Gsell, K. Y., and Brown, S. H. M., 2019, "Characterization of the Passive Mechanical Properties of Spine Muscles across Species," J. Biomech., **88**, pp. 173–179.

[103] Roche, S. M., Gumucio, J. P., Brooks, S. V., Mendias, C. L., and Claflin, D. R., 2015, "Measurement of Maximum Isometric Force Generated by Permeabilized Skeletal Muscle Fibers," J. Vis. Exp., **2015**(100), p. e52695.

[104] Blinks, J. R., 1965, "Influence of Osmotic Strength on Cross-section and Volume of Isolated Single Muscle Fibres," J. Physiol., **177**(1), pp. 42–57.

[105] Lieber, R. L., and Ward, S. R., 2013, "Cellular Mechanisms of Tissue Fibrosis. 4. Structural and Functional Consequences of Skeletal Muscle Fibrosis," Am. J. Physiol. Physiol., **305**(3), pp. C241–C252.

[106] Muiznieks, L. D., and Keeley, F. W., 2013, "Molecular Assembly and Mechanical Properties of the Extracellular Matrix: A Fibrous Protein Perspective," Biochim. Biophys. Acta - Mol. Basis Dis., **1832**(7), pp. 866–875.

[107] Gelse, K., Pöschl, E., and Aigner, T., 2003, "Collagens—Structure, Function, and Biosynthesis," Adv. Drug Deliv. Rev., **55**(12), pp. 1531–1546.

[108] Smith, L. R., Pichika, R., Meza, R. C., Gillies, A. R., Baliki, M. N., Chambers, H. G., and Lieber, R. L., 2019, "Contribution of Extracellular Matrix Components to the Stiffness of Skeletal Muscle Contractures in Patients with Cerebral Palsy," Connect. Tissue Res., pp. 1–12.

[109] Asgari, M., Latifi, N., Heris, H. K., Vali, H., and Mongeau, L., 2017, "In Vitro Fibrillogenesis of Tropocollagen Type III in Collagen Type i Affects Its Relative Fibrillar Topology and Mechanics," Sci. Rep., **7**(1), pp. 1–10.

[110] Miller, T. A., Lesniewski, L. A., Muller-Delp, J. M., Majors, A. K., Scalise, D., and Delp, M. D., 2001, "Hindlimb Unloading Induces a Collagen Isoform Shift in the Soleus Muscle of the Rat," Am. J. Physiol. - Regul. Integr. Comp. Physiol., **281**(5 50-5), pp. R1710–R1717.

[111] Brashear, S. E., Wohlgemuth, R. P., Gonzalez, G., and Smith, L. R., 2021, "Passive Stiffness of Fibrotic Skeletal Muscle in Mdx Mice Relates to Collagen Architecture," J. Physiol., **599**(3), pp. 943–962.

[112] Hill, A. V., 1938, "The Heat of Shortening and the Dynamic Constants of Muscle," Proc. R. Soc. London. Ser. B - Biol. Sci., **126**(843), pp. 136–195.

[113] Zajac, F. E., 1989, "Muscle and Tendon: Properties, Models, Scaling, and Application to Biomechanics and Motor Control.," Crit. Rev. Biomed. Eng., **17**(4), pp. 359–411.

[114] Ward, S. R., Eng, C. M., Smallwood, L. H., and Lieber, R. L., 2009, "Are Current Measurements of Lower Extremity Muscle Architecture Accurate?," Clin. Orthop. Relat. Res., **467**(4), pp. 1074–1082.

[115] Delp, S. L., Suryanarayanan, S., Murray, W. M., Uhlir, J., and Triolo, R. J., 2001, "Architecture of the Rectus Abdominis, Quadratus Lumborum, and Erector Spinae," J.

Biomech., **34**(3), pp. 371–375.

[116] Parvaresh, K. C., Chang, C., Patel, A., Lieber, R. L., Ball, S. T., and Ward, S. R., 2019, "Architecture of the Short External Rotator Muscles of the Hip," BMC Musculoskelet. Disord., **20**(1), pp. 1–6.

[117] Murray, W. M., Buchanan, T. S., and Delp, S. L., 2000, "The Isometric Functional Capacity of Muscles That Cross the Elbow," J. Biomech., **33**(8), pp. 943–952.

[118] Lieber, R. L., Fazeli, B. M., and Botte, M. J., 1990, "Architecture of Selected Wrist Flexor and Extensor Muscles," J. Hand Surg. Am., **15**(2), pp. 244–250.

[119] Luden, N., Minchev, K., Hayes, E., Louis, E., Trappe, T., and Trappe, S., 2008, "Human Vastus Lateralis and Soleus Muscles Display Divergent Cellular Contractile Properties," Am. J. Physiol. - Regul. Integr. Comp. Physiol., **295**(5), pp. R1593–R1598.

[120] Cristea, A., Korhonen, M. T., Häkkinen, K., Mero, A., Alén, M., Sipilä, S., Viitasalo, J. T., Koljonen, M. J., Suominen, H., and Larsson, L., 2008, "Effects of Combined Strength and Sprint Training on Regulation of Muscle Contraction at the Whole-Muscle and Single-Fibre Levels in Elite Master Sprinters," Acta Physiol., **193**(3), pp. 275–289.

[121] Bogduk, N., Johnson, G., and Spalding, D., 1998, "The Morphology and Biomechanics of Latissimus Dorsi," Clin. Biomech., **13**(6), pp. 377–385.

[122] Bayoglu, R., Galibarov, P. E., Verdonschot, N., Koopman, B., and Homminga, J., 2019, "Twente Spine Model: A Thorough Investigation of the Spinal Loads in a Complete and Coherent Musculoskeletal Model of the Human Spine," Med. Eng. Phys., **68**, pp. 35–45.

[123] Zuurbier, C. J., and Huijing, P. A., 1992, "Influence of Muscle Geometry on Shortening Speed of Fibre, Aponeurosis and Muscle," J. Biomech., **25**(9), pp. 1017–1026.

[124] Erdemir, A., McLean, S., Herzog, W., and van den Bogert, A. J., 2007, "Model-Based Estimation of Muscle Forces Exerted during Movements.," Clin. Biomech. (Bristol, Avon), **22**(2), pp. 131–54.

[125] Zajac, F. E., and Winters, J. M., 1990, "Modeling Musculoskeletal Movement Systems: Joint and Body Segmental Dynamics, Musculoskeletal Actuation, and Neuromuscular Control," *Multiple Muscle Systems*, Springer, pp. 121–148.

[126] Thelen, D. G., 2003, "Adjustment of Muscle Mechanics Model Parameters to Simulate Dynamic Contractions in Older Adults," J. Biomech. Eng., **125**(1), pp. 70–77.

[127] Pandy, M. G., Pandy, M. G., and Anderson, F. C., 1995, "Optimal Control of Non-Ballistic Muscular Movements: A Constraint-Based Performance Criterion for Rising from a Chair," J. Biomech. Eng., **117**(1), pp. 15–26.

[128] Pandy, M. G., Zajac, F. E., Sim, E., and Levine, W. S., 1990, "An Optimal Control Model for Maximum-Height Human Jumping," J. Biomech., **23**(12), pp. 1185–1198.

[129] Raasch, C. C., Zajac, F. E., Ma, B., and Levine, W. S., 1997, "Muscle Coordination of Maximum-Speed Pedaling," J. Biomech., **30**(6), pp. 595–602.

[130] Trainor, P. G. S., McLachlan, K. R., and McCall, W. D., 1995, "Modelling of Forces in the Human Masticatory System with Optimization of the Angulations of the Joint Loads," J. Biomech., **28**(7), pp. 829–843.

[131] Arjmand, N., and Shirazi-Adl, A., 2006, "Sensitivity of Kinematics-Based Model

Predictions to Optimization Criteria in Static Lifting Tasks," Med. Eng. Phys., **28**(6), pp. 504–514.

[132] Li, G., Kaufman, K. R., Chao, E. Y. S., and Rubash, H. E., 1999, "Prediction of Antagonistic Muscle Forces Using Inverse Dynamic Optimization during Flexion/Extension of the Knee," J. Biomech. Eng., **121**(3), pp. 316–322.

[133] Happee, R., and Van der Helm, F. C. T., 1995, "The Control of Shoulder Muscles during Goal Directed Movements, an Inverse Dynamic Analysis," J. Biomech., **28**(10), pp. 1179–1191.

[134] Hughes, R. E., Rock, M. G., and An, K.-N., 1999, "Identification of Optimal Strategies for Increasing Whole Arm Strength Using Karush–Kuhn–Tucker Multipliers," Clin. Biomech., **14**(9), pp. 628–634.

[135] Anderson, F. C., and Pandy, M. G., 2001, "Static and Dynamic Optimization Solutions for Gait Are Practically Equivalent," J. Biomech., **34**(2), pp. 153–161.

[136] McLean, S. G., Su, A., and Van Den Bogert, A. J., 2003, "Development and Validation of a 3-D Model to Predict Knee Joint Loading during Dynamic Movement," J. Biomech. Eng., **125**(6), pp. 864–874.

[137] Neptune, R. R., 1999, "Optimization Algorithm Performance in Determining Optimal Controls in Human Movement Analyses.," J. Biomech. Eng., **121**(2), pp. 249–52.

[138] Belytschko, T., Kulak, R. F., Schultz, A. B., and Galante, J. O., 1974, "Finite Element Stress Analysis of an Intervertebral Disc," J. Biomech., **7**(3), pp. 277–285.

[139] Oxland, T. R., 2015, "A History of Spine Biomechanics: Focus on 20th Century Progress," Unfallchirurg, **118**(1), pp. 80–92.

[140] Schmidt, H., Galbusera, F., Rohlmann, A., and Shirazi-Adl, A., 2013, "What Have We Learned from Finite Element Model Studies of Lumbar Intervertebral Discs in the Past Four Decades?," J. Biomech., **46**(14), pp. 2342–2355.

[141] Oxland, T. R., 2016, "Fundamental Biomechanics of the Spine-What We Have Learned in the Past 25 Years and Future Directions," J. Biomech., **49**(6), pp. 817–832.

[142] Schultz, A., Andersson, G., Ortengren, R., Haderspeck, K., and Nachemson, A., 1982, "Loads on the Lumbar Spine. Validation of a Biomechanical Analysis by Measurements of Intradiscal Pressures and Myoelectric Signals," J. Bone Jt. Surg. - Ser. A, **64**(5), pp. 713–720.

[143] McGill, S. M., and Norman, R. W., 1986, "Partitioning of the L4-L5 Dynamic Moment into Disc, Ligamentous, and Muscular Components during Lifting.," Spine (Phila. Pa. 1976)., **11**(7), pp. 666–78.

[144] Bean, J. C., Chaffin, D. B., and Schultz, A. B., 1988, "Biomechanical Model Calculation of Muscle Contraction Forces: A Double Linear Programming Method," J. Biomech., **21**(1), pp. 59–66.

[145] Macintosh, J. E., Valencia, F., Bogduk, N., and Munro, R. R., 1986, "The Morphology of the Human Lumbar Multifidus," Clin. Biomech., **1**(4), pp. 196–204.

[146] Bogduk, N., and Macintosh, J. E., 1987, "1987 Volvo Award in Basic Science: The Morphology of the Lumbar Erector Spinae," Spine (Phila. Pa. 1976)., **12**(7), pp. 658–668.

[147] Macintosh, J. E., and Bogduk, N., 1991, "The Attachments of the Lumbar Erector Spinae," Spine (Phila. Pa. 1976)., **16**(7), pp. 783–792.

[148] Bogduk, N., Macintosh, J. E., and Pearcy, M. J., 1992, "A Universal Model of the Lumbar Back Muscles in the Upright Position," Spine (Phila. Pa. 1976)., **17**(8), pp. 897–913.

[149] Nussbaum, M. A., Chaffin, D. B., and Rechtien, C. J., 1995, "Muscle Lines-of-Action Affect Predicted Forces in Optimization-Based Spine Muscle Modeling," J. Biomech., **28**(4), pp. 401–409.

[150] Stokes, I. A. F., and Gardner-Morse, M., 1999, "Quantitative Anatomy of the Lumbar Musculature," J. Biomech., **32**(3), pp. 311–316.

[151] Christophy, M., Senan, N. A. F., Lotz, J. C., and O'Reilly, O. M., 2012, "A Musculoskeletal Model for the Lumbar Spine," Biomech. Model. Mechanobiol., **11**(1–2), pp. 19–34.

[152] Malakoutian, M., Street, J., Wilke, H. J., Stavness, I., Fels, S., and Oxland, T., 2016, "A Musculoskeletal Model of the Lumbar Spine Using ArtiSynth–Development and Validation," Comput. Methods Biomech. Biomed. Eng. Imaging Vis., **6**(5), pp. 483–490.

[153] Bruno, A. G., Bouxsein, M. L., and Anderson, D. E., 2015, "Development and Validation of a Musculoskeletal Model of the Fully Articulated Thoracolumbar Spine and Rib Cage," J. Biomech. Eng., **137**(8).

[154] Rosatelli, A. L., Ravichandiran, K., and Agur, A. M., 2008, "Three-Dimensional Study of the Musculotendinous Architecture of Lumbar Multifidus and Its Functional Implications," Clin. Anat., **21**(6), pp. 539–546.

[155] Phillips, S., Mercer, S., and Bogduk, N., 2008, "Anatomy and Biomechanics of Quadratus Lumborum," Proc. Inst. Mech. Eng. Part H J. Eng. Med., **222**(2), pp. 151–159.

[156] Ward, S. R., Kim, C. W., Eng, C. M., Gottschalk IV, L. J., Tomiya, A., Garfin, S. R., and Lieber, R. L., 2009, "Architectural Analysis and Intraoperative Measurements Demonstrate the Unique Design of the Multifidus Muscle for Lumbar Spine Stability," J. Bone Jt. Surg. - Ser. A, **91**(1), pp. 176–185.

[157] Marras, W. S., and Sommerich, C. M., 1991, "A Three-Dimensional Motion Model of Loads on the Lumbar Spine: I. Model Structure," Hum. Factors, **33**(2), pp. 123–137.

[158] Cholewicki, J., McGill, S. M., and Norman, R. W., 1995, "Comparison of Muscle Forces and Joint Load from an Optimization and EMG Assisted Lumbar Spine Model: Towards Development of a Hybrid Approach," J. Biomech., **28**(3), pp. 321–331.

[159] Arjmand, N., and Shirazi-Adl, A., 2006, "Model and in Vivo Studies on Human Trunk Load Partitioning and Stability in Isometric Forward Flexions," J. Biomech., **39**(3), pp. 510–521.

[160] de Zee, M., Hansen, L., Wong, C., Rasmussen, J., and Simonsen, E. B., 2007, "A Generic Detailed Rigid-Body Lumbar Spine Model," J. Biomech., **40**(6), pp. 1219–1227.

[161] Cholewicki, J., and McGill, S. M., 1994, "EMG Assisted Optimization: A Hybrid Approach for Estimating Muscle Forces in an Indeterminate Biomechanical Model," J. Biomech., **27**(10), pp. 1287–1289.

[162] Gagnon, D., Larivière, C., and Loisel, P., 2001, "Comparative Ability of EMG,

Optimization, and Hybrid Modelling Approaches to Predict Trunk Muscle Forces and Lumbar Spine Loading during Dynamic Sagittal Plane Lifting," Clin. Biomech., **16**(5), pp. 359–372.

[163] Hajihosseinali, M., Arjmand, N., Shirazi-Adl, A., Farahmand, F., and Ghiasi, M. S., 2014, "A Novel Stability and Kinematics-Driven Trunk Biomechanical Model to Estimate Muscle and Spinal Forces," Med. Eng. Phys., **36**(10), pp. 1296–1304.

[164] Hughes, R. E., Bean, J. C., and Chaffin, D. B., 1995, "Evaluating the Effect of Co-Contraction in Optimization Models," J. Biomech., **28**(7), pp. 875–878.

[165] Li, S. S. W., and Chow, D. H. K., 2020, "Comparison of Predictions Between an EMG-Assisted Approach and Two Optimization-Driven Approaches for Lumbar Spine Loading During Walking With Backpack Loads," Hum. Factors, **62**(4), pp. 565–577.

[166] Delp, S. L., Anderson, F. C., Arnold, A. S., Loan, P., Habib, A., John, C. T., Guendelman, E., and Thelen, D. G., 2007, "OpenSim: Open-Source Software to Create and Analyze Dynamic Simulations of Movement," IEEE Trans. Biomed. Eng., **54**(11), pp. 1940–1950.

[167] Damsgaard, M., Rasmussen, J., Christensen, S. T., Surma, E., and de Zee, M., 2006, "Analysis of Musculoskeletal Systems in the AnyBody Modeling System," Simul. Model. Pract. Theory, **14**(8), pp. 1100–1111.

[168] Lloyd, J. E., Stavness, I., and Fels, S., 2012, "ArtiSynth: A Fast Interactive Biomechanical Modeling Toolkit Combining Multibody and Finite Element Simulation," *Soft Tissue Biomechanical Modeling for Computer Assisted Surgery*, Springer, pp. 355–394.

[169] Han, K. S., Zander, T., Taylor, W. R., and Rohlmann, A., 2012, "An Enhanced and Validated Generic Thoraco-Lumbar Spine Model for Prediction of Muscle Forces," Med. Eng. Phys., **34**(6), pp. 709–716.

[170] Rohlmann, A., Graichen, F., Bender, A., Kayser, R., and Bergmann, G., 2008, "Loads on a Telemeterized Vertebral Body Replacement Measured in Three Patients within the First Postoperative Month," Clin. Biomech., **23**(2), pp. 147–158.

[171] Wilke, H. J., Neef, P., Hinz, B., Seidel, H., and Claes, L., 2001, "Intradiscal Pressure Together with Anthropometric Data - A Data Set for the Validation of Models," Clin. Biomech., **16**(SUPPL. 1), pp. S111–S126.

[172] Vasavada, A. N., Li, S., and Delp, S. L., 1998, "Influence of Muscle Morphometry and Moment Arms on the Moment-Generating Capacity of Human Neck Muscles," Spine (Phila. Pa. 1976)., **23**(4), pp. 412–422.

[173] Holzbaur, K. R. S., Murray, W. M., and Delp, S. L., 2005, "A Model of the Upper Extremity for Simulating Musculoskeletal Surgery and Analyzing Neuromuscular Control," Ann. Biomed. Eng., **33**(6), pp. 829–840.

[174] Sato, K., Kikuchi, S., and Yonezawa, T., 1999, "In Vivo Intradiscal Pressure Measurement in Healthy Individuals and in Patients with Ongoing Back Problems," Spine (Phila. Pa. 1976)., **24**(23), pp. 2468–2474.

[175] Ignasiak, D., Dendorfer, S., and Ferguson, S. J., 2016, "Thoracolumbar Spine Model with Articulated Ribcage for the Prediction of Dynamic Spinal Loading," J. Biomech., **49**(6), pp. 959–966.

[176] Raabe, M. E., and Chaudhari, A. M. W., 2016, "An Investigation of Jogging Biomechanics Using the Full-Body Lumbar Spine Model: Model Development and Validation," J. Biomech., **49**(7), pp. 1238–1243.

[177] Honegger, J. D., Actis, J. A., Gates, D. H., Silverman, A. K., Munson, A. H., and Petrella, A. J., 2020, "Development of a Multiscale Model of the Human Lumbar Spine for Investigation of Tissue Loads in People with and without a Transtibial Amputation during Sit-to-Stand," Biomech. Model. Mechanobiol., pp. 1–20.

[178] Beaucage-Gauvreau, E., Robertson, W. S. P., Brandon, S. C. E., Fraser, R., Freeman, B. J. C., Graham, R. B., Thewlis, D., and Jones, C. F., 2019, "Validation of an OpenSim Full-Body Model with Detailed Lumbar Spine for Estimating Lower Lumbar Spine Loads during Symmetric and Asymmetric Lifting Tasks," Comput. Methods Biomech. Biomed. Engin., **22**(5), pp. 451–464.

[179] Schmid, S., Burkhart, K. A., Allaire, B. T., Grindle, D., and Anderson, D. E., 2020, "Musculoskeletal Full-Body Models Including a Detailed Thoracolumbar Spine for Children and Adolescents Aged 6–18 Years," J. Biomech., **102**, p. 109305.

[180] Kim, Y. E., and Choi, H. W., 2015, "Effect of Disc Degeneration on the Muscle Recruitment Pattern in Upright Posture: A Computational Analysis," Comput. Methods Biomech. Biomed. Engin., **18**(15), pp. 1622–1631.

[181] Shirazi-Adl, A., Sadouk, S., Parnianpour, M., Pop, D., and El-Rich, M., 2002, "Muscle Force Evaluation and the Role of Posture in Human Lumbar Spine under Compression," Eur. Spine J., **11**(6), pp. 519–526.

[182] Zander, T., Rohlmann, A., Calisse, J., and Bergmann, G., 2001, "Estimation of Muscle Forces in the Lumbar Spine during Upper-Body Inclination," Clin. Biomech., **16**(1), pp. S73–S80.

[183] Ignasiak, D., Valenzuela, W., Reyes, M., and Ferguson, S. J., 2018, "The Effect of Muscle Ageing and Sarcopenia on Spinal Segmental Loads," Eur. Spine J., **27**(10), pp. 2650–2659.

[184] Jamshidnejad, S., and Arjmand, N., 2015, "Variations in Trunk Muscle Activities and Spinal Loads Following Posterior Lumbar Surgery: A Combined in Vivo and Modeling Investigation," Clin. Biomech., **30**(10), pp. 1036–1042.

[185] Malakoutian, M., Street, J., Wilke, H. J., Stavness, I., Dvorak, M., Fels, S., and Oxland, T., 2016, "Role of Muscle Damage on Loading at the Level Adjacent to a Lumbar Spine Fusion: A Biomechanical Analysis," Eur. Spine J., **25**(9), pp. 2929–2937.

[186] Beaucage-Gauvreau, E., Brandon, S. C. E., Robertson, W. S. P., Fraser, R., Freeman, B. J. C., Graham, R. B., Thewlis, D., and Jones, C. F., 2020, "A Braced Arm-to-Thigh (BATT) Lifting Technique Reduces Lumbar Spine Loads in Healthy and Low Back Pain Participants," J. Biomech., **100**, p. 109584.

[187] Behjati, M., and Arjmand, N., 2019, "Biomechanical Assessment of the NIOSH Lifting Equation in Asymmetric Load-Handling Activities Using a Detailed Musculoskeletal Model," Hum. Factors, **61**(2), pp. 191–202.

[188] Kim, H. K., and Zhang, Y., 2017, "Estimation of Lumbar Spinal Loading and Trunk Muscle Forces during Asymmetric Lifting Tasks: Application of Whole-Body

Musculoskeletal Modelling in OpenSim," Ergonomics, **60**(4), pp. 563–576.

[189] Han, K. S., Rohlmann, A., Zander, T., and Taylor, W. R., 2013, "Lumbar Spinal Loads Vary with Body Height and Weight," Med. Eng. Phys., **35**(7), pp. 969–977.

[190] Zwambag, D. P., and Brown, S. H. M., 2020, "Experimental Validation of a Novel Spine Model Demonstrates the Large Contribution of Passive Muscle to the Flexion Relaxation Phenomenon," J. Biomech., **102**, p. 109431.

[191] Briggs, A. M., Van Dieën, J. H., Wrigley, T. V., Greig, A. M., Phillips, B., Lo, S. K., and Bennell, K. L., 2007, "Thoracic Kyphosis Affects Spinal Loads and Trunk Muscle Force," Phys. Ther., **87**(5), pp. 595–607.

[192] Bassani, T., Ottardi, C., Costa, F., Brayda-Bruno, M., Wilke, H. J., and Galbusera, F., 2017, "Semiautomated 3D Spine Reconstruction from Biplanar Radiographic Images: Prediction of Intervertebral Loading in Scoliotic Subjects," Front. Bioeng. Biotechnol., **5**(JAN), p. 1.

[193] Overbergh, T., Severijns, P., Beaucage-Gauvreau, E., Jonkers, I., Moke, L., and Scheys, L., 2020, "Development and Validation of a Modeling Workflow for the Generation of Image-Based, Subject-Specific Thoracolumbar Models of Spinal Deformity," J. Biomech., **110**, p. 109946.

[194] Barba, N., Ignasiak, D., Villa, T. M. T., Galbusera, F., and Bassani, T., 2021, "Assessment of Trunk Muscle Activation and Intervertebral Load in Adolescent Idiopathic Scoliosis by Musculoskeletal Modelling Approach," J. Biomech., **114**, p. 110154.

[195] Kamal, Z., and Rouhi, G., 2020, "Stress Distribution Changes in Growth Plates of a Trunk with Adolescent Idiopathic Scoliosis Following Unilateral Muscle Paralysis: A Hybrid Musculoskeletal and Finite Element Model," J. Biomech., **111**, p. 109997.

[196] Schmid, S., Burkhart, K. A., Allaire, B. T., Grindle, D., Bassani, T., Galbusera, F., and Anderson, D. E., 2020, "Spinal Compressive Forces in Adolescent Idiopathic Scoliosis with and without Carrying Loads: A Musculoskeletal Modeling Study," Front. Bioeng. Biotechnol., **8**, p. 159.

[197] Ignasiak, D., 2020, "A Novel Method for Prediction of Postoperative Global Sagittal Alignment Based on Full-Body Musculoskeletal Modeling and Posture Optimization," J. Biomech., **102**, p. 109324.

[198] Michnik, R., Zadoń, H., Nowakowska-Lipiec, K., Jochymczyk-Woźniak, K., Myśliwiec, A., and Mitas, A. W., 2020, "The Effect of the Pelvis Position in the Sagittal Plane on Loads in the Human Musculoskeletal System," Acta Bioeng. Biomech., **22**(3), pp. 1–18.

[199] Bassani, T., Casaroli, G., and Galbusera, F., 2019, "Dependence of Lumbar Loads on Spinopelvic Sagittal Alignment: An Evaluation Based on Musculoskeletal Modeling," PLoS One, **14**(3), p. e0207997.

[200] Stavness, I. K., 2010, "Byte Your Tongue," (December), pp. 1–190.

[201] Abdi, A. H., Malakoutian, M., Oxland, T., and Fels, S., 2019, "Reinforcement Learning for High-Dimensional Continuous Control in Biomechanics: An Intro to ArtiSynth-RL," arXiv.

[202] Kim, J. Y., Paik, H. K., Ahn, S. S., Kang, M. S., Kim, K. H., Park, J. Y., Chin, D. K.,

Kim, K. S., Cho, Y. E., and Kuh, S. U., 2016, "Paraspinal Muscle, Facet Joint, and Disc Problems: Risk Factors for Adjacent Segment Degeneration after Lumbar Fusion," Spine J., **16**(7), pp. 867–875.

[203] Nicolaisen, T., and Jorgensen, K., 1985, "Trunk Strength, Back Muscle Endurance and Low-Back Trouble," Scand. J. Rehabil. Med., **17**(3), pp. 121–127.

[204] Mannion, A. F., 1999, "Fibre Type Characteristics and Function of the Human Paraspinal Muscles: Normal Values and Changes in Association with Low Back Pain," J. Electromyogr. Kinesiol., **9**(6), pp. 363–377.

[205] Goubert, D., De Pauw, R., Meeus, M., Willems, T., Cagnie, B., Schouppe, S., Van Oosterwijck, J., Dhondt, E., and Danneels, L., 2017, "Lumbar Muscle Structure and Function in Chronic versus Recurrent Low Back Pain: A Cross-Sectional Study," Spine J., **17**(9), pp. 1285–1296.

[206] Masaki, M., Aoyama, T., Murakami, T., Yanase, K., Ji, X., Tateuchi, H., and Ichihashi, N., 2017, "Association of Low Back Pain with Muscle Stiffness and Muscle Mass of the Lumbar Back Muscles, and Sagittal Spinal Alignment in Young and Middle-Aged Medical Workers," Clin. Biomech., **49**, pp. 128–133.

[207] Bresnahan, L., Fessler, R. G., and Natarajan, R. N., 2010, "Evaluation of Change in Muscle Activity as a Result of Posterior Lumbar Spine Surgery Using a Dynamic Modeling System," Spine (Phila. Pa. 1976)., **35**(16), pp. E761-7.

[208] DeMers, M. S., Hicks, J. L., and Delp, S. L., 2017, "Preparatory Co-Activation of the Ankle Muscles May Prevent Ankle Inversion Injuries," J. Biomech., **52**, pp. 17–23.

[209] Kamal, Z., Rouhi, G., Arjmand, N., and Adeeb, S., 2019, "A Stability-Based Model of a Growing Spine with Adolescent Idiopathic Scoliosis: A Combination of Musculoskeletal and Finite Element Approaches," Med. Eng. Phys., **64**, pp. 46–55.

[210] Arnold, E. M., Hamner, S. R., Seth, A., Millard, M., and Delp, S. L., 2013, "How Muscle Fiber Lengths and Velocities Affect Muscle Force Generation as Humans Walk and Run at Different Speeds," J. Exp. Biol., **216**(11), pp. 2150–2160.

[211] Fox, A. S., Carty, C. P., Modenese, L., Barber, L. A., and Lichtwark, G. A., 2018, "Simulating the Effect of Muscle Weakness and Contracture on Neuromuscular Control of Normal Gait in Children," Gait Posture, **61**, pp. 169–175.

[212] Millard, M., Uchida, T., Seth, A., and Delp, S. L., 2013, "Flexing Computational Muscle: Modeling and Simulation of Musculotendon Dynamics," J. Biomech. Eng., **135**(2), p. 21005.

[213] Moseley, G. L., Hodges, P. W., and Gandevia, S. C., 2002, "Deep and Superficial Fibers of the Lumbar Multifidus Muscle Are Differentially Active during Voluntary Arm Movements.," Spine (Phila. Pa. 1976)., **27**(2), pp. E29–E36.

[214] Urrutia, J., Besa, P., Lobos, D., Andia, M., Arrieta, C., and Uribe, S., 2018, "Is a Single-Level Measurement of Paraspinal Muscle Fat Infiltration and Cross-Sectional Area Representative of the Entire Lumbar Spine?," Skeletal Radiol., **47**(7), pp. 939–945.

[215] Crawford, R. J., Elliott, J. M., and Volken, T., 2017, "Change in Fatty Infiltration of Lumbar Multifidus, Erector Spinae, and Psoas Muscles in Asymptomatic Adults of Asian or Caucasian Ethnicities," Eur. Spine J., **26**(12), pp. 3059–3067.

[216] Crawford, R. J., Filli, L., Elliott, J. M., Nanz, D., Fischer, M. A., Marcon, M., and Ulbrich, E. J., 2016, "Age- and Level-Dependence of Fatty Infiltration in Lumbar Paravertebral Muscles of Healthy Volunteers," Am. J. Neuroradiol., **37**(4), pp. 742–748.

[217] Lee, S. H., Park, S. W., Kim, Y. B., Nam, T. K., and Lee, Y. S., 2017, "The Fatty Degeneration of Lumbar Paraspinal Muscles on Computed Tomography Scan According to Age and Disc Level," Spine J., **17**(1), pp. 81–87.

[218] Moreau, B., Vergari, C., Gad, H., Sandoz, B., Skalli, W., and Laporte, S., 2016, "Non-Invasive Assessment of Human Multifidus Muscle Stiffness Using Ultrasound Shear Wave Elastography: A Feasibility Study," Proc. Inst. Mech. Eng. Part H J. Eng. Med., **230**(8), pp. 809–814.

[219] Wang, K., McCarter, R., Wright, J., Beverly, J., and Ramirez-Mitchell, R., 1993, "Viscoelasticity of the Sarcomere Matrix of Skeletal Muscles. The Titin-Myosin Composite Filament Is a Dual-Stage Molecular Spring," Biophys. J., **64**(4), pp. 1161–1177.

[220] Zwambag, D. P., Hurtig, M. B., Vernon, H., and Brown, S. H. M., 2018, "Investigation of the Passive Mechanical Properties of Spine Muscles Following Disruption of the Thoracolumbar Fascia and Erector Spinae Aponeurosis, as Well as Facet Injury in a Rat," Spine J., **18**(4), pp. 682–690.

[221] Wood, D. S., Zollman, J., Reuben, J. P., and Brandt, P. W., 1975, "Human Skeletal Muscle: Properties of the 'Chemically Skinned' Fiber," Science (80-.)., **187**(4181), pp. 1075–1076.

[222] Moss, R. L., 1979, "Sarcomere Length-Tension Relations of Frog Skinned Muscle Fibres during Calcium Activation at Short Lengths.," J. Physiol., **292**, p. 177.

[223] Brown, S. H. M., Nolan, C. P. R., and Zwambag, D. P., 2020, "Characteristics of Sarcomere Length Operating Ranges in the Rat Lumbar Spine Extensor Muscles: Comparison to Human," Eur. J. Anat., **24**(3), pp. 205–210.

[224] Zwambag, D. P., Ricketts, T. A., and Brown, S. H. M., 2014, "Sarcomere Length Organization as a Design for Cooperative Function amongst All Lumbar Spine Muscles," J. Biomech., **47**(12), pp. 3087–3093.

[225] Hinz, B., 2010, "The Myofibroblast: Paradigm for a Mechanically Active Cell," J. Biomech., **43**(1), pp. 146–155.

[226] Wipff, P. J., Rifkin, D. B., Meister, J. J., and Hinz, B., 2007, "Myofibroblast Contraction Activates Latent TGF-B1 from the Extracellular Matrix," J. Cell Biol., **179**(6), pp. 1311–1323.

[227] Yeung, T., Georges, P. C., Flanagan, L. A., Marg, B., Ortiz, M., Funaki, M., Zahir, N., Ming, W., Weaver, V., and Janmey, P. A., 2005, "Effects of Substrate Stiffness on Cell Morphology, Cytoskeletal Structure, and Adhesion," Cell Motil. Cytoskeleton, **60**(1), pp. 24–34.

[228] Li, C. X., Talele, N. P., Boo, S., Koehler, A., Knee-Walden, E., Balestrini, J. L., Speight, P., Kapus, A., and Hinz, B., 2017, "MicroRNA-21 Preserves the Fibrotic Mechanical Memory of Mesenchymal Stem Cells," Nat. Mater., **16**(3), pp. 379–389.

[229] Ottenheijm, C. A. C., Voermans, N. C., Hudson, B. D., Irving, T., Stienen, G. J. M., Van

Engelen, B. G., and Granzier, H., 2012, “Titin-Based Stiffening of Muscle Fibers in Ehlers-Danlos Syndrome,” J. Appl. Physiol., **112**(7), pp. 1157–1165.

[230] Meyer, G. A., and Lieber, R. L., 2012, “Skeletal Muscle Fibrosis Develops in Response to Desmin Deletion,” Am. J. Physiol. - Cell Physiol., **302**(11), pp. 1609–1620.

[231] Wood, L. K., Kayupov, E., Gumucio, J. P., Mendias, C. L., Claflin, D. R., and Brooks, S. V., 2014, “Intrinsic Stiffness of Extracellular Matrix Increases with Age in Skeletal Muscles of Mice,” J. Appl. Physiol., **117**(4), pp. 363–369.

[232] Malakoutian, M., Yamamoto, S., Sadaram, S., Speidel, J., Liu, J., Street, J., Brown, S. H. M., and Oxland, T. R., 2021, “The Effect of Vertebral Level on Biomechanical Properties of the Lumbar Paraspinal Muscles in a Rat Model,” J. Mech. Behav. Biomed. Mater., **118**(Under Review).

[233] Bayoglu, R., Geeraedts, L., Groenen, K. H. J., Verdonschot, N., Koopman, B., and Homminga, J., 2017, “Twente Spine Model: A Complete and Coherent Dataset for Musculo-Skeletal Modeling of the Thoracic and Cervical Regions of the Human Spine,” J. Biomech., **58**, pp. 52–63.

[234] Yamamoto, S., Malakoutian, M., Theret, M., Street, J., Rossi, F., Brown, S. H. M., Saito, M., and Oxland, T. R., “The Effect of Posterior Lumbar Spinal Surgery on Biomechanical Properties of Rat Paraspinal Muscles 13 Weeks Post-Surgery,” Spine (Phila. Pa. 1976)., (In Press).

[235] Shahidi, B., Gibbons, M. C., Esparza, M., Zlomislic, V., Allen, R. T., Garfin, S. R., and Ward, S. R., 2020, “Cell Populations and Muscle Fiber Morphology Associated with Acute and Chronic Muscle Degeneration in Lumbar Spine Pathology,” Jor Spine, **3**(2), p. e1087.

[236] Ward, S. R., Takahashi, M., Winters, T. M., Kwan, A., and Lieber, R. L., 2009, “A Novel Muscle Biopsy Clamp Yields Accurate in Vivo Sarcomere Length Values,” J. Biomech., **42**(2), pp. 193–196.

[237] Noonan, A. M., Séguin, C. A., and Brown, S. H. M., 2020, “Paraspinal Muscle Contractile Function Is Impaired in the ENT1 Deficient Mouse Model of Progressive Spine Pathology,” Spine (Phila. Pa. 1976)., Published Ahead of Print.

[238] Padwal, J., Berry, D. B., Hubbard, J. C., Zlomislic, V., Allen, R. T., Garfin, S. R., Ward, S. R., and Shahidi, B., 2020, “Regional Differences between Superficial and Deep Lumbar Multifidus in Patients with Chronic Lumbar Spine Pathology,” BMC Musculoskelet. Disord., **21**(1), pp. 1–9.

[239] Joe, A. W. B., Yi, L., Natarajan, A., Le Grand, F., So, L., Wang, J., Rudnicki, M. A., and Rossi, F. M. V., 2010, “Muscle Injury Activates Resident Fibro/Adipogenic Progenitors That Facilitate Myogenesis,” Nat. Cell Biol., **12**(2), pp. 153–163.

[240] Madaro, L., Passafaro, M., Sala, D., Etxaniz, U., Lugarini, F., Proietti, D., Alfonsi, M. V., Nicoletti, C., Gatto, S., De Bardi, M., Rojas-García, R., Giordani, L., Marinelli, S., Pagliarini, V., Sette, C., Sacco, A., and Puri, P. L., 2018, “Denervation-Activated STAT3–IL-6 Signalling in Fibro-Adipogenic Progenitors Promotes Myofibres Atrophy and Fibrosis,” Nat. Cell Biol., **20**(8), pp. 917–927.

[241] Cooper, R. G., Freemont, A. J., Fitzmaurice, R., Alani, S. M., and Jayson, M. I. V., 1991,

"Paraspinal Muscle Fibrosis: A Specific Pathological Component in Ankylosing Spondylitis," Ann. Rheum. Dis., **50**(11), pp. 755–759.

[242] Matejka, J., Zeman, J., Belatka, J., Zeman, P., and Matejka, T., 2019, "Histochemical and Histological Changes of Paraspinal Muscles in Patients with Thoracic and Lumbar Spine Fractures Treated with Open and Minimally Invasive Stabilisation," J. Back Musculoskelet. Rehabil., **32**(5), pp. 803–810.

[243] Senteler, M., Weisse, B., Rothenfluh, D. A., and Snedeker, J. G., 2016, "Intervertebral Reaction Force Prediction Using an Enhanced Assembly of OpenSim Models," Comput. Methods Biomech. Biomed. Engin., **19**(5), pp. 538–548.

[244] Gardner-Morse, M. G., and Stokes, I. A. F., 2004, "Structural Behavior of Human Lumbar Spinal Motion Segments," J. Biomech., **37**(2), pp. 205–212.

[245] Heuer, F., Schmidt, H., Klezl, Z., Claes, L., and Wilke, H.-J., 2007, "Stepwise Reduction of Functional Spinal Structures Increase Range of Motion and Change Lordosis Angle," J. Biomech., **40**(2), pp. 271–280.

[246] Sagl, B., Dickerson, C. R., and Stavness, I., 2019, "Fast Forward-Dynamics Tracking Simulation: Application to Upper Limb and Shoulder Modeling," IEEE Trans. Biomed. Eng., **66**(2), pp. 335–342.

[247] Eskandari, A. H., Arjmand, N., Shirazi-Adl, A., and Farahmand, F., 2019, "Hypersensitivity of Trunk Biomechanical Model Predictions to Errors in Image-Based Kinematics When Using Fully Displacement-Control Techniques," J. Biomech., **84**, pp. 161–171.

[248] Dehghan-Hamani, I., Arjmand, N., and Shirazi-Adl, A., 2019, "Subject-Specific Loads on the Lumbar Spine in Detailed Finite Element Models Scaled Geometrically and Kinematic-Driven by Radiography Images," Int. j. numer. method. biomed. eng., **35**(4), p. e3182.

[249] Byrne, R. M., Aiyangar, A. K., and Zhang, X., 2020, "Sensitivity of Musculoskeletal Model-Based Lumbar Spinal Loading Estimates to Type of Kinematic Input and Passive Stiffness Properties," J. Biomech., **102**, p. 109659.

[250] Stokes, I. A. F., and Gardner-Morse, M., 2001, "Lumbar Spinal Muscle Activation Synergies Predicted by Multi-Criteria Cost Function," J. Biomech., **34**(6), pp. 733–740.

[251] Frei, H., Oxland, T. R., Rathonyi, G. C., and Nolte, L. P., 2001, "The Effect of Nucleotomy on Lumbar Spine Mechanics in Compression and Shear Loading," Spine (Phila. Pa. 1976)., **26**(19), pp. 2080–2089.

[252] Nachemson, A., 1960, "Lumbar Intradiscal Pressure. Experimental Studies on Post-Mortem Material.," Acta Orthop. Scand. Suppl., **43**(S43), pp. 1–104.

[253] Ghezelbash, F., Schmidt, H., Shirazi-Adl, A., and El-Rich, M., 2020, "Internal Load-Sharing in the Human Passive Lumbar Spine: Review of in Vitro and Finite Element Model Studies," J. Biomech., **102**, p. 109441.

[254] Dreischarf, M., Rohlmann, A., Zhu, R., Schmidt, H., and Zander, T., 2013, "Is It Possible to Estimate the Compressive Force in the Lumbar Spine from Intradiscal Pressure Measurements? A Finite Element Evaluation," Med. Eng. Phys., **35**(9), pp. 1385–1390.

[255] Heuer, F., Schmidt, H., Claes, L., and Wilke, H.-J., 2007, “Stepwise Reduction of Functional Spinal Structures Increase Vertebral Translation and Intradiscal Pressure,” J. Biomech., **40**(4), pp. 795–803.

[256] Van Dieën, J. H., and Kingma, I., 1999, “Total Trunk Muscle Force and Spinal Compression Are Lower in Asymmetric Moments as Compared to Pure Extension Moments,” J. Biomech., **32**(7), pp. 681–687.

[257] Wong, K. W. N., Leong, J. C. Y., Chan, M. K., Luk, K. D. K., and Lu, W. W., 2004, “The Flexion-Extension Profile of Lumbar Spine in 100 Healthy Volunteers,” Spine (Phila. Pa. 1976)., **29**(15), pp. 1636–1641.

[258] Sanchez, G. N., Sinha, S., Liske, H., Chen, X., Nguyen, V., Delp, S. L., and Schnitzer, M. J., 2015, “In Vivo Imaging of Human Sarcomere Twitch Dynamics in Individual Motor Units,” Neuron, **88**(6), pp. 1109–1120.

[259] Winters, T. M., Takahashi, M., Lieber, R. L., and Ward, S. R., 2011, “Whole Muscle Length-Tension Relationships Are Accurately Modeled as Scaled Sarcomeres in Rabbit Hindlimb Muscles,” J. Biomech., **44**(1), pp. 109–115.

[260] Happee, R., 1994, “Inverse Dynamic Optimization Including Muscular Dynamics, a New Simulation Method Applied to Goal Directed Movements,” J. Biomech., **27**(7), pp. 953–960.

[261] Malakoutian, M., Volkheimer, D., Street, J., Dvorak, M. F., Wilke, H. J., and Oxland, T. R., 2015, “Do in Vivo Kinematic Studies Provide Insight into Adjacent Segment Degeneration? A Qualitative Systematic Literature Review,” Eur. Spine J., **24**(9), pp. 1865–1881.

[262] Wilke, H. J., Herkommer, A., Werner, K., and Liebsch, C., 2020, “In Vitro Analysis of the Intradiscal Pressure of the Thoracic Spine,” Front. Bioeng. Biotechnol., **8**, p. 614.

[263] Schmidt, H., Kettler, A., Heuer, F., Simon, U., Claes, L., and Wilke, H. J., 2007, “Intradiscal Pressure, Shear Strain, and Fiber Strain in the Intervertebral Disc under Combined Loading,” Spine (Phila. Pa. 1976)., **32**(7), pp. 748–755.

[264] Dreischarf, M., Shirazi-Adl, A., Arjmand, N., Rohlmann, A., and Schmidt, H., 2016, “Estimation of Loads on Human Lumbar Spine: A Review of in Vivo and Computational Model Studies,” J. Biomech., **49**(6), pp. 833–845.

[265] Glassman, S. D., Coseo, M. P., and Carreon, L. Y., 2016, “Sagittal Balance Is More than Just Alignment: Why PJK Remains an Unresolved Problem,” Scoliosis Spinal Disord., **11**(1), pp. 1–7.

[266] Stokes, I. A. F., and Gardner-Morse, M., 1995, “Lumbar Spine Maximum Efforts and Muscle Recruitment Patterns Predicted by a Model with Multijoint Muscles and Joints with Stiffness,” J. Biomech., **28**(2), pp. 173–186.

[267] Stokes, I. A. F., 1997, “Analysis of Symmetry of Vertebral Body Loading Consequent to Lateral Spinal Curvature,” Stud. Health Technol. Inform., **37**(21), pp. 97–101.

[268] Zoabli, G., Mathieu, P. A., and Aubin, C.-É., 2007, “Back Muscles Biometry in Adolescent Idiopathic Scoliosis,” Spine J., **7**(3), pp. 338–344.

[269] Zapata, K. A., Wang-Price, S. S., Sucato, D. J., and Dempsey-Robertson, M., 2015,

"Ultrasonographic Measurements of Paraspinal Muscle Thickness in Adolescent Idiopathic Scoliosis: A Comparison and Reliability Study," Pediatr. Phys. Ther., **27**(2), pp. 119–125.

[270] Cheung, J., Halbertsma, J. P. K., Veldhuizen, A. G., Sluiter, W. J., Maurits, N. M., Cool, J. C., and van Horn, J. R., 2005, "A Preliminary Study on Electromyographic Analysis of the Paraspinal Musculature in Idiopathic Scoliosis," Eur. Spine J., **14**(2), pp. 130–137.

[271] Kwok, G., Yip, J., Cheung, M.-C., and Yick, K.-L., 2015, "Evaluation of Myoelectric Activity of Paraspinal Muscles in Adolescents with Idiopathic Scoliosis during Habitual Standing and Sitting," Biomed Res. Int., **2015**.

[272] Briggs, A. M., Wrigley, T. V., Van Dieën, J. H., Phillips, B., Lo, S. K., Greig, A. M., and Bennell, K. L., 2006, "The Effect of Osteoporotic Vertebral Fracture on Predicted Spinal Loads in Vivo," Eur. Spine J., **15**(12), pp. 1785–1795.

[273] Galbusera, F., Wilke, H.-J., Brayda-Bruno, M., Costa, F., and Fornari, M., 2013, "Influence of Sagittal Balance on Spinal Lumbar Loads: A Numerical Approach," Clin. Biomech., **28**(4), pp. 370–377.

[274] Roussouly, P., Gollogly, S., Berthonnaud, E., and Dimnet, J., 2005, "Classification of the Normal Variation in the Sagittal Alignment of the Human Lumbar Spine and Pelvis in the Standing Position," Spine (Phila. Pa. 1976)., **30**(3), pp. 346–353.

[275] Stokes, I. A. F., and Gardner-Morse, M., 2004, "Muscle Activation Strategies and Symmetry of Spinal Loading in the Lumbar Spine with Scoliosis," Spine (Phila. Pa. 1976)., **29**(19), pp. 2103–2107.

[276] Wong, C., Gosvig, K., and Sonne-Holm, S., 2017, "The Role of the Paravertebral Muscles in Adolescent Idiopathic Scoliosis Evaluated by Temporary Paralysis," Scoliosis Spinal Disord., **12**(1), pp. 1–8.

[277] Been, E., Barash, A., Marom, A., and Kramer, P. A., 2010, "Vertebral Bodies or Discs: Which Contributes More to Human-like Lumbar Lordosis?," Clin. Orthop. Relat. Res., **468**(7), pp. 1822–1829.

[278] Diebo, B. G., Ferrero, E., Lafage, R., Challier, V., Liabaud, B., Liu, S., Vital, J. M., Errico, T. J., Schwab, F. J., and Lafage, V., 2015, "Recruitment of Compensatory Mechanisms in Sagittal Spinal Malalignment Is Age and Regional Deformity Dependent: A Full-Standing Axis Analysis of Key Radiographical Parameters," Spine (Phila. Pa. 1976)., **40**(9), pp. 642–649.

[279] Schwab, F., Ungar, B., Blondel, B., Buchowski, J., Coe, J., Deinlein, D., Dewald, C., Mehdian, H., Shaffrey, C., Tribus, C., and Lafage, V., 2012, "Scoliosis Research Society-Schwab Adult Spinal Deformity Classification: A Validation Study," Spine (Phila. Pa. 1976)., **37**(12), pp. 1077–1082.

[280] Diebo, B. G., Varghese, J. J., Lafage, R., Schwab, F. J., and Lafage, V., 2015, "Sagittal Alignment of the Spine: What Do You Need to Know?," Clin. Neurol. Neurosurg., **139**, pp. 295–301.

[281] Schwab, F., Patel, A., Ungar, B., Farcy, J. P., and Lafage, V., 2010, "Adult Spinal Deformity-Postoperative Standing Imbalance: How Much Can You Tolerate? An Overview of Key Parameters in Assessing Alignment and Planning Corrective Surgery,"

Spine (Phila. Pa. 1976)., **35**(25), pp. 2224–2231.

[282] Berjano, P., Ismael, M. F., Damilano, M., Scopetta, S., Langella, F., and Lamartina, C., 2014, "Successful Correction of Sagittal Imbalance Can Be Calculated on the Basis of Pelvic Incidence and Age," Eur. Spine J., **23**(6), pp. S587–S596.

[283] Jun, H. S., Kim, J. H., Ahn, J. H., Chang, I. B., Song, J. H., Kim, T. H., Park, M. S., Chan Kim, Y., Kim, S. W., and Oh, J. K., 2016, "The Effect of Lumbar Spinal Muscle on Spinal Sagittal Alignment: Evaluating Muscle Quantity and Quality," Neurosurgery, **79**(6), pp. 847–855.

[284] Shafaq, N., Suzuki, A., Matsumura, A., Terai, H., Toyoda, H., Yasuda, H., Ibrahim, M., and Nakamura, H., 2012, "Asymmetric Degeneration of Paravertebral Muscles in Patients with Degenerative Lumbar Scoliosis," Spine (Phila. Pa. 1976)., **37**(16), pp. 1398–1406.

[285] Mannion, A. F., Meier, M., Grob, D., and Müntener, M., 1998, "Paraspinal Muscle Fibre Type Alterations Associated with Scoliosis: An Old Problem Revisited with New Evidence," Eur. Spine J., **7**(4), pp. 289–293.

[286] Chan, Y. L., Cheng, J. C. Y., Guo, X., King, A. D., Griffith, J. F., and Metreweli, C., 1999, "MRI Evaluation of Multifidus Muscles in Adolescent Idiopathic Scoliosis," Pediatr. Radiol., **29**(5), pp. 360–363.

[287] Shimode, M., Ryouji, A., and Kozo, N., 2003, "Asymmetry of Premotor Time in the Back Muscles of Adolescent Idiopathic Scoliosis," Spine (Phila. Pa. 1976)., **28**(22), pp. 2535–2539.

[288] Elysee, J. C., Lovecchio, F., Lafage, R., Ang, B., Huang, A., Bannwarth, M., Kim, H. J., Schwab, F., and Lafage, V., 2021, "The Relationship of Global Sagittal Malalignment to Fatty Infiltration in the Aging Spine," Eur. Spine J., pp. 1–6.

[289] Ferrero, E., Skalli, W., Lafage, V., Maillot, C., Carlier, R., Feydy, A., Felter, A., Khalifé, M., and Guigui, P., 2020, "Relationships between Radiographic Parameters and Spinopelvic Muscles in Adult Spinal Deformity Patients," Eur. Spine J., **29**(6), pp. 1328–1339.

[290] Yagi, M., Hosogane, N., Watanabe, K., Asazuma, T., and Matsumoto, M., 2016, "The Paravertebral Muscle and Psoas for the Maintenance of Global Spinal Alignment in Patient with Degenerative Lumbar Scoliosis," Spine J., **16**(4), pp. 451–458.

[291] Hyun, S. J., Bae, C. W., Lee, S. H., and Rhim, S. C., 2016, "Fatty Degeneration of the Paraspinal Muscle in Patients with Degenerative Lumbar Kyphosis," Clin. Spine Surg., **29**(10), pp. 441–447.

[292] Ivicsics, M. F., Bishop, N. E., Püschel, K., Morlock, M. M., and Huber, G., 2014, "Increase in Facet Joint Loading after Nucleotomy in the Human Lumbar Spine," J. Biomech., **47**(7), pp. 1712–1717.

[293] Pollintine, P., Dolan, P., Tobias, J. H., and Adams, M. A., 2004, "Intervertebral Disc Degeneration Can Lead to 'Stress-Shielding' of the Anterior Vertebral Body: A Cause of Osteoporotic Vertebral Fracture?," Spine (Phila. Pa. 1976)., **29**(7), pp. 774–782.

[294] Yang, K. H., and King, A. I., 1984, "Mechanism of Facet Load Transmission as a Hypothesis for Low-Back Pain," Spine (Phila. Pa. 1976)., **9**(6), pp. 557–565.

[295] Wisdom, K. M., Delp, S. L., & Kuhl, E., 2015, “Use it or lose it: multiscale skeletal muscle adaptation to mechanical stimuli,” Biomechanics and modeling in mechanobiology, **14**(2), pp. 195-215.

Appendix A Supplementary Materials for Chapter 2

A.1 Correlation Between Fiber Bundle Elastic Modulus and Fascicle Collagen I Deposition

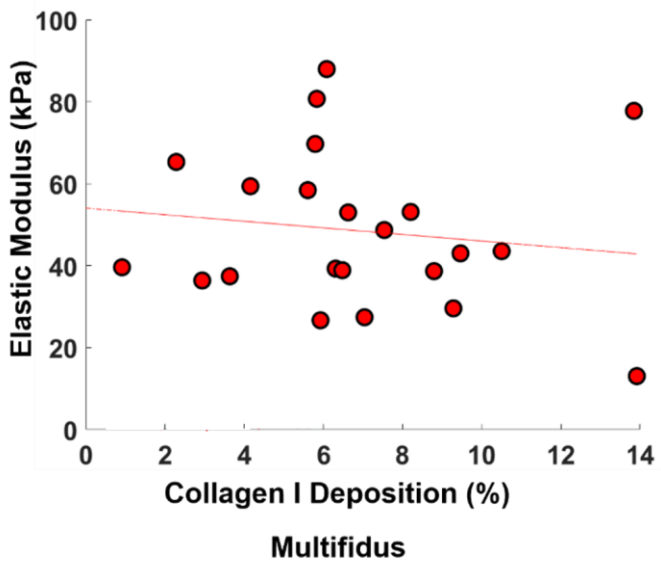

Figure A-1. Linear correlation between tangent modulus of fiber bundles and collagen I deposition of fascicles in multifidus (p=0.54 and R^2 = 0.02). Presence of no correlation between these two parameters is not surprising as they were measured at two different scales. It has been demonstrated for both collagen content and tangent modulus to increase significantly from the fiber bundle scale to fascicle scale [55].

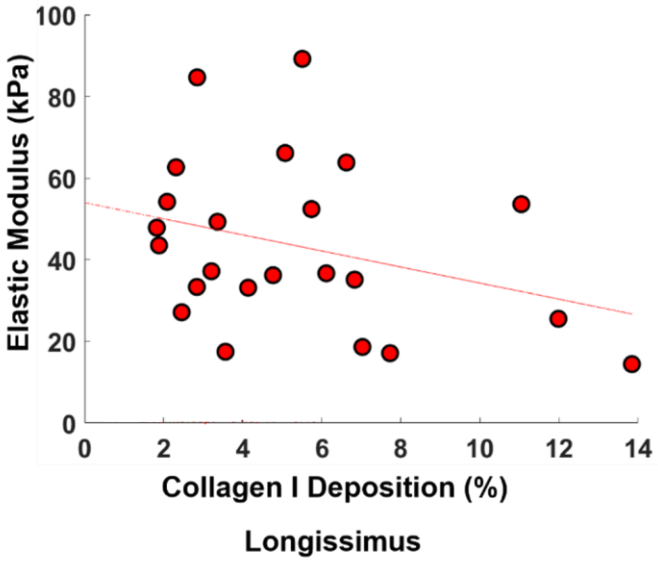

Figure A-2. Linear correlation between tangent modulus of fiber bundles and collagen I deposition of fascicles in Longissimus (p=0.14 and R^2=0.10). Presence of no correlation between these two parameters is not surprising as they were measured at two different scales. It has been demonstrated for both collagen content and tangent modulus to increase significantly from the fiber bundle scale to fascicle scale [55].

Appendix B Supplementary Materials for Chapter 4

B.1 Patients Consent Form for Biomechanical Assessment

PARTICIPANT INFORMATION AND CONSENT FORM[1]

Enhanced Biomechanical Modelling of the Spine for Adult

Principal Investigator: John Street, MD, PhD, FRCSCI
Assistant Professor
Department of Orthopaedics, Division of Spine,
University of British Columbia Faculty of Medicine
Vancouver Spine Surgery Institute (VSSI),
Vancouver General Hospital
Phone: (604) XXX-XXXX

Co-investigators: Thomas Oxland, PhD, Professor, Departments of Orthopaedics and Mechanical Engineering, University of British Columbia

David Wilson, PhD, Professor, Departments of Orthopaedics and Mechanical Engineering, University of British Columbia

Tamir Ailon, MD, MPH, FRCSC, Clinical Instructor, Division of Neurosurgery, University of British Columbia Faculty of Medicine

Sidney Fels, Professor, Department of Electrical and Computer Engineering, University of British Columbia

Steve Brown, Associate Professor, Department of Human Health & Nutritional Sciences, University of Guelph

Stephen Lewis, Professor, University of Toronto

Sponsor: Medtronic Canada
Natural Sciences and Engineering Research Council of Canada (NSERC)

[1] The consent form was put together by Leilani Reichl, Masoud Malakoutian, Noor Shaikh, and Allan Aludino.

Study Contact: Leilani Reichl
Research Coordinator
Phone: (604) XXX-XXXX

1. Invitation

You are being invited to participate in this research study because you have been diagnosed with a degenerative spine condition that requires surgical treatment.

2. Your participation is voluntary

Your participation is voluntary. You have the right to refuse to participate in this study. If you decide to participate, you may still choose to withdraw from the study at any time without any negative consequences to the medical care, education or other services to which you are entitled or are presently receiving.

You should be aware that there is a difference for both you and your doctor between being a patient and being a research participant. As a patient, all medical procedures and treatments are carried out for your benefit only according to standard accepted practice. As a research participant, you and your doctor must also take into account the requirements for the research study. These may include procedures and treatments that are not part of standard practice or are not yet proven. This consent form describes the diagnostic and study procedures that are being carried out for research purposes. Please review the consent document carefully when deciding whether or not you wish to be part of the research and sign this consent only if you accept being a research participant.

If you wish to participate in this study, you will be asked to sign this form.

Please take time to read the following information carefully and to discuss it with your family, friends and doctor before you decide.

3. Who is conducting this study?

The Principal Investigator, Dr. John Street, and the Vancouver Spine Research Program, under VGH's Vancouver Spine Surgery Institute, is conducting this study, along with Co-Investigators from Dr. Tom Oxland's Lab, under the International Collaboration on Repair Discoveries (ICORD). This project is supported by Medtronic Canada and the Natural Sciences and Engineering Research Council of Canada (NSERC) for the work required in doing this clinical research.

4. Background

Adult spine deformity (ASD) occurs when a patient has a loss of natural lumbar lordosis (curvature). ASD is associated with aging of the spine and 20-40% of the population is expected to develop a progressive kyphosis (hunching) or sagittal imbalance (forward tilting). ASD can affect one's ability to stand upright and stare straight ahead, causing symptoms of pain and disability.

Muscle dysfunction in the spine and pelvis are thought to be major factors contributing to the development of sagittal imbalance, and therefore, ASD; however, there are currently no spine models incorporating these elements. Unfortunately, without a spine model that includes features associated with sagittal imbalance, we are unable to better study and understand the impact of age-related muscle properties or activity on ASD.

5. What is the purpose of the study?

The purpose of this study is to create an accurate biomechanical model of ASD that incorporates elements of muscle function in order to improve surgical planning, allow for more individualized surgical treatment, and facilitate the development of more effective spine surgery implants. To achieve this objective, the study involves two parts:

i. To obtain MRI images in a standing position to allow study investigators to better visualize spinal and pelvic muscles in a natural, upright posture.
ii. To obtain muscle tissue samples, via biopsy, during spine surgery.

6. Who can participate in this study?

You may be able to participate in the **Upright MRI** part of this study if you:

- Have been diagnosed with an adult spine deformity requiring treatment
- Had a conventional MRI (in a lying down position) within the last 12 months
- Had upright x-rays of the spine within the last 12 months
- Are 50 years of age or older
- Are able to communicate in English

To be eligible to participate in the **Muscle Biopsy** part of this study, you must meet the above criteria *and*:

- Are scheduled to undergo spine surgery with a posterior midline incision that involves the lumbosacral spine between the L4-S1 levels

7. Who should not participate in this study at this site?

You will not be eligible to participate in **Muscle Biopsy** part of this study if you:

- Had a previous spine injury or surgery
- Have a scoliosis greater than 20°
- Have a body mass index of greater than 35
- Have a pre-existing neurological disorder such as Parkinson's disease, Alzheimer's disease, Huntington's disease, multiple sclerosis, or amyotrophic lateral sclerosis
- Have a pre-existing thromboembolic disease or coagulopathy (disorders related to blood clotting), such as haemophilia or von Willibrand's disease
- Have a pre-existing or ongoing infection (e.g. pneumonia, urinary tract infection, cellulitis)
- Have a pre-existing inflammatory or autoimmune disorder such as rheumatoid arthritis, systemic lupus, psoriasis
- Have a systemic disease that may interfere with safety or evaluation of the condition we're studying (e.g. heart disease, HIV, HTLV-1)
- Have any other medical condition that in the investigator's opinion would render the study procedures dangerous

In addition to the exclusion criteria above, you will not be eligible to participate in the **Upright MRI** part of this study, if you meet any of the criteria below:

- Are not able to stand for the duration of the upright MRI (approximately 45 minutes in total)
- Have a pacemaker, aneurysm clip or other device which is a contraindication to MRI

8. What does the study involve?

If you agree to take part in the study, you will first sign this Consent Form before any study-related procedures are performed. At that time, you will be asked questions about your medical history and current health status to help determine your eligibility.

If you consent to the study, you may choose to participate in:

- The Upright MRI portion of the study only;
- The Muscle Biopsy portion of the study only; or,
- Both the Upright MRI and Muscle Biopsy.

Upright MRI Procedures

On the day of the MRI scan appointment, the previously completed screening form will be reviewed with you by the MRI technologist to ensure your safety during the scanning session. You will then be asked to change into hospital garments and to remove all metal objects (such as hearing aids, dentures, jewelry, watches, hairpins, and ALL piercings) from your body because these objects interfere with imaging and may be attracted to the scanner magnet, or may heat up, with the potential risk of injury.

For the purposes of the study, you will be scanned in the upright open MRI scanner in two different postures:

1. In an upright position (standing)
2. In a supine position (lying down)

The upright open MRI is a vertically open scanner (two parallel discs oriented on edge, 58 cm apart), which allows for a wide range of positioning. An MRI coil (a specifically designed antenna) will be placed around, or next to, your lower back. You will be asked to stand in the scanner or lie down on the MRI table in the scanner. The MRI technologist will place various accessories (foam cushions, support bars, etc.) around you to support your position. Several scans will be taken to capture various views of your lower back, each one lasting less than 5 minutes. You will also be provided with the option of resting between each standing scan in order to allow for recovery of any muscle fatigue. While the total scanning time will be approximately 30-45 minutes, you may spend up to 3 hours in the MRI suite, which includes the time for screening, changing, positioning and scanning, as well as breaks as needed.

Following the research MRI, Study Investigators will compare and measure the imaging obtained in both the upright open MRI scanner and those MRI images obtained as part of your standard of care.

Image 1: Open MRI

Biopsy Procedures

If you are participating in the biopsy part of the study, 8 biopsies will be taken at the time of your spine surgery. Each biopsy will be between 1-2 cm in length and about 3 mm thick. All muscle biopsies will be performed by the attending Spine Surgeon.

If you are having spine surgery, the Spine Surgeon will make an incision on your back which will expose the underlying muscles and spine. Normally, muscle is cut away from the bone and not repaired or reattached. The biopsies will be taken from this tissue that would otherwise be discarded. The entire biopsy process will take less than 4 minutes. Once collected, the muscle tissue will be placed in a sealed container for transfer to a laboratory at the Blusson Spinal Cord Centre (818 West 10th Avenue) in Vancouver where it will be processed and stored for analysis.

Optional Study: Long-Term Sample Storage

The following study is optional. You will be provided with a separate consent that describes the details, and which you will be required to sign if you wish to participate. You can take part in the main study and not take part in the optional study. If you decide not to take part in the optional study, your care will not be affected.

If your muscle tissues are not used up for the purpose of this study, you can choose to participate in the optional study to allow the long-term storage of remaining tissue samples for future analysis. For additional information, please see the separate, optional consent form.

9. What are my responsibilities?

In summary, your participation in this study may involve an Upright MRI, Muscle Biopsy or both.

Upright MRI
Participation in the Upright MRI will require one appointment at Vancouver General Hospital (VGH). The Upright Open MRI is located at VGH, in the Leon Blackmore Pavilion, Ground Level, Room G53. We will provide you with a detailed wayfinding map.

At the time of consent, we will give you a VCH MRI screening form. Because you already had an MRI before, you should be eligible for the upright open MRI provided nothing has changed. We will ask you to complete it at the time you agree to participate in this study to avoid last minute cancellations due to contraindications.

On the day of scanning, it is recommended you have a meal prior to your appointment. You will have to maintain a position and remain as still as you can for several minutes. If you are fasting or on a diet, please let us know and we will reschedule your scan.

Muscle Biopsy
If you choose to participate in the muscle biopsy part of the study, a Spine Surgeon will obtain 8 biopsies from the muscle tissue that is normally exposed during a spine operation. These biopsy samples will then be analyzed in the laboratory. There are no other requirements or procedures to follow for the biopsy other than standard, pre-operative instructions given to you by your Spine Surgeon and healthcare team.

10. What are the possible harms and discomforts?
Upright MRI Procedures
MRI does not use high-energy radiation (like that used in x-rays or CT scans) and there are no known harmful side-effects associated with temporary exposure to the magnetic field used by MRI scanners. However, there are safety considerations and before undergoing an MRI scan which your clinical care team will review with you using a safety checklist.

To ensure safety, we need to know about all metal or metal fragments on or inside your body. As certain types of metal are safe and others are not, we need to assess if it is safe for you to have an MRI scan. Additional risks associated with undergoing an MRI scan include:

- The magnet may cause pacemakers, artificial limbs, and other implanted medical devices that contain metal to malfunction or heat up during the exam. If you have a pacemaker, you would not be allowed to have an MRI scan for this study.
- Any loose metal object may cause damage or injury if it gets pulled toward the magnet. As such, you have to change into hospital pyjamas and remove all metal from your body, including jewellery and keys from your pockets.
- Dyes from tattoos or tattooed eyeliner can cause skin or eye irritation.
- Medication patches can cause a skin burn.
- Exposure to radio waves for long periods of time during the scan could lead to slight warming of the body.

There is a slight risk of claustrophobia (fear associated with confined spaces); however, this is reduced by the open structure of the upright open MRI scanner. During the scan you will hear acoustic noises (very loud "knocking" sounds) from the magnet. You will be required to wear earplugs to minimize the noise. You will be asked to remain as still as possible for the duration of the scanning procedure. In the upright open MRI scanner, you will be imaged while you are standing; there is a risk of fainting when standing still for long periods. To minimize this risk, you will be given ample rest periods between scans during which you can change positions as desired. If you feel uncomfortable at any point during the scan, you will be able to use a call bell to signal the technologist and he or she will help you leave the MRI scanning area.
In addition, you may feel some discomfort in your low back during or following the scanning. Please report to the researcher any undue discomfort or pain experienced during the testing. If the pain or discomfort is deemed to be excessive by you or the investigators, then scanning will cease. Also, we recommend you bring your own pain medication in case you feel you need it during or after the MRI session.

Biopsy Procedures
The biopsy retrieval will not result in increased wound exposure, tissue damage or blood loss beyond what normally occurs during routine midline spine surgery. The biopsy retrieval will not result in any effect on the remainder of the surgical procedure or on your short-term or long-term recovery.

11. What are the potential benefits of participating?
There may not be direct benefits to you from taking part in this study; however, we will be happy to provide you with copies of your imaging session and the final results of the study, if you wish. In addition, images obtained in the upright open MRI scanner will be available to your Spine Surgeon prior to your surgery; although these images will not be used for the purposes of surgical decision making, these results may assist with surgical planning and enable more individualized surgical treatment.

We hope that the information learned from this study can be used in the future to benefit other people with ASD.

12. What are the alternatives to study participation?
The only alternative to this study is non-participation. If you choose not to participate in this study, you will receive the standard of care for your condition. You can discuss these options with your doctor before deciding whether or not to participate in this research project.

13. What if new information becomes available that may affect my decision to participate?
If you choose to enter this study and at a later date new information becomes available that may affect your willingness to remain in this study, it will be discussed with you.

14. What happens if I decide to withdraw my consent to participate?
You may withdraw from this study at any time without giving reasons. If you choose to enter the study and then decide to withdraw at a later time, you have the right to request the

withdrawal of your information and samples collected during the study. This request will be respected to the extent possible. Please note however that there may be exceptions where the data and samples will not be able to be withdrawn, for example, where the data and sample is no longer identifiable (meaning it cannot be linked in any way back to your identity) or where the data has been merged with other data. If your participation in this study includes enrolling in any optional studies or long term follow-up, you will be asked whether you wish to withdraw from these as well. If you would like to request the withdrawal of your data and samples, please let your study doctor know.

15. Can I be asked to leave the study?

If you are not able to follow the requirements of the study or for any other reason, the study doctor may withdraw you from the study and will arrange for your care to continue. Your study doctor might consider it to be in your best interests to withdraw you from the study without your consent if they determine that it would be better for your health. If you are asked to leave the study, the reasons for this will be explained to you and you will have the opportunity to ask questions about this decision.

16. How will my taking part in this study be kept confidential?

Your confidentiality will be respected. However, research records and health or other source records identifying you may be inspected in the presence of the Investigator or his or her designate, by representatives of the UBC Clinical Research Ethics Board for the purpose of monitoring the research. No information or records that disclose your identity will be published without your consent, nor will any information or records that disclose your identity be removed or released without your consent unless required by law.

You will be assigned a unique study number as a participant in this study. This number will not include any personal information that could identify you (e.g., it will not include your Personal Health Number, SIN, or your initials, etc.). Only this number will be used on any research-related information collected about you during the course of this study so that your identity will be kept confidential. Information that contains your identity will remain only with the Principal Investigator and/or designate. The list that matches your name to the unique study number that is used on your research-related information will not be removed or released without your consent unless required by law.

Your rights to privacy are legally protected by federal and provincial laws that require safeguards to ensure that your privacy is respected. You also have the legal right of access to the information about you that has been provided to the sponsor and, if need be, an opportunity to correct any errors in this information. Further details about these laws are available on request to your study doctor.

Your de-identified research data (e.g. your name, birthdate, and other identifiers have been removed) may be published or deposited into a publicly accessible location at the time of publication. This enhances the transparency of the research but also allows others to access

the data. This should not increase risks to you, but it does mean that other researchers may analyze the data for different reasons other than those described in this consent form. Once data is made publicly available, you will not be able to withdraw your data.

17. What happens if something goes wrong?

By signing this form, you do not give up any of your legal rights and you do not release the study doctor, participating institutions, or anyone else from their legal and professional duties. If you become ill or physically injured as a result of participation in this study, medical treatment will be provided at no additional cost to you. The costs of your medical treatment will be paid by your provincial medical plan.

18. What will the study cost me?

You will not be compensated for your participation in this project; however, all research-related medical care and treatment and any related tests that you will receive during your participation in this study will be provided at no cost to you.

19. Who do I contact if I have questions about the study during my participation?

If you have any questions or desire further information about this study before or during participation, or if you experience any adverse effects, you can contact Dr. John Street at (604) XXX-XXXX or the Spine Research Coordinator, Leilani Reichl at (604) XXX-XXXX.

20. Who do I contact if I have any questions or concerns about my rights as a participant?

If you have any concerns or complaints about your rights as a research participant and/or your experiences while participating in this study, contact the Research Participant Complaint Line in the University of British Columbia Office of Research Ethics by e-mail at RSIL@ors.ubc.ca or by phone at (604) XXX-XXXX (Toll Free: 1-877-XXX-XXXX). Please reference the study number [H18-01072] when calling so the Complaint Line staff can better assist you.

21. After the study is finished

Please indicate, by checking the applicable box, whether you are willing to be contacted for future research studies.

☐ Yes, I am willing to be contacted for future research studies.

☐ No, please do not contact me for future research studies.

22. Enhanced Biomechanical Modelling of the Spine for Adult Deformity Surgery

Participant Consent

My signature on this consent form means:

- I have read and understood the information in this consent form.
- I have had enough time to think about the information provided.
- I have been able to ask for advice if needed.
- I have been able to ask questions and have had satisfactory responses to my questions.
- I understand that all of the information collected will be kept confidential and that the results will only be used for scientific purposes.
- I understand that my participation in this study is voluntary.
- I understand that I am completely free to refuse to participate or to withdraw from this study at any time, and that this will not change the quality of care that I receive.
- I authorize access to my health records and samples as described in this consent form.
- I understand that I am not waiving any of my legal rights as a result of signing this consent form.
- I understand that there is no guarantee that this study will provide any benefits to me.

I will receive a signed copy of this consent form for my own records.

☐ I consent to participate in the **Upright MRI** portion of this study.

Participant's Signature	Printed Name	Date

Signature of Person Obtaining Consent	Printed Name	Study Role	Date

☐ I consent to participate in the **Muscle Biopsy** portion of this study.

Participant's Signature	Printed Name	Date	
Signature of Person Obtaining Consent	Printed Name	Study Role	Date

B.2 Patient Consent Form for Histopathological Assessment

PARTICIPANT INFORMATION AND CONSENT FORM[2]

Optional consent for muscle tissue biobanking for future

Principal Investigator: John Street, MD, PhD, FRCSCI
Assistant Professor
Department of Orthopaedics, Division of Spine,
University of British Columbia Faculty of Medicine
Vancouver Spine Surgery Institute (VSSI),
Vancouver General Hospital
Phone: (604) XXX-XXXX

Co-investigators: Thomas Oxland, PhD, Professor, Departments of Orthopaedics and Mechanical Engineering, University of British Columbia

David Wilson, PhD, Professor, Departments of Orthopaedics and Mechanical Engineering, University of British Columbia

Tamir Ailon, MD, MPH, FRCSC, Clinical Instructor, Division of Neurosurgery, University of British Columbia Faculty of Medicine

Sidney Fels, Professor, Department of Electrical and Computer Engineering, University of British Columbia

Steve Brown, Associate Professor, Department of Human Health & Nutritional Sciences, University of Guelph

Stephen Lewis, Professor, University of Toronto

Sponsor: Medtronic of Canada Ltd.
Natural Sciences and Engineering Research Council of Canada (NSERC)

Study Contact: Leilani Reichl
Research Coordinator
Phone: (604) XXX-XXXX

[2] The consent form is put together by Leilani Reichl, Masoud Malakoutian, Noor Shaikh, and Allan Aludino.

22. Invitation

In addition to the main study [e.g. to create an accurate biomechanical model of adult spine deformity (ASD)], you are being invited to allow remnant muscle biopsy tissue to be stored for future use in other optional research studies. This process is referred to as biobanking.

23. Your participation is voluntary

Before you decide to consent to participate in this optional biobanking study and future studies, it is important for you to know why we wish to store your muscle tissue and what will be done with it. This consent form will tell you about why the research is being done, how it is different from the main study, what will be collected and stored, where it will be stored, who will have access to it, how it may be used in the future, and the possible benefits, risks and discomforts associated with giving the sample and with the information obtained from it.

If you wish to participate in this study, you will be invited to sign this form. You have the right to refuse to have your muscle tissue banked without affecting your participation in the main part of the study and without affecting your current medical care. If you decide to participate, you may still choose to withdraw your tissue at any time without giving any reason, and without any negative consequences to your medical care, education, or other services you are receiving now or in the future.

Please take time to read the following information carefully and to discuss it with your family, friends, and doctor before you decide.

24. Who is conducting this study?

The main research study is sponsored by Medtronic of Canada Ltd. and the Natural Sciences and Engineering Research Council of Canada (NSERC) through grants to Dr. Street. The muscle tissue banking process is also being sponsored by Medtronic and NSERC. Some of the tissue analysis will be done by Dr. Oxland's lab at ICORD located in Vancouver, B.C. Current funding levels are expected to maintain the tissue bank for at least 10 years, after which time, tissue samples will be destroyed.

25. Background

It is increasingly common for researchers to invite participants in different kinds of research studies to bank samples of their body tissues for use in future research studies. Often the exact nature of these studies is not entirely known because new discoveries lead research in new, and not always foreseen, directions. However, samples collected for the purposes of one study may not get used completely and can sometimes be used to answer other research questions. For this reason, participants are asked to consider storing the remainder of the sample for future studies that are as yet undetermined.

26. What is the purpose of the study?

The goal of the main study, Enhanced Biomechanical Modelling of the Spine for Adult Deformity Surgery, is to create an accurate biomechanical model of ASD that incorporates elements of muscle function in order to improve surgical planning, allow for more individualized surgical treatment, and facilitate the development of more effective spine surgery implants. The purpose of this optional study is to store muscle tissue samples for possible future analysis and to answer any new clinical questions that may arise. The exact plan for these future studies is not known at this time since it will depend on other discoveries being made in the area of spinal deformity research.

27. Who can participate in this study?

You may participate in this study if you are eligible to participate in the main study on adult deformity.

28. What does the study involve?

As part of the main study, a Spine Surgeon will collect 8 biopsies of your muscle tissue during your spine surgery. This procedure will take up to 4 minutes; otherwise, no additional time for your participation is required.

Once your tissue is collected, your sample will be labelled with a unique code so that no one will know who the sample came from. Dr. Street and those he designates (research coordinator or lab manager) will hold the key that links your identity to the individual code used to label the sample. As part of the main study, your muscle tissue will be analyzed by researchers in Dr. Thomas Oxland's lab located in the Blusson Spinal Cord Centre, Vancouver, B.C. No personal information that directly identifies you will be sent to the lab.

We invite you to allow us to store remnants of your muscle tissue for future analysis that may help us to better understand ASD and identify potential treatments. If you consent to this study, your muscle tissue will be stored in a freezer to preserve it for future testing for 10 years in Dr. Oxland's lab at ICORD. Every measure will be taken to ensure your privacy. The samples will only be used for research described in this consent form and will not be sold. You will not receive the results of this or any future tests and your participation in this part of the study will not become part of your medical record. It is very unlikely that the research testing on your muscle tissue will uncover findings that may affect your current or future health.

29. What are my responsibilities?

After your muscle tissue biopsies have been taken, you do not need to do anything else for this optional study.

30. What are the possible harms and discomforts?

There are no known harms or discomforts associated with the collection of muscle tissue biopsies. The biopsy retrieval will not result in increased wound exposure, tissue damage or blood loss beyond what normally occurs during routine midline spine surgery. The biopsy

retrieval will not result in any effect on the remainder of the surgical procedure or on your short-term or long-term recovery.

31. What are the potential benefits of participating?

The research that may be done with your muscle tissue samples is not expected to benefit you directly.

We hope that the information learned from this study can be used in the future to benefit other patients with ASD.

You will receive no payment for taking part in this study, nor will you receive payment or money if this research ultimately leads to new knowledge or technology with commercial potential.

32. What are the alternatives to study participation?

Should you choose not to participate in the optional study for long-term sample storage, your samples will be destroyed after analysis by incineration (to destroy by burning), instead of being frozen for future use.

33. What if new information becomes available that may affect my decision to participate?

You have the right to know about new information that may affect your health, welfare, or your willingness to participate in the main study and optional studies. You will be provided with this information as soon as it becomes available.

34. What happens if I decide to withdraw my consent to participate?

If you wish for your stored muscle tissue samples to be removed once you leave the study, you may call Dr. Street at 604- XXX-XXXX and he will ensure that your sample is located, removed from the freezer and destroyed. If you prefer, you can also send Dr. Street a letter (at the address listed at the top of this form), asking to be removed from the study, but this is not required. If you do choose to send a letter, Dr. Street will destroy it to protect your privacy after it has been read. Any other information collected about you will also be destroyed. However, if your sample has already been tested at the time you withdraw, it may be impossible to withdraw the results once they have been compiled with the results of others participating in the study or if they have been published. Furthermore, if some of your sample has been shared with other researchers, it may not be possible to remove this part of the sample. In these cases of total withdrawal being impossible, your identity will still be protected and the chance of anyone knowing that you were ever involved in the study is small.

You may withdraw from this study at any time without giving reasons. If you choose to enter the study and then decide to withdraw at a later time, you have the right to request the withdrawal of your information and samples collected during the study. This request will be respected to the extent possible. Please note however that there may be exceptions where the data and samples will not be able to be withdrawn, for example, where the data and sample is no longer identifiable (meaning it cannot be linked in any way back to your identity) or where

the data has been merged with other data. If you would like to request the withdrawal of your data and samples, please let your study doctor know.

35. Can I be asked to leave the study?

The investigator may decide to discontinue the study at any time. He may also decide not to use your sample or withdraw you from the study at any time.

36. How will my taking part in this study be kept confidential?

Your confidentiality will be respected. However, research records and health or other source records identifying you may be inspected in the presence of the Investigator or his or her designate, by representatives of the UBC Clinical Research Ethics Board for the purpose of monitoring the research. No information or records that disclose your identity will be published without your consent, nor will any information or records that disclose your identity be removed or released without your consent unless required by law.

You will be assigned a unique study number as a participant in this study. This number will not include any personal information that could identify you (e.g., it will not include your Personal Health Number, SIN, or your initials, etc.). Only this number will be used on any research-related information collected about you during the course of this study so that your identity will be kept confidential. Information that contains your identity will remain only with the Principal Investigator and/or designate. The list that matches your name to the unique study number that is used on your research-related information will not be removed or released without your consent unless required by law.

Your rights to privacy are legally protected by federal and provincial laws that require safeguards to ensure that your privacy is respected. You also have the legal right of access to the information about you that has been provided to the sponsor and, if need be, an opportunity to correct any errors in this information. Further details about these laws are available on request to your study doctor.

Your de-identified research data (e.g. your name, birthdate, and other identifiers have been removed) may be published or deposited into a publicly accessible location at the time of publication. This enhances the transparency of the research but also allows others to access the data. This should not increase risks to you, but it does mean that other researchers may analyze the data for different reasons other than those described in this consent form. Once data is made publicly available, you will not be able to withdraw your data.

37. What will the study cost me?

You will not have to pay anything to be part of this study, nor will you be paid for participating.

38. What happens if something goes wrong?

By signing this form, you do not give up any of your legal rights and you do not release the study doctor, participating institutions, or anyone else from their legal and professional duties.

If you become ill or physically injured as a result of participation in this study, medical treatment will be provided at no additional cost to you.

39. Who do I contact if I have questions about the study during my participation?

If you have any questions or desire further information about this study before or during participation, or if you experience any adverse effects, you can contact Dr. John Street at (604) XXX-XXXX or the Spine Research Coordinator, Leilani Reichl at (604) XXX-XXXX.

40. Who do I contact if I have any questions or concerns about my rights as a participant?

If you have any concerns or complaints about your rights as a research participant and/or your experiences while participating in this study, contact the Research Participant Complaint Line in the University of British Columbia Office of Research Ethics by e-mail at RSIL@ors.ubc.ca or by phone at (604)XXX-XXXX (Toll Free: 1-877-XXX-XXXX). Please reference the study number [H18-01072] when calling so the Complaint Line staff can better assist you.

41. After the study is finished

Please indicate, by checking the applicable box, whether you are willing to be re-contacted for future research studies not listed here. You may choose not to participate in some or all of the options – just leave the box blank if you do not consent to the use described.

☐ I agree that a member of Dr. Street's research team may contact me in the future for follow-up or further research related to this study

☐ I agree that a member of Dr. Street's research team may contact me in the future to ask if I am interested in participating in other research studies not described in this form.

42. Optional consent for muscle tissue biobanking for future research studies

Participant Consent

My signature on this consent form means:

- I have read and understood the information in this consent form.
- I have had enough time to think about the information provided.
- I have been able to ask for advice if needed.
- I have been able to ask questions and have had satisfactory responses to my questions.
- I understand that all of the information collected will be kept confidential and that the results will only be used for scientific purposes.
- I understand that my participation in this study is voluntary.
- I understand that I am completely free to refuse to participate or to withdraw from this study at any time, and that this will not change the quality of care that I receive.
- I authorize access to my health records and samples as described in this consent form.
- I understand that I am not waiving any of my legal rights as a result of signing this consent form.
- I understand that there is no guarantee that this study will provide any benefits to me.

1. I will receive a signed copy of this consent form for my own records.
2. I consent to participate in this study.

_____	_____	_____
Participant's Signature	Printed Name	Date

_____	_____	_____	_____
Signature of Person Obtaining Consent	Printed Name	Study Role	Date

B.3 Clamp Validation

To assess functionality of the clamp, the in situ sarcomere length of a fresh fiber bundle from rectus femoris in one rat (Figure B-1) was measured using the clamp in two situations. In situation 1, the clamp grabbed a fiber bundle while it was still attached to the bony elements (Figure B-2a); in situation 2, the grabbed fiber bundle by the clamp was detached from the bones (Figure B-2b).

A diode laser transilluminated the fiber bundle in both situations and the resulting diffraction patterns were used for measurement of in situ sarcomere length. Sarcomere length measurement was repeated five times. The mean and standard deviation for in situ sarcomere length was 2.64±0.08 μm in situation 1 and 2.70±0.08 μm in situation 2. This experiment verified that the in situ tension was preserved by the clamp such that after detaching the fiber bundle from the bones its sarcomere length did not decrease.

Obviously after detaching the fiber bundle from the bones (situation 2), the clamp cannot apply further tension to the fiber bundle, therefore the 60 nm larger value measured for in situ sarcomere length in situation 2 compared to situation 1 is attributed to the measurement errors. Our sarcomere length measurement technique requires manual selection of the first order diffraction maximums. Due to large thickness of the fiber bundle tested, the diffraction pattern was not as sharp and clear as when a single fiber or small fiber bundle of ~10-20 fibers is tested. Therefore, a larger standard deviation was observed (i.e. 80 nm) than the typical resolution of 10 nm we perceive when testing single fibers or small fiber bundles (~10-20 fibers).

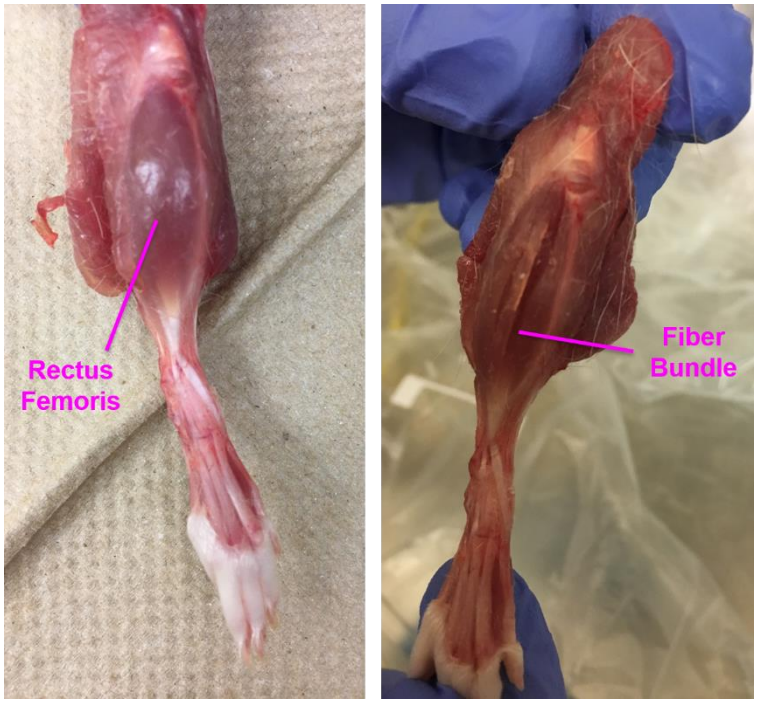

Figure B-1. Rectus femoris of a Sprague-Dawley rat and the fiber bundle tested for in situ sarcomere length measurement.

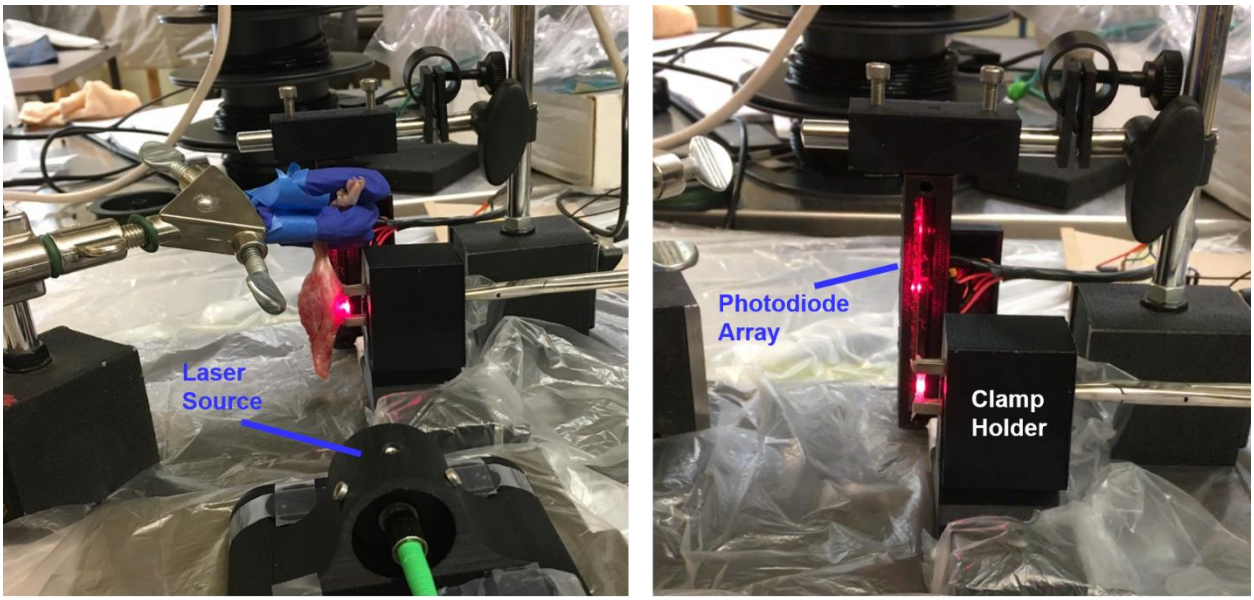

A) Situation 1 **B) Situation 2**

Figure B-2. Validation of the functionality of the specialized muscle biopsy clamp. In situation 1, the clamp grabbed a fiber bundle while it was still attached to the bony elements (A); in situation 2, the grabbed fiber bundle by the clamp was detached from the bones (B).

B.4 Biopsy acquisition instructions

The following instructions were provided to the surgeons for biopsy collection:

- Anatomically, all muscle biopsies should be ideally collected from L5. As a rule of thumb, any muscle tissue medial to facet joints is considered multifidus, and lateral to facet joints, Longissimus.
- Four biopsies will be collected with the special muscle biopsy clamps. These biopsies need to be thin but very delicately taken. For the thickness of the fiber bundle you can consider the thickness of grocery rubber bands (3-5 mm in diameter).
- The other four biopsies will be collected through blunt cut with a scalpel. The larger these pieces of muscle tissue, the better. Please divide them in half once placed in the sterile bowl.
- Please make sure all the biopsies are taken from the muscle belly and not the tendon.

B.5 Tissue Collection Flow Sheet

AT TIME OF OR BOOKING:

- Surgeon to ensure study patient on OR slate with 'Sagittal Deformity Study' indicated in comment field

DAY BEFORE OR:

- Consent form and information package added to patient's hospital chart
- Spine Research e-mails the head nurse later so additions form can be updated with the following requested supplies:
    - Clamps X 4
    - A Container X 1 (holds clamps)
    - B Container X 1 (holds blunt cut samples)

DAY OF OR:

- Spine Surgeon contacts Masoud ≈ 1 hour before sample is ready to be collected
- Masoud arrives in OR and sets up workstation in corner of OR theatre

INTRA-OP:

Part 1: Medtronic Clamp Biopsy Tissue Collection

- Single, sterile 4-pack of Medtronic clamps already in sterile field
- During exposure of spine muscles, Surgeon collects tissue sample in each clamp
- As each sample collected, single clamp passed from Surgeon → Scrub Nurse → Circulating Nurse → Masoud
- Masoud places clamps into Container A already containing formalin storage solution (see Figure 1)
- Once all clamps placed in Container A, spill-proof lid applied (see Figure 5)
- Closed Container A placed in transport box

Part 2: Blunt Cut Biopsy Tissue Collection

- 4 sterile stainless steel bowls already in sterile field
- Surgeon collects 4 blunt cut biopsies
- Each sample pair is placed in steel bowl and passed from Surgeon → Scrub Nurse → Circulating Nurse → Masoud
- Masoud places the tissue samples into Eppendorfs already containing storage solution (see Figures 1 and 6)

POST-OP:

Part 1: Sample Pick-Up

- OR team member requests porter pick-up as a RUSH
- Porter brings transport box containing all biopsy samples to Anatomic Pathology (AP)
- Masoud goes to AP to sign off on tissues, picks up transport box with samples and transfers to ICORD lab

Part 2: Return of Equipment to MDRD

- Once samples removed from biopsy kit equipment, Masoud will rinse/clean clamps and containers of debris
- Cleaned containers will be brought to MDRD dept for cleaning and sterilization (clamps & containers)
- Clamps & containers to be kept by MDRD until next case booked and will be added to case cart

Appendix C Supplementary Materials for Chapter 5

C.1 Formulations for Muscle Force Computation

The anatomic properties (typically measured in cadaveric studies) required as input to the musculoskeletal models include the in situ sarcomere length (l^S_{cad}), PCSA, pennation angle (α_{cad}), and the ratio of fiber to musculotendon length ($\frac{l^F_{cad}}{l^{MT}_{cad}}$). As these parameters taken from the literature were typically measured in cadavers the subscript "cad" was used. Note that absolute values for fiber or tendon lengths are NOT necessary, rather only the ratio of fiber to tendon length is sufficient. Here we explain how in a musculoskeletal model, normalized fiber length $\tilde{l}^F_{model}$and consequently the sarcomere length l^S_{model} are calculated to be used for computation of muscle forces.

To add muscles to a skeletal model, the attachment sites of each muscle fascicle is identified on bony elements based on detailed description of anatomical studies. By connecting those attachment sites, muscle fascicles are formed. As shown in Figure C-1, the resulting length of the connected points (the distance between A and B) is the length of the entire muscle-tendon unit (l^{MT}).

The length of the muscle-tendon in the model may not necessarily be the same as the one measured in cadavers; therefore, direct incorporation of cadaveric muscle properties into the model is generally wrong; instead, they should get scaled by the ratio of the muscle-tendon length of the model at t = 0 (before simulation starts) to the muscle-tendon length of the cadaver (i.e. $\frac{l^{MT}_{model,t=0}}{l^{MT}_{cad}}$).

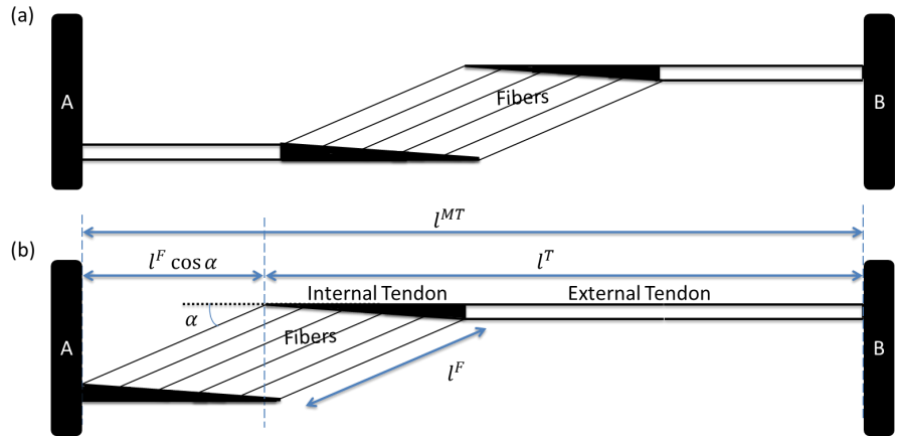

Figure C-1. Muscle anatomic properties including the pennation angle α, musculotendon length l^{MT}, and fiber length l^F. For better demonstration of muscle parameters, (b) is merely a rearrangement of (a).

With rigid tendon assumption, the length of the model tendon l^T_{model} will be constant over time and can be calculated as:

$$l^T_{model} = \frac{l^{MT}_{model,t=0}}{l^{MT}_{cad}}\left(l^{MT}_{cad} - l^F_{cad}\cos\alpha_{cad}\right) = l^{MT}_{model,t=0}\left(1 - \frac{l^F_{cad}}{l^{MT}_{cad}}\cos\alpha_{cad}\right) = cte \tag{C-1}$$

where $l^{MT}_{model,t=0}$ is the length of the muscle-tendon before the simulation starts (i.e. the body is at rest - supine position just as were the embalmed cadavers in which the muscle properties were measured). To avoid confusion, the parameters in the formulations were color coded: grey represented parameters taken from the literature (typically measured in cadavers), which were all constant values; Blue was used for parameters belonging to the model and were all constant values; and Red was used for model parameters that were dynamic and changed as the body moved.

After tendon length of the model was obtained, the model fiber length l^F_{model}, which changes as the body moves, can be computed as:

$$l^F_{model} = \sqrt{(l^{MT}_{model} - l^T_{model})^2 + \left(l^{MT}_{model,t=0} \frac{l^F_{cad}}{l^{MT}_{cad}} \sin \alpha_{cad}\right)^2} \tag{C-2}$$

By fiber length changes, the pennation angle changes, the cosine of which could be calculated as:

$$\cos \alpha = \frac{l^{MT}_{model} - l^T_{model}}{l^F_{model}} \tag{C-3}$$

Fiber optimum length in the model $l^F_{o,model}$ is defined as the fiber length at which sarcomeres are at their optimum length (l^S_o) for generating active forces. This is calculated from the fiber optimum length in the cadaver $l^F_{o,cad}$ as:

$$\begin{aligned} l^F_{o,model} &= \frac{l^{MT}_{model,t=0}}{l^{MT}_{cad}} \times l^F_{o,cad} = \frac{l^{MT}_{model,t=0}}{l^{MT}_{cad}} \times l^F_{cad} \times \frac{l^S_o}{l^S_{cad}} \\ &= l^{MT}_{model,t=0} \times \frac{l^F_{cad}}{l^{MT}_{cad}} \times \frac{l^S_o}{l^S_{cad}} \end{aligned} \tag{C-4}$$

where l^S_o is assumed for both cadavers and models to be equal to 2.8 μm [115]; and l^S_{cad} is the in situ sarcomere length. Finally, normalized fiber length in the model is computed as:

$$\tilde{l}^F_{model} = \frac{l^F_{model}}{l^F_{o,model}} = \frac{\frac{l^F_{model}}{Number\ of\ Sarcomeres}}{\frac{l^F_{o,model}}{Number\ of\ Sarcomeres}} = \frac{l^S_{model}}{l^S_o} = \tilde{l}^S_{model} \tag{C-5}$$

where by "Number of Sarcomeres" it is meant the number of sarcomeres in series that form the length of a muscle fiber; its value is not important here though as it cancels out in the above formula. Therefore, one may obtain the sarcomere length of the model as:

$$l^S_{model} = l^S_o \times \tilde{l}^F_{model} \tag{C-6}$$

The anatomic and biomechanical properties are then used for muscle force computation through the following formulation:

$$\begin{aligned} F_{muscle} = PCSA \\ \times \Big(activation \times SpT \times SpecificTension \times \tilde{f}_{active}(l^S_{model}) \\ + k \times K \times \tilde{f}_{passive}(l^S_{model}) \Big) \times \cos\alpha \end{aligned} \tag{C-7}$$

where K is a constant scaling the normalized passive curve just as does the specific tension for the normalized active curve; SpT and k are the scaling factors for the specific tension and K, respectively, and are both set to 1 by default; l^S_{model} is the model sarcomere length; $\tilde{f}_{active}$ and $\tilde{f}_{passive}$ are force multipliers as functions of $l^S_{model}$and are obtained from the normalized force-

length curve (Figure C-1); and activation is a decimal varying between 0 and 1 representing muscle activation level between turned off and fully activated.

C.2 Calibration

In an in vivo study [26] of four male subjects lying on their right side, the maximum voluntary back-extension torques about the L5-S1 joint along with the corresponding intra-abdominal pressures were measured at multiple lying body postures including 20° extension, 10° extension, 10° flexion, and 30° flexion. To simulate this study, gravity was set to zero in our model and an anteriorly oriented horizontal force was applied to T3 center of mass which had a lever arm of 0.39m about L5-S1. Division of the measured torques in that study by 0.39 gave us the expected equivalent forces to be applied horizontally at T3 and to be resisted by the model **(**Table C-1**).** In our model, for each posture the applied horizontal force was increased by increments of 5 N until the model was not able to resist. As a kinematic accuracy with tracking error of less than 1° was desired, the maximum resisting force by the model was defined as the force beyond which the model could not stay within 1° of the prescribed rotation.

A specific tension of 100 N/cm^2 and three weighting terms of 2.5, 0.025, and 0.005 for the first three cost functions were achieved in our previous model through simulation of 10° extension and 10° flexion postures [152]. We used these same values and simulated 20° extension and 30° flexion, to determine the weighting term for the fourth cost function (w_4) which dealt with six-dimensional springs force minimizations and was introduced in this study. Four values of 1, 5, 10, and 15 were attempted for w_4 to obtain the maximum forces the model could resist to keep the model once within 1° and once within 2° of the prescribed position. With $w4$ = 5 the closest results to the experimental data were achieved by the model, especially for the flexion postures **(**Table C-2**).**

Table C-1. Average of the maximum sagittal plane moment, intra-abdominal pressure (IAP), and diaphragm area at different positions for subjects of the of Daggfeldt et al.'s study [26]**.**

	Extension 20°	Extension 10°	Flexion 10°	Flexion 30°
Moment Magnitude (Nm)	110 (90-130)	180 (150-210)	240 (210-270)	290 (240-340)
IAP (kPa)	12	16	18	18
Diaphragm Area (cm^2)	190 (150-230)	200 (160-240)	210 (180-240)	240 (220-260)
$F_{IAP} = IAP \times Area$ (N)	228	320	378	432
Expected Equivalent Force to be Resisted by the Model (N)	**282**	**461**	**615**	**743**

Table C-2. Maximum resistible forces by the model at 20° extension, 10° extension, 10° flexion, and 30° flexion when values of 1,5,10, and 15 were attempted for w_4 (the weighting term for the FSU forces cost function). Values are reported for tracking errors of 1° and 2°. The weighting term producing closest results to the equivalent forces in Table S1 is presented in bold.

	Tracking Error < 1°				Tracking Error < 2°			
	Extension 20°	Extension 10°	Flexion 10°	Flexion 30°	Extension 20°	Extension 10°	Flexion 10°	Flexion 30°
w4= 15	160 N	170 N	205 N	250 N	225 N	270 N	330 N	400 N
w4= 10	240 N	290 N	350 N	430 N	410 N	480 N	550 N	615 N
w4= 5	**400 N**	**505 N**	**615 N**	**745 N**	410 N	510 N	650 N	765 N
w4= 1	405 N	555 N	650 N	785 N	420 N	560 N	700 N	NP

Once $w4$ = 5 was determined, to refine the value selected for the specific tension, two other values of 80 N/cm^2 and 90 N/cm^2 were attempted, but still 100 N/cm^2 was the only one being able to produce sufficient strength especially when the model is flexed **(**Table C-3**).**

Table C-3. Maximum resistible forces by the model at 20° extension, 10° extension, 10° flexion, and 30° flexion for specific tension. Values are reported for tracking errors of 1° and 2°. The specific tension producing closest results to the equivalent forces in Table C1 is presented in bold.

	Tracking Error < 1°				Tracking Error < 2°			
	Extension 20°	Extension 10°	Flexion 10°	Flexion 30°	Extension 20°	Extension 10°	Flexion 10°	Flexion 30°
ST=100	**400**	**505**	**615**	**745**	405	525	650	765
ST=90	375	470	570	695	385	480	605	695
ST=80	345	435	515	640	360	440	555	640

Appendix D Muscle Stiffness Testing Apparatus

D.1 The Apparatus

Measuring elastic modulus of muscle fibers and fiber bundles required a special apparatus, which I designed and developed during my PhD studies receiving assistance from a graduate student [3] and an undergraduate student [4] in prototyping some of the components (Figure 2-2, Figure D-1, and Figure D-2). The apparatus was customized and built based on the working system in Dr. Steve Brown's lab at the University of Guelph. The major components of the apparatus included a temperature-controlled solution bath, a photodiode array system, a length controller and a highly sensitive force transducer. We bought the force transducer from Aurora scientific (400A, Aurora, Ontario, Canada) and developed the other major components in our lab.

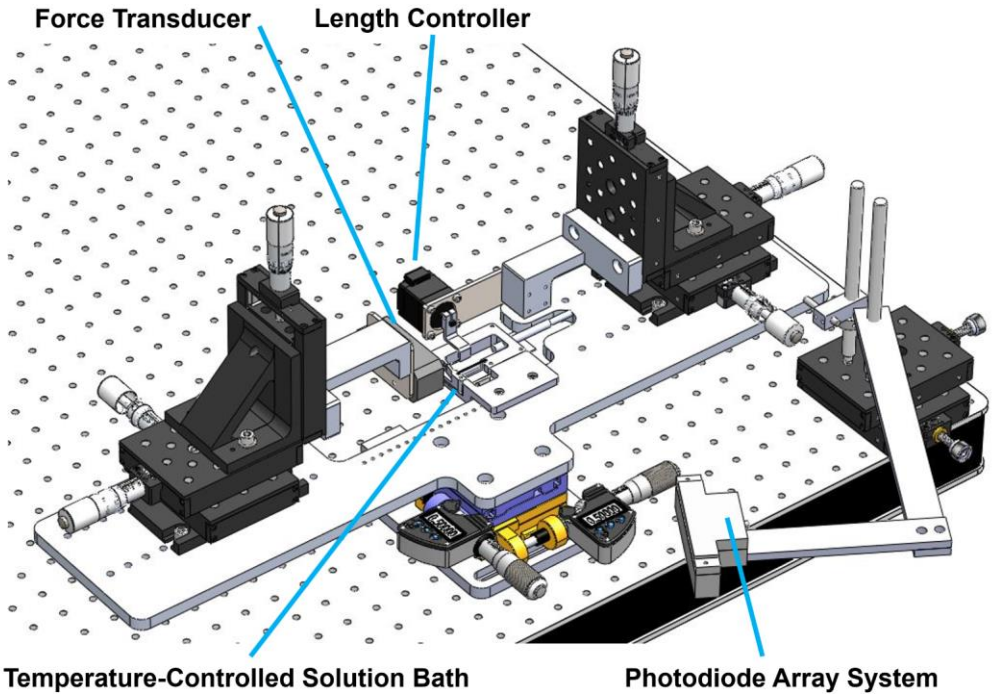

Figure D-1. Schematic of the designed muscle stiffness testing apparatus.

[3] Mr. Sandeep Sadaram
[4] Mrs. Sophie Ramsden

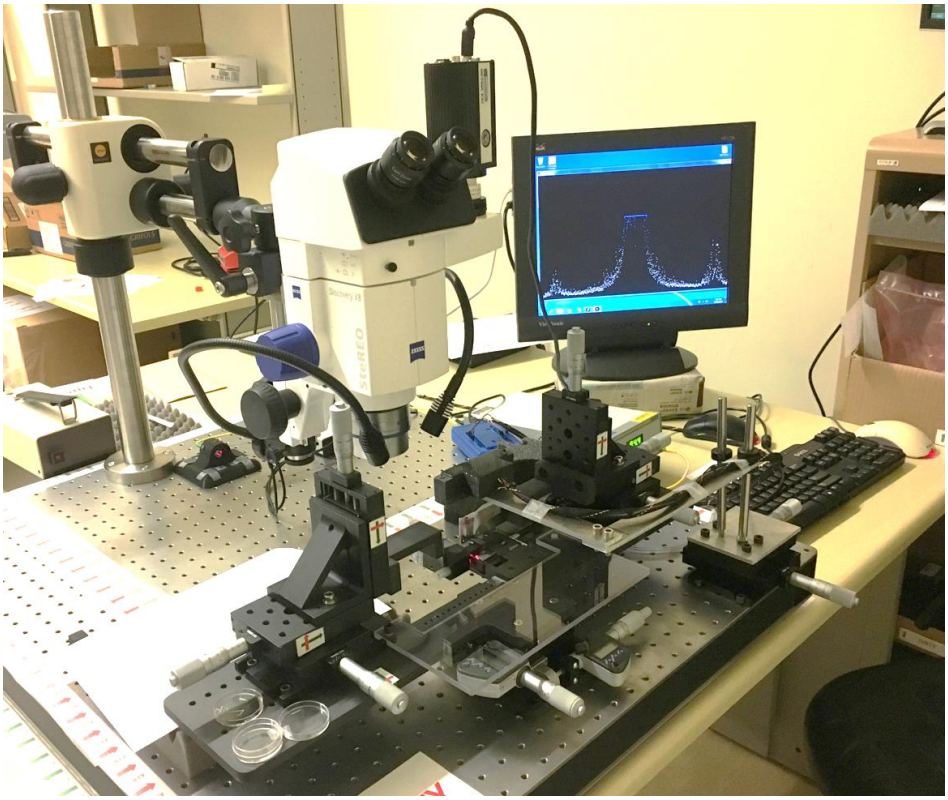

Figure D-2. The manufactured muscle stiffness testing apparatus designed and developed in our lab.

D.2 Temperature-Controlled Solution Bath

Measuring elastic modulus of a fiber/fiber bundle requires the fiber/fiber bundle to be immersed into a physiological relaxing solution, for which we designed and built a temperature-controlled solution bath. During the test to monitor the strain of the muscle fiber/fiber bundle through the diffraction technique, a laser beam needed to enter from the bottom of the bath to transilluminate the fiber/fiber bundle. Therefore, the design of the solution bath was considered to be modular consisting of a solution bath body, a bracket, and a transparent glass (for which we used a microscope slide) in between the two (Figure D-3). With this modular design, the glass (microscope slide) could be easily replaced by a new one when the scratches/dusts on it would affect the quality of the laser beam.

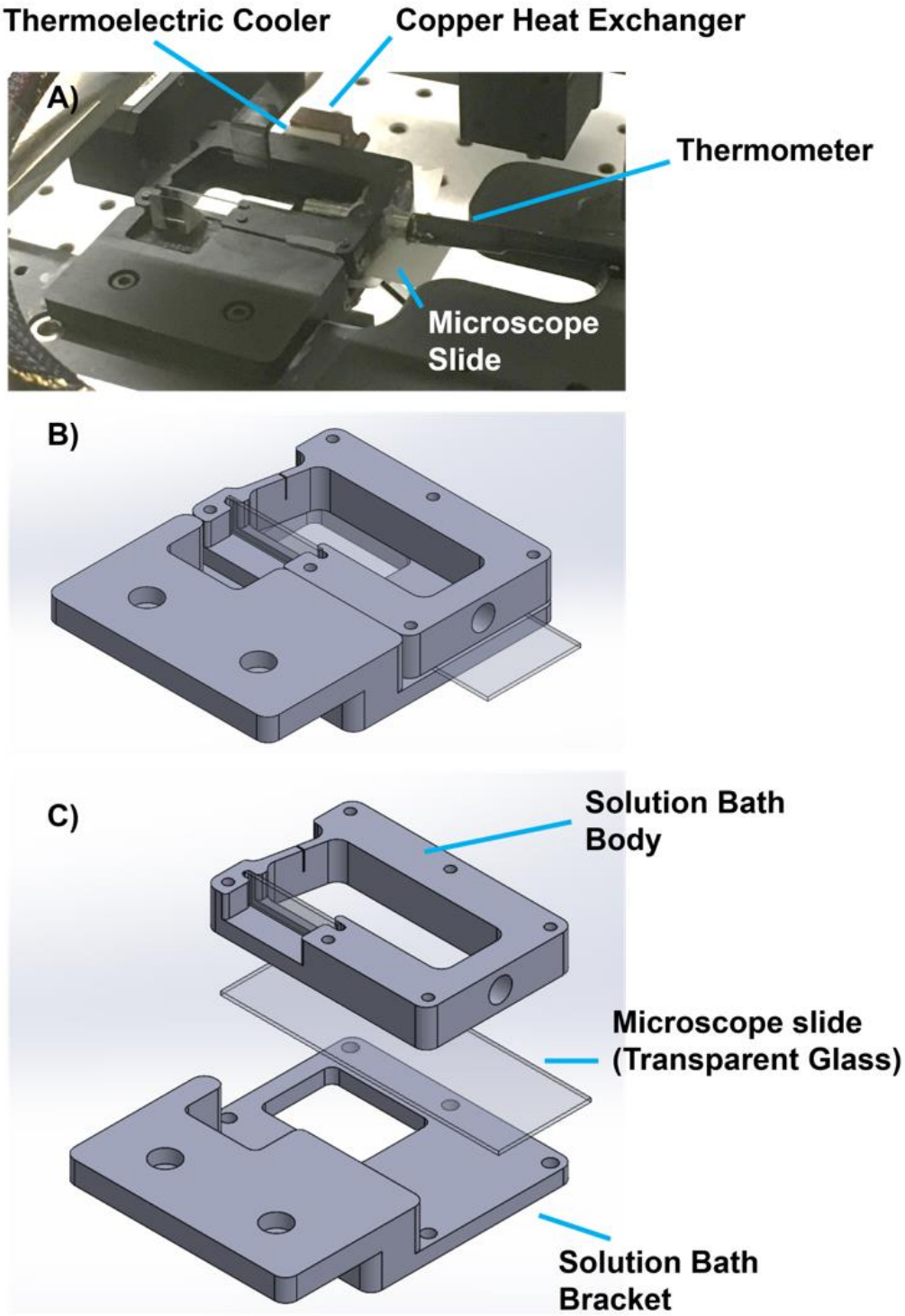

Figure D-3. Temperature-controlled solution bath. The temperature of the solution was monitored using a thermometer and was controlled by an Arduino adjusting the power fed to the thermoelectric cooler (A). The design of the bath was modular (B-C) to allow for convenient replacement of the transparent glass in between the solution bath body and bracket.

A few novel features were provisioned for the solution bath body, which made it a convenient one to work with (Figure D-4). A narrow slit on the left side of the bath enabled insertion of the force transducer pin into the solution bath. With narrow enough slits, the surface tension between water (or more precisely the relaxing solution) and the bath wall prevents any fluid leakage outside the bath. We tested various slit sizes and found slits as wide as 0.71 mm to be able to retain the water within our anodized aluminum bath. Such slit size provided sufficient room for the 0.15 mm in diameter pin attached to the force transducer to stay free from the slit wall. In narrower slits (e.g. 0.3mm) even a slight malalignment of the pin could result in a contact between the slit wall and the pin and affect the accuracy of the force transducer measurements.

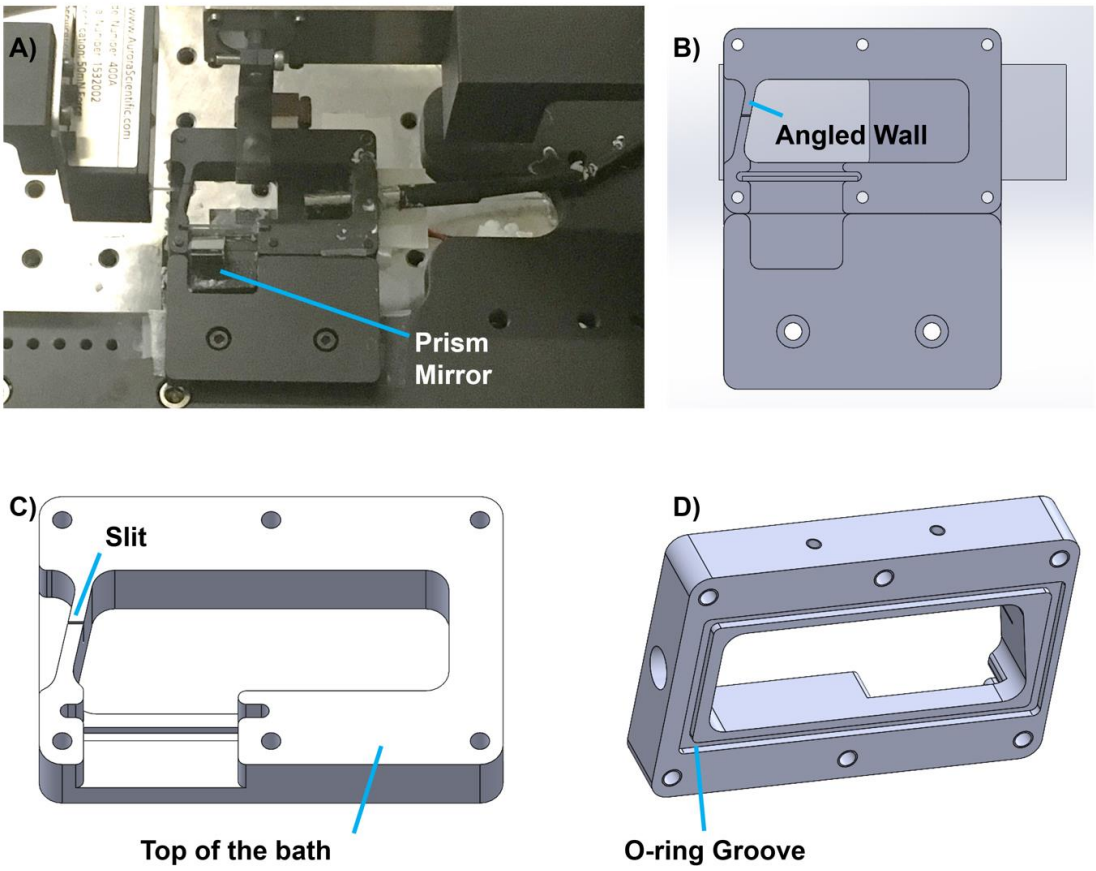

Figure D-4. Special features of the novel solution bath body.

Another novel feature introduced was the angled wall on the left side of the solution bath body. This feature enabled more ergonomic and convenient handling of the fiber/fiber bundle by providing extra room available for the tip of the tester's forceps. The tester needs to extensively use two forceps (18025-10, Fine Science Tools, Vancouver, Canada) to mount a fibre/fiber bundle onto the pins and to secure that by tying suture loops around the pins and the muscle fibre/fiber bundle. This process needs to be done under a stereomicroscope with extra caution and fine control of hand movements so that when pulling the two ends of the suture ties the force transducer is not damaged due to extra force applied on one side of it. The angled wall made this process more ergonomic for the left hand-wrist and more convenient by providing extra room.

At the bottom face of the solution bath body, a groove of 1.3 mm in depth and 2.4 mm in width was milled (Figure D-4.D). Using an 1.7 mm in diameter O-ring and 6 screws which were uniformly tightened, the bath was sealed from the bottom against the microscope glass slide. Nonuniform tightening of the screws could lead to breakage of the glass or leakage of the bath.

At the front face of the solution bath body, a window glass was secured using silicon glue; and a prism mirror was placed in front of it. By moving the stereomicroscope over this mirror, side-view of the fiber/fiber bundle was observed and its side diameter was accurately measured.

For the enzymes within the physiological solution to remain stable during the test, the temperature of the bath is recommended to be around ~15ºC. A waterproof thermometer (DS18B20, Maxim Integrated, San Jose, USA) was inserted into the solution bath through a hole in its right side (and secured by silicon glue) which enabled constant monitoring of the bath temperature (Figure D-3.A). The temperature of the bath was lowered using a thermoelectric cooler (CP30138, CUI Devices, Lake Oswego, OR, USA; Figure D-3.A). A thermoelectric

cooler is a semiconductor that when subjected to a DC voltage acts as a heat pump generating heat on one side while cooling down its other side. Based on thermometer readings, the power of the thermoelectric cooler was controlled using an Arduino. Natural convection was not sufficient to prevent temperature of the hot side of the thermoelectric cooler from going too high and burning; therefore, a copper heat exchanger (WBA-0.60-0.28-CU-01, Custom Thermoelectric, Maryland, USA) was placed in direct contact with the hot side of the thermoelectric cooler (Figure D-3.A). A flow of water at room temperature was constantly pumped from a water bucket (~2 liters) into the heat-exchanger and exited from the other side back into the bucket. Using this mechanism, we were able to maintain the temperature of the solution bath at a constant value of 17°C.

D.3 Photodiode Array System

The photodiode array system was an integral part of the apparatus. The strain of the fiber/fiber bundle after each increment was measured through the diffraction technique. In this technique, a coherent beam transilluminated the mounted fiber/fiber bundle. Due to the organized structure of the sarcomeres within muscle fibers, light interference occurs as the beam passes through the fibers and results in an spectrum of light and dark points (Figure 1-16). As explained in section 1.6.1.1, a number of geometric dimensions including the distance between the first-order light points was required to measure the average length of the sarcomeres present in the transilluminated spot on the fiber/fiber bundle. Although the light points can be indirectly observed when projected on a surface (e.g. a white paper, Figure D-5.A,C, and E), accurate measurement of the sarcomere length requires detecting the exact peak of the light points. To accomplish this, we developed a photodiode arrays system that precisely rendered the diffraction pattern based on projected light intensity (Figure D-5.B,D, and F).

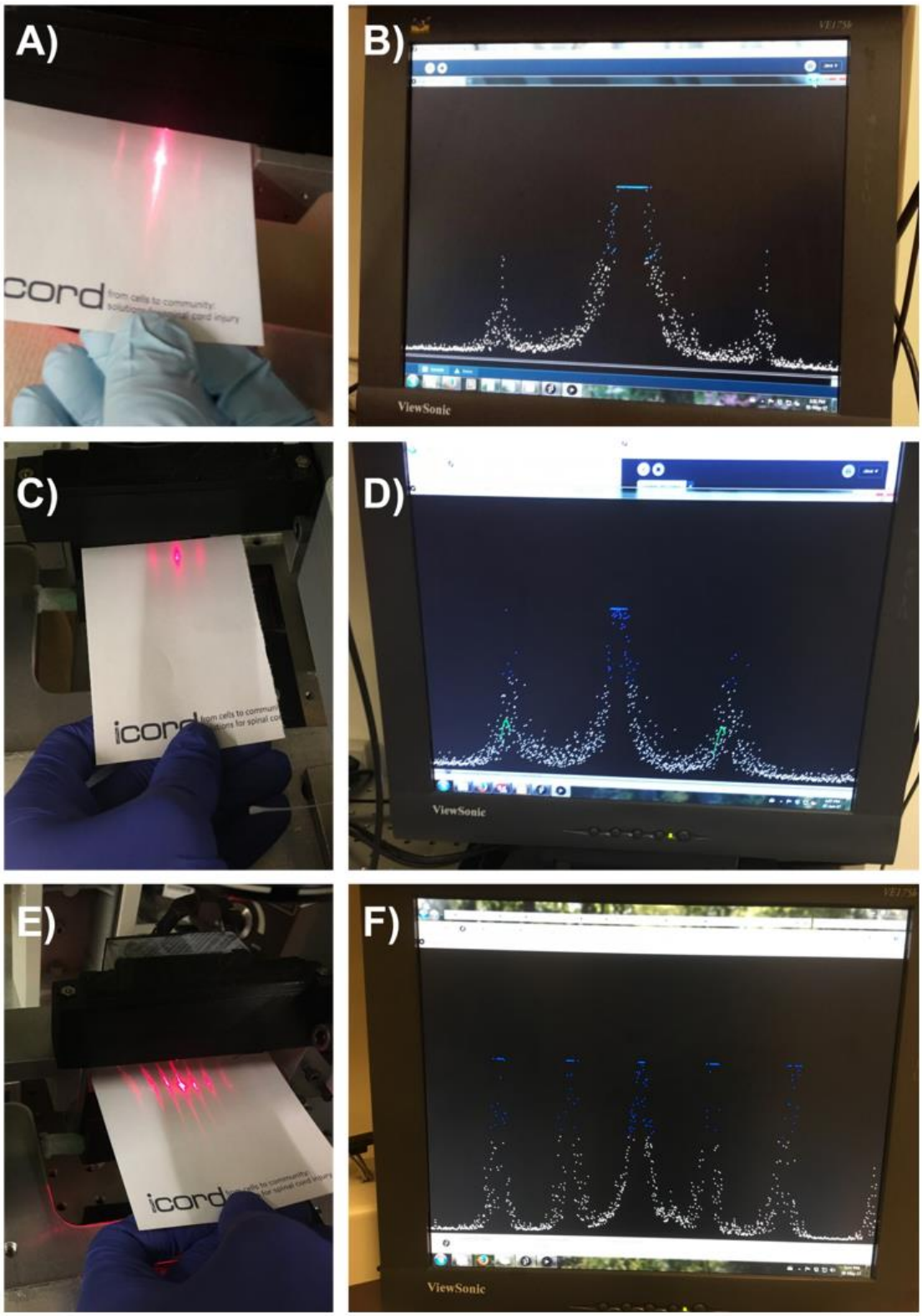

Figure D-5. Muscle fiber diffraction pattern observed by naked eye and with our photodiode array system.

We used a 1280×1 photodiode array (TSL1410R, AMS-TAOS, USA) consisting of 1280 linear pixel elements (each measuring 63.5 µm in length and 55.5 µm in width) in series (Figure D-6). These sensor pixels generate electrical current proportional to the intensity of the light projected onto them. Using an Arduino Mega 2560 (A000067, Arduino, Italy) we were able to scan the diffraction patter every 16 ms although for our application such speed was not necessary at all. Using the open source Processing software package (www.processing.org), we rendered the scanned pattern on the monitor screen. The user could click on the peak of the first order light points and measure the exact distance between them knowing that the physical distance between the two end pixels of the photodiode array is 81.272 mm (Figure D-5).

We 3D printed a deep dark housing for the photodiode array to serve two purposes. First, inside the housing, the photodiode array was fixed and would remain at a constant distance from the fiber/fiber bundle. Second, the depth of the housing would filter our most of the ambient light from projecting onto the photodiode array. The remaining ambient light that would enter anyway was recorded when the laser was turned off and was subtracted when the laser was turned on so the user would only observe the diffraction pattern resulting from the laser beam. A swivel arm was used for convenient handling and coarse positioning of the photodiode array system, while a XY translation stage was used for finer positioning of the photodiode array system (Figure D-7).

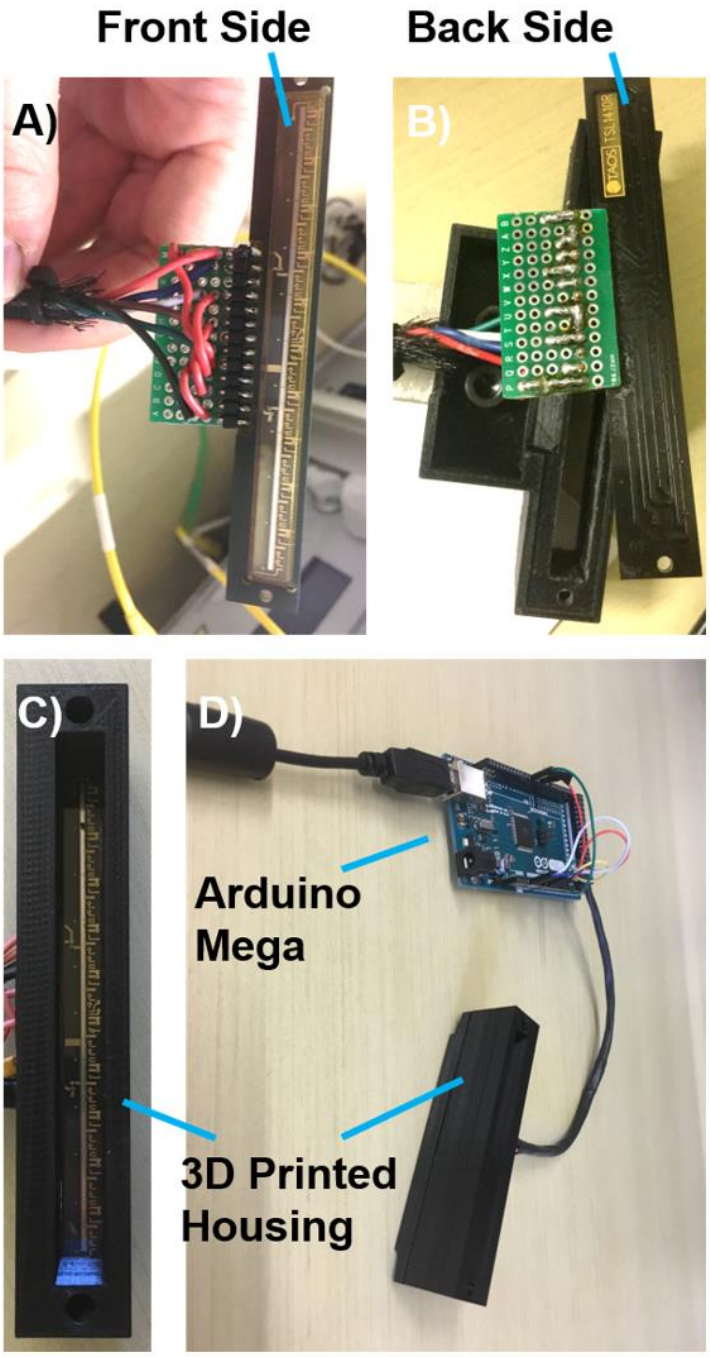

Figure D-6. Photodiode array system. The golden line on the front side is to be exposed to the diffraction pattern (A). The back side of the photodiode array was pressed firm in place so that its position remained fixed with respect to the housing (B). The tall walls of the 3D printed housing around the photodiode array filtered out a large portion of the ambient light from hitting the photodiode array (C and D).

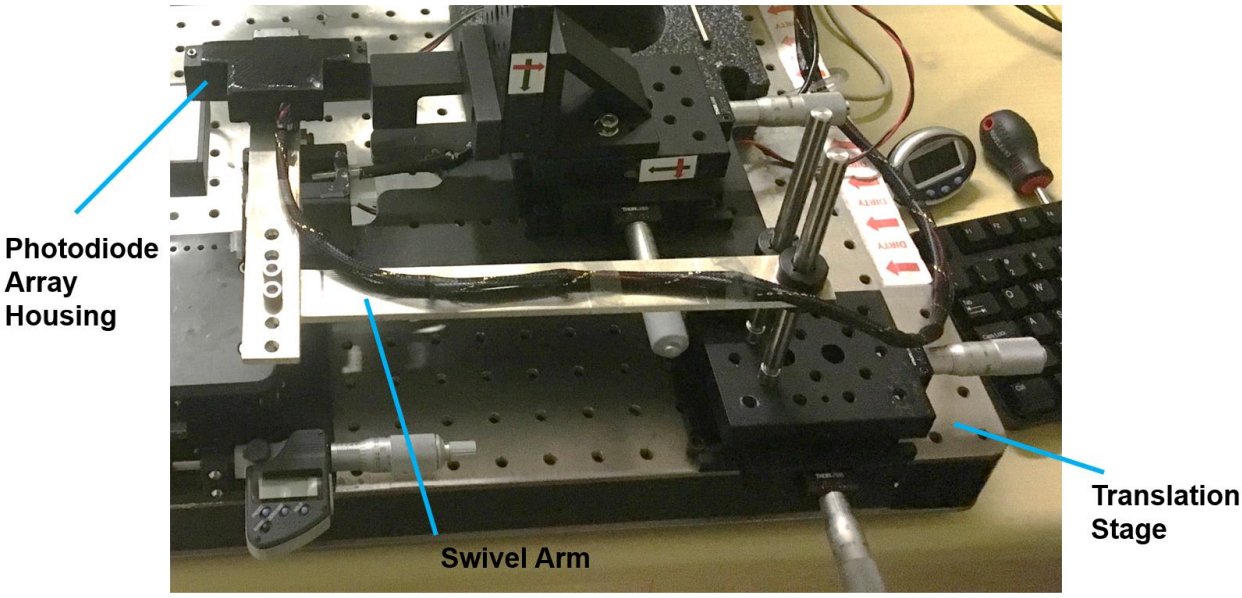

Figure D-7. The mechanism for adjusting position of the photodiode array system. Swivel arm was used for coarse positioning and XY translation stage for fine positioning.

The photodiode array system was calibrated and validated using two diffraction gratings of sizes 2 µm (Edmond Optics, Barrington, NJ, USA) and 3.33 µm (Thorlabs, Newton, NJ, USA). For calibration, the first diffraction grating was immersed into the physiological solution in the bath at the same position that muscle fiber/fiber bundle would be placed for testing. By shining a laser beam through the grating, the diffraction pattern was captured by the photodiode array system (Figure D-8). The distance between the muscle fiber/fiber bundle and photodiode array (i.e. L in in Equation (1-3)) was fine tuned numerically so that the calculated grating size would match the grating nominal size, i.e. 2 µm. For validation, the first grating was replaced by the second grating and its grating size was measured. The measured (calculated) grating size was found to match the nominal value, i.e. 3.33 µm with a precision of 10 nm.

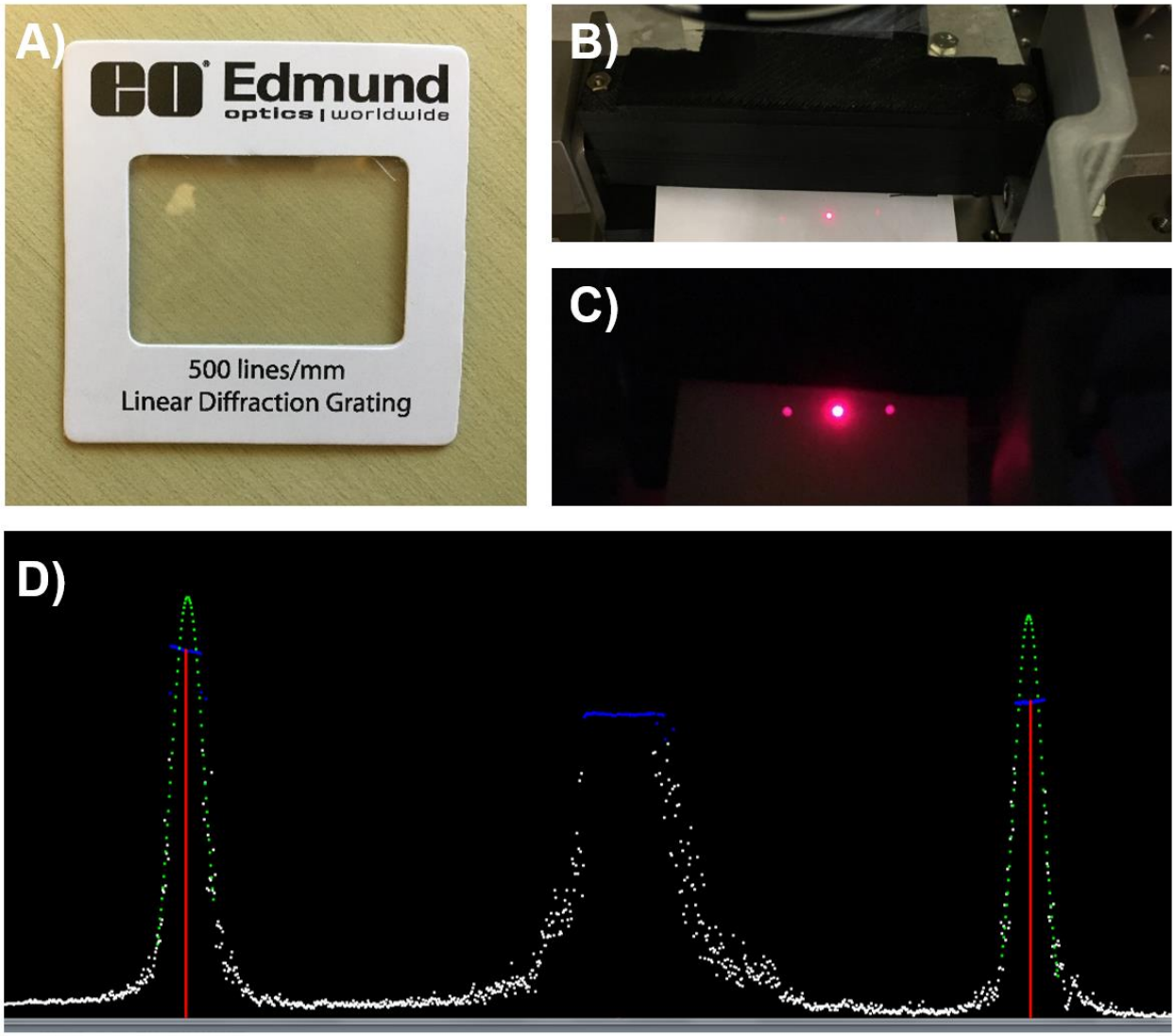

Figure D-8. Diffraction grating and its diffraction pattern. The size of the first diffraction grating was 2 micron (A). Shining the diffraction grating by a laser beam resulted in nice diffraction patterns that could be seen as projected on a piece of paper (B-C) and through our photodiode array system.

D.4 Laser Source

We used S1FC660 Fabry-Perot benchtop laser source from Thorlabs (Newton, NJ, USA). This laser-diode-driven fiber-coupled laser source provided a single mode Guassian beam with a wavelength of 660 nm. The power of the laser source was adjustable using a knob reaching up to 15 mW, but for our experiments we kept it between ~2.5 to 5 mW at most of the times (Figure

D-9). The beam was guided through a single-mode patch cable (P5-630A-PCAPC-1, Thorlabs, Newton, NJ, USA) to enter a collimation package (F230APC-633, Thorlabs, Newton, NJ, USA), resulting in a collimated beam of 0.84 mm in diameter.

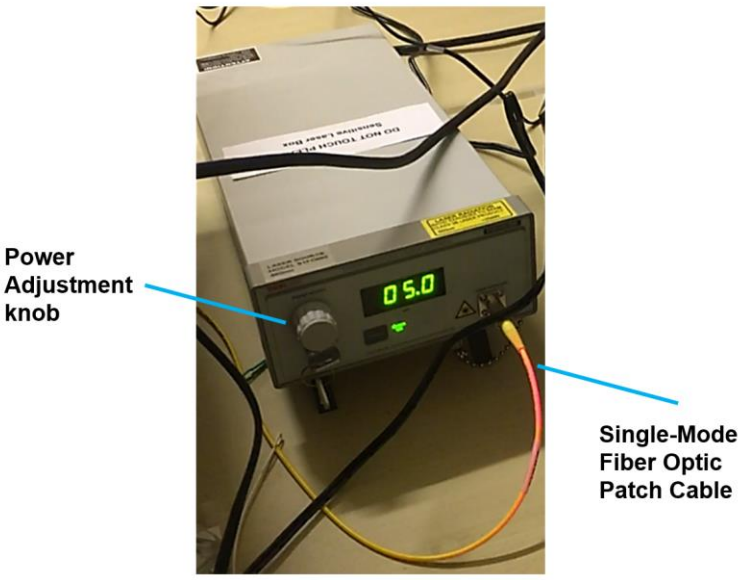

Figure D-9. Laser source with adjustable power up to 15 mW (here set to 5 mW).

I designed and 3D printed a housing for the collimation package to provide easy positioning of the laser beam (Figure D-10). The housing included four magnets at a height of 10 mm from the breadboard table. The magnets allowed smooth slide of the housing for adjusting its position, while providing sufficient grip to the table so as to be kept fixed in a desired location. The collimation package was secured within an unthreaded adapter (AD11NT, Thorlabs, Newton, NJ, USA) and placed inside the housing bore. Using a set screw on top and two screws at sides of the hole, the orientation of the adaptor containing the collimation package could be fine-tuned so as the exiting beam stays horizontal (Figure D-10).

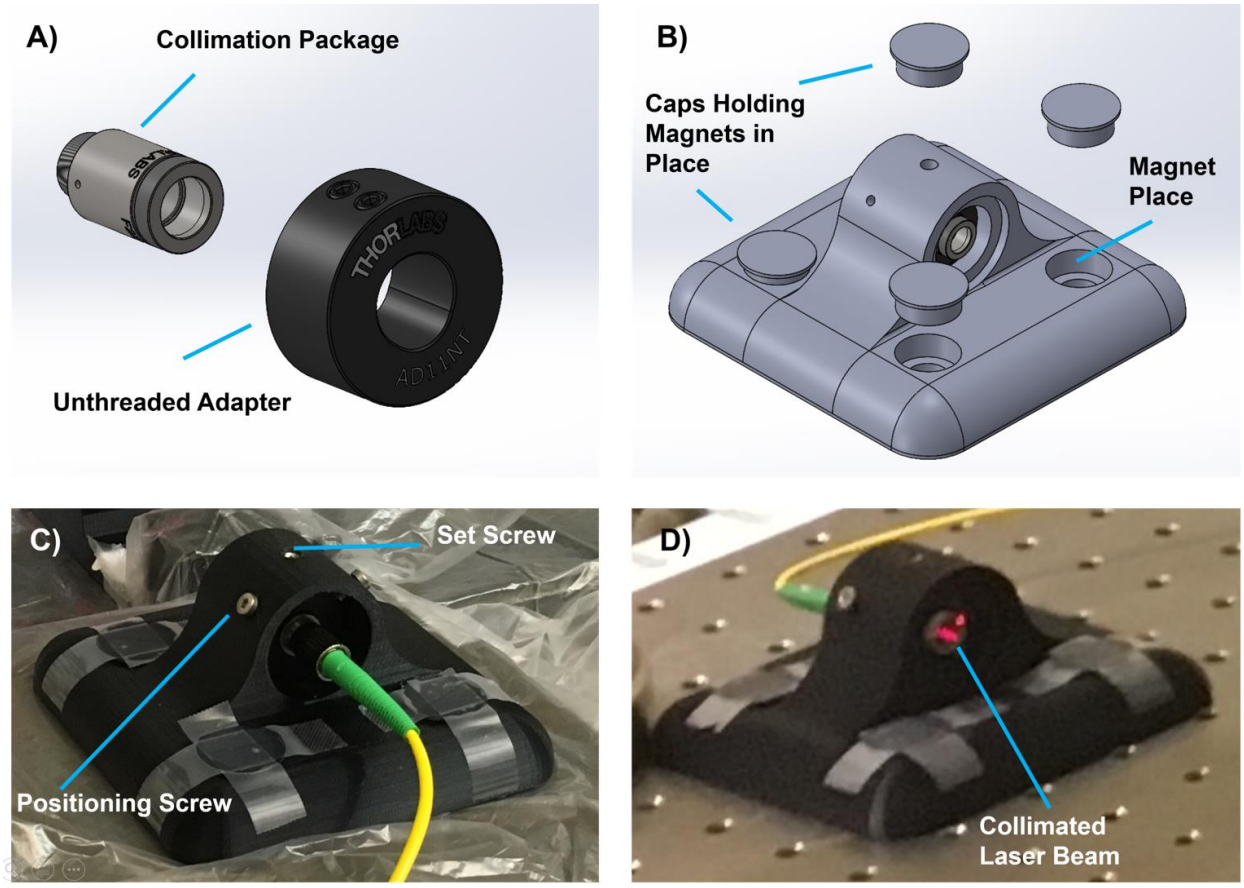

Figure D-10. Housing for the laser collimation package.

The horizontal collimated beam would hit a right-angle prism mirror (MRA10-P01, Thorlabs, Newton, NJ, USA) to be reflected vertically and pass through the transparent bottom of the temperature-controlled solution bath and hit the muscle fiber/fiber bundle and transilluminate it (Figure D-11).

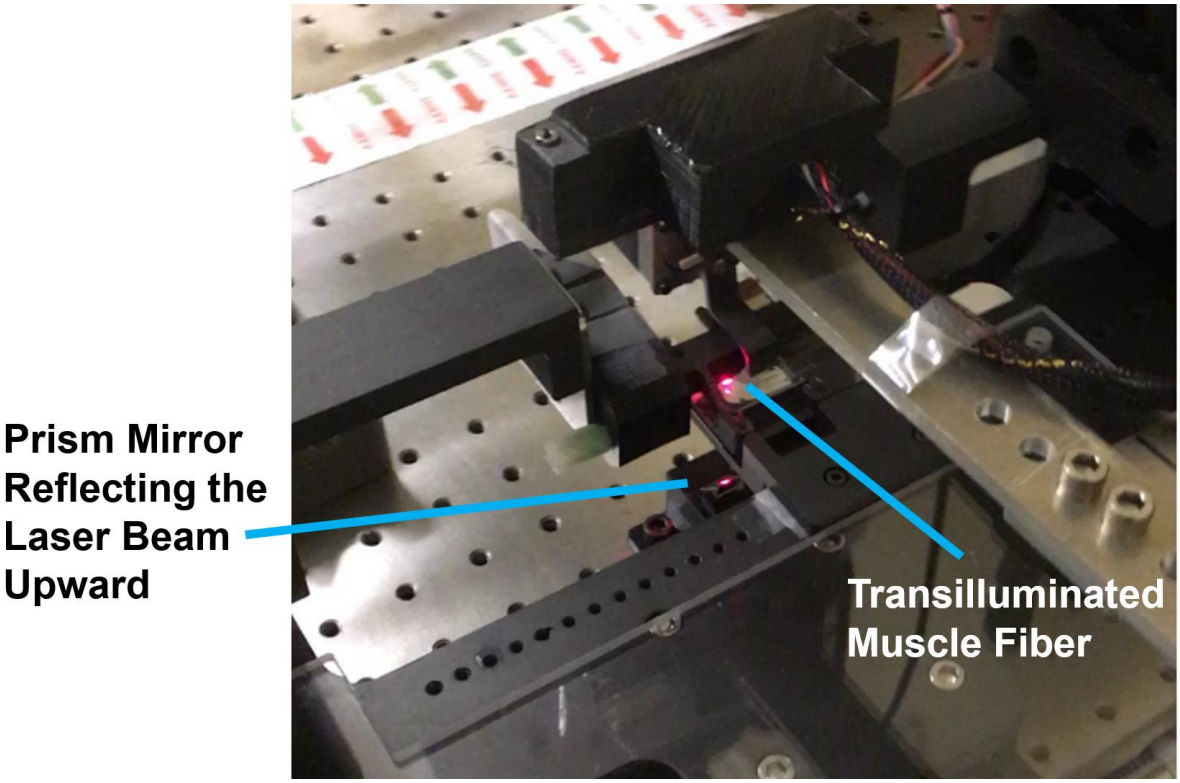

Figure D-11. Prism mirror reflecting the horizontal laser beam vertically.

Under no circumstance the laser beam could be directly looked at. Adjusting the beam direction, however, required an indirect glance to the laser beam. Therefore, standard laser safety glasses (LG13, Thorlabs, Newton, NJ, USA) were used to protect the user from this class 3B laser.

D.5 Length Controller

To stretch the muscle fiber/fiber bundle, increments of 10% strains at a rate of 10% per second were applied. For a 2.5 mm long fiber/fiber bundle this would be equal to a stretch of 250 µm at a rate of 250 µm/s. Such stretch was achieved using a stepper motor (CRK523PMAP, Oriental Motor, Torrance, CA,USA), a motor driver, and an Arduino (Figure D-12).

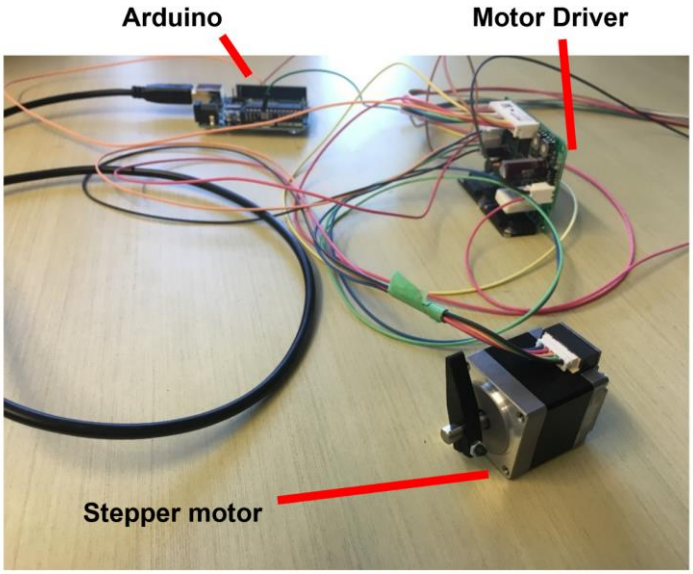

Figure D-12. Length controller consisted of a stepper motor, a motor driver, and an arduino.

Initially, we attached a 3D printed lever arm to the stepper motor and assessed its performance (Figure D-13). Using a dial gauge with a resolution of 25.4 (0.001 inches) the function of the length controller was verified (Figure D-13). We aimed for applying 10 consecutive displacement of 250 µm at the tip of the lever arm, which was in contact with the tip of the spring-loaded dial indicator. We repeated the measurement for three complete cycles (each with 10 incremental stretches). The average of the measured displacement per each increment was 256 µm with a precision of 27 µm (standard deviation). The length controller successfully met our expectations, especially given that the average load on the lever arm by the dial gauge indicator was ~500 mN which is larger than the maximum tension a muscle fiber/fiber bundle would undergo in our tests (~30 mN). In addition, part of the lower precision reported here was due to the coarse resolution of the dial gauge being 25.4 µm. Most importantly, the exact strain of a muscle fiber/fiber bundle after each stretch would be measured accurately using the photodiode array system. Therefore, it was not necessary that the length controller apply an exact 10% strain, rather the accuracy of the stress-strain curve would be guaranteed by the very

accurate photodiode array system. In the final version of the length controller, we replaced the 3D printed lever arm by a modified lever arm which was manufactured out of anodized aluminum (Figure D-14).

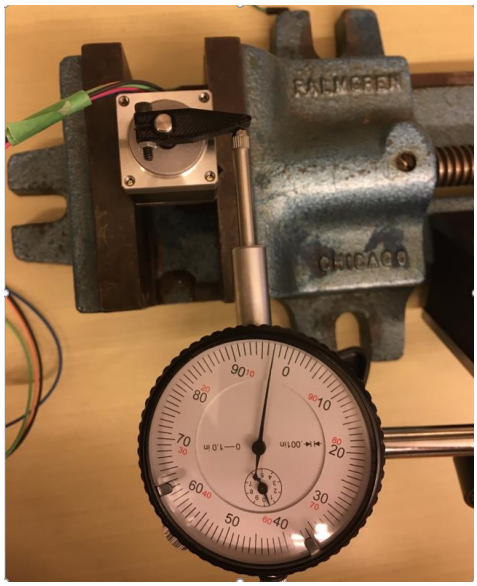

Figure D-13. Verification of the performance of the length controller using a dial gauge.

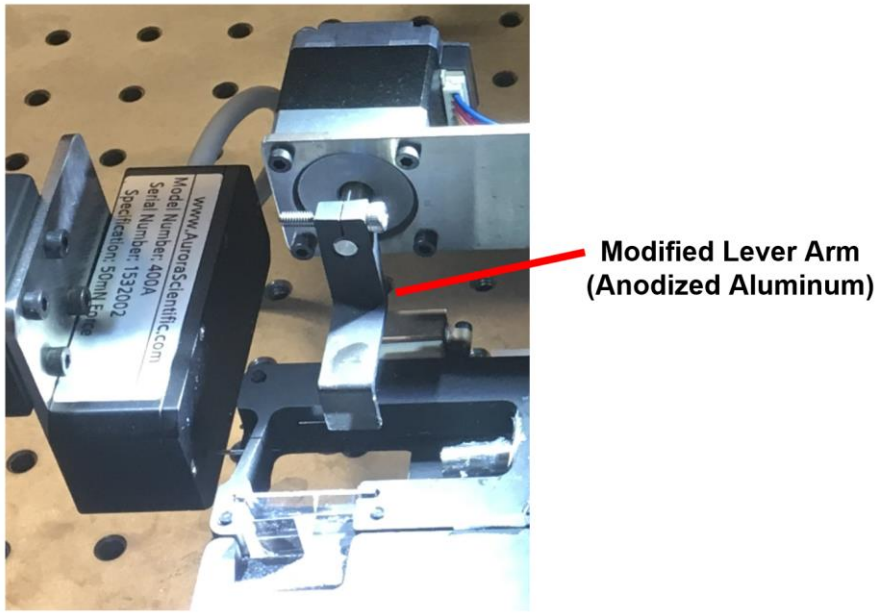

Figure D-14. Final version of the length controller with a modified lever arm.

D.6 Force Transducer

We bought the 400A force transducer from Aurora Scientific (Aurora, Ontario, Canada), whose design was based on a variable displacement capacitor. The resolution of the force transducer was 1 μN with maximum force measurement of 50 mN (and maximum overload force of 250 mN). A scaling factor of 5.013 mN/Volt was used to convert voltage readings to forces. The force transducer was validated by hanging standard weights of 10 mg, 100 mg, 1 g, and 2 g (ASTM Class II Standard Weights Troemner, NJ, USA) repeated for 12 trials each with no measurement having more than 6%, 4%, 2%, and 1% errors, respectively.

D.7 Stereo Microscope

The entire tissue preparation process, ranging from muscle fibers/fiber bundle extraction to installation of the fiber/fiber bundle onto the pins, demanded usage of a stereomicroscope (Figure D-15). We selected SteREO Discovery.V8 stereomicroscope (Zeiss, Germany) and equipped it with a Plan-Apochromatic 0.63x objective lens (435202-9902-000, Zeiss, Germany), which provided a wide filed of view correcting for spherical aberrations. In addition to providing better visualization and hence contributing to better handling of the fiber/fiber bundles, this feature helps in ensuring that both pins are in focus and hence aligned, which is desired for uniaxial tensile testing. For alignment, specifically, it is noteworthy that we would also check the side-view of the fiber/fiber bundles to make final position adjustments ensuring alignment in both planes are achieved.

For measuring the dimensions of the fiber/fiber bundle (from the both top and side views), the XY translation stage on which the base plate was mounted was used (Figure D-16). For example, for measuring the top diameter in the middle of the fiber, the XY stage was moved such that the

center of the crosshair reticule inside the eyepiece of the microscope would coincide with the bottom edge of the fiber/fiber bundle. The micrometer of the Y stage was zeroed at this point and then moved until the crosshair reticule center coincided with the top edge of the fiber/fiber bundle. The micrometer reading at that point is the diameter measured wit ha resolution of 1 micron. After all dimensions were measured using the microscope, the microscope needed to give its place to the photodiode array. This was achieved thanks to the heavy duty ball-bearing-based gliding mechanism in our boom stand (411005-0001-000, Zeiss, Germany) through which the microscope could be easily pushed away and brought back at the end of the experiment with no change in its focus (Figure D-15).

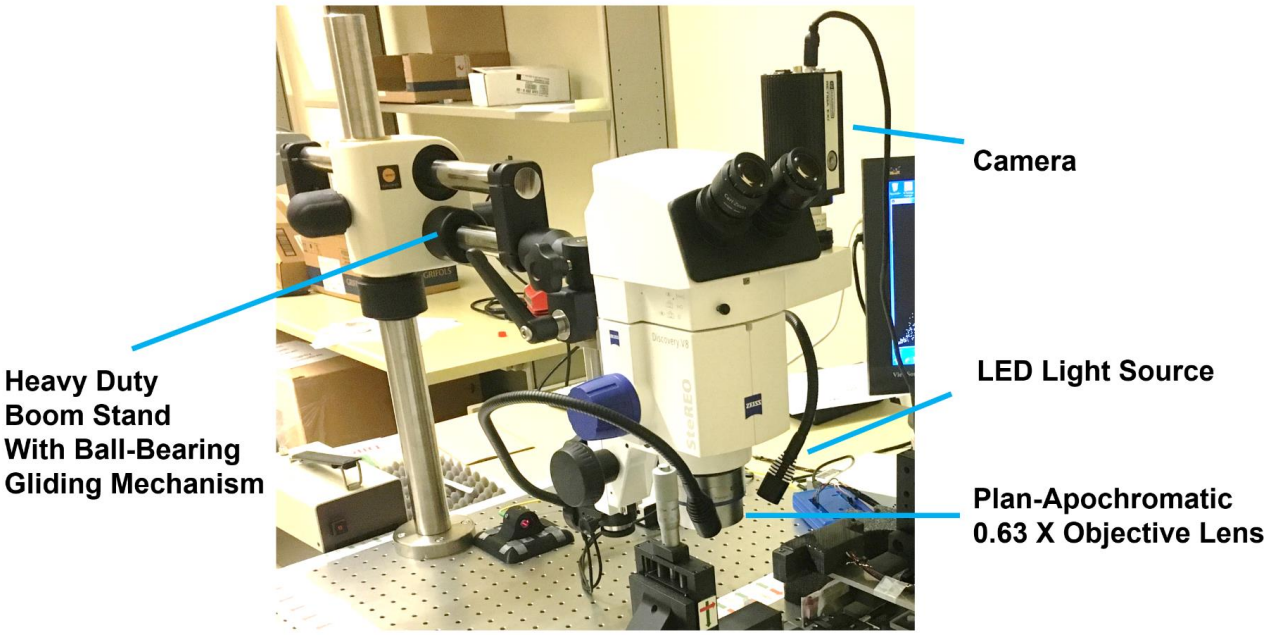

Figure D-15. Zeiss stereomicroscope equiped with a plan-apochromatic objective lens.

D.8 Base Plate and Translation Stages

To adjust position of most of the major components in our apparatus, several translation micro-stages were used (Figure D-16). While the force transducer and length controller required a XYZ translation stage, the photodiode array system and the base plate were mounted on a XY translation stage.

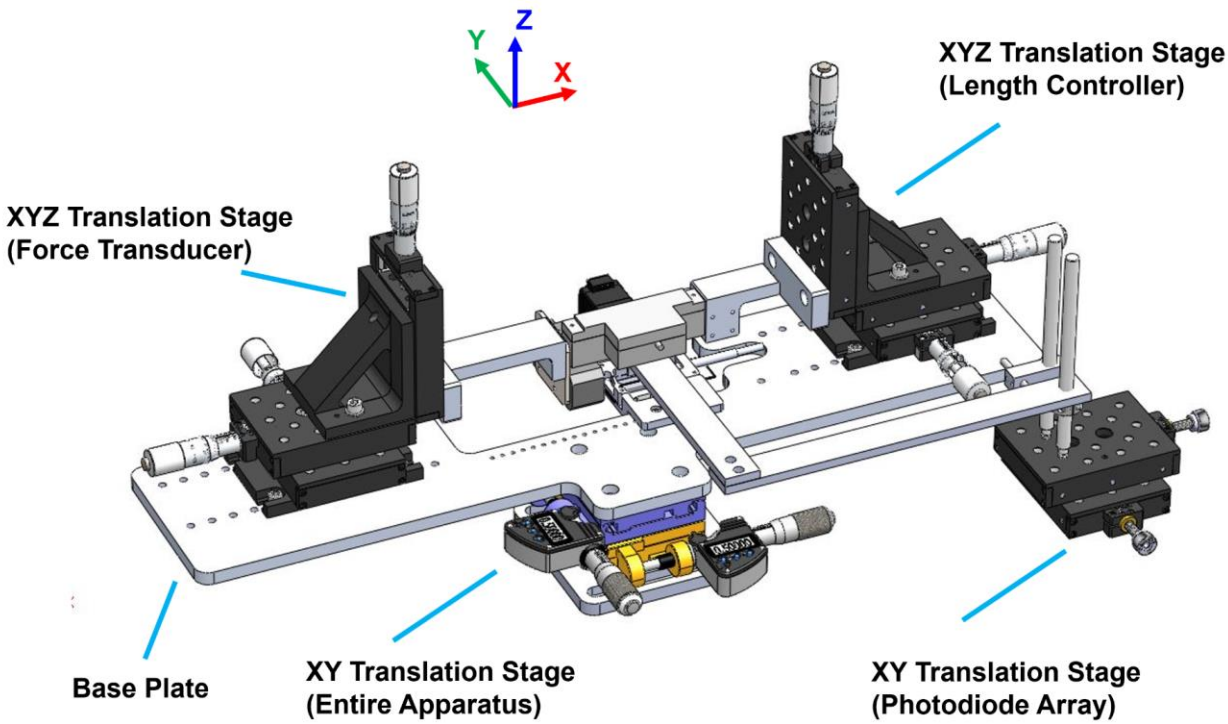

Figure D-16. Base plate and translation stages.